Diss. ETH No. 13363

Precise Predictions for Four-Fermion Production in Electron-Positron Annihilation

A dissertation submitted to the
SWISS FEDERAL INSTITUTE OF TECHNOLOGY ZURICH
(ETH Zürich)

for the degree of
Doctor of Natural Sciences

presented by
Markus Roth
Dipl. Phys. Univ. Würzburg
born March 8, 1969
German citizen

accepted on the recommendation of
Prof. Zoltan Kunszt, examiner
PD Dr. Ansgar Denner, co-examiner
Prof. Jürg Fröhlich, co-examiner

1999

Contents

Abstract

At present, the W boson is investigated experimentally at LEP2 via its pair production. In order to achieve precise theoretical predictions for the measurement of the W-boson mass and the non-abelian triple-gauge-boson couplings, the inclusion of radiative corrections is required. Since the W bosons decay very rapidly into light fermion pairs, the actual processes under investigation are $e^+e^- \to 4$ fermions.

The full $\mathcal{O}(\alpha)$ corrections to these processes are not available at present. Since the main contributions originate from diagrams with two resonant W-boson propagators, an expansion of the amplitude around the poles of the two resonant W bosons is a reasonable approach, which is also gauge-invariant. In the double-pole approximation, the contributions are classified in factorizable and non-factorizable corrections. The amplitudes of the factorizable corrections are composed of those for the on-shell W-pair production and the on-shell W-decays multiplied by the two propagators of the resonant W bosons. All other corrections are called non-factorizable, because they do not factorize into a simple product of W-pair production and W decays.

As a first step of this work, the non-factorizable corrections of the processes $e^+e^- \to 4$ fermions are calculated in double-pole approximation. The non-factorizable corrections are implemented into an existing Monte Carlo program and various distributions are studied. It turns out that the non-factorizable corrections are negligible with respect to the experimental accuracy of LEP2; however, they should become relevant for a future linear collider with higher luminosity.

A further building block of the radiative corrections to four-fermion production are the bremsstrahlung processes $e^+e^- \to 4$ fermions$+\gamma$. These processes are of physics interest in their own right. For instance, the radiative processes can be used to obtain information on the quartic-gauge-boson couplings $\gamma\gamma WW$, γZWW, and $\gamma\gamma ZZ$, which are part of the tree-level amplitude. The tree-level helicity amplitudes for the processes $e^+e^- \to 4$ fermions and $e^+e^- \to 4$ fermions$+\gamma$ for all possible final-state fermions are calculated. A multi-channel Monte Carlo program for both classes of processes is constructed. This is a particularly difficult task owing to the very complex peaking structure of the differential cross section.

In order to include radiative corrections into the Monte Carlo program, the infrared and collinear singularities must be extracted from the bremsstrahlung process. This is done by applying the dipole-subtraction method to four-fermion production. This subtraction method has already been worked out in massless QCD for dimensional regularization. In the Electroweak Standard Model it is more convenient to regularize the amplitude with an infinitesimal photon mass and small fermion masses. Hence, the subtraction method is reformulated for mass regularization.

Finally, the doubly-resonant virtual corrections are implemented into the Monte Carlo program for the processes $e^+e^- \to 4\,\text{fermions}(+\gamma)$. Therefore, the results of the non-factorizable corrections and the already existing results of the on-shell W-pair production and on-shell W-decay are used. For the real corrections the complete bremsstrahlung process $e^+e^- \to 4\,\text{fermions} + \gamma$ is taken into account. All results are combined in a four-fermion generator, which is the first Monte Carlo generator including the complete $\mathcal{O}(\alpha)$ corrections to the processes $e^+e^- \to W^+W^- \to 4\,\text{fermions}$ in double-pole approximation. This generator is used to produce numerical results for the total cross section, angular, and invariant-mass distributions.

Zusammenfassung

Am Beschleuniger LEP2 wird zur Zeit die W-Paar-Produktion experimentell untersucht. Um genaue theoretische Vorhersagen für die Bestimmung der W-Boson-Masse und die Untersuchung der Drei-Eichboson-Kopplungen zu erhalten, müssen Strahlungskorrekturen berücksichtigt werden. Weil die W-Bosonen sehr schnell in je zwei leichte Fermionen zerfallen, werden in Wirklichkeit die Prozesse $e^+e^- \to 4\,$Fermionen untersucht.

Die vollständigen Strahlungskorrekturen in $\mathcal{O}(\alpha)$ sind zu diesen Prozessen noch nicht bekannt. Der Hauptbeitrag stammt von Diagrammen mit zwei resonanten W-Boson-Propagatoren. Deshalb besteht ein naheliegender und auch eichinvarianter Ansatz darin, die Amplitude um die Pole der beiden W-Bosonen zu entwickeln. In dieser Doppelpolnäherung können die Strahlungskorrekturen in faktorisierbare und nicht-faktorisierbare Korrekturen klassifiziert werden. Die Amplitude der faktorisierbaren Korrekturen setzt sich aus den Amplituden der W-Paar-Produktion, den beiden Amplituden der W-Boson-Zerfälle und den zwei Propagatoren der resonanten W-Bosonen zusammen. Alle übrigen Korrekturen werden mit nicht-faktorisierbar bezeichnet, weil sie nicht aus einem einfachen Produkt von Beiträgen zur Produktion und zu den Zerfällen geschrieben werden können.

In einem ersten Schritt wurden in der vorliegenden Arbeit die nicht-faktorisierbaren Korrekturen zu den Prozessen $e^+e^- \to 4\,$Fermionen in Doppelpolnäherung berechnet. Sie wurden in ein existierendes Monte-Carlo-Programm eingebaut, und verschiedene Verteilungen wurden studiert. Dabei zeigte sich, dass diese Korrekturen vernachlässigbar gegenüber dem experimentellen Fehler von LEP2 sind. Jedoch werden sie für einen zukünftigen Linearbeschleuniger mit höherer Luminosität voraussichtlich wichtig.

Ein weiterer notwendiger Bestandteil der Strahlungskorrekturen zur Vier-Fermion-Produktion sind die Bremsstrahlungsprozesse $e^+e^- \to 4\,$Fermionen$\,+\,\gamma$. Mit diesen Prozessen können auch die Vier-Eichboson-Kopplungen $\gamma\gamma WW$, γZWW und $\gamma\gamma ZZ$ studiert werden, die auf Born-Niveau enthalten sind. Die Helizitäts-Amplituden zu den Prozessen $e^+e^- \to 4\,$Fermionen und $e^+e^- \to 4\,$Fermionen$+\gamma$ für alle Endzustände wurden berechnet, und ein Monte-Carlo-Programm für beide Klassen von Prozessen geschrieben. Die Schwierigkeit lag dabei in dem sehr komplexen und stark variierenden Verhalten des differentiellen Wirkungsquerschnittes.

Um Strahlungskorrekturen mit Hilfe eines Monte-Carlo-Programms zu berechnen, müssen die infraroten und kollinearen Singularitäten vom Bremsstrahlungsprozess abgespalten werden. Dazu wurde die Dipol-Subtraktionsmethode auf die Vier-Fermion-Produktion angewandt. Diese Subtraktionsmethode existierte in der Literatur für masselose QCD und dimensionale Regularisierung. Für das Elektroschwache Standardmodell werden normalerweise die Singularitäten mit einer infinitesimalen Photonmasse und kleinen Fermion-

massen regularisiert. Daher wurde die Subtraktionsmethode für die Massenregularisierung umgeschrieben.

Alle doppeltresonanten virtuellen Korrekturen wurden in das vorher erwähnte Monte-Carlo-Programm für die Prozesse $e^+e^- \rightarrow 4\,\text{Fermionen}(+\gamma)$ eingebaut. Dazu wurden die nicht-faktorisierbaren Korrekturen und die schon existierenden Ergebnisse für die W-Paar-Produktion und W-Zerfälle verwendet. Für die reellen Korrekturen wurde der komplette Bremsstrahlungsprozess $e^+e^- \rightarrow 4\,\text{Fermionen}+\gamma$ berücksichtigt. Dieses Programm ist der erste Monte-Carlo-Generator, der alle Strahlungskorrekturen in $\mathcal{O}(\alpha)$ zur Vier-Fermion-Produktion in Doppelpolnäherung beinhaltet. Mit ihm wurden numerische Ergebnisse für den totalen Wirkungsquerschnitt, Winkelverteilungen und invariante-Massen-Verteilungen erzeugt.

Chapter 1

Introduction

The Glashow–Salam–Weinberg model [1], known as the Electroweak Standard Model (SM), is very successful in describing electroweak phenomena. Since the SM is a spontaneously broken gauge theory, it is renormalizable [2] and hence observables can be, in principle, calculated to any finite order in perturbation theory.

An important feature of the SM lies in the appearance of elementary gauge-boson-self-interactions resulting from the non-abelian structure of the gauge group. The γWW and ZWW vertices can be studied in detail at the e^+e^- collider LEP2 [3]. Beside the investigation of the triple-gauge-boson-couplings, LEP2 also allows for a precise determination of the W-boson mass. Two methods are used [4, 5]: the measurement of the total cross section near threshold and the reconstruction method, where the Breit-Wigner resonance shape is reconstructed from the decay products of the W bosons.

LEP2 is operating above the W-pair production threshold and produces about 10^4 W pairs. Hence, the typical experimental accuracy is of the order of one to a few per cent. The accuracy of the W-boson mass measurement is expected to be $\lesssim 50\,\text{MeV}$ at LEP2 [4] and about $15\,\text{MeV}$ for a future linear collider [6]. This experimental accuracy should be matched or better exceeded by the precision of the theoretical predictions. Since W bosons decay very rapidly into light fermions, the actual reaction under investigation is $e^+e^- \to W^+W^- \to 4\,\text{fermions}$.
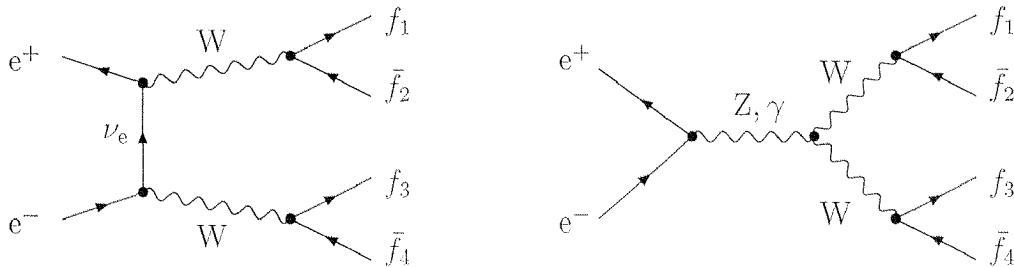

Figure 1.1: Diagrams with two resonant W-boson propagators contributing to $e^+e^- \to 4f$

In the LEP2 energy region, the lowest-order cross section is dominated by the diagrams that involve two resonant W bosons, as shown in Fig. 1.1. All other lowest-order diagrams are typically suppressed by a factor $\Gamma_W/M_W \approx 2.5\%$, but may be enhanced in certain phase-space regions. Since all these contributions are required at the one-per-cent level, the complete lowest-order matrix element has to be taken into account.

Furthermore, the implementation of the finite width of unstable particles, such as the W bosons, has to be done properly. A finite width is necessary in the phase-space region where the unstable particle becomes resonant, i.e. nearly on shell, otherwise the cross section has a non-integrable unphysical singularity. The finite width is naturally introduced via Dyson summation, where the width arises from the imaginary parts of the resummed self-energy diagrams:

$$\frac{1}{k^2 - M_0^2} \sum_{n=0}^{\infty} \left[\frac{-\Sigma_V(k^2)}{k^2 - M_0^2} \right]^n = \frac{1}{k^2 - M_0^2 + \Sigma_V(k^2)}, \qquad (1.0.1)$$

where M_0 symbolizes the bare mass of the unstable particle, and Σ_V denotes the one-particle-irreducible self-energy.

However, since only a part of higher-order corrections are included in this way, the whole result is gauge-dependent, and wrong results can be obtained in certain phase-space regions [7, 8, 9, 10]. The reason is that Ward identities are violated and, hence, gauge breaking terms can be amplified in the presence of small scales, or unitarity cancellations do not take place properly. Ward identities are, in particular, crucial for processes with nearly on-shell virtual photons or for the production of longitudinal polarized gauge bosons at high energies.

For the calculation of the tree-level processes $e^+e^- \to 4f$ and $e^+e^- \to 4f\gamma$, three schemes for the implementation of the finite W-boson width are compared in Chapter 2: the constant-width scheme, where the imaginary part of the self-energy is replaced by a constant, the running-width scheme with the naive running $\Gamma(k^2) = \Gamma_V \theta(k^2) k^2/M_V^2$, and the complex-mass scheme, where the boson masses are replaced by complex masses in all couplings and propagators and, in particular, in the definition of the weak mixing angle. In general, the first two schemes violate Ward identities [9, 10], while the third scheme fulfils all Ward identities.

A gauge-invariant approach for the introduction of the finite width is the *pole expansion* [11, 12] outlined in the following. The complete matrix element for a process, with an unstable particle in the intermediate state, can be written as

$$\mathcal{M} = \frac{r}{k^2 - M^2} + n, \qquad (1.0.2)$$

where the residue is denoted by r, and the mass of the unstable particle by M. The symbol n summarizes all terms that are regular at $k^2 = M^2$. Both the location of the complex pole, which corresponds to the mass of the unstable particle, and the residue are gauge-invariant quantities. For stable particles the mass lies on the real axis, for unstable particles in the complex plane.

In perturbation theory, the complex mass M is determined by the location of the pole after Dyson summation (1.0.1):

$$M^2 = M_0^2 - \Sigma_V(M^2) = M_V^2 - iM_V\Gamma_V, \qquad (1.0.3)$$

where Γ_V and M_V denote the finite width and the real mass of the unstable particle, respectively. After expanding the self-energy about M^2, the inverse propagator reads

$$k^2 - M_0^2 + \Sigma_V(k^2) = [1 + \Sigma_V'(M^2)](k^2 - M^2) + \mathcal{O}\left((k^2 - M^2)^2\right),$$

and the matrix element can be rewritten in the form [12]:

$$\mathcal{M} = \frac{R(k^2,\theta)}{k^2 - M_0^2 + \Sigma_V(k^2)} + N(k^2,\theta) = \frac{R(M^2,\theta)}{[1 + \Sigma_V'(M^2)](k^2 - M^2)}$$
$$+ \left[\frac{R(k^2,\theta)}{k^2 - M_0^2 + \Sigma_V(k^2)} - \frac{R(M^2,\theta)}{[1 + \Sigma_V'(M^2)](k^2 - M^2)}\right] + N(k^2,\theta), \quad (1.0.4)$$

where N includes the non-resonant diagrams, and θ summarizes all kinematic variables, except for the invariant mass k^2 of the unstable particle. Since the complete amplitude is gauge-invariant, the single terms of the Laurent expansion about the squares of the complex mass are also gauge-invariant. The first term on the right-hand side of (1.0.4) corresponds to the leading term in a Laurent expansion about $k^2 = M^2$, and dominates the cross section in the resonance region. The remaining terms are finite in the limit $k^2 \to M^2$. Therefore, a reasonable and gauge-invariant approximation is to neglect the non-leading terms and to keep only the resonant term. This simplifies the calculation considerably, since all obviously non-resonant diagrams can be left out from the calculation from the beginning.

In Chapter 3 and 4, the pole scheme is applied to the radiative corrections of four-fermion production. Radiative corrections are, in general, required in the theoretical predictions for four-fermion production, in order to match the accuracy of LEP2 of about one per cent. The full $\mathcal{O}(\alpha)$ calculation involves 10^3-10^4 diagrams and is, therefore, extremely complicated. Since the non-doubly-resonant radiative corrections are of the order of $\alpha \Gamma_W \ln(\dots)/(\pi M_W) \approx 0.1\%$, the restriction to the doubly-resonant corrections is a reasonable approach.

After the introduction of the finite W-boson width, the matrix element reads

$$\mathcal{M} = \frac{R_{+-}(k_+^2, k_-^2, \theta)}{(k_+^2 - M^2)(k_-^2 - M^2)} + \frac{R_+(k_+^2, k_-^2, \theta)}{k_+^2 - M^2} + \frac{R_-(k_+^2, k_-^2, \theta)}{k_-^2 - M^2} + N(k_+^2, k_-^2, \theta), \quad (1.0.5)$$

where $k_\pm$ are the momenta of the resonant virtual $W^\pm$ bosons and the factor $[1 + \Sigma_V'(M^2)]$ is already included in the definition of R_{+-}, R_+, and R_-[1]. In double-pole approximation, the matrix element is expanded about the squares of the W-boson masses and all non-doubly-resonant terms are neglected:

$$\mathcal{M}^{\mathrm{DPA}} = \frac{R_{+-}(M^2, M^2, \theta)}{(k_+^2 - M^2)(k_-^2 - M^2)}. \quad (1.0.6)$$

The double-pole approximation simplifies the calculation considerably, since only diagrams with two resonant W-boson propagators have to be calculated. Furthermore, a

---

[1]We use the the on-shell renormalization scheme of Ref. [13], where $\mathrm{Re}\{\Sigma_V'(M_V^2)\} = 0$. In this renormalization scheme, the deviation of the self-energy at the complex pole $\Sigma_V'(M^2)$ yields only $\mathcal{O}(\alpha^2)$ corrections. Hence, the factor $[1 + \Sigma_V'(M^2)]$ is neglected in the following chapters.

large part of the doubly-resonant radiative corrections are included in the factorizable corrections. The factorizable corrections are composed of the on-shell W-pair production, the two resonant W-boson propagators, and the two on-shell W-boson decays. The remaining radiative corrections are called non-factorizable and are explicitly calculated and discussed in Chapter 3.

The double-pole approximation is a good approximation if the doubly-resonant contributions dominate the cross section. If these are suppressed, as close to the W-pair production threshold, the other contributions become important. This is also true if non-doubly-resonant terms are enhanced, as e.g. by nearly on-shell photons. These terms can be suppressed by applying appropriate cuts on the phase space.

Note that the pole expansion only works if the on-shell limit exists. Since the non-factorizable corrections, given in Section 3.3, involve on-shell-divergent terms, like $\ln(k_{\pm}^2 - M^2)$, the pole expansion of these corrections has not such a simple form as in (1.0.6). Thus, the non-factorizing corrections are calculated for off-shell W bosons, while the limit $k_{\pm}^2 \to M^2$ is performed whenever possible.

With the results of Chapter 2 and 3, a Monte Carlo generator is constructed in Chapter 4 that includes all doubly-resonant $\mathcal{O}(\alpha)$ radiative corrections to four-fermion production. More precise, this generator includes the complete tree-level matrix element, the virtual corrections in double-pole approximation, and the complete bremsstrahlung process. The cancellation of the soft and collinear singularities is achieved within the subtraction method as discussed in Section 4.2. Although the real non-factorizable corrections are calculated in Chapter 3 in double-pole approximation, the complete bremsstrahlung process is taken into account in Chapter 4. In this way, the problem of overlapping resonances is avoided (see Section 4.1.3). The Monte Carlo program of Chapter 4 is the first generator that includes the complete $\mathcal{O}(\alpha)$ corrections to the processes $e^+e^- \to W^+W^- \to 4$ fermions in double-pole approximation.

Chapter 2

Tree-level processes $e^+e^- \to 4f(+\gamma)$

While the most important process at LEP2 for the studies of the gauge sector in the Electroweak Standard Model is certainly $e^+e^- \to W^+W^- \to 4f$, many other reactions have now become accessible. Besides the 4-fermion-production processes, including single W-boson production, single Z-boson production, or Z-boson-pair production, LEP2 and especially a future linear collider allow us to investigate another class of processes, namely $e^+e^- \to 4f\gamma$.

The physical interest in the processes $e^+e^- \to 4f\gamma$ is twofold. First of all, they are an important building block for the radiative corrections to $e^+e^- \to 4f$, and their effect must be taken into account in order to get precise predictions for the observables that are used for the measurement of the W-boson mass and the triple-gauge-boson couplings. On the other hand, those processes themselves involve interesting physics. They include, in particular, triple-gauge-boson-production processes such as $W^+W^-\gamma$, $ZZ\gamma$, or $Z\gamma\gamma$ production and can therefore be used to obtain information on the quartic gauge-boson couplings $\gamma\gamma WW$, γZWW, and $\gamma\gamma ZZ$. While only a few events of this kind are expected at LEP2, these studies can be performed in more detail at future linear e^+e^- colliders [14].

Some results for $e^+e^- \to 4f\gamma$ with an observable photon already exist in the literature. In Refs. [15, 16] the contributions to the matrix elements involving two resonant W bosons have been calculated and implemented into a Monte Carlo generator. This generator has been extended to include collinear bremsstrahlung [17] and used to discuss the effect of hard photons at LEP2 [18]. The complete cross section for the process $e^+e^- \to u\bar{d}e^-\bar{\nu}_e\gamma$ has been discussed in Ref. [19]. In Ref. [20], the complete matrix elements for the processes $e^+e^- \to 4f\gamma$ have been calculated using an iterative numerical algorithm without referring to Feynman diagrams. We are, however, interested in explicit analytical results on the amplitudes for various reasons. In particular, we want to have full control over the implementation of the finite width of the virtual vector bosons and to select single diagrams, such as the doubly-resonant ones. No results for $e^+e^- \to 4f\gamma$ with e^+e^- pairs in the final state have been published in the past. The results of this section are published in Ref. [21] and agree very well with the recent calculations of Ref. [22], where finite-mass effects due to nearly collinear photon emission are discussed for the process $e^+e^- \to u\bar{d}\mu^-\bar{\nu}_\mu\gamma$.

In order to perform the calculation as efficient as possible we have reduced all processes to a small number of generic contributions. For $e^+e^- \to 4f$, the calculation is similar to the one in Ref. [23], and the generic contributions correspond to individual Feynman

diagrams. In the case of $e^+e^- \to 4f\gamma$ we have combined groups of diagrams in such a way that the resulting generic contributions can be classified in the same way as those for $e^+e^- \to 4f$. As a consequence, the generic contributions are individually gauge-invariant with respect to the external photon. The number and the complexity of diagrams in the generic contributions for $e^+e^- \to 4f\gamma$ has been reduced by using a non-linear gauge-fixing condition for the W-boson field [24]. In this way, many cancellations between diagrams are avoided, without any further algebraic manipulations. Finally, for the helicity amplitudes corresponding to the generic contributions concise results have been obtained by using the Weyl–van der Waerden formalism (see Ref. [25] and references therein).

After the matrix elements have been calculated, the finite widths of the resonant particles have to be introduced. We have done this in different ways and compared the different treatments for $e^+e^- \to 4f$ and $e^+e^- \to 4f\gamma$. In particular, we have discussed a "complex-mass scheme", which preserves all Ward identities and is still rather simple to apply.

The matrix elements to $e^+e^- \to 4f$ and $e^+e^- \to 4f\gamma$ exhibit a complex peaking behaviour owing to propagators of massless particles and Breit–Wigner resonances, so that the integration over the 8- and 11-dimensional phase spaces, respectively, is not straightforward. In order to obtain numerically stable results, we adopt the multi-channel integration method [23, 26] and reduce the Monte Carlo error by the adaptive weight optimization procedure described in Ref. [27]. In the multi-channel approach, we define a suitable mapping of random numbers into phase-space variables for each arising propagator structure. These variables are generated according to distributions that approximate this specific peaking behaviour of the integrand. For $e^+e^- \to 4f$ and $e^+e^- \to 4f\gamma$ we identify up to 128 and 928 channels, respectively, which necessitates an efficient and generic procedure for the phase-space generation.

2.1 Analytical results

2.1.1 Notation and conventions

We consider reactions of the types

$$e^+(p_+, \sigma_+) + e^-(p_-, \sigma_-) \to f_1(k_1, \sigma_1) + \bar{f}_2(k_2, \sigma_2) + f_3(k_3, \sigma_3) + \bar{f}_4(k_4, \sigma_4), \qquad (2.1.1)$$

$$e^+(p_+, \sigma_+) + e^-(p_-, \sigma_-) \to f_1(k_1, \sigma_1) + \bar{f}_2(k_2, \sigma_2) + f_3(k_3, \sigma_3) + \bar{f}_4(k_4, \sigma_4) + \gamma(k_5, \lambda). \qquad (2.1.2)$$

The arguments label the momenta $p_\pm$, k_i and helicities $\sigma_i = \pm 1/2$, $\lambda = \pm 1$ of the corresponding particles. We often use only the signs to denote the helicities. The fermion masses are neglected everywhere.

For the Feynman rules we use the conventions of Ref. [13, 28]. In particular, all fields and momenta are incoming. It is convenient to use a non-linear gauge-fixing term [24] of the form

$$\mathcal{L}_{\text{fix}} = -\left| \partial^\mu W_\mu^+ + ie(A^\mu - \frac{c_{\text{W}}}{s_{\text{W}}} Z^\mu) W_\mu^+ - iM_{\text{W}}\phi^+ \right|^2$$
$$- \frac{1}{2}(\partial^\mu Z_\mu - M_{\text{Z}}\chi)^2 - \frac{1}{2}(\partial^\mu A_\mu)^2, \qquad (2.1.3)$$

where $\phi^\pm$ and χ are the would-be Goldstone bosons of the $W^\pm$ and Z fields, respectively. With this choice, the $\phi^\pm W^\mp A$ vertices vanish, and the bosonic couplings that are relevant for $e^+e^- \to 4f\gamma$ read

$$= -ieg_{VWW}\left[g_{\nu\rho}(k_- - k_+)_\mu - 2g_{\mu\nu}k_{V,\rho} + 2g_{\mu\rho}k_{V,\nu}\right],$$

$$= -2ieg_{VWW}\,g_{\mu\nu}g_{\rho\sigma}, \tag{2.1.4}$$

with $V = A, Z$, and the coupling factors

$$g_{AWW} = 1, \qquad g_{ZWW} = -\frac{c_{\mathrm{W}}}{s_{\mathrm{W}}}. \tag{2.1.5}$$

Note that the gauge-boson propagators have the same simple form as in the 't Hooft–Feynman gauge, i.e. they are proportional to the metric tensor $g_{\mu\nu}$. This gauge choice eliminates some diagrams and simplifies others owing to the simpler structure of the photon–gauge-boson couplings.

The vector-boson–fermion–fermion couplings have the usual form

$$= ie\gamma_\mu \sum_\sigma g^\sigma_{V\bar{f}_i f_j}\omega_\sigma, \tag{2.1.6}$$

where $\omega_\pm = (1 \pm \gamma_5)/2$. The corresponding coupling factors read

$$g^\sigma_{A\bar{f}_i f_i} = -Q_i, \qquad g^\sigma_{Z\bar{f}_i f_i} = -\frac{s_{\mathrm{W}}}{c_{\mathrm{W}}}Q_i + \frac{I^3_{\mathrm{w},i}}{c_{\mathrm{W}}s_{\mathrm{W}}}\delta_{\sigma-}, \qquad g^\sigma_{W\bar{f}_i f'_i} = \frac{1}{\sqrt{2}s_{\mathrm{W}}}\delta_{\sigma-}, \tag{2.1.7}$$

where Q_i and $I^3_{\mathrm{w},i} = \pm 1/2$ denote the relative charge and the weak isospin of the fermion f_i, respectively, and f'_i is the weak-isospin partner of f_i. The colour factor of a fermion f_i is denoted by $N^c_{f_i}$, i.e. $N^c_{\mathrm{lepton}} = 1$ and $N^c_{\mathrm{quark}} = 3$.

2.1.2 Classification of final states for $e^+e^- \to 4f$

The final states for $e^+e^- \to 4f$ have already been classified in Refs. [29, 23, 30]. We introduce a classification that is very close to the one of Refs. [29, 30]. It is based on

the production mechanism, i.e. whether the reactions proceed via charged-current (CC), or neutral-current (NC) interactions, or via both interaction types. The classification can be performed by considering the quantum numbers of the final-state fermion pairs. In the following, f and F denote different fermions ($f \neq F$) that are neither electrons nor electron neutrinos ($f, F \neq e^-, \nu_e$), and their weak-isospin partners are denoted by f' and F', respectively. We find the following 11 classes of processes (in parenthesis the corresponding classification of Ref. [30] is given):

(i) CC reactions:

   (a) $e^+e^- \to f\bar{f}'F\bar{F}'$,   (*CC11* family),

   (b) $e^+e^- \to \nu_e e^+ f\bar{f}'$,   (*CC20* family),

   (c) $e^+e^- \to f\bar{f}'e^-\bar{\nu}_e$,   (*CC20* family),

(ii) NC reactions:

   (a) $e^+e^- \to f\bar{f}F\bar{F}$,   (*NC32* family),

   (b) $e^+e^- \to f\bar{f}f\bar{f}$,   (*NC4·16* family),

   (c) $e^+e^- \to e^-e^+ f\bar{f}$,   (*NC48* family),

   (d) $e^+e^- \to e^-e^+e^-e^+$,   (*NC4·36* family),

(iii) Mixed CC/NC reactions:

   (a) $e^+e^- \to f\bar{f}f'\bar{f}'$,   (*mix43* family),

   (b) $e^+e^- \to \nu_e\bar{\nu}_e f\bar{f}$,   (*NC21* family),

   (c) $e^+e^- \to \nu_e\bar{\nu}_e\nu_e\bar{\nu}_e$,   (*NC4·9* family),

   (d) $e^+e^- \to \nu_e\bar{\nu}_e e^-e^+$,   (*mix56* family).

The radiation of an additional photon does not change this classification.

2.1.3   Generic diagrams and amplitudes for $e^+e^- \to 4f$

In order to explain and to illustrate our generic approach we first list the results for $e^+e^- \to 4f$. All these processes can be composed from only two generic diagrams, the abelian and non-abelian diagrams shown in Fig. 2.1. All external fermions $f_{a,...,f}$ are assumed to be incoming, and the momenta and helicities are denoted by $p_{a,...,f}$ and $\sigma_{a,...,f}$, respectively. The helicity amplitudes of these diagrams are calculated within the Weyl–van der Waerden (WvdW) formalism following the conventions of Ref. [25] (see also references therein).

Leptonic and semi-leptonic final states

We first treat purely leptonic and semi-leptonic final states. In this case, none of the gauge bosons in the generic graphs of Fig. 2.1 can be a gluon, and the colour structure trivially

8
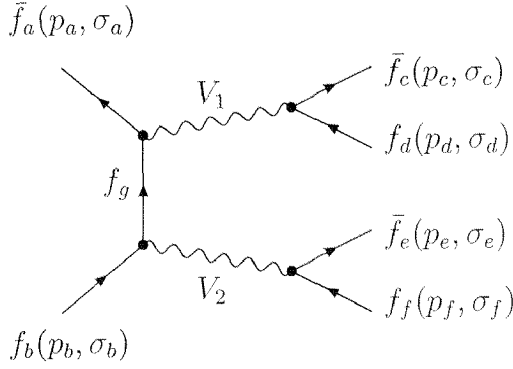
a) abelian graph   b) non-abelian graph
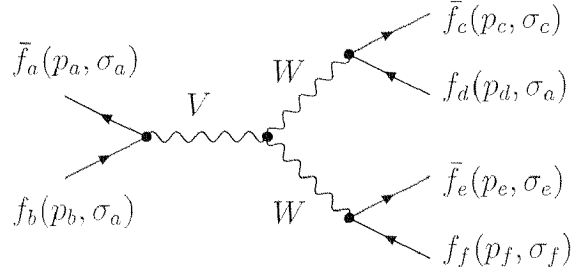
Figure 2.1: Generic diagrams for $e^+e^- \rightarrow 4f$

leads to a global factor $N^c_{f_1}N^c_{f_3}$, which is equal to 1 or 3, after summing the squared amplitude over the colour degrees of freedom. The results for the generic amplitudes are

$$
\mathcal{M}^{\sigma_a,\sigma_b,\sigma_c,\sigma_d,\sigma_e,\sigma_f}_{V_1V_2}(p_a,p_b,p_c,p_d,p_e,p_f)
$$
$$
= -4e^4 \delta_{\sigma_a,-\sigma_b}\delta_{\sigma_c,-\sigma_d}\delta_{\sigma_e,-\sigma_f}\, g^{\sigma_b}_{V_1\bar{f}_af_g}g^{\sigma_b}_{V_2\bar{f}_gf_b}g^{\sigma_d}_{V_1\bar{f}_cf_d}g^{\sigma_f}_{V_2\bar{f}_ef_f}
$$
$$
\times \frac{P_{V_1}(p_c+p_d)P_{V_2}(p_e+p_f)}{(p_b+p_e+p_f)^2}\, A^{\sigma_a,\sigma_c,\sigma_e}_2(p_a,p_b,p_c,p_d,p_e,p_f), \qquad (2.1.8)
$$

$$
\mathcal{M}^{\sigma_a,\sigma_b,\sigma_c,\sigma_d,\sigma_e,\sigma_f}_{VWW}(p_a,p_b,p_c,p_d,p_e,p_f)
$$
$$
= -4e^4 \delta_{\sigma_a,-\sigma_b}\delta_{\sigma_c,+}\delta_{\sigma_d,-}\delta_{\sigma_e,+}\delta_{\sigma_f,-}\,(Q_c-Q_d)g_{VWW}g^{\sigma_b}_{V\bar{f}_af_b}g^-_{W\bar{f}_cf_d}g^-_{W\bar{f}_ef_f}
$$
$$
\times P_V(p_a+p_b)P_W(p_c+p_d)P_W(p_e+p_f)\, A^{\sigma_a}_3(p_a,p_b,p_c,p_d,p_e,p_f), \qquad (2.1.9)
$$

where the vector-boson propagators are abbreviated by

$$
P_V(p) = \frac{1}{p^2-M^2_V}, \qquad V=A,Z,W,g, \qquad M_A=M_g=0. \qquad (2.1.10)
$$

(The case of the gluon is included for later convenience.) The auxiliary functions $A^{\sigma_a,\sigma_c,\sigma_e}_2$ and $A^{\sigma_a}_3$ are expressed in terms of WvdW spinor products,

$$
A^{+++}_2(p_a,p_b,p_c,p_d,p_e,p_f) = \langle p_ap_c\rangle\langle p_bp_f\rangle^*(\langle p_bp_d\rangle^*\langle p_bp_e\rangle + \langle p_dp_f\rangle^*\langle p_ep_f\rangle),
$$
$$
A^{++-}_2(p_a,p_b,p_c,p_d,p_e,p_f) = A^{+++}_2(p_a,p_b,p_c,p_d,p_f,p_e),
$$
$$
A^{+-+}_2(p_a,p_b,p_c,p_d,p_e,p_f) = A^{+++}_2(p_a,p_b,p_d,p_c,p_e,p_f),
$$
$$
A^{+--}_2(p_a,p_b,p_c,p_d,p_e,p_f) = A^{+++}_2(p_a,p_b,p_d,p_c,p_f,p_e),
$$
$$
A^{-,\sigma_c,\sigma_d}_2(p_a,p_b,p_c,p_d,p_e,p_f) = \left(A^{+,-\sigma_c,-\sigma_d}_2(p_a,p_b,p_c,p_d,p_e,p_f)\right)^*, \qquad (2.1.11)
$$

$$
A^+_3(p_a,p_b,p_c,p_d,p_e,p_f) = \langle p_bp_d\rangle^*\langle p_bp_f\rangle^*\langle p_ap_b\rangle\langle p_cp_e\rangle + \langle p_bp_d\rangle^*\langle p_dp_f\rangle^*\langle p_ap_e\rangle\langle p_cp_d\rangle
$$
$$
+ \langle p_bp_f\rangle^*\langle p_dp_f\rangle^*\langle p_ap_c\rangle\langle p_ep_f\rangle,
$$
$$
A^-_3(p_a,p_b,p_c,p_d,p_e,p_f) = A^+_3(p_b,p_a,p_c,p_d,p_e,p_f). \qquad (2.1.12)
$$

9

The spinor products are defined by

$$\langle pq\rangle = \epsilon^{AB} p_A q_B = 2\sqrt{p_0 q_0}\left[\mathrm{e}^{-\mathrm{i}\phi_p}\cos\frac{\theta_p}{2}\sin\frac{\theta_q}{2} - \mathrm{e}^{-\mathrm{i}\phi_q}\cos\frac{\theta_q}{2}\sin\frac{\theta_p}{2}\right], \qquad (2.1.13)$$

where p_A, q_A are the associated momentum spinors for the momenta

$$\begin{aligned}
p^\mu &= p_0(1,\sin\theta_p\cos\phi_p,\sin\theta_p\sin\phi_p,\cos\theta_p),\\
q^\mu &= p_0(1,\sin\theta_q\cos\phi_q,\sin\theta_q\sin\phi_q,\cos\theta_q).
\end{aligned} \qquad (2.1.14)$$

Incoming fermions are turned into outgoing ones by crossing, which is performed by inverting the corresponding fermion momenta and helicities. If the generic functions are called with negative momenta $-p$, $-q$, it is understood that only the complex conjugate spinor products get the corresponding sign change. We illustrate this by simple examples:

$$\begin{aligned}
A(p,q) &= \langle pq\rangle = A(p,-q) = A(-p,q) = A(-p,-q),\\
B(p,q) &= \langle pq\rangle^* = -B(p,-q) = -B(-p,q) = B(-p,-q).
\end{aligned} \qquad (2.1.15)$$

We have checked the results for the generic diagrams against those of Ref. [23] and found agreement.

Using the results for the generic diagrams of Fig. 2.1, the helicity amplitudes for all possible processes involving six external fermions can be built up. It is convenient to construct first the amplitudes for the process types CC(a) and NC(a) (see Section 2.1.2) in terms of the generic functions (2.1.8) and (2.1.9), because these amplitudes are the basic subamplitudes of the other channels. The full amplitude for each process type can be built up from those subamplitudes by appropriate substitutions and linear combinations.

We first list the helicity amplitudes for the CC processes:

$$\begin{aligned}
\mathcal{M}_{\mathrm{CCa}}^{\sigma_+,\sigma_-,\sigma_1,\sigma_2,\sigma_3,\sigma_4}&(p_+,p_-,k_1,k_2,k_3,k_4)\\
&= \mathcal{M}_{WW}^{\sigma_+,\sigma_-,-\sigma_1,-\sigma_2,-\sigma_3,-\sigma_4}(p_+,p_-,-k_1,-k_2,-k_3,-k_4)\\
&\quad + \sum_{V=\gamma,Z}\Big[\ \mathcal{M}_{VWW}^{\sigma_+,\sigma_-,-\sigma_1,-\sigma_2,-\sigma_3,-\sigma_4}(p_+,p_-,-k_1,-k_2,-k_3,-k_4)\\
&\qquad + \mathcal{M}_{VW}^{-\sigma_1,-\sigma_2,\sigma_+,\sigma_-,-\sigma_3,-\sigma_4}(-k_1,-k_2,p_+,p_-,-k_3,-k_4)\\
&\qquad + \mathcal{M}_{VW}^{-\sigma_3,-\sigma_4,\sigma_+,\sigma_-,-\sigma_1,-\sigma_2}(-k_3,-k_4,p_+,p_-,-k_1,-k_2)\\
&\qquad + \mathcal{M}_{WV}^{-\sigma_1,-\sigma_2,-\sigma_3,-\sigma_4,\sigma_+,\sigma_-}(-k_1,-k_2,-k_3,-k_4,p_+,p_-)\\
&\qquad + \mathcal{M}_{WV}^{-\sigma_3,-\sigma_4,-\sigma_1,-\sigma_2,\sigma_+,\sigma_-}(-k_3,-k_4,-k_1,-k_2,p_+,p_-)\Big], \qquad (2.1.16)
\end{aligned}$$

$$\begin{aligned}
\mathcal{M}_{\mathrm{CCb}}^{\sigma_+,\sigma_-,\sigma_1,\sigma_2,\sigma_3,\sigma_4}&(p_+,p_-,k_1,k_2,k_3,k_4)\\
&= \mathcal{M}_{\mathrm{CCa}}^{\sigma_+,\sigma_-,\sigma_1,\sigma_2,\sigma_3,\sigma_4}(p_+,p_-,k_1,k_2,k_3,k_4)\\
&\quad - \mathcal{M}_{\mathrm{CCa}}^{\sigma_+,-\sigma_2,\sigma_1,-\sigma_-,\sigma_3,\sigma_4}(p_+,-k_2,k_1,-p_-,k_3,k_4), \qquad (2.1.17)
\end{aligned}$$

$$\begin{aligned}
\mathcal{M}_{\mathrm{CCc}}^{\sigma_+,\sigma_-,\sigma_1,\sigma_2,\sigma_3,\sigma_4}&(p_+,p_-,k_1,k_2,k_3,k_4)\\
&= \mathcal{M}_{\mathrm{CCa}}^{\sigma_+,\sigma_-,\sigma_1,\sigma_2,\sigma_3,\sigma_4}(p_+,p_-,k_1,k_2,k_3,k_4)\\
&\quad - \mathcal{M}_{\mathrm{CCa}}^{-\sigma_3,\sigma_-,\sigma_1,\sigma_2,-\sigma_+,\sigma_4}(-k_3,p_-,k_1,k_2,-p_+,k_4). \qquad (2.1.18)
\end{aligned}$$

The ones for the NC processes are given by

$$\mathcal{M}_{\mathrm{NCa}}^{\sigma_+,\sigma_-,\sigma_1,\sigma_2,\sigma_3,\sigma_4}(p_+,p_-,k_1,k_2,k_3,k_4)$$
$$= \sum_{V_1,V_2=\gamma,Z}\Big[\ \mathcal{M}_{V_1V_2}^{\sigma_+,\sigma_-,-\sigma_1,-\sigma_2,-\sigma_3,-\sigma_4}(p_+,p_-,-k_1,-k_2,-k_3,-k_4)$$
$$+\ \mathcal{M}_{V_1V_2}^{\sigma_+,\sigma_-,-\sigma_3,-\sigma_4,-\sigma_1,-\sigma_2}(p_+,p_-,-k_3,-k_4,-k_1,-k_2)$$
$$+\ \mathcal{M}_{V_1V_2}^{-\sigma_1,-\sigma_2,\sigma_+,\sigma_-,-\sigma_3,-\sigma_4}(-k_1,-k_2,p_+,p_-,-k_3,-k_4)$$
$$+\ \mathcal{M}_{V_1V_2}^{-\sigma_3,-\sigma_4,\sigma_+,\sigma_-,-\sigma_1,-\sigma_2}(-k_3,-k_4,p_+,p_-,-k_1,-k_2)$$
$$+\ \mathcal{M}_{V_1V_2}^{-\sigma_1,-\sigma_2,-\sigma_3,-\sigma_4,\sigma_+,\sigma_-}(-k_1,-k_2,-k_3,-k_4,p_+,p_-)$$
$$+\ \mathcal{M}_{V_1V_2}^{-\sigma_3,-\sigma_4,-\sigma_1,-\sigma_2,\sigma_+,\sigma_-}(-k_3,-k_4,-k_1,-k_2,p_+,p_-)\Big], \qquad (2.1.19)$$

$$\mathcal{M}_{\mathrm{NCb}}^{\sigma_+,\sigma_-,\sigma_1,\sigma_2,\sigma_3,\sigma_4}(p_+,p_-,k_1,k_2,k_3,k_4)$$
$$=\ \mathcal{M}_{\mathrm{NCa}}^{\sigma_+,\sigma_-,\sigma_1,\sigma_2,\sigma_3,\sigma_4}(p_+,p_-,k_1,k_2,k_3,k_4)$$
$$-\ \mathcal{M}_{\mathrm{NCa}}^{\sigma_+,\sigma_-,\sigma_3,\sigma_2,\sigma_1,\sigma_4}(p_+,p_-,k_3,k_2,k_1,k_4), \qquad (2.1.20)$$

$$\mathcal{M}_{\mathrm{NCc}}^{\sigma_+,\sigma_-,\sigma_1,\sigma_2,\sigma_3,\sigma_4}(p_+,p_-,k_1,k_2,k_3,k_4)$$
$$=\ \mathcal{M}_{\mathrm{NCa}}^{\sigma_+,\sigma_-,\sigma_1,\sigma_2,\sigma_3,\sigma_4}(p_+,p_-,k_1,k_2,k_3,k_4)$$
$$-\ \mathcal{M}_{\mathrm{NCa}}^{-\sigma_1,\sigma_-,-\sigma_+,\sigma_2,\sigma_3,\sigma_4}(-k_1,p_-,-p_+,k_2,k_3,k_4), \qquad (2.1.21)$$

$$\mathcal{M}_{\mathrm{NCd}}^{\sigma_+,\sigma_-,\sigma_1,\sigma_2,\sigma_3,\sigma_4}(p_+,p_-,k_1,k_2,k_3,k_4)$$
$$=\ \mathcal{M}_{\mathrm{NCa}}^{\sigma_+,\sigma_-,\sigma_1,\sigma_2,\sigma_3,\sigma_4}(p_+,p_-,k_1,k_2,k_3,k_4)$$
$$-\ \mathcal{M}_{\mathrm{NCa}}^{\sigma_+,\sigma_-,\sigma_3,\sigma_2,\sigma_1,\sigma_4}(p_+,p_-,k_3,k_2,k_1,k_4)$$
$$-\ \mathcal{M}_{\mathrm{NCa}}^{-\sigma_1,\sigma_-,-\sigma_+,\sigma_2,\sigma_3,\sigma_4}(-k_1,p_-,-p_+,k_2,k_3,k_4)$$
$$-\ \mathcal{M}_{\mathrm{NCa}}^{-\sigma_3,\sigma_-,\sigma_1,\sigma_2,-\sigma_+,\sigma_4}(-k_3,p_-,k_1,k_2,-p_+,k_4)$$
$$+\ \mathcal{M}_{\mathrm{NCa}}^{-\sigma_1,\sigma_-,\sigma_3,\sigma_2,-\sigma_+,\sigma_4}(-k_1,p_-,k_3,k_2,-p_+,k_4)$$
$$+\ \mathcal{M}_{\mathrm{NCa}}^{-\sigma_3,\sigma_-,-\sigma_+,\sigma_2,\sigma_1,\sigma_4}(-k_3,p_-,-p_+,k_2,k_1,k_4). \qquad (2.1.22)$$

Finally, the helicity amplitudes for reactions of mixed CC/NC type read

$$\mathcal{M}_{\mathrm{CC/NCa}}^{\sigma_+,\sigma_-,\sigma_1,\sigma_2,\sigma_3,\sigma_4}(p_+,p_-,k_1,k_2,k_3,k_4)$$
$$=\ \mathcal{M}_{\mathrm{NCa}}^{\sigma_+,\sigma_-,\sigma_1,\sigma_2,\sigma_3,\sigma_4}(p_+,p_-,k_1,k_2,k_3,k_4)$$
$$-\ \mathcal{M}_{\mathrm{CCa}}^{\sigma_+,\sigma_-,\sigma_1,\sigma_4,\sigma_3,\sigma_2}(p_+,p_-,k_1,k_4,k_3,k_2), \qquad (2.1.23)$$

$$\mathcal{M}_{\mathrm{CC/NCb}}^{\sigma_+,\sigma_-,\sigma_1,\sigma_2,\sigma_3,\sigma_4}(p_+,p_-,k_1,k_2,k_3,k_4)$$
$$=\ \mathcal{M}_{\mathrm{NCa}}^{\sigma_+,\sigma_-,\sigma_1,\sigma_2,\sigma_3,\sigma_4}(p_+,p_-,k_1,k_2,k_3,k_4)$$
$$-\ \mathcal{M}_{\mathrm{CCa}}^{-\sigma_3,-\sigma_4,\sigma_1,-\sigma_-,-\sigma_+,\sigma_2}(-k_3,-k_4,k_1,-p_-,-p_+,k_2), \qquad (2.1.24)$$

$$\mathcal{M}_{\mathrm{CC/NCc}}^{\sigma_+,\sigma_-,\sigma_1,\sigma_2,\sigma_3,\sigma_4}(p_+,p_-,k_1,k_2,k_3,k_4)$$
$$=\ \mathcal{M}_{\mathrm{NCa}}^{\sigma_+,\sigma_-,\sigma_1,\sigma_2,\sigma_3,\sigma_4}(p_+,p_-,k_1,k_2,k_3,k_4)$$
$$-\ \mathcal{M}_{\mathrm{NCa}}^{\sigma_+,\sigma_-,\sigma_3,\sigma_2,\sigma_1,\sigma_4}(p_+,p_-,k_3,k_2,k_1,k_4)$$

$$- \mathcal{M}_{\mathrm{CCa}}^{-\sigma_1,-\sigma_2,-\sigma_+,\sigma_4,\sigma_3,-\sigma_-} \left(-k_1,-k_2,k_3,-p_-,-p_+,k_4\right)$$
$$+ \mathcal{M}_{\mathrm{CCa}}^{-\sigma_1,-\sigma_4,-\sigma_+,\sigma_2,\sigma_3,-\sigma_-} \left(-k_1,-k_4,k_3,-p_-,-p_+,k_2\right)$$
$$+ \mathcal{M}_{\mathrm{CCa}}^{-\sigma_3,-\sigma_2,-\sigma_+,\sigma_4,\sigma_1,-\sigma_-} \left(-k_3,-k_2,k_1,-p_-,-p_+,k_4\right)$$
$$- \mathcal{M}_{\mathrm{CCa}}^{-\sigma_3,-\sigma_4,-\sigma_+,\sigma_2,\sigma_1,-\sigma_-} \left(-k_3,-k_4,k_1,-p_-,-p_+,k_2\right), \tag{2.1.25}$$

$$\mathcal{M}_{\mathrm{CC/NCd}}^{\sigma_+,\sigma_-,\sigma_1,\sigma_2,\sigma_3,\sigma_4} \left(p_+,p_-,k_1,k_2,k_3,k_4\right)$$
$$= \quad \mathcal{M}_{\mathrm{NCa}}^{\sigma_+,\sigma_-,\sigma_1,\sigma_2,\sigma_3,\sigma_4} \left(p_+,p_-,k_1,k_2,k_3,k_4\right)$$
$$- \mathcal{M}_{\mathrm{NCa}}^{-\sigma_3,\sigma_-,\sigma_1,\sigma_2,-\sigma_+,\sigma_4} \left(-k_3,p_-,k_1,k_2,-p_+,k_4\right)$$
$$- \mathcal{M}_{\mathrm{CCa}}^{\sigma_+,\sigma_-,\sigma_1,\sigma_4,\sigma_3,\sigma_2} \left(p_+,p_-,k_1,k_4,k_3,k_2\right)$$
$$+ \mathcal{M}_{\mathrm{CCa}}^{\sigma_+,-\sigma_4,\sigma_1,-\sigma_-,\sigma_3,\sigma_2} \left(p_+,-k_4,k_1,-p_-,k_3,k_2\right)$$
$$+ \mathcal{M}_{\mathrm{CCa}}^{-\sigma_3,\sigma_-,\sigma_1,\sigma_4,-\sigma_+,\sigma_2} \left(-k_3,p_-,k_1,k_4,-p_+,k_2\right)$$
$$- \mathcal{M}_{\mathrm{CCa}}^{-\sigma_3,-\sigma_4,\sigma_1,-\sigma_-,-\sigma_+,\sigma_2} \left(-k_3,-k_4,k_1,-p_-,-p_+,k_2\right). \tag{2.1.26}$$

The relative signs between contributions of the basic subamplitudes $\mathcal{M}_{\mathrm{CCa}}$ and $\mathcal{M}_{\mathrm{NCa}}$ to the full matrix elements account for the sign changes resulting from interchanging external fermion lines.

For the CC reactions, the amplitudes $\mathcal{M}_{\mathrm{CCa}}$ are the smallest gauge-invariant subset of diagrams [31]. In the case of NC reactions, the amplitudes $\mathcal{M}_{\mathrm{NCa}}$ are composed of three separately gauge-invariant subamplitudes consisting of the first two lines, the two lines in the middle, and the last two lines of (2.1.19).

Hadronic final states

Next we inspect purely hadronic final states, i.e. the cases where all final-state fermions f_i are quarks. This concerns only the channels CC(a), NC(a), NC(b), and CC/NC(a) given in Section 2.1.2. The colour structure of the quarks leads to two kinds of modifications. Firstly, the summation of the squared amplitudes over the colour degrees of freedom can become non-trivial, and secondly, the possibility of virtual-gluon exchange between the quarks has to be taken into account. More precisely, there are diagrams of type (a) in Fig. 2.1 in which one of the gauge bosons $V_{1,2}$ is a gluon. The other gauge boson of $V_{1,2}$ can only be a photon or Z boson, since this boson has to couple to the incoming e^+e^- pair. Consequently, there is an impact of gluon-exchange diagrams only for the channels NC(a), NC(b), and CC/NC(a), but not for CC(a). This can be easily seen by inspecting the generic diagrams in Fig. 2.1: the presence of a gluon exchange requires two quark–antiquark pairs $q\bar{q}$ in the final state.

We first inspect the colour structure of the purely electroweak diagrams. Since the colour structure of each diagram contributing to the basic channels CC(a) and NC(a) is the same, the corresponding amplitudes factorize into a simple colour part and the "colour-singlet amplitudes" $\mathcal{M}_{\mathrm{CCa}}$ and $\mathcal{M}_{\mathrm{NCa}}$, given in (2.1.16) and (2.1.19), respectively. The amplitudes for NC(b) and CC/NC(a) are composed from the ones of CC(a) and NC(a) in a way that is analogous to the singlet case, but now the colour indices c_i of the quarks f_i have to be taken into account. Indicating the electroweak amplitudes for fully hadronic final states by "had,ew", and writing colour indices explicitly, we get

$$\mathcal{M}_{\mathrm{CCa,had,ew},c_1,c_2,c_3,c_4}^{\sigma_+,\sigma_-,\sigma_1,\sigma_2,\sigma_3,\sigma_4} \left(p_+,p_-,k_1,k_2,k_3,k_4\right)$$

$$= \mathcal{M}_{\text{CCa}}^{\sigma_+,\sigma_-,\sigma_1,\sigma_2,\sigma_3,\sigma_4}(p_+,p_-,k_1,k_2,k_3,k_4)\,\delta_{c_1c_2}\delta_{c_3c_4}, \quad (2.1.27)$$

$$\mathcal{M}_{\text{NCa,had,ew},c_1,c_2,c_3,c_4}^{\sigma_+,\sigma_-,\sigma_1,\sigma_2,\sigma_3,\sigma_4}(p_+,p_-,k_1,k_2,k_3,k_4)$$
$$= \mathcal{M}_{\text{NCa}}^{\sigma_+,\sigma_-,\sigma_1,\sigma_2,\sigma_3,\sigma_4}(p_+,p_-,k_1,k_2,k_3,k_4)\,\delta_{c_1c_2}\delta_{c_3c_4}, \quad (2.1.28)$$

$$\mathcal{M}_{\text{NCb,had,ew},c_1,c_2,c_3,c_4}^{\sigma_+,\sigma_-,\sigma_1,\sigma_2,\sigma_3,\sigma_4}(p_+,p_-,k_1,k_2,k_3,k_4)$$
$$= \mathcal{M}_{\text{NCa}}^{\sigma_+,\sigma_-,\sigma_1,\sigma_2,\sigma_3,\sigma_4}(p_+,p_-,k_1,k_2,k_3,k_4)\,\delta_{c_1c_2}\delta_{c_3c_4}$$
$$- \mathcal{M}_{\text{NCa}}^{\sigma_+,\sigma_-,\sigma_3,\sigma_2,\sigma_1,\sigma_4}(p_+,p_-,k_3,k_2,k_1,k_4)\,\delta_{c_3c_2}\delta_{c_1c_4}, \quad (2.1.29)$$

$$\mathcal{M}_{\text{CC/NCa,had,ew},c_1,c_2,c_3,c_4}^{\sigma_+,\sigma_-,\sigma_1,\sigma_2,\sigma_3,\sigma_4}(p_+,p_-,k_1,k_2,k_3,k_4)$$
$$= \mathcal{M}_{\text{NCa}}^{\sigma_+,\sigma_-,\sigma_1,\sigma_2,\sigma_3,\sigma_4}(p_+,p_-,k_1,k_2,k_3,k_4)\,\delta_{c_1c_2}\delta_{c_3c_4}$$
$$- \mathcal{M}_{\text{CCa}}^{\sigma_+,\sigma_-,\sigma_1,\sigma_4,\sigma_3,\sigma_2}(p_+,p_-,k_1,k_4,k_3,k_2)\,\delta_{c_1c_4}\delta_{c_3c_2}. \quad (2.1.30)$$

In the calculation of the gluon-exchange diagrams we can also make use of the "colour-singlet" result (2.1.8) for the generic diagram (a) of Fig. 2.1, after splitting off the colour structure appropriately. Since each of these diagrams involves exactly one internal gluon, exchanged by the two quark lines, the corresponding matrix elements can be deduced in a simple way from the diagrams in which the gluon is replaced by a photon. The gluon-exchange contributions to the channels NC(b) and CC/NC(a) can again be composed from the ones for NC(a). Making use of the auxiliary function

$$\mathcal{M}_{\text{g}}^{\sigma_+,\sigma_-,\sigma_1,\sigma_2,\sigma_3,\sigma_4}(p_+,p_-,k_1,k_2,k_3,k_4)$$
$$= \frac{g_{\text{s}}^2}{Q_1 Q_3 e^2}\sum_{V=\gamma,Z}\Big[\ \mathcal{M}_{V\gamma}^{-\sigma_1,-\sigma_2,\sigma_+,\sigma_-,-\sigma_3,-\sigma_4}(-k_1,-k_2,p_+,p_-,-k_3,-k_4)$$
$$+ \mathcal{M}_{V\gamma}^{-\sigma_3,-\sigma_4,\sigma_+,\sigma_-,-\sigma_1,-\sigma_2}(-k_3,-k_4,p_+,p_-,-k_1,-k_2)$$
$$+ \mathcal{M}_{\gamma V}^{-\sigma_1,-\sigma_2,-\sigma_3,-\sigma_4,\sigma_+,\sigma_-}(-k_1,-k_2,-k_3,-k_4,p_+,p_-)$$
$$+ \mathcal{M}_{\gamma V}^{-\sigma_3,-\sigma_4,-\sigma_1,-\sigma_2,\sigma_+,\sigma_-}(-k_3,-k_4,-k_1,-k_2,p_+,p_-)\Big], \quad (2.1.31)$$

where $g_{\text{s}} = \sqrt{4\pi\alpha_{\text{s}}}$ is the strong gauge coupling, the matrix elements involving gluon exchange explicitly read

$$\mathcal{M}_{\text{NCa,had,gluon},c_1,c_2,c_3,c_4}^{\sigma_+,\sigma_-,\sigma_1,\sigma_2,\sigma_3,\sigma_4}(p_+,p_-,k_1,k_2,k_3,k_4)$$
$$= \mathcal{M}_{\text{g}}^{\sigma_+,\sigma_-,\sigma_1,\sigma_2,\sigma_3,\sigma_4}(p_+,p_-,k_1,k_2,k_3,k_4)\,\tfrac{1}{4}\lambda_{c_1c_2}^a\lambda_{c_3c_4}^a, \quad (2.1.32)$$

$$\mathcal{M}_{\text{NCb,had,gluon},c_1,c_2,c_3,c_4}^{\sigma_+,\sigma_-,\sigma_1,\sigma_2,\sigma_3,\sigma_4}(p_+,p_-,k_1,k_2,k_3,k_4)$$
$$= \mathcal{M}_{\text{g}}^{\sigma_+,\sigma_-,\sigma_1,\sigma_2,\sigma_3,\sigma_4}(p_+,p_-,k_1,k_2,k_3,k_4)\,\tfrac{1}{4}\lambda_{c_1c_2}^a\lambda_{c_3c_4}^a$$
$$- \mathcal{M}_{\text{g}}^{\sigma_+,\sigma_-,\sigma_3,\sigma_2,\sigma_1,\sigma_4}(p_+,p_-,k_3,k_2,k_1,k_4)\,\tfrac{1}{4}\lambda_{c_3c_2}^a\lambda_{c_1c_4}^a, \quad (2.1.33)$$

$$\mathcal{M}_{\text{CC/NCa,had,gluon},c_1,c_2,c_3,c_4}^{\sigma_+,\sigma_-,\sigma_1,\sigma_2,\sigma_3,\sigma_4}(p_+,p_-,k_1,k_2,k_3,k_4)$$
$$= \mathcal{M}_{\text{g}}^{\sigma_+,\sigma_-,\sigma_1,\sigma_2,\sigma_3,\sigma_4}(p_+,p_-,k_1,k_2,k_3,k_4)\,\tfrac{1}{4}\lambda_{c_1c_2}^a\lambda_{c_3c_4}^a. \quad (2.1.34)$$

The colour structure is easily evaluated by making use of the completeness relation $\lambda_{ij}^a\lambda_{kl}^a = -\tfrac{2}{3}\delta_{ij}\delta_{kl} + 2\delta_{il}\delta_{jk}$ for the Gell-Mann matrices λ_{ij}^a.

The complete matrix elements for the fully hadronic channels result from the sum of the purely electroweak and the gluon-exchange contributions,

$$\mathcal{M}^{\sigma+,\sigma-,\sigma_1,\sigma_2,\sigma_3,\sigma_4}_{\ldots,\mathrm{had},c_1,c_2,c_3,c_4} = \mathcal{M}^{\sigma+,\sigma-,\sigma_1,\sigma_2,\sigma_3,\sigma_4}_{\ldots,\mathrm{had,ew},c_1,c_2,c_3,c_4} + \mathcal{M}^{\sigma+,\sigma-,\sigma_1,\sigma_2,\sigma_3,\sigma_4}_{\ldots,\mathrm{had,gluon},c_1,c_2,c_3,c_4}. \tag{2.1.35}$$

The gluon-exchange contributions are separately gauge-invariant.

For clarity, we explicitly write down the colour-summed squared matrix elements for the fully hadronic channels. Abbreviating $\mathcal{M}^{\sigma+,\sigma-,\sigma_a,\sigma_b,\sigma_c,\sigma_d}_{\ldots}(p_+,p_-,k_a,k_b,k_c,k_d)$ by $\mathcal{M}_{\ldots}(a,b,c,d)$ we obtain

$$\sum_{\mathrm{colour}} |\mathcal{M}_{\mathrm{CCa,had}}(1,2,3,4)|^2 = 9|\mathcal{M}_{\mathrm{CCa}}(1,2,3,4)|^2, \tag{2.1.36}$$

$$\sum_{\mathrm{colour}} |\mathcal{M}_{\mathrm{NCa,had}}(1,2,3,4)|^2 = 9|\mathcal{M}_{\mathrm{NCa}}(1,2,3,4)|^2 + 2|\mathcal{M}_{\mathrm{g}}(1,2,3,4)|^2, \tag{2.1.37}$$

$$\sum_{\mathrm{colour}} |\mathcal{M}_{\mathrm{NCb,had}}(1,2,3,4)|^2$$
$$= 9|\mathcal{M}_{\mathrm{NCa}}(1,2,3,4)|^2 + 9|\mathcal{M}_{\mathrm{NCa}}(3,2,1,4)|^2 - 6\,\mathrm{Re}\left\{\mathcal{M}_{\mathrm{NCa}}(1,2,3,4)\mathcal{M}^*_{\mathrm{NCa}}(3,2,1,4)\right\}$$
$$+ 2|\mathcal{M}_{\mathrm{g}}(1,2,3,4)|^2 + 2|\mathcal{M}_{\mathrm{g}}(3,2,1,4)|^2 + \tfrac{4}{3}\,\mathrm{Re}\left\{\mathcal{M}_{\mathrm{g}}(1,2,3,4)\mathcal{M}^*_{\mathrm{g}}(3,2,1,4)\right\}$$
$$- 8\,\mathrm{Re}\left\{\mathcal{M}_{\mathrm{NCa}}(1,2,3,4)\mathcal{M}^*_{\mathrm{g}}(3,2,1,4)\right\} - 8\,\mathrm{Re}\left\{\mathcal{M}_{\mathrm{NCa}}(3,2,1,4)\mathcal{M}^*_{\mathrm{g}}(1,2,3,4)\right\}, \tag{2.1.38}$$

$$\sum_{\mathrm{colour}} |\mathcal{M}_{\mathrm{CC/NCa,had}}(1,2,3,4)|^2$$
$$= 9|\mathcal{M}_{\mathrm{NCa}}(1,2,3,4)|^2 + 9|\mathcal{M}_{\mathrm{CCa}}(1,4,3,2)|^2 - 6\,\mathrm{Re}\left\{\mathcal{M}_{\mathrm{NCa}}(1,2,3,4)\mathcal{M}^*_{\mathrm{CCa}}(1,4,3,2)\right\}$$
$$+ 2|\mathcal{M}_{\mathrm{g}}(1,2,3,4)|^2 - 8\,\mathrm{Re}\left\{\mathcal{M}_{\mathrm{CCa}}(1,4,3,2)\mathcal{M}^*_{\mathrm{g}}(1,2,3,4)\right\}. \tag{2.1.39}$$

Owing to the colour structure of the diagrams, a non-zero interference between purely electroweak and gluon-exchange contributions is only possible if the four final-state fermions can be combined into one single closed fermion line in the squared diagram. This implies that fermion pairs must couple to different resonances in the electroweak and the gluon-exchange diagrams, leading to a global suppression of such interference effects in the phase-space integration (see Section 2.3.5).

2.1.4 Generic functions and amplitudes for $\mathrm{e^+e^-} \to 4f + \gamma$

The generic functions for $\mathrm{e^+e^-} \to 4f\gamma$ can be constructed in a similar way. The idea is to combine the contributions of all those graphs to one generic function that reduce to the same graph after removing the radiated photon. These combined contributions to $\mathrm{e^+e^-} \to 4f\gamma$ are classified in the same way as the diagrams for the corresponding process $\mathrm{e^+e^-} \to 4f$, i.e. the graphs of Fig. 2.1 also represent the generic functions for $\mathrm{e^+e^-} \to 4f\gamma$. Finally, all amplitudes for $\mathrm{e^+e^-} \to 4f\gamma$ can again be constructed from only two generic functions. Note that the number of individual Feynman diagrams ranges between 14 and 1008 for the various processes. We note that the generic functions can in fact be used to

construct the amplitudes for all processes involving exactly six external fermions and one external photon, such as $e^-e^- \to 4f\gamma$ and $e^\pm\gamma \to 5f$.

As a virtue of this approach, the so-defined generic functions fulfill the QED Ward identity for the external photon, i.e. replacing the photon polarization vector by the photon momentum yields zero for each generic function. This is simply a consequence of electromagnetic charge conservation. Consequently, in the actual calculation in the WvdW formalism the gauge spinor of the photon drops out in each contribution separately.

Assuming the external fermions as incoming and the photon as outgoing, the generic functions read

$$
\mathcal{M}_{V_1 V_2}^{\sigma_a,\sigma_b,\sigma_c,\sigma_d,\sigma_e,\sigma_f,\lambda}(Q_a,Q_b,Q_c,Q_d,Q_e,Q_f,p_a,p_b,p_c,p_d,p_e,p_f,k)
$$
$$
= -4\sqrt{2}e^5 \delta_{\sigma_a,-\sigma_b}\delta_{\sigma_c,-\sigma_d}\delta_{\sigma_e,-\sigma_f}\, g_{V_1 \bar{f}_a f_g}^{\sigma_b} g_{V_2 \bar{f}_g f_b}^{\sigma_b} g_{V_1 \bar{f}_c f_d}^{\sigma_d} g_{V_2 \bar{f}_e f_f}^{\sigma_f}
$$
$$
\times\, A_2^{\sigma_a,\sigma_c,\sigma_e,\lambda}(Q_a,Q_b,Q_c,Q_d,Q_e,Q_f,p_a,p_b,p_c,p_d,p_e,p_f,k), \tag{2.1.40}
$$

$$
\mathcal{M}_{VWW}^{\sigma_a,\sigma_b,\sigma_c,\sigma_d,\sigma_e,\sigma_f,\lambda}(Q_a,Q_b,Q_c,Q_d,Q_e,Q_f,p_a,p_b,p_c,p_d,p_e,p_f,k)
$$
$$
= -4\sqrt{2}e^5 \delta_{\sigma_a,-\sigma_b}\delta_{\sigma_c,+}\delta_{\sigma_d,-}\delta_{\sigma_e,+}\delta_{\sigma_f,-}\,(Q_c-Q_d)g_{VWW}\, g_{V\bar{f}_a f_b}^{\sigma_b} g_{W\bar{f}_c f_d}^{-} g_{W\bar{f}_e f_f}^{-}
$$
$$
\times\, A_3^{\sigma_a,\lambda}(Q_a,Q_b,Q_c,Q_d,Q_e,Q_f,p_a,p_b,p_c,p_d,p_e,p_f,k), \tag{2.1.41}
$$

with the auxiliary functions

$$
A_2^{++++}(Q_a,Q_b,Q_c,Q_d,Q_e,Q_f,p_a,p_b,p_c,p_d,p_e,p_f,k) = -\langle p_a p_c\rangle\Bigg\{
$$
$$
P_{V_1}(p_c+p_d)P_{V_2}(p_e+p_f)
$$
$$
\times\Bigg[\frac{\langle p_b p_f\rangle^*}{\langle p_a k\rangle}\Bigg(\frac{Q_c-Q_d}{(p_b+p_e+p_f)^2}\frac{\langle p_a p_c\rangle}{\langle p_c k\rangle}(\langle p_b p_d\rangle^*\langle p_b p_e\rangle+\langle p_d p_f\rangle^*\langle p_e p_f\rangle)
$$
$$
+\frac{Q_f-Q_e}{(p_a+p_c+p_d)^2}\frac{\langle p_a p_e\rangle}{\langle p_e k\rangle}(\langle p_a p_d\rangle^*\langle p_a p_e\rangle+\langle p_c p_d\rangle^*\langle p_c p_e\rangle)\Bigg)
$$
$$
+\frac{Q_b(\langle p_a p_d\rangle^*\langle p_a p_e\rangle+\langle p_c p_d\rangle^*\langle p_c p_e\rangle)(\langle p_b p_f\rangle^*\langle p_a p_b\rangle-\langle p_f k\rangle^*\langle p_a k\rangle)}{(p_a+p_c+p_d)^2\langle p_a k\rangle\langle p_b k\rangle}
$$
$$
+\frac{(Q_a+Q_c-Q_d)\langle p_b p_f\rangle^*\langle p_c p_d\rangle^*\langle p_a p_c\rangle(\langle p_b k\rangle^*\langle p_b p_e\rangle-\langle p_f k\rangle^*\langle p_e p_f\rangle)}{(p_a+p_c+p_d)^2(p_b+p_e+p_f)^2\langle p_a k\rangle}\Bigg]
$$
$$
-\frac{Q_d-(Q_c-Q_d)2(p_d\cdot k)P_{V_1}(p_c+p_d)}{(p_b+p_e+p_f)^2}P_{V_1}(p_c+p_d-k)P_{V_2}(p_e+p_f)\langle p_b p_f\rangle^*
$$
$$
\times\frac{\langle p_c p_d\rangle(\langle p_b p_d\rangle^*\langle p_b p_e\rangle+\langle p_d p_f\rangle^*\langle p_e p_f\rangle)+\langle p_c k\rangle(\langle p_b k\rangle^*\langle p_b p_e\rangle-\langle p_f k\rangle^*\langle p_e p_f\rangle)}{\langle p_c k\rangle\langle p_d k\rangle}
$$
$$
+\frac{Q_f-(Q_e-Q_f)2(p_f\cdot k)P_{V_2}(p_e+p_f)}{(p_a+p_c+p_d)^2}P_{V_1}(p_c+p_d)P_{V_2}(p_e+p_f-k)
$$
$$
\times\frac{(\langle p_b p_f\rangle^*\langle p_e p_f\rangle+\langle p_b k\rangle^*\langle p_e k\rangle)(\langle p_a p_d\rangle^*\langle p_a p_e\rangle+\langle p_c p_d\rangle^*\langle p_c p_e\rangle)}{\langle p_e k\rangle\langle p_f k\rangle}\Bigg\},
$$

$$
A_2^{++-+}(Q_a,Q_b,Q_c,Q_d,Q_e,Q_f,p_a,p_b,p_c,p_d,p_e,p_f,k)
$$
$$
= A_2^{++++}(Q_a,Q_b,Q_c,Q_d,-Q_f,-Q_e,p_a,p_b,p_c,p_d,p_f,p_e,k),
$$

$$A_2^{+-++}(Q_a, Q_b, Q_c, Q_d, Q_e, Q_f, p_a, p_b, p_c, p_d, p_e, p_f, k)$$
$$= A_2^{++++}(Q_a, Q_b, -Q_d, -Q_c, Q_e, Q_f, p_a, p_b, p_d, p_c, p_e, p_f, k),$$
$$A_2^{+--+}(Q_a, Q_b, Q_c, Q_d, Q_e, Q_f, p_a, p_b, p_c, p_d, p_e, p_f, k)$$
$$= A_2^{++++}(Q_a, Q_b, -Q_d, -Q_c, -Q_f, -Q_e, p_a, p_b, p_d, p_c, p_f, p_e, k),$$
$$A_2^{-+++}(Q_a, Q_b, Q_c, Q_d, Q_e, Q_f, p_a, p_b, p_c, p_d, p_e, p_f, k)$$
$$= A_2^{++++}(Q_b, Q_a, -Q_e, -Q_f, -Q_c, -Q_d, p_b, p_a, p_e, p_f, p_c, p_d, k),$$
$$A_2^{-+-+}(Q_a, Q_b, Q_c, Q_d, Q_e, Q_f, p_a, p_b, p_c, p_d, p_e, p_f, k)$$
$$= A_2^{++++}(Q_b, Q_a, Q_f, Q_e, -Q_c, -Q_d, p_b, p_a, p_f, p_e, p_c, p_d, k),$$
$$A_2^{--++}(Q_a, Q_b, Q_c, Q_d, Q_e, Q_f, p_a, p_b, p_c, p_d, p_e, p_f, k)$$
$$= A_2^{++++}(Q_b, Q_a, -Q_e, -Q_f, Q_d, Q_c, p_b, p_a, p_e, p_f, p_d, p_c, k),$$
$$A_2^{---+}(Q_a, Q_b, Q_c, Q_d, Q_e, Q_f, p_a, p_b, p_c, p_d, p_e, p_f, k)$$
$$= A_2^{++++}(Q_b, Q_a, Q_f, Q_e, Q_d, Q_c, p_b, p_a, p_f, p_e, p_d, p_c, k),$$
$$A_2^{\sigma_a, \sigma_c, \sigma_d, -}(Q_a, Q_b, Q_c, Q_d, Q_e, Q_f, p_a, p_b, p_c, p_d, p_e, p_f, k)$$
$$= \left(A_2^{-\sigma_a, -\sigma_c, -\sigma_d, +}(Q_a, Q_b, Q_c, Q_d, Q_e, Q_f, p_a, p_b, p_c, p_d, p_e, p_f, k) \right)^* \Big|_{P_{V_{1,2}}(p) \to P_{V_{1,2}}^*(p)}, \tag{2.1.42}$$

and

$$A_3^{++}(Q_a, Q_b, Q_c, Q_d, Q_e, Q_f, p_a, p_b, p_c, p_d, p_e, p_f, k)$$
$$= P_V(p_a + p_b) P_W(p_c + p_d) P_W(p_e + p_f) \frac{(Q_c - Q_d)\langle p_c p_e \rangle}{\langle p_c k \rangle \langle p_e k \rangle}$$
$$\times (\quad \langle p_b p_d \rangle^* \langle p_b p_f \rangle^* \langle p_a p_b \rangle \langle p_c p_e \rangle + \langle p_b p_d \rangle^* \langle p_d p_f \rangle^* \langle p_a p_e \rangle \langle p_c p_d \rangle$$
$$+ \langle p_b p_f \rangle^* \langle p_d p_f \rangle^* \langle p_a p_c \rangle \langle p_e p_f \rangle)$$
$$+ P_V(p_a + p_b - k) P_W(p_c + p_d) P_W(p_e + p_f) \frac{Q_b}{\langle p_a k \rangle \langle p_b k \rangle}$$
$$\times \{ \quad \langle p_d p_f \rangle^* [\quad \langle p_a p_e \rangle \langle p_c p_d \rangle (\langle p_b p_d \rangle^* \langle p_a p_b \rangle - \langle p_d k \rangle^* \langle p_a k \rangle)$$
$$+ \langle p_a p_c \rangle \langle p_e p_f \rangle (\langle p_b p_f \rangle^* \langle p_a p_b \rangle - \langle p_f k \rangle^* \langle p_a k \rangle)]$$
$$+ \langle p_c p_e \rangle (\langle p_b p_d \rangle^* \langle p_a p_b \rangle - \langle p_d k \rangle^* \langle p_a k \rangle)(\langle p_b p_f \rangle^* \langle p_a p_b \rangle - \langle p_f k \rangle^* \langle p_a k \rangle)\}$$
$$+ P_V(p_a + p_b) P_W(p_c + p_d - k) P_W(p_e + p_f) \frac{Q_d - (Q_c - Q_d)2(p_d \cdot k) P_W(p_c + p_d)}{\langle p_c k \rangle \langle p_d k \rangle}$$
$$\times \{ \quad \langle p_b p_f \rangle^* [\quad \langle p_a p_c \rangle \langle p_e p_f \rangle (\langle p_d p_f \rangle^* \langle p_c p_d \rangle - \langle p_f k \rangle^* \langle p_c k \rangle)$$
$$+ \langle p_c p_e \rangle \langle p_a p_b \rangle (\langle p_b p_d \rangle^* \langle p_c p_d \rangle + \langle p_b k \rangle^* \langle p_c k \rangle)]$$
$$+ \langle p_a p_e \rangle (\langle p_d p_f \rangle^* \langle p_c p_d \rangle - \langle p_f k \rangle^* \langle p_c k \rangle)(\langle p_b p_d \rangle^* \langle p_c p_d \rangle + \langle p_b k \rangle^* \langle p_c k \rangle)\}$$
$$+ P_V(p_a + p_b) P_W(p_c + p_d) P_W(p_e + p_f - k) \frac{Q_f + (Q_f - Q_e)2(p_f \cdot k) P_W(p_e + p_f)}{\langle p_e k \rangle \langle p_f k \rangle}$$
$$\times \{ \quad \langle p_b p_d \rangle^* [\quad \langle p_c p_e \rangle \langle p_a p_b \rangle (\langle p_b p_f \rangle^* \langle p_e p_f \rangle + \langle p_b k \rangle^* \langle p_e k \rangle)$$
$$+ \langle p_a p_e \rangle \langle p_c p_d \rangle (\langle p_d p_f \rangle^* \langle p_e p_f \rangle + \langle p_d k \rangle^* \langle p_e k \rangle)]$$
$$+ \langle p_a p_c \rangle (\langle p_b p_f \rangle^* \langle p_e p_f \rangle + \langle p_b k \rangle^* \langle p_e k \rangle)(\langle p_d p_f \rangle^* \langle p_e p_f \rangle + \langle p_d k \rangle^* \langle p_e k \rangle)\},$$
$$A_3^{-+}(Q_a, Q_b, Q_c, Q_d, Q_e, Q_f, p_a, p_b, p_c, p_d, p_e, p_f, k)$$
$$= A_3^{++}(-Q_b, -Q_a, Q_c, Q_d, Q_e, Q_f, p_b, p_a, p_c, p_d, p_e, p_f, k),$$

$$A_3^{\sigma_a,-}(Q_a, Q_b, Q_c, Q_d, Q_e, Q_f, p_a, p_b, p_c, p_d, p_e, p_f, k) \tag{2.1.43}$$

$$= \left(A_3^{-\sigma_a,+}(Q_a, Q_b, -Q_d, -Q_c, -Q_f, -Q_e, p_a, p_b, p_d, p_c, p_f, p_e, k) \right)^* \Big|_{P_{V,W}(p) \to P_{V,W}^*(p)}.$$

The replacements $P_V \to P_V^*$ after the complex conjugation in the last lines of (2.1.43) and (2.1.44) ensure that the vector-boson propagators remain unaffected. Note that the vector-boson masses do not enter explicitly in the above results, but only via P_V. In gauges such as the 't Hooft–Feynman or the unitary gauge this feature is obtained only after combining different Feynman graphs for $e^+e^- \to 4f\gamma$; in the non-linear gauge (2.1.3) this is the case diagram by diagram.

The helicity amplitudes for $e^+e^- \to 4f\gamma$ follow from the generic functions $\mathcal{M}_{V_1 V_2}$ and $\mathcal{M}_{VWW}$ of (2.1.41) in exactly the same way as described in Section 2.1.3 for $e^+e^- \to 4f$. This holds also for the gluon-exchange matrix elements and for the colour factors. Moreover, the classification of gauge-invariant sets of diagrams for $e^+e^- \to 4f$ immediately yields such sets for $e^+e^- \to 4f\gamma$, if the additional photon is attached to all graphs of a set in all possible ways.

We have checked analytically that the electromagnetic Ward identity for the external photon is fulfilled for each generic contribution separately. In addition, we have numerically compared the amplitudes for all processes with amplitudes generated by *Madgraph* [32] for zero width of the vector bosons and found complete agreement. We could not compare our results with *Madgraph* for finite width, because *Madgraph* uses the unitary gauge for massive vector-boson propagators and the 't Hooft–Feynman gauge for the photon propagators, while we are using the non-linear gauge (2.1.3). Therefore, the matrix elements differ after introduction of finite vector-boson widths. While the calculation with *Madgraph* is fully automized, in our calculation we have full control over the matrix element and can, in particular, investigate various implementations of the finite width.

A comparison of our results with those of Refs. [15, 16], which include only the matrix elements that involve two resonant W bosons, immediately reveals the virtues of our generic approach.

2.1.5 Implementation of finite gauge-boson widths

We have implemented the finite widths of the W and Z bosons in different ways:

- *fixed width* in all propagators: $P_V(p) = [p^2 - M_V^2 + iM_V\Gamma_V]^{-1}$,

- *running width* in time-like propagators: $P_V(p) = [p^2 - M_V^2 + ip^2(\Gamma_V/M_V)\theta(p^2)]^{-1}$,

- *complex-mass scheme:* complex gauge-boson masses everywhere, i.e. $\sqrt{M_V^2 - iM_V\Gamma_V}$ instead of M_V in the propagators and in the couplings. This results, in particular, in a constant width in all propagators,

$$P_V(p) = [p^2 - M_V^2 + iM_V\Gamma_V]^{-1}, \tag{2.1.44}$$

and in a complex weak mixing angle:

$$c_W^2 = 1 - s_W^2 = \frac{M_W^2 - iM_W\Gamma_W}{M_Z^2 - iM_Z\Gamma_Z}. \tag{2.1.45}$$

The virtues and drawbacks of the first two schemes have been discussed in Ref. [10]. Both violate SU(2) gauge invariance, the running width also U(1) gauge invariance. The complex-mass scheme obeys all Ward identities and thus gives a consistent description of the finite-width effects in any tree-level calculation. While the complex-mass scheme works in general, it is particularly simple for $e^+e^- \to 4f\gamma$ in the non-linear gauge (2.1.3). In this case, no couplings involving explicit gauge-boson masses appear, and it is sufficient to introduce the finite gauge-boson widths in the propagators [cf. (2.1.44)] and to introduce the complex weak mixing angle (2.1.45) in the couplings. We note that a generalization of this scheme to higher orders requires to introduce complex mass counterterms in order to compensate for the complex masses in the propagators [33]. We did not consider the fermion-loop scheme [7, 9, 10, 34], which is also fully consistent for lowest-order predictions, since it requires the calculation of fermionic one-loop corrections to $e^+e^- \to 4f\gamma$ which is beyond the scope of this work.

2.2 The Monte Carlo program

The cross section for $e^+e^- \to 4f(\gamma)$ is given by

$$
d\sigma = \frac{(2\pi)^{4-3n}}{2s} \left[\prod_{i=1}^{n} d^4 k_i \, \delta\left(k_i^2\right) \theta(k_i^0) \right] \delta^{(4)}\left(p_+ + p_- - \sum_{i=1}^{n} k_i \right)
$$
$$
\times |\mathcal{M}(p_+, p_-, k_1, \ldots, k_n)|^2, \tag{2.2.1}
$$

where $n = 4, 5$ is the number of outgoing particles. The helicity amplitudes $\mathcal{M}$ for $e^+e^- \to 4f(\gamma)$ have been calculated in Sections 2.1.3 and 2.1.4. The phase-space integration is performed with the help of a Monte Carlo technique, since the Monte Carlo method allows us to calculate a variety of observables simultaneously and to easily implement cuts in order to account for the experimental situation.

The helicity amplitudes in (2.2.1) exhibit a complicated peaking behaviour in different regions of the integration domain. In order to obtain a numerically stable result and to reduce the Monte Carlo integration error we use a multi-channel Monte Carlo method [23, 26], which is briefly outlined in the following.

Before turning to the multi-channel method, we consider the treatment of a single channel. We choose a suitable set Φ of $3n - 4$ phase-space variables to describe a point in phase space, and determine the corresponding physical region V and the relation $k_i(\Phi)$ between the phase-space variables Φ and the momenta $k_1, \ldots, k_n$. The phase-space integration of (2.2.1) reads

$$
I_n = \int d\sigma = \int_V d\Phi \, \rho\left(k_i(\Phi)\right) f\left(k_i(\Phi)\right), \tag{2.2.2}
$$
$$
f\left(k_i(\Phi)\right) = \frac{(2\pi)^{4-3n}}{2s} |\mathcal{M}\left(p_+, p_-, k_1(\Phi), \ldots, k_n(\Phi)\right)|^2,
$$

where ρ is the phase-space density. For the random generation of the events, we further transform the integration variables Φ to $3n - 4$ new variables $\mathbf{r} = (r_i)$ with a hypercube as integration domain: $\Phi = \mathbf{h}(\mathbf{r})$ with $0 \leq r_i \leq 1$. We obtain

$$I_n = \int_V \mathrm{d}\Phi\, \rho\Big(k_i(\Phi)\Big)\, f\Big(k_i(\Phi)\Big) = \int_0^1 \mathrm{d}\mathbf{r}\, \frac{f\Big(k_i(\mathbf{h}(\mathbf{r}))\Big)}{g\Big(k_i(\mathbf{h}(\mathbf{r}))\Big)}\,, \qquad (2.2.3)$$

where g is the probability density of events generated in phase space, defined by

$$\frac{1}{g\Big(k_i(\Phi)\Big)} = \rho\Big(k_i(\Phi)\Big)\left|\frac{\partial \mathbf{h}(\mathbf{r})}{\partial \mathbf{r}}\right|_{\mathbf{r}=\mathbf{h}^{-1}(\Phi)}. \qquad (2.2.4)$$

If f varies strongly, the efficiency of the Monte Carlo method can be considerably enhanced by choosing the mapping of random numbers $\mathbf{r}$ to Φ in such a way that the resulting density g mimics the behaviour of $|f|$. For this *importance sampling*, the choice of Φ is guided by the peaking structure of f, which is determined by the propagators in a characteristic Feynman diagram.

We choose the variables Φ in such a way that the invariants corresponding to the propagators are included. Accordingly, we decompose the n-particle final state into $2 \rightarrow 2$ scattering processes with subsequent $1 \rightarrow 2$ decays. The variables Φ consist of Lorentz invariants s_i, t_i, defined as the squares of time- and space-like momenta, respectively, and of polar and azimuthal angles θ_i and ϕ_i, defined in appropriate frames. A detailed description of the parameterization of an n-particle phase space in terms of invariants and angles can be found in Appendix C. The parameterization of the invariants s_i and t_i in $\Phi = \mathbf{h}(\mathbf{r})$ is chosen in such a way that the propagator structure of the function f is compensated by a similar behaviour in the density g. More precisely, if f contains Breit–Wigner resonances or distributions like $s_i^{-\nu}$, which are relevant for massless propagators, appropriate parameterizations of s_i are given by:

- Breit–Wigner resonances:

$$s_i = M_V^2 + M_V \Gamma_V \tan[y_1 + (y_2 - y_1)r_i] \qquad (2.2.5)$$
$$\text{with } y_{1,2} = \arctan\left(\frac{s_{\text{min,max}} - M_V^2}{M_V \Gamma_V}\right);$$

- propagators of massless particles:

$$\nu \neq 1: \qquad s_i = \left[s_{\text{max}}^{1-\nu} r_i + s_{\text{min}}^{1-\nu}(1 - r_i)\right]^{1/(1-\nu)},$$
$$\nu = 1: \qquad s_i = \exp\left[\ln(s_{\text{max}})r_i + \ln(s_{\text{min}})(1 - r_i)\right]. \qquad (2.2.6)$$

For the choice of ν see Appendix C. The remaining variables in $\Phi = \mathbf{h}(\mathbf{r})$, i.e. those for which f is expected not to exhibit a peaking behaviour, are generated as follows:

$$s_i = s_{\text{max}}r_i + s_{\text{min}}(1 - r_i), \qquad \phi_i = 2\pi r_i, \qquad \cos\theta_i = 2r_i - 1. \qquad (2.2.7)$$

The absolute values of the invariants t_i are generated in the same way as s_i. The resulting density g of events in phase space is obtained as the product of the corresponding Jacobians, as given in (2.2.4). In the Appendix C, we provide explicit examples for the generation of events with a specific choice of mappings $k_i(\Phi)$ and $\mathbf{h}(\mathbf{r})$, and for the calculation of the corresponding density g.

The differential cross sections of the processes $e^+e^- \to 4f$ and especially $e^+e^- \to 4f\gamma$ possess very complex peaking structures so that the peaks in the integrand $f(\Phi)$ in (2.2.3) cannot be described properly by only one single density $g(\Phi)$. The *multi-channel approach* [23, 26] suggests a solution to this problem. For each peaking structure we choose a suitable set Φ_k, and accordingly a mapping of random numbers r_i into Φ_k: $\Phi_k = \mathbf{h}_k(\mathbf{r})$ with $0 \le r_i \le 1$, so that the resulting density g_k describes this particular peaking behaviour of f. All densities g_k are combined into one density g_{tot} that is expected to smoothes the integrand over the whole phase-space integration region. The phase-space integral of (2.2.3) reads

$$I_n = \sum_{k=1}^{M} \int_V \mathrm{d}\Phi_k\, \rho_k\Big(k_i(\Phi_k)\Big)\, g_k\Big(k_i(\Phi_k)\Big)\, \frac{f\Big(k_i(\Phi_k)\Big)}{g_{\text{tot}}\Big(k_i(\Phi_k)\Big)} = \sum_{k=1}^{M} \int_0^1 \mathrm{d}\mathbf{r}\, \frac{f\Big(k_i(\mathbf{h}_k(\mathbf{r}))\Big)}{g_{\text{tot}}\Big(k_i(\mathbf{h}_k(\mathbf{r}))\Big)}, \quad (2.2.8)$$

with

$$g_{\text{tot}}\Big(k_i(\Phi_k)\Big) = \sum_{l=1}^{M} g_l\Big(k_i(\Phi_k)\Big), \qquad \frac{1}{g_l\Big(k_i(\Phi_k)\Big)} = \rho_l\Big(k_i(\Phi_k)\Big) \left|\frac{\partial \mathbf{h}_l(\mathbf{r})}{\partial \mathbf{r}}\right|_{\mathbf{r}=\mathbf{h}_k^{-1}(\Phi_k)} \quad (2.2.9)$$

The different mappings $\mathbf{h}_k(\mathbf{r})$ are called channels, and M is the number of all channels.

In order to reduce the Monte Carlo error further, we adopt the method of weight optimization of Ref. [27] and introduce *a-priori weights* $\alpha_k, k = 1, \ldots, M$ ($\alpha_k \ge 0$ and $\sum_{k=1}^{M} \alpha_k = 1$). The channel k that is used to generate the event is picked randomly with probability α_k, i.e.

$$I_n = \sum_{k=1}^{M} \alpha_k \int_V \mathrm{d}\Phi_k\, \rho_k\Big(k_i(\Phi_k)\Big) g_k\Big(k_i(\Phi_k)\Big)\, \frac{f\Big(k_i(\Phi_k)\Big)}{g_{\text{tot}}\Big(k_i(\Phi_k)\Big)}$$

$$= \int_0^1 \mathrm{d}r_0 \sum_{k=1}^{M} \theta(r_0 - \beta_{k-1})\theta(\beta_k - r_0) \int_V \mathrm{d}\Phi_k\, \rho_k\Big(k_i(\Phi_k)\Big) g_k\Big(k_i(\Phi_k)\Big)\, \frac{f\Big(k_i(\Phi_k)\Big)}{g_{\text{tot}}\Big(k_i(\Phi_k)\Big)}$$

$$= \int_0^1 \mathrm{d}r_0 \sum_{k=1}^{M} \theta(r_0 - \beta_{k-1})\theta(\beta_k - r_0) \int_0^1 \mathrm{d}\mathbf{r}\, \frac{f\Big(k_i(\mathbf{h}_k(\mathbf{r}))\Big)}{g_{\text{tot}}\Big(k_i(\mathbf{h}_k(\mathbf{r}))\Big)}, \quad (2.2.10)$$

where $\beta_0 = 0, \beta_j = \sum_{k=1}^{j} \alpha_k, j = 1, \ldots, M-1$, $\beta_M = \sum_{k=1}^{M} \alpha_k = 1$, and

$$g_{\text{tot}}\Big(k_i(\Phi_k)\Big) = \sum_{l=1}^{M} \alpha_l g_l\Big(k_i(\Phi_k)\Big), \quad (2.2.11)$$

is the total density of the event.

For the processes $e^+e^- \to 4f$ we have between 6 and 128 different channels, for $e^+e^- \to 4f\gamma$ between 14 and 928 channels. Each channel smoothes a particular combination of

20

propagators that results from a characteristic Feynman diagram. We have written phase-space generators in a generic way for several classes of channels determined by the chosen set of invariants s_i, t_i. The channels within one class differ in the choice of the mappings (2.2.5), (2.2.6), and (2.2.7) and the order of the external particles. We did not include special channels for interference contributions.

The α_k-dependence of the quantity

$$W(\alpha) = \frac{1}{N} \sum_{j=1}^{N} [w(r_0^j, \mathbf{r}^j)]^2, \tag{2.2.12}$$

where $w = f/g_{\text{tot}}$ is the weight assigned to the Monte Carlo point $(r_0^j, \mathbf{r}^j)$ of the jth event, can be exploited to minimize the expected Monte Carlo error

$$\delta \bar{I}_n = \sqrt{\frac{W(\alpha) - \bar{I}_n^2}{N}}, \tag{2.2.13}$$

with the Monte Carlo estimate of I_n

$$\bar{I}_n = \frac{1}{N} \sum_{j=1}^{N} w(r_0^j, \mathbf{r}^j) \tag{2.2.14}$$

by trying to choose an optimal set of a-priori weights. We perform the search for an optimal set of α_k by using an *adaptive optimization* method, as described in Ref. [27]. After a certain number of generated events a new set of a-priori weights α_k^{new} is calculated according to

$$\alpha_k^{\text{new}} \propto \alpha_k \sqrt{\frac{1}{N} \sum_{j=1}^{N} \frac{g_k\left(k_i(\mathbf{h}_k(\mathbf{r}^j))\right) [w(r_0^j, \mathbf{r}^j)]^2}{g_{\text{tot}}\left(k_i(\mathbf{h}_k(\mathbf{r}^j))\right)}}, \qquad \sum_{k=1}^{M} \alpha_k^{\text{new}} = 1. \tag{2.2.15}$$

Based on the above approach, we have written two independent Monte Carlo programs. While the general strategy is similar, the programs differ in the explicit phase-space generation.

2.3 Numerical results

If not stated otherwise we use the complex-mass scheme and the following parameters:

$$\alpha = 1/128.89, \qquad \alpha_s = 0.12,$$
$$M_{\text{W}} = 80.26 \, \text{GeV}, \qquad \Gamma_{\text{W}} = 2.05 \, \text{GeV},$$
$$M_{\text{Z}} = 91.1884 \, \text{GeV}, \qquad \Gamma_{\text{Z}} = 2.46 \, \text{GeV}. \tag{2.3.1}$$

In the complex-mass scheme, the weak mixing angle is defined in (2.1.45), in all other schemes it is fixed by $c_{\text{W}} = M_{\text{W}}/M_{\text{Z}}, \; s_{\text{W}}^2 = 1 - c_{\text{W}}^2$.

The energy in the centre-of-mass (CM) system of the incoming electron and positron is denoted by $\sqrt{s}$. Concerning the phase-space integration, we apply the canonical cuts of the ADLO/TH detector,

$$\theta(l, \text{beam}) > 10°, \qquad \theta(l, l') > 5°, \qquad \theta(l, q) > 5°,$$

$$\theta(\gamma, \text{beam}) > 1°, \qquad \theta(\gamma, l) > 5°, \qquad \theta(\gamma, q) > 5°,$$

$$E_\gamma > 0.1\,\text{GeV}, \qquad E_l > 1\,\text{GeV}, \qquad E_q > 3\,\text{GeV},$$

$$m(q, q') > 5\,\text{GeV}, \tag{2.3.2}$$

where $\theta(i, j)$ specifies the angle between the particles i and j in the CM system, and l, q, γ, and "beam" denote charged leptons, quarks, photons, and the beam electrons or positrons, respectively. The invariant mass of a quark pair qq' is denoted by $m(q, q')$. The cuts coincide with those defined in Ref. [30], except for the additional angular cut between charged leptons. The canonical cuts exclude all collinear and infrared singularities from phase space for all processes.

Although our helicity amplitudes and Monte Carlo programs allow for a treatment of arbitrary polarization configurations, we consider only unpolarized quantities.

All results are produced with 10^7 events. The calculation of the cross section for $e^+e^- \to e^+e^-\mu^+\mu^-$ requires about 50 minutes on a DEC ALPHA workstation with 500 MHz, the calculation of the cross section for $e^+e^- \to e^+e^-\mu^+\mu^-\gamma$ takes about 5 hours. The numbers in parentheses in the following tables correspond to the statistical errors of the results of the Monte Carlo integrations.

2.3.1 Comparison with existing results

In order to compare our results for $e^+e^- \to 4f$ with Tables 6–8 of Ref. [35], we use the corresponding set of phase-space cuts and input parameters, i.e. the canonical cuts defined in (2.3.2), a CM energy of $\sqrt{s} = 190\,\text{GeV}$, and the parameters $\alpha = \alpha(2M_W) = 1/128.07$, $\alpha_s = 0.12$, $M_W = 80.23\,\text{GeV}$, $\Gamma_W = 2.0337\,\text{GeV}$, $M_Z = 91.1888\,\text{GeV}$, and $\Gamma_Z = 2.4974\,\text{GeV}$. The value of s_W, which enters the couplings, is calculated from $\alpha(2M_W)/(2s_W^2) = G_\mu M_W^2/(\pi\sqrt{2})$ with $G_\mu = 1.16639 \times 10^{-5}\,\text{GeV}^{-2}$.

In Table 2.1, we list the integrated cross sections for various processes $e^+e^- \to 4f$ with running widths and constant widths, and for the corresponding processes $e^+e^- \to 4f\gamma$ with constant widths. For processes involving gluon-exchange diagrams we give the cross sections resulting from the purely electroweak diagrams and those including the gluon-exchange contributions. The latter results include also the interference terms between purely electroweak and gluon-exchange diagrams. In Table 2.1 we provide a complete list of processes for vanishing fermion masses. All processes $e^+e^- \to 4f(\gamma)$ not explicitly listed are equivalent to one of the given processes.

For NC processes $e^+e^- \to 4f$ with four neutrinos or four quarks in the final state we find small deviations of roughly 0.2% between the results with constant and running widths. Assuming that a running width has been used in Ref. [35], we find very good agreement.

Unfortunately we cannot compare with most of the publications [17, 18, 19, 20] for the bremsstrahlung processes $e^+e^- \to 4f\gamma$. In those papers, either the cuts are not

$\sigma/$ fb	$e^+e^- \to 4f$ running width	$e^+e^- \to 4f$ constant width	$e^+e^- \to 4f\gamma$ constant width
$\nu_e\bar\nu_e e^- e^+$	256.7(3)	257.1(7)	89.4(2)
$\nu_\mu\mu^+ e^- \bar\nu_e$	227.4(1)	227.5(1)	79.1(1)
$\nu_\mu\bar\nu_\mu\mu^- \mu^+$	228.7(1)	228.8(1)	81.0(2)
$\nu_\mu\mu^+\tau^-\bar\nu_\tau$	218.55(9)	218.57(9)	76.7(1)
$e^- e^+ e^- e^+$	109.1(3)	109.4(3)	38.8(4)
$e^- e^+ \mu^- \mu^+$	116.6(3)	116.4(3)	43.4(4)
$\mu^- \mu^+ \mu^- \mu^+$	5.478(5)	5.478(5)	3.37(1)
$\mu^- \mu^+ \tau^- \tau^+$	11.02(1)	11.02(1)	6.78(3)
$e^- e^+ \nu_\mu\bar\nu_\mu$	14.174(9)	14.150(9)	5.36(1)
$\nu_e\bar\nu_e\mu^- \mu^+$	17.78(6)	17.73(6)	6.63(2)
$\nu_\tau\bar\nu_\tau\mu^- \mu^+$	10.108(8)	10.103(8)	4.259(9)
$\nu_e\bar\nu_e\nu_e\bar\nu_e$	4.089(1)	4.082(1)	0.7278(7)
$\nu_e\bar\nu_e\nu_\mu\bar\nu_\mu$	8.354(2)	8.337(2)	1.512(1)
$\nu_\mu\bar\nu_\mu\nu_\mu\bar\nu_\mu$	4.069(1)	4.057(1)	0.7434(7)
$\nu_\mu\bar\nu_\mu\nu_\tau\bar\nu_\tau$	8.241(2)	8.218(2)	1.511(1)
$u\bar d e^- \bar\nu_e$	693.5(3)	693.6(3)	220.8(4)
$u\bar d \mu^- \bar\nu_\mu$	666.7(3)	666.7(3)	214.5(4)
$e^- e^+ u\bar u$	86.87(9)	86.82(9)	32.3(2)
$e^- e^+ d\bar d$	43.02(4)	42.95(4)	16.17(8)
$u\bar u \mu^- \mu^+$	24.69(2)	24.69(2)	12.70(4)
$d\bar d \mu^- \mu^+$	23.73(1)	23.73(1)	10.43(2)
$\nu_e\bar\nu_e u\bar u$	24.00(2)	23.95(2)	6.84(1)
$\nu_e\bar\nu_e d\bar d$	20.657(8)	20.62(1)	4.319(6)
$u\bar u \nu_\mu\bar\nu_\mu$	21.080(5)	21.050(5)	6.018(9)
$d\bar d \nu_\mu\bar\nu_\mu$	19.863(5)	19.817(5)	4.156(5)
$u\bar u d\bar d$	2064.1(9), 2140.8(9)	2064.3(9), 2141(1)	615(1), 672(1)
$u\bar d s\bar c$	2015.2(8)	2015.3(8)	598(1)
$u\bar u u\bar u$	25.738(7), 71.28(4)	25.721(7), 71.30(4)	9.78(2), 42.1(1)
$d\bar d d\bar d$	23.494(6), 51.35(3)	23.448(6), 51.32(3)	5.527(7), 28.68(4)
$u\bar u c\bar c$	51.61(1), 144.72(9)	51.57(1), 144.75(9)	19.61(4), 86.1(2)
$u\bar u s\bar s$	49.68(1), 126.52(8)	49.62(1), 126.52(8)	15.17(2), 75.1(2)
$d\bar d s\bar s$	47.13(1), 104.79(6)	47.02(1), 104.74(6)	11.10(2), 59.2(1)

Table 2.1: Integrated cross sections for all representative processes $e^+e^- \to 4f$ with running widths and constant widths and for the corresponding processes $e^+e^- \to 4f\gamma$ with constant widths. If two numbers are given, the first results from pure electroweak diagrams and the second involves in addition gluon-exchange contributions.

σ/fb	$\theta_{\gamma,\min}, E_{\gamma,\min}$	1 GeV	5 GeV	10 GeV	15 GeV
leptonic process	1°	53.54(8)	27.57(3)	16.96(2)	11.22(2)
	5°	32.65(4)	16.98(3)	10.48(2)	6.94(1)
	10°	23.48(3)	12.30(2)	7.61(2)	5.04(1)
	15°	18.03(2)	9.51(2)	5.90(1)	3.90(1)
semi-leptonic process	1°	141.9(2)	71.90(8)	43.56(5)	28.26(4)
	5°	86.8(1)	44.25(6)	26.78(4)	17.40(3)
	10°	62.29(7)	31.92(5)	19.40(4)	12.61(3)
	15°	47.42(5)	24.50(4)	14.97(3)	9.77(2)

Table 2.2: Comparison with Table 2 of Ref. [15]: Cross sections resulting from diagrams involving two resonant W bosons for purely leptonic and semi-leptonic final states and several photon separation cuts

(completely) specified, or collinear photon emission is not excluded, and the corresponding fermion-mass effects are taken into account. Note that the contributions of collinear photons dominate the results given there.

We have compared our results with the ones given in Refs. [15, 16], where the total cross sections for $e^+e^- \to 4f\gamma$ have been calculated for purely leptonic and semi-leptonic final states. As done in Refs. [15, 16] only diagrams involving two resonant W bosons have been taken into account for this comparison. Table 2.2 contains our results corresponding to Table 2.2 of Ref. [15]. Based on Refs. [15, 16], we have chosen $\sqrt{s} = 200\,\text{GeV}$ and the input parameters $\alpha = 1/137.03599$, $M_W = 80.9\,\text{GeV}$, $\Gamma_W = 2.14\,\text{GeV}$, $M_Z = 91.16\,\text{GeV}$, $\Gamma_Z = 2.46\,\text{GeV}$, s_W obtained from $\alpha/(2s_W^2) = G_\mu M_W^2/(\pi\sqrt{2})$ with $G_\mu = 1.16637 \times 10^{-5}\,\text{GeV}^{-2}$, and constant gauge-boson widths. The energy of the photon is required to be larger than $E_{\gamma,\min}$, and the angle between the photon and any charged fermion must be larger than $\theta_{\gamma,\min}$. A maximal photon energy is required, $E_\gamma < 60\,\text{GeV}$, in order to exclude contributions from the Z resonance. Our results are consistent with those of Refs. [15, 16] within the statistical error of 1% given there. In some cases we find deviations of 2%.[1]

2.3.2 Comparison of finite-width schemes

As discussed in Refs. [7, 9, 10, 34], particular care has to be taken when implementing the finite gauge-boson widths. Differences between results obtained with running or constant widths can already be seen in Table 2.1, where a typical LEP2 energy is considered. In Table 2.3 we compare predictions for integrated cross sections obtained by using a constant width, a running width, or the complex-mass scheme for several energies. We consider

---

[1] Note that the input specified in Refs. [15, 16] is not completely clear even if the information of both publications is combined.

$\sigma\,/\,\mathrm{fb}$	$\sqrt{s}$	189 GeV	500 GeV	2 TeV	10 TeV
$e^+e^- \to u\,\bar{d}\,\mu^-\bar{\nu}_\mu$	constant width	703.5(3)	237.4(1)	13.99(2)	0.624(3)
	running width	703.4(3)	238.9(1)	34.39(3)	498.8(1)
	complex-mass scheme	703.1(3)	237.3(1)	13.98(2)	0.624(3)
$e^+e^- \to u\,\bar{d}\,\mu^-\bar{\nu}_\mu\,\gamma$	constant width	224.0(4)	83.4(3)	6.98(5)	0.457(6)
	running width	224.6(4)	84.2(3)	19.2(1)	368(6)
	complex-mass scheme	223.9(4)	83.3(3)	6.98(5)	0.460(6)
$e^+e^- \to u\,\bar{d}\,e^-\bar{\nu}_e$	constant width	730.2(3)	395.3(2)	211.0(2)	32.38(6)
	running width	729.8(3)	396.9(2)	231.5(2)	530.2(6)
	complex-mass scheme	729.8(3)	395.1(2)	210.9(2)	32.37(6)
$e^+e^- \to u\,\bar{d}\,e^-\bar{\nu}_e\,\gamma$	constant width	230.0(4)	136.5(5)	84.0(7)	16.8(5)
	running width	230.6(4)	137.3(5)	95.7(7)	379(6)
	complex-mass scheme	229.9(4)	136.4(5)	84.1(6)	16.8(5)

Table 2.3: Comparison of different width schemes for several processes and energies

two semi-leptonic final states for $e^+e^- \to 4f(\gamma)$. The numbers show that the constant width and the complex-mass scheme yield the same results within the statistical accuracy for $e^+e^- \to 4f$ and $e^+e^- \to 4f\gamma$. In contrast, the results with the running width produce totally wrong results for high energies. The difference of the running width with respect to the other implementations of the finite width is up to 1% already for 500 GeV. Thus, the running width should not be used for linear-collider energies. As already stated above, our default treatment of the finite width is the complex-mass scheme in this chapter.

2.3.3 Survey of photon-energy spectra

In Fig. 2.2 we show the photon-energy spectra of several processes for the typical LEP2 energy of 189 GeV and a possible linear-collider energy of 500 GeV. The upper plots contain CC and CC/NC processes, the plots in the middle and the lower plots contain NC processes. Several spectra show threshold or peaking structures. These structures are caused by diagrams in which the photon is emitted from the initial state. The two important classes of diagrams are shown in Fig. 2.3.

The first class, shown in Fig. 2.3a, corresponds to triple-gauge-boson-production subprocesses which yield dominant contributions as long as the two virtual gauge bosons V_1 and V_2 can become simultaneously resonant. If the real photon takes the energy E_γ, defined in the CM system, only the energy $\sqrt{s'}$, with

$$s' = s - 2\sqrt{s}\,E_\gamma, \tag{2.3.3}$$
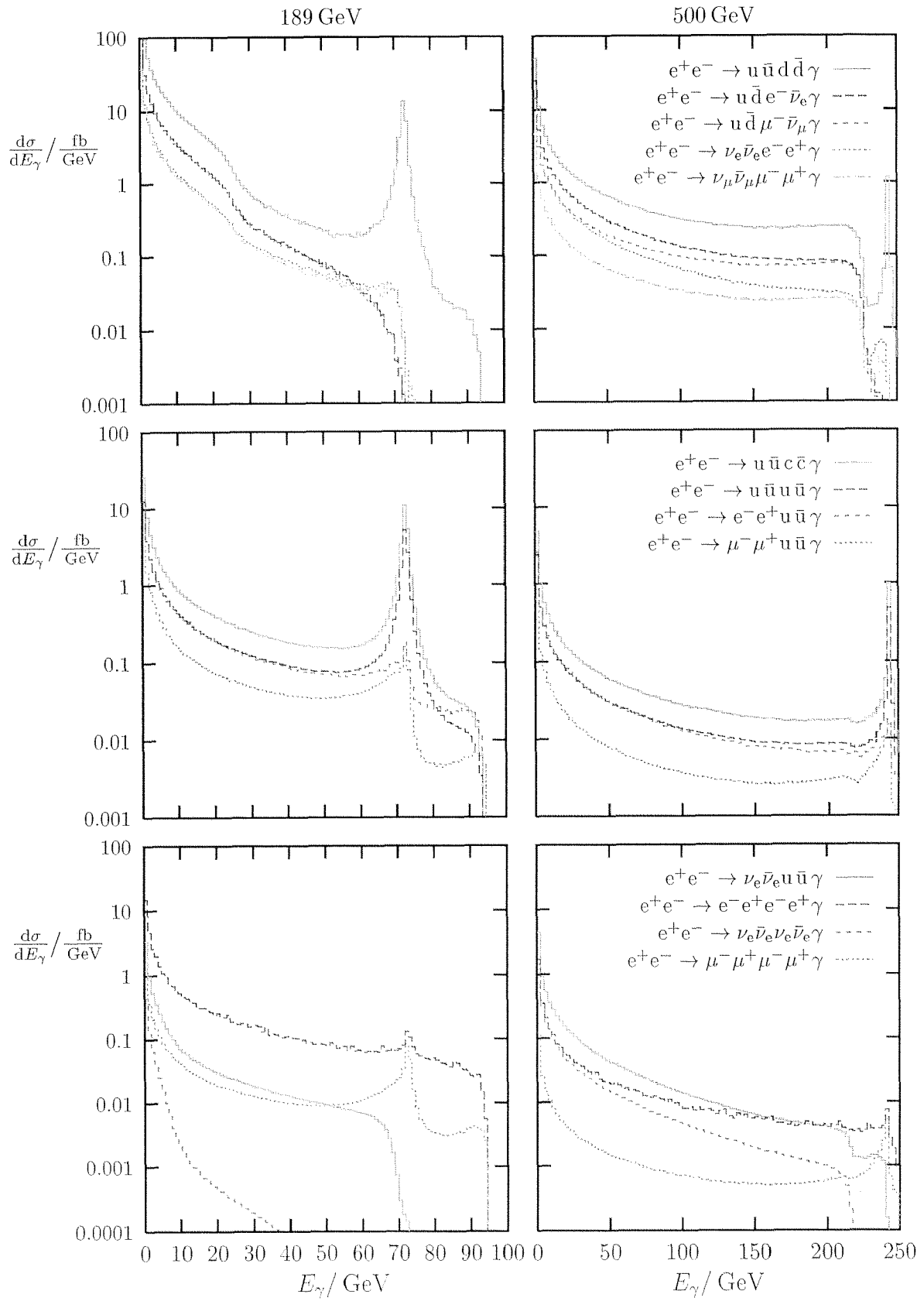
Figure 2.2: Photon-energy spectra for several processes and for $\sqrt{s} = 189\,\text{GeV}$ and $500\,\text{GeV}$
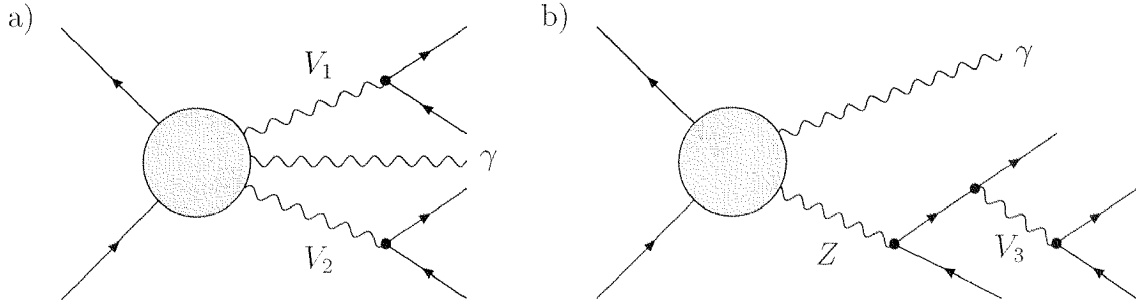
Figure 2.3: Diagrams for important subprocesses, where $V_1, V_2 = W, Z, \gamma$, and $V_3 = \gamma, g$

$\sqrt{s}$	189 GeV				500 GeV			
$V_1 V_2$	WW	ZZ	γZ	$\gamma\gamma$	WW	ZZ	γZ	$\gamma\gamma$
$E_\gamma^{V_1 V_2}$ / GeV	26.3	6.5	72.5	94.5	224	217	242	250

Table 2.4: Photon energies $E_\gamma^{V_1 V_2}$ corresponding to thresholds

is available for the production of the gauge-boson pair $V_1 V_2$. If at least one of the gauge bosons is massive, and if the photon becomes too hard, the two gauge bosons cannot be produced on shell anymore, so that the spectrum falls off for E_γ above the corresponding threshold $E_\gamma^{V_1 V_2}$. Using the threshold condition for the on-shell production of the $V_1 V_2$ pair,

$$\sqrt{s'} > M_{V_1} + M_{V_2}, \tag{2.3.4}$$

the value of $E_\gamma^{V_1 V_2}$ is determined by

$$E_\gamma^{V_1 V_2} = \frac{s - (M_{V_1} + M_{V_2})^2}{2\sqrt{s}}. \tag{2.3.5}$$

The values of the photon energies that cause such thresholds can be found in Table 2.4. The value $E_\gamma^{\gamma\gamma}$ corresponds to the upper endpoint of the photon-energy spectrum, which is given by the beam energy $\sqrt{s}/2$. Since $\sqrt{s'}$ is fully determined by s and E_γ, the contribution of the $V_1 V_2$-production subprocess to the E_γ spectrum qualitatively follows the energy dependence of the total cross section for $V_1 V_2$ production (cf. Ref. [35], Fig. 1) above the corresponding thresholds. The cross sections for $\gamma\gamma$ and γZ production strongly increase with decreasing energy, while the ones for ZZ and WW production are comparably flat. Thus, the $\gamma\gamma$ and γZ-production subprocesses introduce contributions in the photon-energy spectra with resonance-like structures, whereas the ones with ZZ or WW pairs yield edges.

The second class of important diagrams, shown in Fig. 2.3b corresponds to the production of a photon and a resonant Z boson that decays into four fermions. These diagrams

are important if the gauge boson V_3 is also resonant, i.e. a photon or a gluon with small invariant mass. In this case, the kinematics fixes the energy of the real photon to

$$E_\gamma = E_\gamma^{\gamma Z} = \frac{s - M_Z^2}{2\sqrt{s}}, \tag{2.3.6}$$

which corresponds to the γZ threshold in Table 2.4. This subprocess gives rise to resonance structures at $E_\gamma^{\gamma Z}$, which are even enhanced by α_s/α in the presence of gluon exchange.

In the photon-energy spectra of Fig. 2.2 all these threshold and resonance effects are visible. The effect of the γZ peak can be nicely seen in different photon-energy spectra, in particular in those where gluon-exchange diagrams contribute (cf. also Fig. 2.5). The effect of the WW threshold is present in the upper two plots of Fig. 2.2. In the plot for $\sqrt{s} = 189\,\mathrm{GeV}$ the threshold for single W production causes the steep drop of the spectrum for the pure CC processes above $70\,\mathrm{GeV}$. Note that the CC cross sections are an order of magnitude larger than the NC cross sections if the WW channel is open. The ZZ threshold is visible in the middle and lower plots for $\sqrt{s} = 500\,\mathrm{GeV}$. The γZ threshold (resulting from the graphs of Fig. 2.3a) is superimposed on the γZ peak (resulting from the graphs of Fig. 2.3b) and therefore best recognizable in those channels where the γZ peak is absent or suppressed, i.e. where a neutrino pair is present in the final state or where at least no gluon-exchange diagrams contribute. Processes with four neutrinos in the final state do not involve photonic diagrams and are therefore small above the ZZ threshold. The effects of the triple-photon-production subprocess appear as a tendency of some photon-energy spectra to increase near the maximal value of E_γ for two charged fermion–antifermion pairs in the final state.

2.3.4 Triple-gauge-boson-production subprocesses

In Fig. 2.4 we compare predictions that are based on the full set of diagrams with those that include only the graphs associated with the triple-gauge-boson-production subprocesses, i.e. the graphs in Fig. 2.3a. In addition we consider the contributions of the $ZZ\gamma$-production subprocess alone. For CC processes, the photon-energy spectra resulting from the $W^+W^-\gamma$-production subprocess are close to those resulting from all diagrams at LEP2 energies, but large differences are found for higher energies and $e^\pm$ in the final state. Note that the spectra are shown on a logarithmic scale. Even at LEP2 energies the differences between the predictions for different final states may be important, as can be seen, for instance, in Table 2.1 by comparing the cross sections of $e^+e^- \to u\,\bar{d}\,\mu^-\bar{\nu}_\mu\gamma$ and $e^+e^- \to u\,\bar{d}\,e^-\bar{\nu}_e\gamma$. In the case of NC processes, already for $189\,\mathrm{GeV}$ the contributions from $ZZ\gamma$, $Z\gamma\gamma$, and $\gamma\gamma\gamma$ production are not sufficient: in the vicinity of the γZ peak sizeable contributions result from the γZ-production subprocess (Fig. 2.3b) even for the $\mu^+\mu^-u\,\bar{u}\,\gamma$ final state. For $e^+e^- \to e^-e^+u\,\bar{u}\,\gamma$ other diagrams become dominating everywhere. The contribution of $ZZ\gamma$ production is always small and could only be enhanced by invariant-mass cuts. Note that the triple-gauge-boson-production diagrams form a gauge-invariant subset for NC processes, while this is not the case for CC processes.
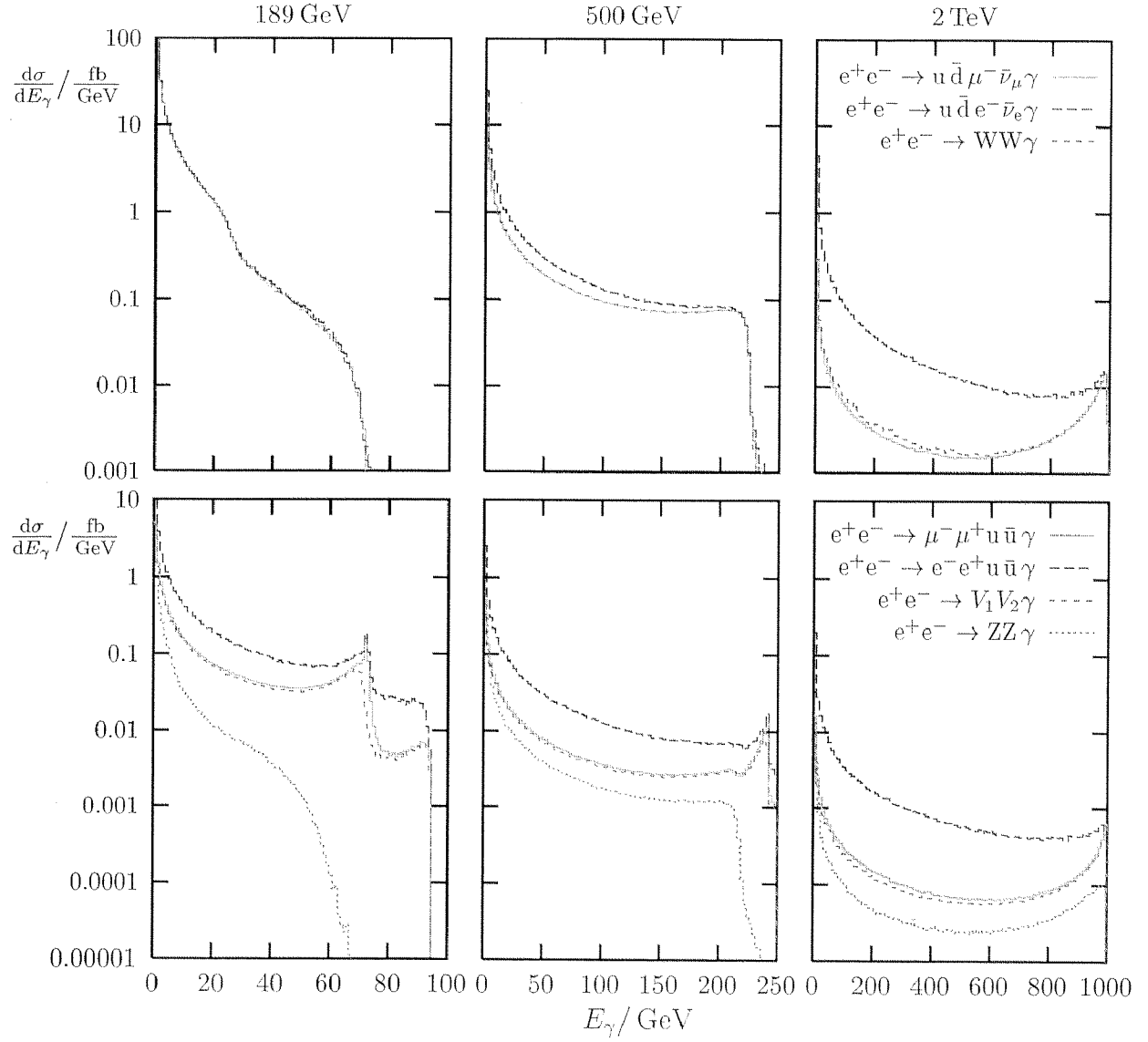
28

Figure 2.4: Photon-energy spectra resulting from the triple-gauge-boson-production sub-processes compared to those resulting from all diagrams (V_1V_2 includes ZZ, γZ, and $\gamma\gamma$)

σ / fb	ew and gluon	purely ew	gluon	interference
$e^+e^- \to u\,\bar{u}\,c\,\bar{c}$	52.98(4)	21.560(6)	31.38(3)	0.04(5)
$e^+e^- \to u\,\bar{u}\,c\,\bar{c}\,\gamma$	29.8(1)	10.38(4)	19.6(1)	$-0.1(1)$
$e^+e^- \to u\,\bar{u}\,u\,\bar{u}$	26.25(2)	10.765(3)	15.34(1)	0.14(2)
$e^+e^- \to u\,\bar{u}\,u\,\bar{u}\,\gamma$	14.83(7)	5.16(2)	9.52(5)	0.15(9)
$e^+e^- \to d\,\bar{d}\,u\,\bar{u}$	901.2(6)	876.4(5)	24.24(2)	0.6(8)
$e^+e^- \to d\,\bar{d}\,u\,\bar{u}\,\gamma$	290(1)	275(1)	14.82(8)	0(1)

Table 2.5: Full lowest order cross section (ew and gluon) and contributions of purely electroweak diagrams (ew), of gluon-exchange diagrams (gluon), and their interference for 500 GeV

2.3.5   Relevance of gluon-exchange contributions

In the analytical calculation of the matrix elements for $e^+e^- \to 4f(\gamma)$ in Section 2.1 we have seen that NC processes with four quarks in the final state involve, besides purely electroweak, also gluon-exchange diagrams. Table 2.5 illustrates the impact of these diagrams on the integrated cross sections for a CM energy of 500 GeV. The results for the interference are obtained by subtracting the purely electroweak and the gluon contribution from the total cross section. For pure NC processes the contributions of gluon-exchange diagrams dominate over the purely electroweak graphs. This can be understood from the fact that the gluon-exchange diagrams are enhanced by the strong coupling constant, and, as discussed in Section 2.3.3, that the diagrams with gluons replaced by photons yield a sizeable contribution to the cross section. For the mixed CC/NC processes the purely electroweak diagrams dominate the cross section. Here, the contributions from the $W^+W^-\gamma$-production subprocess are large compared to all other diagrams, even if the latter are enhanced by the strong coupling. At 500 GeV the gluon-exchange diagrams contribute to the cross section at the level of several per cent. The interference contributions are relatively small. As discussed at the end of Section 2.1.3, this is due to the fact that interfering electroweak and gluon-exchange diagrams involve different resonances. Note that the interference vanishes for $e^+e^- \to u\,\bar{u}\,c\,\bar{c}\,\gamma$, and the corresponding numbers in Table 2.5 are only due to the Monte Carlo integration error.

In Fig. 2.5 we show the photon-energy spectra for the processes $e^+e^- \to u\,\bar{u}\,d\,\bar{d}\,\gamma$ and $e^+e^- \to u\,\bar{u}\,u\,\bar{u}\,\gamma$ together with the separate contributions from purely electroweak and gluon-exchange diagrams. The pure electroweak contributions are similar to the ones for $e^+e^- \to u\,\bar{d}\,\mu^-\bar{\nu}_\mu\,\gamma$ and $e^+e^- \to e^-e^+u\,\bar{u}\,\gamma$ in Fig. 2.2. For the NC process $e^+e^- \to u\,\bar{u}\,u\,\bar{u}\,\gamma$, the photon-energy spectrum is dominated by the gluon-exchange contribution, which shows a strong peak at 72.5 GeV owing to the γZ-production subprocess. For the CC/NC process $e^+e^- \to u\,\bar{u}\,d\,\bar{d}\,\gamma$, the electroweak diagrams dominate below the WW threshold, whereas the gluon-exchange diagrams dominate at the γZ peak and above. The interference between purely electroweak and gluon-exchange diagrams is generally small.
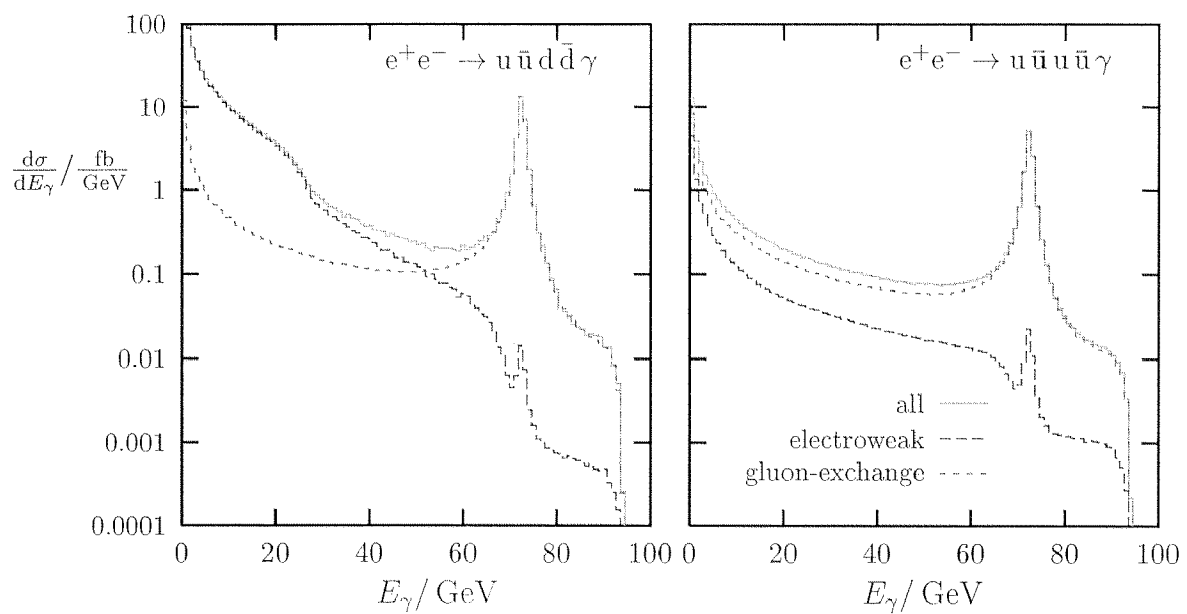
Figure 2.5: Electroweak and gluon-exchange contributions to the photon-energy spectra for $e^+e^- \to u\bar{u}d\bar{d}\gamma$ and $e^+e^- \to u\bar{u}u\bar{u}\gamma$ at $\sqrt{s} = 189\,\text{GeV}$

Chapter 3

Non-factorizable photonic corrections to $e^+e^- \to W^+W^- \to 4f$

In this chapter we define and explicitly calculate the non-factorizable photonic corrections. It has been shown that they vanish in inclusive quantities, i.e. if the invariant masses of both W bosons are integrated out [36]. However, for non-inclusive quantities these corrections do not vanish in general. The non-factorizable photonic corrections have already been investigated by two groups. Melnikov and Yakovlev [37] have given the analytical results only in an implicit form and restrict the numerical evaluation to a special phase-space configuration. Beenakker, Berends and Chapovsky have provided both the complete formulae and an adequate numerical evaluation [38, 39], but do not find agreement with all results of Ref. [37]. For this reason, it is worth-while to present the results of a third independent calculation. The material of this chapter has been published in Refs. [40, 41].

We start out by discussing the definition of the virtual and real photonic non-factorizable corrections in double-pole approximation in detail. Since only soft photons are relevant in double-pole approximation, the virtual non-factorizable correction is just a factor to the lowest-order cross section. For the corresponding real correction, the situation is similar, but in addition an integration over the photon momentum has to be performed. This requires a specification of the phase-space parameterization, which includes, in particular, the invariant masses of the W bosons. Usually these are defined via the invariant masses of the respective final-state fermion pairs and are chosen as independent variables [37, 38, 39]. Experimentally, however, the invariant mass of a W boson is identified with the invariant mass of the associated jet pair that necessarily includes soft and collinear photons. Therefore, the influence of the choice for the invariant masses of the W bosons on the non-factorizable corrections should be investigated in order to provide sound predictions for physical situations.

Besides the non-factorizable doubly-resonant corrections, the most important effect of the instability of the W bosons is the modification of the Coulomb singularity. Since the off-shell Coulomb singularity results from a scalar integral that also contributes to the doubly-resonant non-factorizable corrections, it seems to be natural to approximate this integral in such a way that both effects are simultaneously included. This requires going beyond the strict double-pole approximation.

3.1 Definition of the approximation

3.1.1 Conventions and notations

We discuss corrections to the process

$$e^+(p_+) + e^-(p_-) \rightarrow W^+(k_+) + W^-(k_-) \rightarrow f_1(k_1) + \bar{f}_2(k_2) + f_3(k_3) + \bar{f}_4(k_4). \quad (3.1.1)$$

The relative charges of the fermions f_i are represented by Q_i with $i = 1, \ldots, 4$. The masses of the external fermions, $m_i^2 = k_i^2$ and $m_e^2 = p_\pm^2$, are neglected, except where this would lead to mass singularities. The momenta of the intermediate W bosons are defined by

$$k_+ = k_1 + k_2, \qquad k_- = k_3 + k_4, \quad (3.1.2)$$

their complex mass squared and their respective invariant masses are denoted by

$$M^2 = M_W^2 - iM_W\Gamma_W, \qquad M_\pm = \sqrt{k_\pm^2}, \quad (3.1.3)$$

respectively, and we introduce the variables

$$K_+ = k_+^2 - M^2, \qquad K_- = k_-^2 - M^2. \quad (3.1.4)$$

Furthermore, we define the following kinematical invariants

$$
\begin{aligned}
t &= (p_\pm - k_\pm)^2, & u &= (p_\pm - k_\mp)^2, \\
t_{+i} &= (p_+ - k_i)^2, & u_{-i} &= (p_- - k_i)^2, & i &= 1, 2, \\
t_{-i} &= (p_- - k_i)^2, & u_{+i} &= (p_+ - k_i)^2, & i &= 3, 4,
\end{aligned}
\quad (3.1.5)
$$

and

$$
\begin{aligned}
s &= (p_+ + p_-)^2 = (k_+ + k_-)^2, \\
s_{ij} &= (k_i + k_j)^2, \\
s_{ijk} &= (k_i + k_j + k_k)^2, & i, j, k &= 1, 2, 3, 4,
\end{aligned}
\quad (3.1.6)
$$

which obey the relations

$$
\begin{aligned}
s &= k_+^2 + k_-^2 + s_{13} + s_{14} + s_{23} + s_{24}, & s_{12} &= k_+^2, & s_{34} &= k_-^2, \\
s_{ijk} &= s_{ij} + s_{ik} + s_{jk}, & i, j, k &= 1, 2, 3, 4.
\end{aligned}
\quad (3.1.7)
$$

3.1.2 Doubly-resonant virtual corrections

The aim of this chapter is to evaluate the non-factorizable corrections to the process (3.1.1) in double-pole approximation (DPA). The DPA takes into account only the leading terms in an expansion around the poles originating from the two resonant W propagators.
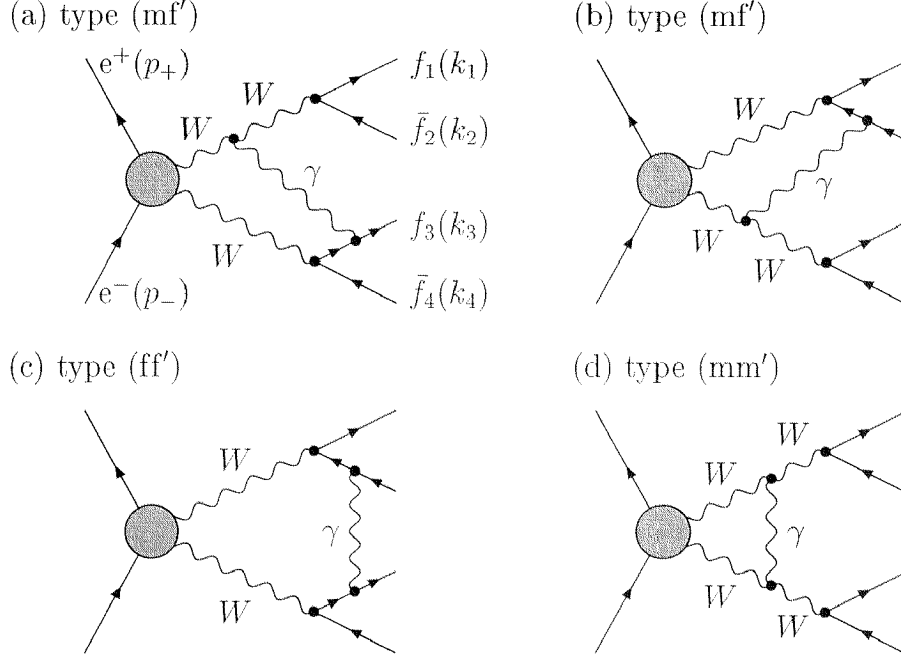
Figure 3.1: Examples of non-factorizable photonic corrections in $\mathcal{O}(\alpha)$. The shaded blobs stand for all tree-level graphs contributing to $e^+e^- \to W^+W^-$. Whenever Feynman diagrams with intermediate would-be Goldstone bosons $\phi^\pm$ instead of $W^\pm$ bosons are relevant, the inclusion of such graphs is implicitly understood.

In DPA, the lowest-order matrix element for the process (3.1.1) factorizes into the matrix element for the on-shell W-pair production, $\mathcal{M}_{\mathrm{Born}}^{e^+e^- \to W^+W^-}(p_+, p_-, k_+, k_-)$, the (transverse parts of the) propagators of these bosons, and the matrix elements for the decays of these on-shell bosons, $\mathcal{M}_{\mathrm{Born}}^{W^+ \to f_1 \bar{f}_2}(k_+, k_1, k_2)$ and $\mathcal{M}_{\mathrm{Born}}^{W^- \to f_3 \bar{f}_4}(k_-, k_3, k_4)$:

$$\mathcal{M}_{\mathrm{Born}} = \sum_{\lambda_+, \lambda_-} \frac{\mathcal{M}_{\mathrm{Born}}^{e^+e^- \to W^+W^-} \mathcal{M}_{\mathrm{Born}}^{W^+ \to f_1 \bar{f}_2} \mathcal{M}_{\mathrm{Born}}^{W^- \to f_3 \bar{f}_4}}{K_+ K_-}. \tag{3.1.8}$$

The sum runs over the physical polarizations $\lambda_\pm$ of the $W^\pm$ bosons.

The higher-order corrections to (3.1.1) can be separated into factorizable and non-factorizable contributions [5, 12, 42]. In the factorizable contributions the production of two W bosons and their subsequent decays are independent. The corresponding Feynman diagrams can be split into three parts by cutting only the two W-boson lines. The corresponding matrix element factorizes in the same way as the lowest-order matrix element (3.1.8).

The non-factorizable corrections comprise all those contributions in which W-pair production and/or the subsequent W decays are not independent. Obviously, this includes all Feynman diagrams in which a particle is exchanged between the production subprocess and one of the decay subprocesses or between the decay subprocesses. Examples for such manifestly non-factorizable corrections are the diagrams (a), (b), and (c) in Fig. 3.1. If the additional exchanged particle is massive, the corresponding correction has no double pole for on-shell W bosons. However, if a photon is exchanged between the different subprocesses, this leads to a doubly-resonant contribution originating from the soft-photon

34

region. This can be directly seen from the usual soft-photon approximation (SPA), which yields contributions proportional to the (doubly-resonant) lowest-order contribution.

The doubly-resonant contributions can be extracted on the basis of a simple power-counting argument. For instance, the loop integral corresponding to diagram (c) in Fig. 3.1 is of the following form:

$$
\begin{aligned}
I &= \int \mathrm{d}^4 q \frac{N(q, k_i)}{(q^2 - \lambda^2)[(q - k_3)^2 - m_3^2][(q - k_-)^2 - M_W^2][(q + k_+)^2 - M_W^2][(q + k_2)^2 - m_2^2]} \\
&= \int \mathrm{d}^4 q \frac{N(q, k_i)}{(q^2 - \lambda^2)(q^2 - 2qk_3)(q^2 - 2qk_- + k_-^2 - M_W^2)(q^2 + 2qk_+ + k_+^2 - M_W^2)(q^2 + 2qk_2)},
\end{aligned}
$$

$$(3.1.9)$$

where we have introduced an infinitesimal photon mass λ to regularize the infrared (IR) singularity. The function $N(q, k_i)$ involves the numerator of the Feynman integral, i.e. a polynomial in the momenta q and k_i, and possible further denominator factors originating from propagators (hidden in the blob of the diagrams) that are regular for $q = 0$ and $k_\pm^2 = M_W^2$. For on-shell W bosons ($k_\pm^2 = M_W^2$), the integral has a quadratic IR singularity. For off-shell W bosons, part of the IR singularity is regularized by the off-shellness, $k_\pm^2 - M_W^2 \neq 0$, such that the usual logarithmic IR singularity remains. Vice versa, the off-shell result develops a pole if either W boson becomes on shell, and is thus doubly-resonant. Therefore, the quadratic IR singularity in the on-shell limit is characteristic of the doubly-resonant non-factorizable contributions. All terms that involve a factor q in the numerator are less IR-singular and therefore do not lead to doubly-resonant contributions and can be omitted. Similarly, q can be neglected in all denominator factors included in $N(q, k_i)$. In summary, q can be put to zero in $N(q, k_i)$ in DPA. We have checked this for various examples explicitly. As a consequence, we are left with only scalar integrals, and the non-factorizable virtual corrections are proportional to the lowest-order matrix element. We call the resulting approximation *extended soft-photon approximation* (ESPA). It differs from the usual SPA only by the fact that q is not neglected in the resonant W propagators. In ESPA, diagram (c) in Fig. 3.1 gives the following contribution to the matrix element:

$$
\mathcal{M}^{\bar{f}_2 f_3} = \mathrm{i}e^2 Q_2 Q_3 \mathcal{M}_{\text{Born}} \int \frac{\mathrm{d}^4 q}{(2\pi)^4} \frac{4k_2 k_3}{(q^2 - \lambda^2)(q^2 - 2qk_3)(q^2 + 2qk_2)}
$$
$$
\times \frac{(k_-^2 - M_W^2)(k_+^2 - M_W^2)}{[(q - k_-)^2 - M_W^2][(q + k_+)^2 - M_W^2]}. \quad (3.1.10)
$$

The q^2 terms in the last four denominators are not relevant in the soft-photon limit and were omitted in Refs. [37, 38, 39]. In fact, using the above power-counting argument it can easily be seen that the differences of doubly-resonant contributions with and without these q^2 terms are non-doubly-resonant. We have chosen to keep the q^2 terms, because we want to use the standard techniques for the evaluation of virtual scalar integrals [43]. In DPA, i.e. if we perform the limit $k_\pm^2 \to M_W^2$ after evaluating the integral, we should obtain the same result.

In order to arrive at physical results, we have to incorporate the finite width of the W bosons. In DPA this can be done in at least two different ways:

As a first possibility, we perform the integrals for zero width and afterwards put $k_\pm^2 = M_W^2$ where this does not give rise to singularities. In all other places, i.e. in the resonant propagators and in logarithms of the form $\ln(k_\pm^2 - M_W^2 + i\epsilon)$, we replace $k_\pm^2 - M_W^2 + i\epsilon$ by $K_\pm = k_\pm^2 - M_W^2 + iM_W\Gamma_W$. Since the width is only relevant in the on-shell limit, it is clear that the (physical) on-shell width has to be used.

Alternatively, we introduce the width in the W propagators before integration. This has to be done with caution. If we introduce the finite width by resumming W-self-energy insertions, the width depends on the invariant mass of the W boson and thus on the integration momentum. Fortunately, the contribution we are interested in results only from the soft-photonic region where the virtual W bosons are almost on shell. Therefore, we can insert the on-shell width inside the loop integral. After performing the integral, we put $k_\pm^2 = M_W^2$ and $\Gamma_W = 0$ where this does not lead to singularities. In DPA this gives the same results as the above treatment.

In the following we write $M^2 = M_W^2 - iM_W\Gamma_W$ instead of M_W^2 in the loop integrals. It is always understood that M^2 and $k_\pm^2$ are replaced by M_W^2 where possible after evaluation of the integrals.

If we implement the width into the integrand, it is clear that only the part of the integration region with $|q_0| \lesssim \Gamma_W$ contributes in DPA. If $|q_0| \gg \Gamma_W$, one of the W propagators must be non-resonant and the contribution becomes negligible.

Once the width is introduced, it becomes evident that the relative error of the DPA is of the order of Γ_W/scale. Let E_{CM} be the center-of-mass (CM) energy and $\Delta E = E_{CM} - 2M_W$ be the available kinetic energy of the W bosons. Then, for $\Delta E \gtrsim M_W$ the scale is given by M_W, for $\Gamma_W \lesssim \Delta E \lesssim M_W$ it is given by ΔE and for $\Delta E \lesssim \Gamma_W$ it is given by Γ_W. This shows that the DPA is only sensible several Γ_W's above threshold. This is simply due to the fact that, close to threshold, the phase space where both W propagators can become doubly-resonant is very small, and the singly-resonant diagrams become important.

3.1.3 Classification and gauge-independent definition of the non-factorizable doubly-resonant virtual corrections

Manifestly non-factorizable corrections arise from photon exchange between the final states of the two W bosons (ff'), between initial and final state (if), and between one of the intermediate resonant W bosons and the final state of the other W boson (mf'). Examples for these types of corrections are shown in Fig. 3.1 (c), Fig. 3.2 (a), and Fig. 3.1 (a,b), respectively. In addition, there are diagrams where the photon does not couple to uniquely distinguishable subprocesses. These contributions can be classified into photon-exchange contributions between one of the intermediate resonant W bosons and the final state of the same W boson (mf), between the intermediate and the initial state (im), between the two intermediate W bosons (mm'), and within a single W-boson line, i.e. the photonic part of the W-self-energy corrections (mm). Diagrams contributing to these types of corrections are given in Fig. 3.2 (c), Fig. 3.2 (b), Fig. 3.1 (d), and Fig. 3.2 (d), respectively. Because the photon coupling to the W boson can be attributed to the decay or the production subprocesses, these diagrams involve both factorizable and non-factorizable corrections.

In order to define the non-factorizable corrections, we have to specify how the factorizable contributions are split off. This should be done in such a way that the non-factorizable
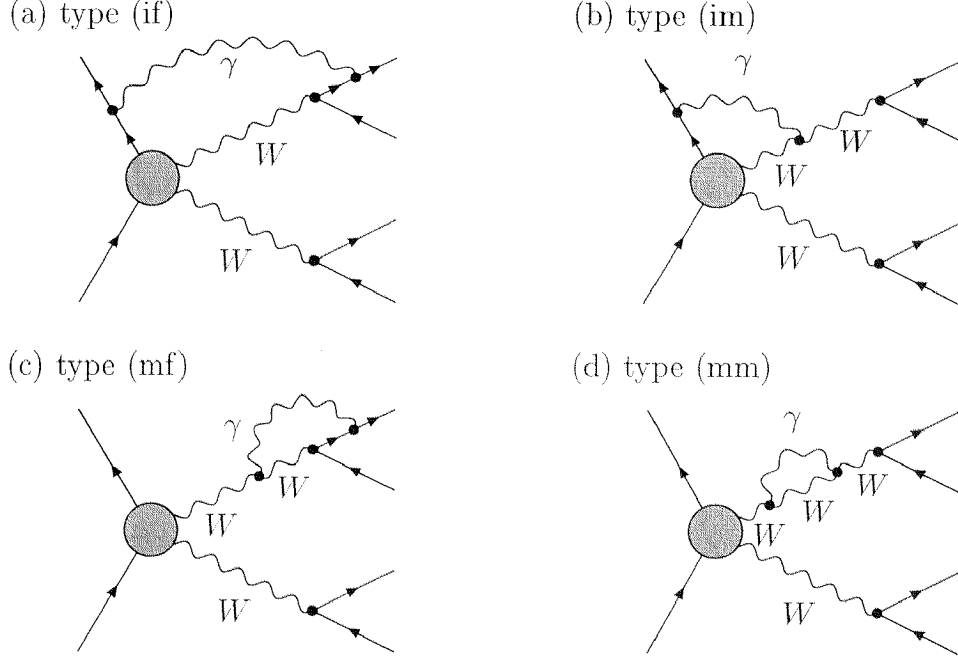
Figure 3.2: Further examples of non-factorizable photonic corrections in $\mathcal{O}(\alpha)$.

corrections become gauge-independent. In Refs. [38, 39] this was reached by exploiting the fact that in ESPA the matrix element can be viewed as a product of the lowest-order matrix element with two conserved currents. Taking all interferences between the positively and the negatively charged currents arising from the outgoing W bosons and fermions gives a gauge-independent result.

We have chosen a different definition of the non-factorizable corrections, which, however, turns out to be equivalent to the one of Refs. [38, 39] in DPA. Our approach has the advantage of providing a clear procedure how to combine factorizable and non-factorizable contributions to the full $\mathcal{O}(\alpha)$ correction in DPA. Because the complete matrix element is gauge-independent order by order, the sum of all doubly-resonant $\mathcal{O}(\alpha)$ corrections must be gauge-independent. On the other hand, the factorizable doubly-resonant corrections can be defined by the product of gauge-independent on-shell matrix elements for W-pair production and W decays and the (transverse parts of the) W propagators,

$$
\mathcal{M}_{\mathrm{f}} = \sum_{\lambda_+,\lambda_-} \frac{1}{K_+ K_-} \Big(\delta\mathcal{M}^{\mathrm{e}^+\mathrm{e}^- \to \mathrm{W}^+\mathrm{W}^-} \mathcal{M}_{\mathrm{Born}}^{\mathrm{W}^+ \to f_1\bar{f}_2} \mathcal{M}_{\mathrm{Born}}^{\mathrm{W}^- \to f_3\bar{f}_4}
$$

$$
+ \mathcal{M}_{\mathrm{Born}}^{\mathrm{e}^+\mathrm{e}^- \to \mathrm{W}^+\mathrm{W}^-} \delta\mathcal{M}^{\mathrm{W}^+ \to f_1\bar{f}_2} \mathcal{M}_{\mathrm{Born}}^{\mathrm{W}^- \to f_3\bar{f}_4} + \mathcal{M}_{\mathrm{Born}}^{\mathrm{e}^+\mathrm{e}^- \to \mathrm{W}^+\mathrm{W}^-} \mathcal{M}_{\mathrm{Born}}^{\mathrm{W}^+ \to f_1\bar{f}_2} \delta\mathcal{M}^{\mathrm{W}^- \to f_3\bar{f}_4} \Big),
$$

(3.1.11)

where $\delta\mathcal{M}^{\mathrm{e}^+\mathrm{e}^- \to \mathrm{W}^+\mathrm{W}^-}$, $\delta\mathcal{M}^{\mathrm{W}^+ \to f_1\bar{f}_2}$, and $\delta\mathcal{M}^{\mathrm{W}^- \to f_3\bar{f}_4}$ denote the one-loop amplitudes of the respective subprocesses. We can define the non-factorizable doubly-resonant corrections by subtracting the factorizable doubly-resonant corrections from the complete doubly-resonant corrections. This definition allows us to calculate the complete doubly-resonant corrections by simply adding the factorizable corrections, defined via the on-shell matrix elements, to our results. Our definition can be applied diagram by diagram. In this way, all diagrams that are neither manifestly factorizable nor manifestly non-factorizable can

be split. Such diagrams receive doubly-resonant contributions from the complete range of the photon momentum q, and not only from the soft-photon region. This is obviously due to the presence of two explicit resonant propagators. However, after subtracting the factorizable contributions, all doubly-resonant terms that are not IR-singular in the on-shell limit cancel exactly, i.e. only the soft-photon region contributes. Consequently, also in this case q can be neglected everywhere except for the denominators that become IR-singular in the on-shell limit. As an example, we give the non-factorizable correction originating from diagram (d) of Fig. 3.1:[1]

$$\mathcal{M}_{\text{nf}}^{\text{W}^+\text{W}^-} \sim ie^2 \mathcal{M}_{\text{Born}} \left\{ \int \frac{\mathrm{d}^4 q}{(2\pi)^4} \frac{4k_+ k_-}{q^2[(q+k_+)^2 - M^2][(q-k_-)^2 - M^2]} \right. $$
$$ \left. - \left[\int \frac{\mathrm{d}^4 q}{(2\pi)^4} \frac{4k_+ k_-}{(q^2 - \lambda^2)(q^2 + 2qk_+)(q^2 - 2qk_-)} \right]_{k_\pm^2 = M_\text{W}^2} \right\}. \quad (3.1.12)$$

This example shows that the on-shell subtraction introduces additional IR singularities. If the IR singularities in the non-factorizable real corrections are regularized in the same way, they cancel in the sum. In (3.1.12) an infinitesimal photon mass λ is used as IR regulator, but we have repeated the same calculation also by using a finite W-decay width as IR regulator instead of λ, leading to the same results in the sum of virtual and real photonic corrections.

We illustrate our definition of the non-factorizable corrections also for the photonic contribution to the W-self-energy correction [diagram (d) of Fig. 3.2]. The non-factorizable part of the W^+ self-energy reads

$$\mathcal{M}_{\text{nf}}^{\text{W}^+\text{W}^+} \sim -ie^2 \mathcal{M}_{\text{Born}} \left\{ \int \frac{\mathrm{d}^4 q}{(2\pi)^4} \frac{4k_+^2}{q^2[(q+k_+)^2 - M^2](k_+^2 - M^2)} \right. $$
$$ - \frac{1}{k_+^2 - M^2} \left[\int \frac{\mathrm{d}^4 q}{(2\pi)^4} \frac{4k_+^2}{q^2(q^2 + 2qk_+)} \right]_{k_+^2 = M^2} $$
$$ \left. + \left[\int \frac{\mathrm{d}^4 q}{(2\pi)^4} \frac{4k_+^2}{(q^2 - \lambda^2)(q^2 + 2qk_+)^2} \right]_{k_+^2 = M_\text{W}^2} \right\}. \quad (3.1.13)$$

The first integral results from the off-shell self-energy diagram, the second from the corresponding mass-renormalization term, and the third integral is the negative of the on-shell limit of the first two integrals. The integrals in (3.1.13) are UV-divergent and can be easily evaluated in dimensional regularization.

The gauge independence of the non-factorizable corrections has been ensured by construction. The consistent evaluation of gauge theories requires, besides gauge independence of the physical matrix elements, the validity of Ward identities. It was found in Ref. [7, 8, 9, 10] that the violation of Ward identities can lead to completely wrong predictions. The procedure described above for extracting the non-factorizable corrections from the full matrix element does not lead to problems with the Ward identities that rule the gauge cancellations inside matrix elements. This is due to the fact that the non-factorizable corrections are proportional to the Born matrix element. Therefore, if Ward

---

[1] We use the sign $\sim$ to indicate an equality within DPA, i.e. up to non-doubly-resonant terms.

identities and gauge cancellations are under control in lowest order, the same is true for the non-factorizable corrections.

Finally, we show how our definition of the non-factorizable corrections can be rephrased in terms of products of appropriately defined currents. By using

$$\frac{1}{(q \pm k_\pm)^2 - M^2} = \frac{1}{q^2 \pm 2qk_\pm}\left[1 - \frac{k_\pm^2 - M^2}{(q \pm k_\pm)^2 - M^2}\right], \qquad (3.1.14)$$

and the fact that in DPA $k_\pm^2$ can be put to M_W^2 before integration in integrals that do not depend on M^2, the contribution (3.1.12) can be expressed as

$$\mathcal{M}_{\mathrm{nf}}^{W^+W^-} \sim ie^2 \mathcal{M}_{\mathrm{Born}} \int \frac{\mathrm{d}^4 q}{(2\pi)^4} \frac{4k_+k_-}{(q^2 - \lambda^2)(q^2 + 2qk_+)(q^2 - 2qk_-)}\left[-\frac{k_+^2 - M^2}{(q + k_+)^2 - M^2}\right.$$
$$\left. - \frac{k_-^2 - M^2}{(q - k_-)^2 - M^2} + \frac{k_+^2 - M^2}{(q + k_+)^2 - M^2}\frac{k_-^2 - M^2}{(q - k_-)^2 - M^2}\right]. \quad (3.1.15)$$

The other non-factorizable corrections that involve photons coupled to W bosons can be rewritten in a similar way. Finally, all non-factorizable virtual corrections can be cast into the following form:

$$\mathcal{M}_{\mathrm{nf}}^{\mathrm{virt}} \sim i\mathcal{M}_{\mathrm{Born}} \int \frac{\mathrm{d}^4 q}{(2\pi)^4} \frac{1}{q^2 - \lambda^2}\left[j_{\mathrm{virt},+}^{e^+e^- \to W^+W^-,\mu} j_{\mathrm{virt},\mu}^{W^+ \to f_1\bar{f}_2} + j_{\mathrm{virt},-}^{e^+e^- \to W^+W^-,\mu} j_{\mathrm{virt},\mu}^{W^- \to f_3\bar{f}_4}\right.$$
$$\left. + j_{\mathrm{virt}}^{W^+ \to f_1\bar{f}_2,\mu} j_{\mathrm{virt},\mu}^{W^- \to f_3\bar{f}_4}\right] \qquad (3.1.16)$$

with

$$j_{\mathrm{virt},\pm,\mu}^{e^+e^- \to W^+W^-} = e\left(\frac{2k_{+\mu}}{q^2 + 2qk_+} + \frac{2k_{-\mu}}{q^2 - 2qk_-} \pm \frac{2p_{-\mu}}{q^2 \pm 2qp_-} \mp \frac{2p_{+\mu}}{q^2 \pm 2qp_+}\right),$$

$$j_{\mathrm{virt},\mu}^{W^+ \to f_1\bar{f}_2} = e\left(Q_1\frac{2k_{1\mu}}{q^2 + 2qk_1} - Q_2\frac{2k_{2\mu}}{q^2 + 2qk_2} - \frac{2k_{+\mu}}{q^2 + 2qk_+}\right)\frac{k_+^2 - M^2}{(k_+ + q)^2 - M^2},$$

$$j_{\mathrm{virt},\mu}^{W^- \to f_3\bar{f}_4} = -e\left(Q_3\frac{2k_{3\mu}}{q^2 - 2qk_3} - Q_4\frac{2k_{4\mu}}{q^2 - 2qk_4} + \frac{2k_{-\mu}}{q^2 - 2qk_-}\right)\frac{k_-^2 - M^2}{(k_- - q)^2 - M^2}. \quad (3.1.17)$$

The last term in (3.1.16) originates from the Feynman graphs shown in Fig. 3.1 and those where the final-state fermions are appropriately interchanged [interference terms (ff'), (mf'), and (mm')]. The contributions involving the current $j_{\mathrm{virt},\mu}^{e^+e^- \to W^+W^-}$ contain the interference terms (if), (mf), (im), (mm), and the remaining contributions of (mf') and (mm'). The contribution of the W^+ self-energy is given, for instance, by the product of the two terms involving $k_{+\mu}$ in $j_{\mathrm{virt},\mu}^{e^+e^- \to W^+W^-}$ and $j_{\mathrm{virt},\mu}^{W^+ \to f_1\bar{f}_2}$.

In DPA, the q^2 terms in the denominators of (3.1.17) can be neglected, and the currents are conserved. The currents $j_{\mathrm{virt},\mu}^{W^+ \to f_1\bar{f}_2}$ and $j_{\mathrm{virt},\mu}^{W^- \to f_3\bar{f}_4}$ are the ones mentioned in Refs. [38, 39]. For the virtual corrections, this shows that our definition of non-factorizable doubly-resonant corrections coincides with the one of Refs. [38, 39] in DPA.
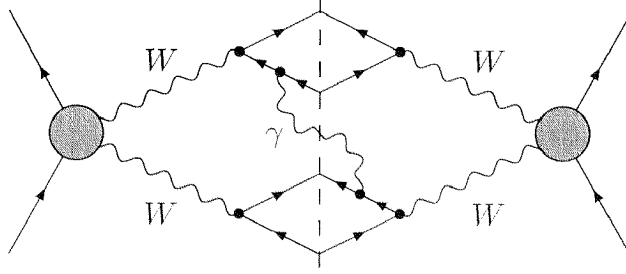
Figure 3.3: Example of a non-factorizable real correction.

3.1.4 Doubly-resonant real corrections

The photonic virtual corrections discussed above are IR-singular and have to be combined with the corresponding real corrections in order to arrive at a sensible physical result. The real corrections originate from the process

$$e^+(p_+) + e^-(p_-) \ \rightarrow \ W^+(k'_+) + W^-(k'_-) \, [+ \gamma(q)]$$
$$\rightarrow \ f_1(k'_1) + \bar{f}_2(k'_2) + f_3(k'_3) + \bar{f}_4(k'_4) + \gamma(q). \tag{3.1.18}$$

Note that we have marked the fermion momenta k'_i by primes in order to distinguish them from the respective momenta without real photon emission. The momenta of the W bosons are $k'_+ = k'_1 + k'_2$ and $k'_- = k'_3 + k'_4$ if the photon is emitted in the initial state or in the final state of the other W boson, and $\bar{k}_+ = k'_1 + k'_2 + q$ or $\bar{k}_- = k'_3 + k'_4 + q$ if the photon is emitted in the final state of the respective W boson.

The non-factorizable corrections induced by the process (3.1.18) arise from interferences between diagrams where the photon is emitted from different subprocesses. A typical non-factorizable contribution is shown in Fig. 3.3. Including the integration over the photon phase space, this contribution has the following form:

$$\mathcal{I} = \int \frac{\mathrm{d}^3 \mathbf{q}}{2q_0} \frac{N(q, k'_i) \delta(p_+ + p_- - k'_1 - k'_2 - k'_3 - k'_4 - q)}{[(q + k'_2)^2 - m_2^2][(q + k'_+)^2 - M^2](k'^2_- - M^2)}$$
$$\times \left\{ \frac{1}{[(q + k'_3)^2 - m_3^2](k'^2_+ - M^2)[(q + k'_-)^2 - M^2]} \right\}^* \Bigg|_{q_0 = \sqrt{\mathbf{q}^2 + \lambda^2}}$$
$$= \int \frac{\mathrm{d}^3 \mathbf{q}}{2q_0} \frac{N(q, k'_i) \delta(p_+ + p_- - k'_1 - k'_2 - k'_3 - k'_4 - q)}{(2qk'_2)(2qk'_+ + k'^2_+ - M^2)(k'^2_- - M^2)}$$
$$\times \frac{1}{(2qk'_3)[k'^2_+ - (M^*)^2][2qk'_- + k'^2_- - (M^*)^2]} \Bigg|_{q_0 = \sqrt{\mathbf{q}^2 + \lambda^2}}, \tag{3.1.19}$$

where we again use a photon mass λ to regularize the IR singularities, and $N(q, k'_i)$ has the same meaning as above. Again, the doubly-resonant contributions are characterized by a quadratic IR singularity for $k'^2_\pm = M_W^2$, $\Gamma_W \rightarrow 0$, and only soft-photon emission is relevant in DPA. For this reason, the W bosons are nearly on shell, and the on-shell width is appropriate. As for the virtual corrections, the introduction of the width before or after phase-space integration leads to the same results in DPA. As already indicated in (3.1.19), in the following real integrals we use M^2 with the understanding that it has to be replaced by M_W^2 after integration where possible.

40

The aim is to integrate over the photon momentum analytically and to relate the fermion momenta k_i' to the ones of the process without photon emission, k_i. Primed and unprimed momenta differ by terms of the order of the photon momentum: $k_i' = k_i + \mathcal{O}(q_0)$. In DPA we can neglect q in $N(q, k_i')$, leading to the replacement $N(q, k_i') \to N(0, k_i)$. Moreover, we can extend the integration region for q_0 to infinity, because large photon momenta yield negligible contributions in DPA. After extension of the integration region the integral becomes Lorentz-invariant.

While the correction factor to the lowest-order cross section is universal in SPA for all observables, the correction factor is non-universal in ESPA. In order to define this correction factor in a unique way, one has to specify the parameterization of phase space, i.e. the variables that are kept fixed when the photon momentum is integrated over. This fact has not been addressed in the literature so far.

Let us consider this problem in more detail. It can be traced back to the appearance of the photon momentum q in the δ-function for momentum conservation. In the usual SPA q is neglected in this δ-function, which is sensible if the exact matrix element is a slowly varying function of q in the vicinity of $q = 0$. However, in the presence of resonant propagators, in which q cannot be neglected, the simple omission of q in the momentum-conservation δ-function leads to ambiguous results: putting $q = 0$ in the δ-function and identifying k_i' with k_i in (3.1.19) yields

$$\mathcal{I} \to \int \frac{\mathrm{d}^3\mathbf{q}}{2q_0} \frac{N(0, k_i)\delta(p_+ + p_- - k_1 - k_2 - k_3 - k_4)}{(2qk_2)(2qk_+ + k_+^2 - M^2)(k_-^2 - M^2)}$$
$$\times \frac{1}{(2qk_3)[k_+^2 - (M^*)^2][2qk_- + k_-^2 - (M^*)^2]}\bigg|_{q_0=\sqrt{\mathbf{q}^2+\lambda^2}}. \qquad (3.1.20)$$

On the other hand, eliminating k_+' in the denominator of (3.1.19) with the help of the δ-function, putting $q = 0$ in the δ-function, restoring k_+' with the modified δ-function, and setting $k_i' \to k_i$ results in

$$\mathcal{I} \to \int \frac{\mathrm{d}^3\mathbf{q}}{2q_0} \frac{N(0, k_i)\delta(p_+ + p_- - k_1 - k_2 - k_3 - k_4)}{(2qk_2)(k_+^2 - M^2)(k_-^2 - M^2)}$$
$$\times \frac{1}{(2qk_3)[-2qk_+ + k_+^2 - (M^*)^2][2qk_- + k_-^2 - (M^*)^2]}\bigg|_{q_0=\sqrt{\mathbf{q}^2+\lambda^2}}. \qquad (3.1.21)$$

Both expressions differ by a doubly-resonant contribution. The difference is in general confined to the W propagators and originates from the fact that not only soft photons but also photons with energies of the order of $|k_\pm^2 - M_W^2|/M_W$ or, after the inclusion of the finite width, of order Γ_W contribute in DPA. Since photons with finite energies contribute, it is evident that the integral over the photon momentum depends on the choice of the phase-space variables that are kept fixed.

As a consequence, one has to choose a definite parameterization of phase space and to exploit the δ-function carefully, in order to define the non-factorizable corrections uniquely. For instance, if the vector $k_+' = k_1' + k_2'$ is kept fixed, the alternative (3.1.21) is excluded. However, because of momentum conservation, not all external momenta can be kept fixed independently.

It is, however, possible to keep, for instance, the invariant masses of the final-state fermion pairs $k_+'^2 = (k_1' + k_2')^2$ and $k_-'^2 = (k_3' + k_4')^2$ fixed when integrating over the photon momentum. If we require $(k_1' + k_2')^2 = k_+'^2 = k_+^2 = (k_1 + k_2)^2$, we obtain for the denominator of the W^+ boson

$$(q + k_+')^2 - M^2 = 2qk_+' + k_+'^2 - M^2 = 2qk_+ + k_+^2 - M^2 + \mathcal{O}(q_0^2)$$
$$= (q + k_+)^2 - M^2 + \mathcal{O}(q_0^2), \tag{3.1.22}$$

where $k_i' = k_i + \mathcal{O}(q_0)$ was used. Based on the power-counting argument given above, the terms of order q_0^2 can be neglected in DPA, and we find

$$(q + k_+')^2 - M^2 \sim (q + k_+)^2 - M^2. \tag{3.1.23}$$

If we choose to eliminate k_+', as done in the derivation of (3.1.21), we find, on the other hand,

$$(q + k_+')^2 - M^2 = (p_+ + p_- - k_-')^2 - M^2 = (p_+ + p_- - k_-)^2 - M^2 + \mathcal{O}(q_0)$$
$$= k_+^2 - M^2 + \mathcal{O}(q_0). \tag{3.1.24}$$

The $\mathcal{O}(q_0)$ terms are relevant in DPA [and in fact given by (3.1.22)]. As a consequence, (3.1.21) is not correct if we choose to fix $k_+'^2 = k_+^2$ when integrating over the photon momentum. For fixed $k_+'^2 = k_+^2$, (3.1.22) leads to the unique result (3.1.20) for the W^+ propagator in DPA, independently of the other phase-space parameters. If we choose, on the other hand, to fix $\bar{k}_+^2 = k_+^2$, which corresponds to a different definition of the invariant mass of the W^+ boson, we obtain

$$(q + k_+')^2 - M^2 = \bar{k}_+^2 - M^2, \tag{3.1.25}$$

and thus (3.1.21) instead of (3.1.20). Consequently, the different approaches (3.1.20) and (3.1.21) correspond to different definitions of the invariant mass of the W^+ boson which decays into the fermion pair $(f_1, \bar{f}_2)$. In order to define the DPA for real radiation, one has to specify at least the definition of the invariant masses of the W bosons that are kept fixed. In the following we always fix $k_+^2 = (k_1' + k_2')^2 = (k_1 + k_2)^2$ and $k_-^2 = (k_3' + k_4')^2 = (k_3 + k_4)^2$, as it was also implicitly done in Refs. [37, 38, 39]. Once the invariant masses of the W bosons are fixed in this way, the resulting formulae for the non-factorizable corrections hold independently of the choice of all other phase-space variables.

We stress that the results obtained within this parameterization of phase space differ from those in other parameterizations by doubly-resonant corrections. As already indicated in the introduction, in an experimentally more realistic approach the invariant masses of W bosons are identified with invariant masses of jet pairs, which also include part of the photon radiation. Since this situation can only be described with Monte Carlo programs, our results (as well as those of Refs. [37, 38, 39]) should be regarded as an estimate of the non-factorizable corrections.

3.1.5 Classification and gauge-independent definition of the non-factorizable doubly-resonant real corrections

The doubly-resonant real corrections can be classified in exactly the same way as the virtual corrections. For each virtual diagram there is exactly a real contribution, which
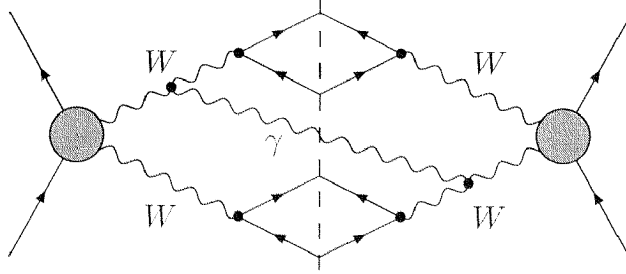
Figure 3.4: Real bremsstrahlung diagram containing non-factorizable and factorizable contributions.

we denote in the same way, e.g. ff' refers to all interferences where the photon is emitted by two fermions corresponding to the two different W bosons.

As in the case of the virtual corrections, one has to define the non-factorizable real corrections in a gauge-independent way. To this end, we proceed analogously and define the non-factorizable real corrections as the difference of the complete real corrections and the factorizable real corrections in DPA. The factorizable corrections are defined by the products of the matrix elements for on-shell W-pair production and decay with additional photon emission. There are three contributions to the factorizable real corrections, one where the photon is radiated during the production process and two where it is emitted during one of the W-boson decays. The corresponding matrix elements read

$$
\mathcal{M}_{\text{real},1} = \sum_{\lambda_+,\lambda_-} \frac{\mathcal{M}_{\text{Born}}^{e^+e^- \to W^+W^-\gamma} \mathcal{M}_{\text{Born}}^{W^+ \to f_1 \bar{f}_2} \mathcal{M}_{\text{Born}}^{W^- \to f_3 \bar{f}_4}}{(k_+^2 - M^2)(k_-^2 - M^2)},
$$

$$
\mathcal{M}_{\text{real},2} = \sum_{\lambda_+,\lambda_-} \frac{\mathcal{M}_{\text{Born}}^{e^+e^- \to W^+W^-} \mathcal{M}_{\text{Born}}^{W^+ \to f_1 \bar{f}_2 \gamma} \mathcal{M}_{\text{Born}}^{W^- \to f_3 \bar{f}_4}}{[(k_+ + q)^2 - M^2](k_-^2 - M^2)},
$$

$$
\mathcal{M}_{\text{real},3} = \sum_{\lambda_+,\lambda_-} \frac{\mathcal{M}_{\text{Born}}^{e^+e^- \to W^+W^-} \mathcal{M}_{\text{Born}}^{W^+ \to f_1 \bar{f}_2} \mathcal{M}_{\text{Born}}^{W^- \to f_3 \bar{f}_4 \gamma}}{(k_+^2 - M^2)[(k_- + q)^2 - M^2]}, \tag{3.1.26}
$$

in analogy to (3.1.8). Note that the matrix elements $\mathcal{M}_{\text{real},2}$ and $\mathcal{M}_{\text{real},3}$ involve an explicit q-dependent propagator. The factorizable corrections are given by the squares of these three matrix elements, and include by definition no interferences between them.

As an example for the extraction of non-factorizable corrections from real diagrams that involve both factorizable and non-factorizable corrections, we consider the contribution of the diagram in Fig. 3.4. After subtraction of the factorizable contribution, which originates from $|\mathcal{M}_{\text{real},1}|^2$, it gives rise to the following correction factor to the square $|\mathcal{M}_{\text{Born}}|^2$ of the lowest-order matrix element (3.1.8):

$$
\delta_{\text{real}}^{W^+W^-} = e^2 \int \frac{d^3\mathbf{q}}{(2\pi)^3 2q_0} 2 \, \text{Re} \left\{ \frac{4k_+ k_-}{[(k_+ + q)^2 - M^2][(k_- + q)^2 - (M^*)^2]} \right.
$$
$$
\left. - \left[\frac{4k_+ k_-}{2qk_+ 2qk_-} \right]_{k_\pm^2 = M_W^2} \right\} \Bigg|_{q_0 = \sqrt{\mathbf{q}^2 + \lambda^2}}. \tag{3.1.27}
$$

43

Note that the form of the correction factor is only correct for fixed $(k_1' + k_2')^2$ and $(k_3' + k_4')^2$. For other conventions the off-shell contribution changes, whereas the on-shell contribution stays the same. Using the relations (3.1.14) for $q^2 = 0$, in DPA we can rewrite (3.1.27) as

$$
\delta_{\text{real}}^{W^+W^-} \sim -e^2 \int \frac{d^3\mathbf{q}}{(2\pi)^3 2q_0} 2\,\text{Re}\left\{ \frac{k_+ k_-}{(qk_+)(qk_-)}\left[\frac{k_+^2 - M^2}{(k_+ + q)^2 - M^2} + \frac{k_-^2 - (M^*)^2}{(k_- + q)^2 - (M^*)^2} \right. \right.
$$
$$
\left. \left. - \frac{k_+^2 - M^2}{(k_+ + q)^2 - M^2}\frac{k_-^2 - (M^*)^2}{(k_- + q)^2 - (M^*)^2} \right] \right\}\bigg|_{q_0 = \sqrt{\mathbf{q}^2 + \lambda^2}}. \tag{3.1.28}
$$

In the same way, all other contributions that originate from a photon coupled to a W boson can be rewritten such that the complete real non-factorizable corrections can finally be expressed as the following correction factor to the lowest-order cross section,

$$
\delta_{\text{real,nf}} \sim -\int \frac{d^3\mathbf{q}}{(2\pi)^3 2q_0} 2\,\text{Re}\left[j_{\text{real}}^{e^+e^- \to W^+W^-,\mu}\left(j_{\text{real},\mu}^{W^+ \to f_1\bar{f}_2}\right)^* + j_{\text{real}}^{e^+e^- \to W^+W^-,\mu}\left(j_{\text{real},\mu}^{W^- \to f_3\bar{f}_4}\right)^* \right.
$$
$$
\left. + j_{\text{real}}^{W^+ \to f_1\bar{f}_2,\mu}\left(j_{\text{real},\mu}^{W^- \to f_3\bar{f}_4}\right)^* \right]\bigg|_{q_0 = \sqrt{\mathbf{q}^2 + \lambda^2}} \tag{3.1.29}
$$

with the currents

$$
j_{\text{real},\mu}^{e^+e^- \to W^+W^-} = e\left(\frac{k_{+\mu}}{qk_+} - \frac{k_{-\mu}}{qk_-} + \frac{p_{-\mu}}{qp_-} - \frac{p_{+\mu}}{qp_+} \right),
$$
$$
j_{\text{real},\mu}^{W^+ \to f_1\bar{f}_2} = e\left(Q_1\frac{k_{1\mu}}{qk_1} - Q_2\frac{k_{2\mu}}{qk_2} - \frac{k_{+\mu}}{qk_+} \right)\frac{k_+^2 - M^2}{(k_+ + q)^2 - M^2},
$$
$$
j_{\text{real},\mu}^{W^- \to f_3\bar{f}_4} = e\left(Q_3\frac{k_{3\mu}}{qk_3} - Q_4\frac{k_{4\mu}}{qk_4} + \frac{k_{-\mu}}{qk_-} \right)\frac{k_-^2 - M^2}{(k_- + q)^2 - M^2}. \tag{3.1.30}
$$

The factor (3.1.29) for the non-factorizable correction can be viewed as the interference contributions in the square of the matrix element (ε denotes the polarization vector of the photon)

$$
\mathcal{M}_{\text{real}} = \mathcal{M}_{\text{Born}}\,\varepsilon^{\mu}\left(j_{\text{real},\mu}^{e^+e^- \to W^+W^-} + j_{\text{real},\mu}^{W^+ \to f_1\bar{f}_2} + j_{\text{real},\mu}^{W^- \to f_3\bar{f}_4} \right), \tag{3.1.31}
$$

which is just the sum of the three matrix elements $\mathcal{M}_{\text{real},i}$, $i = 1, 2, 3$, in ESPA (including radiation from the external fermions and the internal W bosons). The respective squares of these three contributions correspond to the factorizable corrections. Note that $\mathcal{M}_{\text{Born}}^{e^+e^- \to W^+W^-}\varepsilon^{\mu}j_{\text{real},\mu}^{e^+e^- \to W^+W^-}$ is the soft-photon matrix element for on-shell W-pair production. Similarly, $\mathcal{M}_{\text{Born}}^{W^+ \to f_1\bar{f}_2}\varepsilon^{\mu}j_{\text{real},\mu}^{W^+ \to f_1\bar{f}_2}$ and $\mathcal{M}_{\text{Born}}^{W^- \to f_3\bar{f}_4}\varepsilon^{\mu}j_{\text{real},\mu}^{W^- \to f_3\bar{f}_4}$ correspond to the soft-photon matrix elements for the decays of the on-shell W bosons, apart from the extra factors $(k_\pm^2 - M^2)/[(k_\pm + q)^2 - M^2]$. These factors result from the definition of the lowest-order matrix element in terms of $k_\pm$ and from the fact that we impose $k_\pm'^2 = k_\pm^2$ and not $\bar{k}_\pm^2 = k_\pm^2$.

Obviously, the currents (3.1.30) are conserved, and the corresponding Ward identity for the $U(1)_{\text{em}}$ symmetry of the emitted photon is fulfilled.

3.2   Calculation of scalar integrals

In this section we set our conventions for the scalar integrals. We describe the reduction of the virtual and real 5-point functions to 4-point functions and indicate how the scalar integrals were evaluated. More details and the explicit results for the scalar integrals can be found in the appendix.

3.2.1   Reduction of 5-point functions

Reduction of virtual 5-point functions

The virtual 2-, 3-, 4-, and 5-point functions are defined as

$$
B_0(p_1, m_0, m_1) = \frac{1}{i\pi^2} \int d^4 q \, \frac{1}{N_0 N_1},
$$

$$
C_0(p_1, p_2, m_0, m_1, m_2) = \frac{1}{i\pi^2} \int d^4 q \, \frac{1}{N_0 N_1 N_2},
$$

$$
D_{\{0,\mu\}}(p_1, p_2, p_3, m_0, m_1, m_2, m_3) = \frac{1}{i\pi^2} \int d^4 q \, \frac{\{1, q_\mu\}}{N_0 N_1 N_2 N_3},
$$

$$
E_{\{0,\mu\}}(p_1, p_2, p_3, p_4, m_0, m_1, m_2, m_3, m_4) = \frac{1}{i\pi^2} \int d^4 q \, \frac{\{1, q_\mu\}}{N_0 N_1 N_2 N_3 N_4}, \tag{3.2.1}
$$

with the denominator factors

$$
N_0 = q^2 - m_0^2 + i\epsilon, \qquad N_i = (q + p_i)^2 - m_i^2 + i\epsilon, \qquad i = 1, \ldots, 4, \tag{3.2.2}
$$

where $i\epsilon$ ($\epsilon > 0$) denotes an infinitesimal imaginary part.

The reduction of the virtual 5-point function to 4-point functions is based on the fact that in four dimensions the integration momentum depends linearly on the four external momenta p_i [13, 44]. This gives rise to the identity

$$
0 = \begin{vmatrix} 2q^2 & 2qp_1 & \ldots & 2qp_4 \\ 2p_1 q & 2p_1^2 & \ldots & 2p_1 p_4 \\ \vdots & \vdots & \ddots & \vdots \\ 2p_4 q & 2p_4 p_1 & \ldots & 2p_4^2 \end{vmatrix} = \begin{vmatrix} 2N_0 + Y_{00} & 2qp_1 & \ldots & 2qp_4 \\ N_1 - N_0 + Y_{10} - Y_{00} & 2p_1^2 & \ldots & 2p_1 p_4 \\ \vdots & \vdots & \ddots & \vdots \\ N_4 - N_0 + Y_{40} - Y_{00} & 2p_4 p_1 & \ldots & 2p_4^2 \end{vmatrix} \tag{3.2.3}
$$

with

$$
Y_{00} = 2m_0^2, \quad Y_{i0} = Y_{0i} = m_0^2 + m_i^2 - p_i^2, \quad Y_{ij} = m_i^2 + m_j^2 - (p_i - p_j)^2, \quad i, j = 1, 2, 3, 4. \tag{3.2.4}
$$

Dividing this equation by $N_0 N_1 \cdots N_4$ and integrating over $d^4 q$ yields

$$
0 = \frac{1}{i\pi^2} \int d^4 q \, \frac{1}{N_0 N_1 \cdots N_4} \begin{vmatrix} 2N_0 + Y_{00} & 2qp_1 & \ldots & 2qp_4 \\ N_1 - N_0 + Y_{10} - Y_{00} & 2p_1^2 & \ldots & 2p_1 p_4 \\ \vdots & \vdots & \ddots & \vdots \\ N_4 - N_0 + Y_{40} - Y_{00} & 2p_4 p_1 & \ldots & 2p_4^2 \end{vmatrix}. \tag{3.2.5}
$$

Expanding the determinant along the first column, we obtain

$$
0 = \left[2D_0(0) + Y_{00}E_0 \right] \begin{vmatrix} 2p_1p_1 & \ldots & 2p_1p_4 \\ \vdots & \ddots & \vdots \\ 2p_4p_1 & \ldots & 2p_4p_4 \end{vmatrix}
$$

$$
+ \sum_{k=1}^{4} (-1)^k \left\{ D_\mu(k) - \left[D_\mu(0) + p_{4\mu}D_0(0) \right] + p_{4\mu}D_0(0) + (Y_{k0} - Y_{00})E_\mu \right\}
$$

$$
\times \begin{vmatrix} 2p_1^\mu & \ldots & 2p_4^\mu \\ 2p_1p_1 & \ldots & 2p_1p_4 \\ \vdots & \ddots & \vdots \\ 2p_{k-1}p_1 & \ldots & 2p_{k-1}p_4 \\ 2p_{k+1}p_1 & \ldots & 2p_{k+1}p_4 \\ \vdots & \ddots & \vdots \\ 2p_4p_1 & \ldots & 2p_4p_4 \end{vmatrix} , \tag{3.2.6}
$$

where $D_0(k)$ denotes the 4-point function that is obtained from the 5-point function E_0 by omitting the kth propagator N_k^{-1}. The terms involving $p_{4\mu}D_0(0)$ have been added for later convenience.

All integrals in (3.2.6) are UV-finite and Lorentz-covariant. Therefore, the vector integrals possess the following decompositions

$$
E_\mu = \sum_{i=1}^{4} E_i p_{i\mu},
$$

$$
D_\mu(k) = \sum_{\substack{i=1 \\ i \neq k}}^{4} D_i(k) p_{i\mu}, \qquad k = 1, 2, 3, 4,
$$

$$
D_\mu(0) + p_{4\mu}D_0(0) = \sum_{i=1}^{3} D_i(0)(p_i - p_4)_\mu. \tag{3.2.7}
$$

The last decomposition becomes obvious after performing a shift $q \to q - p_4$ in the integral. From (3.2.7) it follows immediately that the terms in (3.2.6) that involve $D_\mu(k)$ drop out when multiplied with the determinants, because the resulting determinants vanish. Similarly, $D_\mu(0) + p_{4\mu}D_0(0)$ vanishes after summation over k. Finally, the term $p_{4\mu}D_0(0)$ contributes only for $k = 4$, where it can be combined with the first term in (3.2.6). Rewriting the resulting equation as a determinant and reinserting the explicit form of the tensor integrals leads to

$$
0 = \frac{1}{i\pi^2} \int d^4q \, \frac{1}{N_0 N_1 \cdots N_4} \begin{vmatrix} N_0 + Y_{00} & 2qp_1 & \ldots & 2qp_4 \\ Y_{10} - Y_{00} & 2p_1p_1 & \ldots & 2p_1p_4 \\ \vdots & \vdots & \ddots & \vdots \\ Y_{40} - Y_{00} & 2p_4p_1 & \ldots & 2p_4p_4 \end{vmatrix} . \tag{3.2.8}
$$

Using

$$2p_i p_j = Y_{ij} - Y_{i0} - Y_{0j} + Y_{00},$$
$$2q p_j = N_j - N_0 + Y_{0j} - Y_{00}, \tag{3.2.9}$$

adding the first column to each of the other columns, and then enlarging the determinant by one column and one row, this can be written as

$$0 = \begin{vmatrix} 1 & Y_{00} & \dots & Y_{04} \\ 0 & D_0(0) + Y_{00}E_0 & \dots & D_0(4) + Y_{04}E_0 \\ 0 & Y_{10} - Y_{00} & \dots & Y_{14} - Y_{04} \\ \vdots & \vdots & \ddots & \vdots \\ 0 & Y_{40} - Y_{00} & \dots & Y_{44} - Y_{04} \end{vmatrix}. \tag{3.2.10}$$

Equation (3.2.10) is equivalent to

$$0 = \begin{vmatrix} -E_0 & D_0(0) & D_0(1) & D_0(2) & D_0(3) & D_0(4) \\ 1 & Y_{00} & Y_{01} & Y_{02} & Y_{03} & Y_{04} \\ 1 & Y_{10} & Y_{11} & Y_{12} & Y_{13} & Y_{14} \\ 1 & Y_{20} & Y_{21} & Y_{22} & Y_{23} & Y_{24} \\ 1 & Y_{30} & Y_{31} & Y_{32} & Y_{33} & Y_{34} \\ 1 & Y_{40} & Y_{41} & Y_{42} & Y_{43} & Y_{44} \end{vmatrix}, \tag{3.2.11}$$

which expresses the scalar 5-point function E_0 in terms of five scalar 4-point functions

$$E_0 = \frac{1}{\det(Y)} \sum_{i=0}^{4} \det(Y_i)\, D_0(i), \tag{3.2.12}$$

where $Y = (Y_{ij})$, and Y_i is obtained from Y by replacing all entries in the ith column with 1.

In the special case of an infrared singular 5-point function we have

$$Y_{00} = 2\lambda^2 \to 0, \qquad Y_{01} = m_1^2 - p_1^2 = 0, \qquad Y_{04} = m_4^2 - p_4^2 = 0, \tag{3.2.13}$$

and the determinants fulfill the relations

$$0 = \det(Y) - Y_{02}\det(Y_2) - Y_{03}\det(Y_3), \tag{3.2.14}$$
$$0 = (Y_{24} - Y_{02})\det(Y) + Y_{02}Y_{14}\det(Y_1) + (Y_{02}Y_{34} - Y_{03}Y_{24})\det(Y_3) + Y_{02}Y_{44}\det(Y_4),$$
$$0 = (Y_{31} - Y_{03})\det(Y) + Y_{03}Y_{11}\det(Y_1) + (Y_{03}Y_{21} - Y_{02}Y_{31})\det(Y_2) + Y_{03}Y_{41}\det(Y_4),$$

which allow the simplification of (3.2.12).

Reduction of real 5-point functions

The real 3-, 4-, and 5-point functions are defined as

$$
\mathcal{C}_0(p_1, p_2, \lambda, m_1, m_2) = \frac{2}{\pi} \int_{q_0 < \Delta E} \frac{\mathrm{d}^3 \mathbf{q}}{2 q_0} \left. \frac{1}{N_1' N_2'} \right|_{q_0 = \sqrt{\mathbf{q}^2 + \lambda^2}},
$$

$$
\mathcal{D}_0(p_1, p_2, p_3, \lambda, m_1, m_2, m_3) = \frac{2}{\pi} \int \frac{\mathrm{d}^3 \mathbf{q}}{2 q_0} \left. \frac{1}{N_1' N_2' N_3'} \right|_{q_0 = \sqrt{\mathbf{q}^2 + \lambda^2}},
$$

$$
\mathcal{E}_0(p_1, p_2, p_3, p_4, \lambda, m_1, m_2, m_3, m_4) = \frac{2}{\pi} \int \frac{\mathrm{d}^3 \mathbf{q}}{2 q_0} \left. \frac{1}{N_1' N_2' N_3' N_4'} \right|_{q_0 = \sqrt{\mathbf{q}^2 + \lambda^2}}, \qquad (3.2.15)
$$

with

$$
N_i' = 2 q p_i + p_i^2 - m_i^2, \qquad i = 1, \ldots, 4. \qquad (3.2.16)
$$

The shift of the integration boundary of q_0 to infinity leads to an artificial UV divergence in the 3-point function $\mathcal{C}_0$, which is regularized by an energy cutoff $\Delta E \to \infty$. In the following we only need differences of 3-point functions that are independent of ΔE and Lorentz-invariant.

Because of the appearance of UV-singular integrals in intermediate steps, the reasoning of the previous section cannot directly be applied to $\mathcal{E}_0$. Therefore, we rewrite the real 5-point function as an integral over a closed anticlockwise contour $\mathcal{C}$ in the q_0 plane and introduce a Lorentz-invariant UV regulator Λ:

$$
\mathcal{E}_0(p_1, p_2, p_3, p_4, \lambda, m_1, m_2, m_3, m_4) = \lim_{\Lambda \to \infty} \frac{1}{\mathrm{i} \pi^2} \int_{\mathcal{C}} \mathrm{d}^4 q \, \frac{1}{N_0' N_1' \cdots N_4'} \frac{-\Lambda^2}{q^2 - \Lambda^2} \qquad (3.2.17)
$$

with

$$
N_0' = q^2 - \lambda^2. \qquad (3.2.18)
$$

The contour $\mathcal{C}$ is chosen such that it includes the poles at $q_0 = \sqrt{\mathbf{q}^2 + \lambda^2}$ and $q_0 = \sqrt{\mathbf{q}^2 + \Lambda^2}$, but none else (see Fig. 3.5)[2].

The integral (3.2.17) can be reduced similarly to the virtual 5-point function. Owing to the different propagators N_i', (3.2.3) leads to

$$
0 = \lim_{\Lambda \to \infty} \frac{1}{\mathrm{i} \pi^2} \int_{\mathcal{C}} \mathrm{d}^4 q \, \frac{1}{N_0' N_1' \cdots N_4'} \frac{-\Lambda^2}{q^2 - \Lambda^2}
\begin{vmatrix}
2 N_0' & 2 q p_1 & \ldots & 2 q p_4 \\
N_1' + Y_{10} & 2 p_1^2 & \ldots & 2 p_1 p_4 \\
\vdots & \vdots & \ddots & \vdots \\
N_4' + Y_{40} & 2 p_4 p_1 & \ldots & 2 p_4^2
\end{vmatrix}
\qquad (3.2.19)
$$

instead of (3.2.5), with Y_{ij} from (3.2.4), and λ^2 can be set to zero in all Y_{ij}, in particular we have $Y_{00} = 2\lambda^2 \to 0$. After expanding the determinant along the first column and

---

[2] It is straightforward to check that the naive power counting for the UV behaviour in (3.2.17) is valid for time-like momenta p_i; light-like p_i can be treated as a limiting case. The basic idea for the proof is to deform the contour $\mathcal{C}$ to the vertical line $\mathrm{Re}\{q_0\} = |\mathbf{q}| - \epsilon$ with a small $\epsilon > 0$, which is allowed for sufficiently large $|\mathbf{q}|$, more precisely when all particle poles appear left from the line $\mathrm{Re}\{q_0\} = |\mathbf{q}| - \epsilon$.
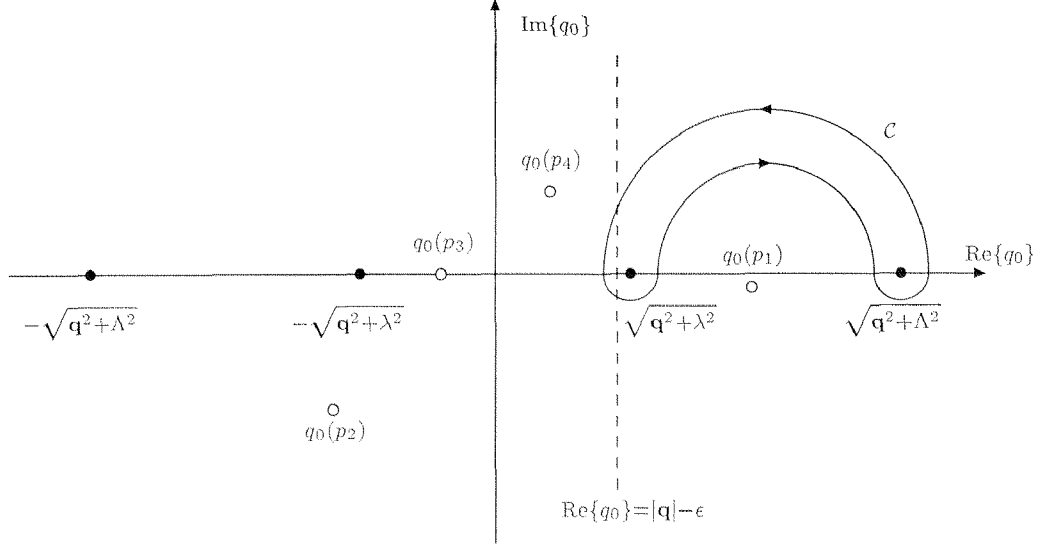
Figure 3.5: Illustration of the contour $\mathcal{C}$ of (3.2.17) in the complex q_0 plane. The open circles indicate the "particle poles" located at $q_0(p_i) = (2\mathbf{q}\mathbf{p}_i - p_i^2 + m_i^2)/(2p_{i0})$.

using the Lorentz decompositions of the integrals where N_k' is cancelled, we see that these terms vanish, and we are left with

$$0 = \lim_{\Lambda \to \infty} \frac{1}{i\pi^2} \int_{\mathcal{C}} \mathrm{d}^4 q \, \frac{1}{N_0' N_1' \cdots N_4'} \frac{-\Lambda^2}{q^2 - \Lambda^2} \begin{vmatrix} 2N_0' & 2qp_1 & \dots & 2qp_4 \\ Y_{10} & 2p_1^2 & \dots & 2p_1 p_4 \\ \vdots & \vdots & \ddots & \vdots \\ Y_{40} & 2p_4 p_1 & \dots & 2p_4^2 \end{vmatrix}. \tag{3.2.20}$$

Using

$$\begin{aligned} 2p_i p_j &= Y_{ij} - Y_{i0} - Y_{0j}, \\ 2qp_j &= N_j' + Y_{0j}, \end{aligned} \tag{3.2.21}$$

adding the first column to the other columns and extending the determinant leads to

$$0 = \lim_{\Lambda \to \infty} \frac{1}{i\pi^2} \int_{\mathcal{C}} \mathrm{d}^4 q \, \frac{1}{N_0' N_1' \cdots N_4'} \frac{-\Lambda^2}{q^2 - \Lambda^2} \begin{vmatrix} 1 & 0 & Y_{01} & \dots & Y_{04} \\ 0 & 2N_0' & N_1' + 2N_0' + Y_{01} & \dots & N_4' + 2N_0' + Y_{04} \\ 0 & Y_{10} & Y_{11} - Y_{01} & \dots & Y_{14} - Y_{04} \\ \vdots & \vdots & \vdots & \ddots & \vdots \\ 0 & Y_{40} & Y_{41} - Y_{01} & \dots & Y_{44} - Y_{04} \end{vmatrix}.$$

$$\tag{3.2.22}$$

Subtracting the first row from the second, adding the first row to the other rows, and exchanging the first two rows, we arrive at

$$
0 = \lim_{\Lambda \to \infty} \frac{1}{i\pi^2} \int_{\mathcal{C}} \mathrm{d}^4 q \, \frac{1}{N_0' N_1' \cdots N_4'} \frac{-\Lambda^2}{q^2 - \Lambda^2}
\begin{vmatrix}
-1 & 2N_0' & N_1' + 2N_0' & \cdots & N_4' + 2N_0' \\
1 & 0 & Y_{01} & \cdots & Y_{04} \\
1 & Y_{10} & Y_{11} & \cdots & Y_{14} \\
\vdots & \vdots & \vdots & \ddots & \vdots \\
1 & Y_{40} & Y_{41} & \cdots & Y_{44}
\end{vmatrix}.
\tag{3.2.23}
$$

Now we perform the contour integral using power counting for $\Lambda \to \infty$ (see footnote 2). In the contribution of the pole at $q_0 = \sqrt{\mathbf{q}^2 + \lambda^2}$ we have $N_0' = 0$ in the numerator; the limit $\Lambda \to \infty$ can be trivially taken and reproduces usual bremsstrahlung integrals, as defined in (3.2.15). In the contribution of the pole at $q_0 = \sqrt{\mathbf{q}^2 + \Lambda^2}$ the term containing N_0' in the numerator survives and will be calculated below, but all other terms vanish after taking the limit $\Lambda \to \infty$.

Thus, we find

$$
0 =
\begin{vmatrix}
-\mathcal{E}_0 & \tilde{\mathcal{D}}_0(0) & \mathcal{D}_0(1) + \tilde{\mathcal{D}}_0(0) & \mathcal{D}_0(2) + \tilde{\mathcal{D}}_0(0) & \mathcal{D}_0(3) + \tilde{\mathcal{D}}_0(0) & \mathcal{D}_0(4) + \tilde{\mathcal{D}}_0(0) \\
1 & Y_{00} & Y_{01} & Y_{02} & Y_{03} & Y_{04} \\
1 & Y_{10} & Y_{11} & Y_{12} & Y_{13} & Y_{14} \\
1 & Y_{20} & Y_{21} & Y_{22} & Y_{23} & Y_{24} \\
1 & Y_{30} & Y_{31} & Y_{32} & Y_{33} & Y_{34} \\
1 & Y_{40} & Y_{41} & Y_{42} & Y_{43} & Y_{44}
\end{vmatrix},
\tag{3.2.24}
$$

or

$$
\mathcal{E}_0 = \frac{1}{\det(Y)} \left\{ \det(Y_0) \, \tilde{\mathcal{D}}_0(0) + \sum_{i=1}^{4} \det(Y_i) \left[\mathcal{D}_0(i) + \tilde{\mathcal{D}}_0(0) \right] \right\}.
\tag{3.2.25}
$$

Here

$$
\tilde{\mathcal{D}}_0(0) = \lim_{\Lambda \to \infty} \frac{2}{i\pi^2} \int_{\mathcal{C}} \mathrm{d}^4 q \, \frac{1}{N_1' \cdots N_4'} \frac{-\Lambda^2}{q^2 - \Lambda^2},
\tag{3.2.26}
$$

and the 4-point bremsstrahlung integrals $\mathcal{D}_0(i)$, $i = 1, 2, 3, 4$, result from $\mathcal{E}_0$ by omitting the ith denominator N_i'. The result (3.2.24) differs from (3.2.10) only by the extra $\tilde{\mathcal{D}}_0(0)$'s added to the $\mathcal{D}_0(i)$'s.

The integral $\tilde{\mathcal{D}}_0(0)$ stems from the terms involving N_0' in the numerator in (3.2.23) and can be expressed as follows:

$$
\tilde{\mathcal{D}}_0(0) = \frac{2}{i\pi^2} \int_{\mathcal{C}'} \mathrm{d}^4 q' \, \frac{1}{2q' p_1 \cdots 2q' p_4} \frac{-1}{q'^2 - 1},
\tag{3.2.27}
$$

where the contour $\mathcal{C}'$ surrounds $q_0' = \sqrt{\mathbf{q}'^2 + 1}$. Performing the contour integral over $\mathrm{d}q_0'$ yields

$$
\tilde{\mathcal{D}}_0(0) = \frac{4}{\pi} \int \frac{\mathrm{d}^3 \mathbf{q}'}{2q_0'} \, \frac{1}{2q' p_1 \cdots 2q' p_4} \bigg|_{q_0' = \sqrt{\mathbf{q}'^2 + 1}}.
\tag{3.2.28}
$$

Now the vector q' is time-like. Since also the vectors p_i are time-like (or at least light-like), the scalar products $q'p_i$ cannot become zero. After redefining the momenta,

$$p_i = \sigma_i \tilde{p}_i, \qquad \sigma_i = \pm 1, \qquad \tilde{p}_{i0} > 0, \tag{3.2.29}$$

and extracting the signs σ_i, this integral can be evaluated by a Feynman-parameter representation and momentum integration in polar coordinates resulting in:

$$\tilde{\mathcal{D}}_0(0) = -\sigma_1 \sigma_2 \sigma_3 \sigma_4 \int_0^\infty dx_1\, dx_2\, dx_3\, dx_4\, \delta\left(1 - \sum_{i=1}^4 x_i\right) \left[\left(\sum_{i=1}^4 x_i \tilde{p}_i\right)^2\right]^{-2}. \tag{3.2.30}$$

This is just the Feynman-parameter representation of a virtual 4-point function such that we finally obtain

$$\tilde{\mathcal{D}}_0(0) = -\sigma_1 \sigma_2 \sigma_3 \sigma_4 D_0\left(\tilde{p}_2 - \tilde{p}_1, \tilde{p}_3 - \tilde{p}_1, \tilde{p}_4 - \tilde{p}_1, \sqrt{p_1^2}, \sqrt{p_2^2}, \sqrt{p_3^2}, \sqrt{p_4^2}\right). \tag{3.2.31}$$

Explicit reduction of the virtual 5-point function for the photon exchange between $\bar{f}_2$ and f_3

For the photon exchange between $\bar{f}_2$ and f_3 the following scalar integrals are relevant:

$$\begin{aligned}
E_0 &= E_0(-k_3, -k_-, k_+, k_2, \lambda, m_3, M, M, m_2), \\
D_0(0) &= D_0(-k_4, k_+ + k_3, k_2 + k_3, 0, M, M, 0), \\
D_0(1) &= D_0(-k_-, k_+, k_2, 0, M, M, m_2), \\
D_0(2) &= D_0(-k_3, k_+, k_2, \lambda, m_3, M, m_2), \\
D_0(3) &= D_0(-k_3, -k_-, k_2, \lambda, m_3, M, m_2), \\
D_0(4) &= D_0(-k_3, -k_-, k_+, 0, m_3, M, M).
\end{aligned} \tag{3.2.32}$$

Since we neglect the external fermion masses, the last two relations (3.2.14) simplify to

$$0 = (s_{23} + s_{24}) \det(Y) + K_- s_{23} \det(Y_1) - \left[K_+(s_{23} + s_{24}) + K_- M_+^2\right] \det(Y_3),$$

$$0 = (s_{13} + s_{23}) \det(Y) + K_+ s_{23} \det(Y_4) - \left[K_-(s_{13} + s_{23}) + K_+ M_-^2\right] \det(Y_2). \tag{3.2.33}$$

These relations allow us to eliminate $\det(Y_1)$ and $\det(Y_4)$ from (3.2.12), resulting in:

$$\begin{aligned}
E_0(-k_3, -k_-, k_+, k_2, \lambda, m_3, M, M, m_2) &= \frac{\det(Y_0)}{\det(Y)} D_0(0) \\
&+ \frac{\det(Y_3)}{\det(Y) K_- s_{23}} \left\{ [K_+(s_{23} + s_{24}) + K_- M_+^2] D_0(1) + K_- s_{23} D_0(3) \right\} \\
&+ \frac{\det(Y_2)}{\det(Y) K_+ s_{23}} \left\{ [K_-(s_{13} + s_{23}) + K_+ M_-^2] D_0(4) + K_+ s_{23} D_0(2) \right\} \\
&- \frac{s_{13} + s_{23}}{K_+ s_{23}} D_0(4) - \frac{s_{23} + s_{24}}{K_- s_{23}} D_0(1).
\end{aligned} \tag{3.2.34}$$

The matrix Y reads

$$Y = \begin{pmatrix} 0 & 0 & -K_- & -K_+ & 0 \\ * & 0 & M^2 & (-K_+ - s_{13} - s_{23}) & -s_{23} \\ * & * & 2M^2 & 2M^2 - s & (-K_- - s_{23} - s_{24}) \\ * & * & * & 2M^2 & M^2 \\ * & * & * & * & 0 \end{pmatrix}. \qquad (3.2.35)$$

Neglecting terms that do not contribute to the correction factor in DPA, the corresponding determinants are given by

$$\det(Y) \sim 2s_{23}\left[K_+ K_- s_{14} s_{23} - (K_+ M_W^2 + K_- s_{13})(K_- M_W^2 + K_+ s_{24})\right],$$

$$\det(Y_0) \sim -\kappa_W^2,$$

$$\det(Y_1) \sim K_+\left[M_W^4(s_{23} - s_{24}) + (s_{23} + s_{24})(s_{13} s_{24} - s_{14} s_{23})\right]$$
$$\quad + K_- M_W^2(-M_W^4 + 2s_{13} s_{23} + s_{13} s_{24} + s_{14} s_{23}),$$

$$\det(Y_2) \sim -s_{23}\left[K_+(M_W^4 + s_{13} s_{24} - s_{14} s_{23}) + 2K_- M_W^2 s_{13}\right],$$

$$\det(Y_3) = \det(Y_2)|_{K_+ \leftrightarrow K_-, s_{13} \leftrightarrow s_{24}},$$

$$\det(Y_4) = \det(Y_1)|_{K_+ \leftrightarrow K_-, s_{13} \leftrightarrow s_{24}}, \qquad (3.2.36)$$

where the shorthand κ_W is defined in Appendix A.1.

Explicit reduction of the real 5-point function for the photon exchange between $\bar{f}_2$ and f_3

In this case the integrals appearing in (3.2.25) read

$$\mathcal{E}_0 = \mathcal{E}_0(k_3, k_-, k_+, k_2, \lambda, m_3, M^*, M, m_2),$$

$$\tilde{\mathcal{D}}_0(0) = -\mathcal{D}_0(k_4, k_+ - k_3, k_2 - k_3, 0, M_-, M_+, 0),$$

$$\mathcal{D}_0(1) = \mathcal{D}_0(k_-, k_+, k_2, 0, M^*, M, m_2),$$

$$\mathcal{D}_0(2) = \mathcal{D}_0(k_3, k_+, k_2, \lambda, m_3, M, m_2),$$

$$\mathcal{D}_0(3) = \mathcal{D}_0(k_3, k_-, k_2, \lambda, m_3, M^*, m_2),$$

$$\mathcal{D}_0(4) = \mathcal{D}_0(k_3, k_-, k_+, 0, m_3, M^*, M). \qquad (3.2.37)$$

In analogy to the virtual 5-point function, we can express the real 5-point function with the help of the relations (we denote the matrix Y for the real 5-point function with a prime, in order to distinguish it from the one for the virtual 5-point function):

$$0 = (s_{23} + s_{24})\det(Y') + K_-^* s_{23}\det(Y_1') - \left[K_+(s_{23} + s_{24}) - K_-^* M_+^2\right]\det(Y_3'),$$

$$0 = (s_{13} + s_{23})\det(Y') + K_+ s_{23}\det(Y_4') - \left[K_-^*(s_{13} + s_{23}) - K_+ M_-^2\right]\det(Y_2'), \quad (3.2.38)$$

by

$$\mathcal{E}_0(k_3, k_-, k_+, k_2, \lambda, m_3, M^*, M, m_2) = \frac{\det(Y_0')}{\det(Y')}\tilde{\mathcal{D}}_0(0)$$

$$+ \frac{\det(Y_3')}{\det(Y')K_-^* s_{23}} \left\{ \left[K_+(s_{23} + s_{24}) - K_-^* M_+^2 \right] \left[\mathcal{D}_0(1) + \tilde{\mathcal{D}}_0(0) \right] + K_-^* s_{23} \left[\mathcal{D}_0(3) + \tilde{\mathcal{D}}_0(0) \right] \right\}$$

$$+ \frac{\det(Y_2')}{\det(Y')K_+ s_{23}} \left\{ \left[K_-^* (s_{13} + s_{23}) - K_+ M_-^2 \right] \left[\mathcal{D}_0(4) + \tilde{\mathcal{D}}_0(0) \right] + K_+ s_{23} \left[\mathcal{D}_0(2) + \tilde{\mathcal{D}}_0(0) \right] \right\}$$

$$- \frac{s_{13} + s_{23}}{K_+ s_{23}} \left[\mathcal{D}_0(4) + \tilde{\mathcal{D}}_0(0) \right] - \frac{s_{23} + s_{24}}{K_-^* s_{23}} \left[\mathcal{D}_0(1) + \tilde{\mathcal{D}}_0(0) \right]. \tag{3.2.39}$$

For the matrix Y' we find

$$Y' = \begin{pmatrix} 0 & 0 & -K_-^* & -K_+ & 0 \\ * & 0 & (M^*)^2 & (-K_+ + s_{13} + s_{23}) & s_{23} \\ * & * & 2(M^*)^2 & (-2K_+ - 2K_-^* + s - (M^*)^2 - M^2) & (-K_-^* + s_{23} + s_{24}) \\ * & * & * & 2M^2 & M^2 \\ * & * & * & * & 0 \end{pmatrix}. \tag{3.2.40}$$

Replacing $-K_-^*$ by K_- and $(M^*)^2$ by M^2 and multiplying the second and third columns and rows by -1, this becomes equal to (3.2.35) in DPA.

In DPA, $\tilde{\mathcal{D}}_0(0)$ can be neglected in the terms $\mathcal{D}_0(i) + \tilde{\mathcal{D}}_0(0)$ in (3.2.25) and (3.2.39), and the reduction of the real 5-point function becomes algebraically identical to the reduction of the virtual 5-point function, apart from the differences in signs of some momenta. As a consequence, the results for the virtual corrections can be translated to the real case if we substitute $K_- \to -K_-^*$ in all algebraic factors such as the determinants and $E_0 \to \mathcal{E}_0$, $D_0(0) \to \tilde{\mathcal{D}}_0(0)$, $D_0(1) \to -\mathcal{D}_0(1)$, $D_0(2) \to -\mathcal{D}_0(2)$, $D_0(3) \to \mathcal{D}_0(3)$ and $D_0(4) \to \mathcal{D}_0(4)$. In particular, the determinants are related by

$$\det(Y') \sim + \det(Y)\big|_{K_- \to -K_-^*}, \qquad \det(Y_0') \sim + \det(Y_0) \sim -\kappa_W^2,$$

$$\det(Y_1') \sim - \det(Y_1)\big|_{K_- \to -K_-^*}, \qquad \det(Y_2') \sim - \det(Y_2)\big|_{K_- \to -K_-^*},$$

$$\det(Y_3') \sim + \det(Y_3)\big|_{K_- \to -K_-^*}, \qquad \det(Y_4') \sim + \det(Y_4)\big|_{K_- \to -K_-^*}. \tag{3.2.41}$$

3.2.2 Calculation of 3- and 4-point functions

The scalar loop integrals have been evaluated following the methods of Ref. [43]. Our explicit results are listed in Appendix A.3. For vanishing W-boson width they agree with the general results of Ref. [43]. For finite W-boson width the virtual 4-point functions are in agreement with those of Refs. [38, 39] in DPA. This shows explicitly that the q^2 terms in the W-boson and fermion propagators are irrelevant in DPA.

An evaluation of the bremsstrahlung integrals, which follows closely the techniques for calculating loop integrals, is sketched in Appendix A.2. The final results in DPA are listed in Appendix A.3, and the 4-point functions agree with those of Refs. [38, 39]. We have analytically reproduced all exact results for the occurring bremsstrahlung 3- and 4-point integrals by independent methods. In addition, we have evaluated the IR-finite integrals

$\mathcal{D}_0(1)$, $\mathcal{D}_0(4)$, and $\mathcal{E}_0 - \mathcal{D}_0(3)/K_+$ by a direct Monte Carlo integration over the photon momentum, yielding perfect agreement with our exact analytical results for these integrals. Note that this, in particular, checks the reduction of the bremsstrahlung 5-point function described in the previous section.

Our results for the 3-point functions cannot directly be compared with those of Refs. [38, 39], because different approaches have been used. While our results are IR-singular owing to the subtracted on-shell integrals, the results of Refs. [38, 39] are artificially UV-singular owing to the neglect of q^2 in the W propagators. However, when adding the real and virtual 3-point functions the two results agree. This confirms that our definition of the non-factorizable corrections is equivalent to the one of Refs. [38, 39] in DPA. Thus, it turns out that in DPA the subtraction of the on-shell contribution is effectively equivalent to the neglect of the q^2 terms in all but the photon propagators.

3.3 Analytic results for the non-factorizable corrections

3.3.1 General properties of non-factorizable corrections

In Ref. [37] it was shown from the integral representation that the non-factorizable corrections associated with photon exchange between initial and final state vanish in DPA. This was confirmed in Refs. [38, 39]. Via explicit evaluation of all integrals we have checked that the cancellation between virtual and real integrals takes place diagram by diagram once the factorizable contributions are subtracted. In this way all interference terms (if), (mf), (im), and (mm) drop out. Examples for the virtual Feynman diagrams contributing to these types of corrections are shown in Fig. 3.2.

The only non-vanishing non-factorizable corrections are due to the contributions (ff'), (mf'), and (mm'). The corresponding virtual diagrams are shown in Fig. 3.1, apart from permutations of the final-state fermions. Two of the corresponding real diagrams are pictured in Figs. 3.3 and 3.4. Since these corrections depend only on s-channel invariants, the non-factorizable corrections are independent of the production angle of the W bosons, as was also pointed out in Refs. [38, 39].

3.3.2 Generic form of the correction factor

The non-factorizable corrections $d\sigma_{\mathrm{nf}}$ to the fully differential lowest-order cross-section $d\sigma_{\mathrm{Born}}$ resulting from the matrix element (3.1.8) take the form of a correction factor to the lowest-order cross-section:

$$d\sigma_{\mathrm{nf}} = \delta_{\mathrm{nf}}\, d\sigma_{\mathrm{Born}}. \tag{3.3.1}$$

Upon splitting the contributions that result from photons coupled to the W bosons according to $1 = Q_{\mathrm{W}+} = Q_1 - Q_2$ and $1 = -Q_{\mathrm{W}-} = Q_4 - Q_3$ into contributions associated with definite final-state fermions, the complete correction factor to the lowest-order cross-section can be written as

$$\delta_{\mathrm{nf}} = \sum_{a=1,2} \sum_{b=3,4} (-1)^{a+b+1}\, Q_a Q_b\, \frac{\alpha}{\pi}\, \mathrm{Re}\{\Delta(k_+, k_a; k_-, k_b)\}. \tag{3.3.2}$$

In the following, only $\Delta = \Delta(k_+, k_2; k_-, k_3)$ is given; the other terms follow by obvious substitutions. As discussed above, Δ gets contributions from *intermediate–intermediate* ($\Delta_{\mathrm{mm'}}$), *intermediate–final* ($\Delta_{\mathrm{mf'}}$), and *final–final* ($\Delta_{\mathrm{ff'}}$) interactions:

$$\Delta = \Delta_{\mathrm{mm'}} + \Delta_{\mathrm{mf'}} + \Delta_{\mathrm{ff'}}. \tag{3.3.3}$$

The quantity ($\Delta_{\mathrm{mm'}}$ is independent of the final-state fermions. The individual contributions read

$$\Delta_{\mathrm{mm'}} \sim \left(2M_{\mathrm{W}}^2 - s\right)\Big\{ C_0(k_+, -k_-, 0, M, M) - \big[C_0(k_+, -k_-, \lambda, M_{\mathrm{W}}, M_{\mathrm{W}})\big]_{k_\pm^2 = M_{\mathrm{W}}^2}$$
$$- \mathcal{C}_0(k_+, k_-, 0, M, M^*) + \big[\mathcal{C}_0(k_+, k_-, \lambda, M_{\mathrm{W}}, M_{\mathrm{W}})\big]_{k_\pm^2 = M_{\mathrm{W}}^2} \Big\}, \tag{3.3.4}$$

$$\Delta_{\mathrm{mf'}} \sim -(s_{23} + s_{24})\big[K_+ D_0(1) - K_+ \mathcal{D}_0(1)\big] - (s_{13} + s_{23})\big[K_- D_0(4) - K_-^* \mathcal{D}_0(4)\big], \tag{3.3.5}$$

$$\Delta_{\mathrm{ff'}} \sim -K_+ s_{23}\big[K_- E_0 - K_-^* \mathcal{E}_0\big], \tag{3.3.6}$$

with the arguments of the 5- and 4-point functions as defined in (3.2.32) and (3.2.37).

The sum $\Delta_{\mathrm{mf'}} + \Delta_{\mathrm{ff'}}$ can be simplified by inserting the decompositions of the 5-point functions (3.2.34) and (3.2.39). In DPA this leads to

$$\Delta_{\mathrm{mf'}} + \Delta_{\mathrm{ff'}} \sim -\frac{K_+ K_- s_{23} \det(Y_0)}{\det(Y)} D_0(0) + \frac{K_+ K_-^* s_{23} \det(Y_0')}{\det(Y')} \tilde{\mathcal{D}}_0(0)$$
$$- \frac{K_+ \det(Y_3)}{\det(Y)} \Big\{ [K_+(s_{23} + s_{24}) + K_- M_{\mathrm{W}}^2] D_0(1) + K_- s_{23} D_0(3) \Big\}$$
$$- \frac{K_- \det(Y_2)}{\det(Y)} \Big\{ [K_-(s_{13} + s_{23}) + K_+ M_{\mathrm{W}}^2] D_0(4) + K_+ s_{23} D_0(2) \Big\}$$
$$+ \frac{K_+ \det(Y_3')}{\det(Y')} \Big\{ [K_+(s_{23} + s_{24}) - K_-^* M_{\mathrm{W}}^2] \mathcal{D}_0(1) + K_-^* s_{23} \mathcal{D}_0(3) \Big\}$$
$$+ \frac{K_-^* \det(Y_2')}{\det(Y')} \Big\{ [K_-^*(s_{13} + s_{23}) - K_+ M_{\mathrm{W}}^2] \mathcal{D}_0(4) + K_+ s_{23} \mathcal{D}_0(2) \Big\}. \tag{3.3.7}$$

Note that $\Delta_{\mathrm{mf'}}$ is exactly cancelled by the contributions of the last two terms in (3.2.34) and (3.2.39).

Inserting the expressions for the scalar integrals from Appendix A.3 and using the first of the relations (3.2.14), various terms, notably all IR divergences and mass-singular logarithms, cancel between the real and virtual corrections, and in DPA we are left with

$$\Delta_{\mathrm{mm'}} \sim \frac{2M_{\mathrm{W}}^2 - s}{s\beta_{\mathrm{W}}} \Bigg[-\mathcal{L}i_2\Big(\frac{K_-}{K_+}, x_{\mathrm{W}}\Big) + \mathcal{L}i_2\Big(\frac{K_-}{K_+}, x_{\mathrm{W}}^{-1}\Big) + \mathcal{L}i_2\Big(-\frac{K_-^*}{K_+}, x_{\mathrm{W}}\Big)$$
$$- \mathcal{L}i_2\Big(-\frac{K_-^*}{K_+}, x_{\mathrm{W}}^{-1}\Big) + 2\pi i \ln\Big(\frac{K_+ + K_-^* x_{\mathrm{W}}}{iM_{\mathrm{W}}^2}\Big) \Bigg] + \text{imaginary parts}, \tag{3.3.8}$$

$$\Delta_{\mathrm{mf'}} + \Delta_{\mathrm{ff'}} \sim -\frac{K_+ K_- s_{23} \det(Y_0)}{\det(Y)} D_0(0) - \frac{K_+ \det(Y_3)}{\det(Y)} F_3 - \frac{K_- \det(Y_2)}{\det(Y)} F_2$$
$$+ \frac{K_+ K_-^* s_{23} \det(Y_0')}{\det(Y')} \tilde{\mathcal{D}}_0(0) + \frac{K_+ \det(Y_3')}{\det(Y')} \mathcal{F}_3 + \frac{K_-^* \det(Y_2')}{\det(Y')} \mathcal{F}_2$$
$$+ \text{imaginary parts}, \tag{3.3.9}$$

with $D_0(0)$ and $\tilde{D}_0(0)$ given in (A.18) and (A.26), respectively, and

$$
F_3 = -2\,\mathcal{L}i_2\left(\frac{K_+}{K_-}, -\frac{s_{23}+s_{24}}{M_W^2} - i\epsilon\right) + \sum_{\tau=\pm 1}\left[\mathcal{L}i_2\left(\frac{K_+}{K_-}, x_W^\tau\right) - \mathcal{L}i_2\left(-\frac{M_W^2}{s_{23}+s_{24}} + i\epsilon, x_W^\tau\right)\right]
$$
$$
- \mathrm{Li}_2\left(-\frac{s_{24}}{s_{23}}\right) + 2\ln\left(-\frac{s_{23}}{M_W^2} - i\epsilon\right)\ln\left(-\frac{K_-}{M_W^2}\right) - \ln^2\left(-\frac{s_{23}+s_{24}}{M_W^2} - i\epsilon\right),
$$

$$
\mathcal{F}_3 = F_3\Big|_{K_-\to-K_-^*} + 2\pi i\left[2\ln\left(1 - \frac{K_+}{K_-^*}\frac{s_{23}+s_{24}}{M_W^2}\right) - \ln\left(1 + \frac{K_+}{K_-^* x_W}\right) - \ln\left(1 + \frac{x_W M_W^2}{s_{23}+s_{24}}\right)\right.
$$
$$
\left. + \ln\left(\frac{iK_-^*}{s_{23}+s_{24}}\right)\right],
$$

$$
F_2 = F_3\Big|_{K_+\leftrightarrow K_-,\,s_{24}\leftrightarrow s_{13}},
$$

$$
\mathcal{F}_2 = F_2\Big|_{K_-\to-K_-^*} + 2\pi i\left\{\ln\left(1 + \frac{K_-^* x_W}{K_+}\right) - \ln\left(1 + \frac{x_W M_W^2}{s_{13}+s_{23}}\right) + \ln\left[\frac{K_+ s_{23}}{iM_W^2(s_{13}+s_{23})}\right]\right\}.
$$
$$
(3.3.10)
$$

The variables β_W, x_W and the dilogarithms Li_2, $\mathcal{L}i_2$ are defined in Appendix A.1.

The above results contain logarithms and dilogarithms the arguments of which depend on $K_\pm$. It is interesting to see whether enhanced logarithms of the form $\ln(K_\pm/M_W^2)$ appear in the limits $K_\pm \to 0$. It turns out that such logarithms are absent from the non-factorizable corrections, irrespective of the ratio in which the two limits $K_\pm \to 0$ are realized.

Moreover, the non-factorizable corrections vanish in the high-energy limit. This feature of the non-factorizable corrections has been checked by analytical and numerical calculations.

3.3.3 Non-factorizable virtual corrections

In Chapter 4 the factorizable and non-factorizable radiative corrections to four-fermion production are investigated. In order to overcome the problem of overlapping resonances for the DPA of the real corrections discussed in Section 4.1.3, the complete real process, involving resonant and non-resonant diagrams, is evaluated by Monte Carlo integration. On the other hand, only the doubly-resonant part of the virtual corrections is taken into account. Therefore, the results of the non-factorizable virtual corrections are required separately.

As in Section 3.3.2, the non-factorizable virtual corrections factorize to the lowest-order cross section:

$$
d\sigma_{nf}^{virt} = \delta_{nf}^{virt}\,d\sigma_{Born} \tag{3.3.11}
$$

with

$$
\delta_{nf}^{virt} = \sum_{a=1,2}\sum_{b=3,4}(-1)^{a+b+1}\,Q_a Q_b\,\frac{\alpha}{\pi}\,\mathrm{Re}\{\Delta^{virt}(k_+, k_a; k_-, k_b)\}. \tag{3.3.12}
$$

The explicit results of the term $\Delta^{\mathrm{virt}} = \Delta^{\mathrm{virt}}(k_+, k_2; k_-, k_3)$ are listed in the following:

$$\Delta^{\mathrm{virt}} = \Delta^{\mathrm{virt}}_{\mathrm{mm}} + \Delta^{\mathrm{virt}}_{\mathrm{mf}} + \Delta^{\mathrm{virt}}_{\mathrm{im}} + \Delta^{\mathrm{virt}}_{\mathrm{mm}'} + \Delta^{\mathrm{virt}}_{\mathrm{if}} + \Delta^{\mathrm{virt}}_{\mathrm{mf}'} + \Delta^{\mathrm{virt}}_{\mathrm{ff}'}. \tag{3.3.13}$$

with the individual contributions of the diagrams shown in Fig. 3.1 and Fig. 3.2

$$\Delta^{\mathrm{virt}}_{\mathrm{mm}} \sim \frac{2M_{\mathrm{W}}^2}{k_+^2 - M^2} \left\{ B_0(k_+, 0, M) - \left[B_0(k_+, 0, M) \right]_{k_+^2 = M^2} \right\}$$
$$- 2M_{\mathrm{W}}^2 \left[B_0'(k_+, \lambda, M_{\mathrm{W}}) \right]_{k_+^2 = M_{\mathrm{W}}^2} + (k_+ \leftrightarrow k_-), \tag{3.3.14}$$

$$\Delta^{\mathrm{virt}}_{\mathrm{mf}} \sim M_{\mathrm{W}}^2 \left\{ C_0(k_2, k_+, 0, m_2, M) - \left[C_0(k_2, k_+, \lambda, m_2, M_{\mathrm{W}}) \right]_{k_+^2 = M_{\mathrm{W}}^2} \right\}$$
$$+ (k_2 \leftrightarrow k_3, k_+ \leftrightarrow k_-), \tag{3.3.15}$$

$$\Delta^{\mathrm{virt}}_{\mathrm{im}} \sim 2k_+ p_+ \left\{ C_0(p_+, k_+, 0, m_{\mathrm{e}}, M) - \left[C_0(p_+, k_+, \lambda, m_{\mathrm{e}}, M_{\mathrm{W}}) \right]_{k_+^2 = M_{\mathrm{W}}^2} \right\}$$
$$+ (p_+ \leftrightarrow p_-, k_+ \leftrightarrow k_-) - (k_+ \leftrightarrow k_-) - (p_+ \leftrightarrow p_-), \tag{3.3.16}$$

$$\Delta^{\mathrm{virt}}_{\mathrm{mm}'} \sim -2k_+ k_- \left\{ C_0(k_+, -k_-, 0, M, M) - \left[C_0(k_+, -k_-, \lambda, M_{\mathrm{W}}, M_{\mathrm{W}}) \right]_{k_\pm^2 = M_{\mathrm{W}}^2} \right\}, \tag{3.3.17}$$

$$\Delta^{\mathrm{virt}}_{\mathrm{if}} \sim 2p_+ k_2 K_+ D_0(p_+, k_+, k_2, \lambda, m_{\mathrm{e}}, M, m_2)$$
$$- (p_+ \leftrightarrow p_-) - (k_2 \leftrightarrow k_3, k_+ \leftrightarrow k_-) + (k_2 \leftrightarrow k_3, k_+ \leftrightarrow k_-, p_+ \leftrightarrow p_-), \tag{3.3.18}$$

$$\Delta^{\mathrm{virt}}_{\mathrm{mf}'} \sim -2k_2 k_- K_+ D_0(1) - 2k_3 k_+ K_- D_0(4), \tag{3.3.19}$$

$$\Delta^{\mathrm{virt}}_{\mathrm{ff}'} \sim -2k_2 k_3 K_+ K_- E_0. \tag{3.3.20}$$

The other terms, $\Delta^{\mathrm{virt}}(k_+, k_a; k_-, k_b)$, can be obtained by obvious substitutions.

Contributions of the diagrams (if), (im), (mf), and (mm) of Fig. 3.2 cancel in the sum of virtual and real corrections in DPA but remain for the virtual corrections. After combining several diagrams the result becomes relatively simple:

$$\Delta^{\mathrm{virt}}_{\mathrm{mm}} \sim -2\ln\left(\frac{K_+}{M_{\mathrm{W}}^2}\right) - 2\ln\left(\frac{K_-}{M_{\mathrm{W}}^2}\right) + 4\ln\left(\frac{\lambda}{M_{\mathrm{W}}}\right) + 4, \tag{3.3.21}$$

$$\Delta^{\mathrm{virt}}_{\mathrm{mm}'} \sim \frac{2M_{\mathrm{W}}^2 - s}{s\beta_{\mathrm{W}}} \left[-\mathcal{L}i_2\left(\frac{K_-}{K_+}, x_{\mathrm{W}}\right) + \mathcal{L}i_2\left(\frac{K_-}{K_+}, x_{\mathrm{W}}^{-1}\right) + \mathrm{Li}_2(1 - x_{\mathrm{W}}^2) + \pi^2 + \ln^2(-x_{\mathrm{W}}) \right.$$
$$\left. + 2\ln\left(\frac{K_+}{\lambda M_{\mathrm{W}}}\right) \ln(x_{\mathrm{W}}) - 2\pi \mathrm{i} \ln(1 - x_{\mathrm{W}}^2) \right] + \text{imaginary parts}, \tag{3.3.22}$$

and

$$\Delta^{\mathrm{virt}}_{\mathrm{mf}} + \Delta^{\mathrm{virt}}_{\mathrm{im}} + \Delta^{\mathrm{virt}}_{\mathrm{if}} + \Delta^{\mathrm{virt}}_{\mathrm{mf}'} + \Delta^{\mathrm{virt}}_{\mathrm{ff}'} \sim \ln\left(\frac{\lambda^2}{M_{\mathrm{W}}^2}\right) \ln\left(\frac{-s_{23} - \mathrm{i}\epsilon}{M_{\mathrm{W}}^2}\right)$$
$$- \frac{K_+ K_- s_{23} \det(Y_0)}{\det(Y)} D_0(0) - \frac{K_+ \det(Y_3)}{\det(Y)} F_3 - \frac{K_- \det(Y_2)}{\det(Y)} F_2$$
$$+ 2\ln\left(\frac{-K_+}{\lambda M_{\mathrm{W}}}\right) \ln\left(\frac{u_{-2}(M_{\mathrm{W}}^2 - t)}{t_{+2}(M_{\mathrm{W}}^2 - u)}\right) + 2\ln\left(\frac{-K_-}{\lambda M_{\mathrm{W}}}\right) \ln\left(\frac{u_{+3}(M_{\mathrm{W}}^2 - t)}{t_{-3}(M_{\mathrm{W}}^2 - u)}\right)$$

$$+ \mathrm{Li}_2\left(1 - \frac{t - M_W^2}{t_{+2}}\right) + \mathrm{Li}_2\left(1 - \frac{t - M_W^2}{t_{-3}}\right)$$

$$- \mathrm{Li}_2\left(1 - \frac{u - M_W^2}{u_{+3}}\right) - \mathrm{Li}_2\left(1 - \frac{u - M_W^2}{u_{-2}}\right). \tag{3.3.23}$$

where $D_0(0)$ can be found in (A.18) and the variables β_W, x_W and the dilogarithms Li_2, $\mathcal{L}i_2$ are defined in Appendix A.1.

All mass singularities vanish in the non-factorizable virtual correction factor $\delta_{\mathrm{nf}}^{\mathrm{virt}}$. Infrared singularities remain which have to be cancelled by the corresponding real corrections.

3.3.4 Inclusion of the exact off-shell Coulomb singularity

For non-relativistic W bosons, i.e. for a small on-shell velocity β_W, the long range of the Coulomb interaction leads to a large radiative correction, known as the Coulomb singularity. For on-shell W bosons, this correction behaves like $1/\beta_W$ near threshold, but including the instability of the W bosons the long-range interaction is effectively truncated, and the $1/\beta_W$ singularity is regularized. Therefore, for realistic predictions in the threshold region, the on-shell Coulomb singularity should be replaced by the corresponding off-shell correction. The precise form of this off-shell Coulomb singularity [45] reveals that corrections of some per cent occur even a few W-decay widths above threshold. As explained above, the DPA becomes valid only several widths above threshold. Nevertheless, there exists an overlapping region in which the inclusion of the Coulomb singularity within the double-pole approach is reasonable.

The Feynman graph relevant for the Coulomb singularity is diagram (d) of Fig. 3.1. The non-factorizable corrections contain just the difference between the off-shell and the on-shell contributions of this diagram. Therefore, the difference between off-shell and on-shell Coulomb singularity is in principle included in $\Delta_{\mathrm{mm'}}$, as defined in (3.3.4). The genuine form of $\Delta_{\mathrm{mm'}}$ in DPA, which is given by (3.3.8), does not contain the full effect of the Coulomb singularity, because in both C_0 functions of (3.3.4) the on-shell limit $K_\pm \to 0$ was taken under the assumption of a finite β_W. In order to include the correct difference between off-shell and on-shell Coulomb singularity in $\Delta_{\mathrm{mm'}}$, the on-shell limit of the C_0 functions of (3.3.4) has to be taken for arbitrary β_W. The full off-shell Coulomb singularity can be included by adding

$$\frac{2M_W^2 - s}{s}\left[\frac{2\pi\mathrm{i}}{\bar{\beta}}\ln\left(\frac{\beta + \Delta_M - \bar{\beta}}{\beta + \Delta_M + \bar{\beta}}\right) - \frac{2\pi\mathrm{i}}{\beta_W}\ln\left(\frac{K_+ + K_- + s\beta_W\Delta_M}{2\beta_W^2 s}\right)\right] \tag{3.3.24}$$

to the genuine DPA result (3.3.8) for $\Delta_{\mathrm{mm'}}$. The quantities β, $\bar{\beta}$, and Δ_M are defined in (A.1). After combination with the factorizable doubly-resonant corrections, all doubly-resonant corrections and the correct off-shell Coulomb singularity are included. The on-shell Coulomb singularity contained in the factorizable corrections is compensated by a corresponding contribution in the non-factorizable ones. Note, however, that this subtracted on-shell Coulomb singularity appears as an artefact if the non-factorizable corrections are discussed separately.

3.3.5 Non-local cancellations

In Ref. [36] it was pointed out that the non-factorizable photonic corrections completely cancel in DPA if the phase-space integration over both invariant masses of the W bosons is performed. This cancellation is due to a symmetry of the non-factorizable corrections.

The lowest-order cross section in DPA is symmetric with respect to the "reflections"

$$K_+ = (k_+^2 - M_W^2) + iM_W\Gamma_W \quad \leftrightarrow \quad -(k_+^2 - M_W^2) + iM_W\Gamma_W = -K_+^*,$$

$$K_- = (k_-^2 - M_W^2) + iM_W\Gamma_W \quad \leftrightarrow \quad -(k_-^2 - M_W^2) + iM_W\Gamma_W = -K_-^*. \qquad (3.3.25)$$

Therefore, Δ can be symmetrized in $K_+ \to -K_+^*$ or $K_- \to -K_-^*$ if the respective invariant mass is integrated out. For instance, if k_-^2 is integrated out, Δ can be replaced by

$$\frac{1}{2}\left(\Delta + \Delta\big|_{K_- \leftrightarrow -K_-^*}\right)$$

$$\sim i\pi\left\{\frac{s - 2M_W^2}{\beta_W s}\ln\left(\frac{K_- x_W + K_+^*}{K_- x_W - K_+}\right)\right.$$

$$+ K_+ s_{23}\kappa_W\left[\frac{K_-}{\det(Y)} - \frac{K_-^*}{\det(Y')}\right]\left[\ln\left(-x_W\frac{s_{23}}{M_W^2}\right) + \ln\left(1 + \frac{s_{13}}{s_{23}}(1-z)\right)\right.$$

$$\left. + \ln\left(1 + \frac{s_{24}}{s_{23}}(1-z)\right) - \ln\left(1 + \frac{s_{13}}{M_W^2}zx_W\right) - \ln\left(1 + \frac{s_{24}}{M_W^2}zx_W\right)\right]$$

$$- \left[\frac{K_- \det(Y_2)}{\det(Y)} + \frac{K_-^* \det(Y_2')}{\det(Y')}\right]\left[\ln\left(x_W + \frac{s_{13}+s_{23}}{M_W^2}\right) - \ln\left(-x_W\frac{s_{23}}{M_W^2}\right)\right]$$

$$- \frac{K_+ \det(Y_3)}{\det(Y)}\left[\ln\left(x_W + \frac{s_{23}+s_{24}}{M_W^2}\right) - 2\ln\left(1 + \frac{K_+}{K_-}\frac{s_{23}+s_{24}}{M_W^2}\right)\right]$$

$$- \frac{K_+ \det(Y_3')}{\det(Y')}\left[\ln\left(x_W + \frac{s_{23}+s_{24}}{M_W^2}\right) - 2\ln\left(1 - \frac{K_+}{K_-^*}\frac{s_{23}+s_{24}}{M_W^2}\right)\right]$$

$$+ \frac{2s_{23}M_W^2(K_+^2 s_{24} - K_-^2 s_{13})}{\det(Y)}\ln\left(1 - \frac{K_+}{K_- x_W}\right)$$

$$\left. + \frac{2s_{23}M_W^2(K_+^2 s_{24} - K_-^{*2} s_{13})}{\det(Y')}\ln\left(1 + \frac{K_+}{K_-^* x_W}\right)\right\}$$

$$+ \text{ imaginary parts}, \qquad (3.3.26)$$

with z defined in (A.20). Note that this expression is considerably simpler than the full result for Δ. In particular, all dilogarithms have dropped out.

Symmetrizing (3.3.26) also in $K_+ \leftrightarrow -K_+^*$ leads to further simplifications if the relations (3.2.41) for the determinants are used. Under the assumptions that $(s_{13} + s_{23}) > -M_W^2 x_W$, $(s_{23} + s_{24}) > -M_W^2 x_W$, and that κ_W is imaginary, the real part of the result vanishes. These assumptions are fulfilled on resonance, $k_\pm^2 = M_W^2$; off resonance, there are regions in phase space where the assumptions are violated. The volume of those regions of phase space is suppressed by factors $|k_\pm^2 - M_W^2|/M_W^2$ and thus negligible in DPA. Therefore we can use the above assumptions and find that Δ vanishes in DPA after averaging over the four points in the (k_+^2, k_-^2) plane that are related by the reflections (3.3.25):

$$\Delta + \Delta\big|_{K_+ \to -K_+^*} + \Delta\big|_{K_- \to -K_-^*} + \Delta\big|_{K_\pm \to -K_\pm^*} \sim 0. \qquad (3.3.27)$$

This explicitly confirms the results of Ref. [36]. In particular, the non-factorizable corrections vanish in the limit $|k_\pm^2 - M_W^2| \ll \Gamma_W M_W$, i.e. for on-shell W bosons.

The above considerations lead to the following simplified recipe for the non-factorizable corrections to single invariant-mass distributions, i.e. as long as at least one of the invariant masses $k_\pm^2$ is integrated out: the full factor Δ can be replaced according to

$$\Delta \;\rightarrow\; \frac{1}{2}\left(\Delta + \Delta\big|_{K_- \leftrightarrow -K_-^*}\right) + \frac{1}{2}\left(\Delta + \Delta\big|_{K_+ \leftrightarrow -K_+^*}\right), \qquad (3.3.28)$$

where the first term on the r.h.s. is given in (3.3.26), and the second follows from the first by interchanging $K_+ \leftrightarrow K_-$ and $s_{13} \leftrightarrow s_{24}$. Note that no double counting is introduced, since the first (second) term does not contribute if k_+^2 (k_-^2) is integrated out. In order to introduce the exact Coulomb singularity, one simply has to add the additional term of (3.3.24) to (3.3.26) and (3.3.28).

3.3.6 Non-factorizable corrections to related processes

Since all non-factorizable corrections involving the initial e^+e^- state cancel, the above results for the correction factor also apply to other W-pair production processes, such as $\gamma\gamma \rightarrow WW \rightarrow 4\,\mathrm{fermions}$ and $q\bar{q} \rightarrow WW \rightarrow 4\,\mathrm{fermions}$.

The presented analytical results can also be carried over to Z-pair-mediated four-fermion production, $e^+e^- \rightarrow ZZ \rightarrow 4\,\mathrm{fermions}$. In this case, $\Delta_{ff'}$ yields the complete non-factorizable correction, where all quantities such as M_W and Γ_W defined for the W bosons are to be replaced by the ones for the Z bosons. The fact that $Q_1 = Q_2$ and $Q_3 = Q_4$ has two important consequences. Firstly, it implies the cancellation of mass singularities contained in $\Delta_{ff'}$ when all contributions are summed as in (3.3.2). Secondly, it leads to the antisymmetry of δ_{nf} under each of the interchanges $k_1 \leftrightarrow k_2$ and $k_3 \leftrightarrow k_4$. It is interesting to note that (3.3.2) with (3.3.3) are directly applicable, since $\Delta_{mf'}$ and $\Delta_{mm'}$ cancel in the sum of (3.3.2). Therefore, a practical way to calculate the non-factorizable corrections to $e^+e^- \rightarrow ZZ \rightarrow 4\,\mathrm{fermions}$ consists in taking $\Delta_{ff'} + \Delta_{mf'}$ from (3.3.9) and (3.3.10), and setting $\Delta_{mm'}$ to zero.

3.4 Numerical results

We used the parameters

$$\alpha^{-1} = 137.0359895, \quad M_Z = 91.187\,\mathrm{GeV}, \quad M_W = 80.22\,\mathrm{GeV}, \quad \Gamma_W = 2.08\,\mathrm{GeV}, \qquad (3.4.1)$$

which coincide with those of Ref. [38], for the numerical evaluation.

In order to exclude errors, we have written two independent programs for the correction factor (3.3.2) and compared all building blocks numerically. These subroutines are implemented in the Monte Carlo generator EXCALIBUR [23][3] as a correction factor to the three

---

[3]Since the Monte Carlo program of Chapter 2 was programmed after the results of the non-factorizable corrections were published, the Monte Carlo program EXCALIBUR was used for the results of this chapter.

(doubly-resonant) W-pair-production signal diagrams. In all numerical results below, only these signal diagrams are included, and no phase-space cuts have been applied.

If not stated otherwise the results for the figures have been obtained from 50 million phase-space points using the histogram routine of EXCALIBUR with 40 bins for each figure. For each entry in the tables, 10 million phase-space points were generated.

3.4.1 Comparison with existing results

The non-factorizable photonic corrections have already been evaluated by two groups. As was noted in the introduction, the authors of Refs. [38, 39] have not confirmed[4] the results of Ref. [37]. Therefore, we first compare our findings with the results of these two groups.

Melnikov and Yakovlev [37] give the relative non-factorizable corrections only to the completely differential cross section for the process $e^+e^- \to WW \to \nu_e e^+ e^- \bar{\nu}_e$ as a function of the invariant mass M_+ of the $\nu_e e^+$ system for all other phase-space parameters fixed. All momenta of the final-state fermions lie in a plane, and the momenta $\mathbf{k}_2$ and $\mathbf{k}_3$ of the final-state positron and electron point into opposite directions. The angle between the W^- boson and the positron is fixed to $\theta_{W^- e^+} = 150°$, and the CM energy is chosen as $\sqrt{s} = 180\,\text{GeV}$. The invariant mass of the $e^- \bar{\nu}_e$ system takes the values $M_- = 78$ and $82\,\text{GeV}$. The other parameters are $\alpha = 1/137$, $M_W = 80\,\text{GeV}$, and $\Gamma_W = 2.0\,\text{GeV}$. In Fig. 3.6 we show our results for the non-factorizable photonic corrections for this phase-space configuration. The intermediate–intermediate (mm′) corrections agree reasonably with those of Ref. [37], but the other curves differ qualitatively and quantitatively[5]. We mention that Fig. 3.6 has been reproduced [47] by the authors of Refs. [38, 39] within the expected level of accuracy. While the individual contributions shown in Fig. 3.6 are at the level of 10% owing to mass singularities, the sum, which is free of mass singularities, is below 1.2%.

Beenakker et al. [38] have evaluated the relative non-factorizable corrections to the distributions $d\sigma/dM_+dM_-$, $d\sigma/dM_+$, and $d\sigma/dM_{av}$, where $M_{av} = (M_- + M_+)/2$. Our corresponding results for the set of parameters given in (3.4.1) are shown in Fig. 3.7 for the single invariant-mass distributions and in Table 3.1 for the double invariant-mass distribution. The deviation between the distributions $d\sigma/dM_+$ and $d\sigma/dM_-$ in Fig. 3.7, which should be identical, gives an indication on the Monte Carlo error of our calculation. The single and double invariant-mass distributions agree very well with those of Ref. [38]. The worst agreement is found for small invariant masses and amounts to 0.03%. In fact, the agreement is better than expected, in view of the fact that our results differ from those of Ref. [38] by non-doubly resonant corrections. In the numerical evaluations of Ref. [38] the phase space and the Born matrix element are taken entirely on shell [47]. Moreover,

---

[4]While the result of Refs. [38, 39] (as our result) for the complete non-factorizable correction is free of mass-singular logarithms, the result of Ref. [37] contains logarithms of ratios of fermion masses. However, the authors of Ref. [37] have informed us [46] that the results of Ref. [37] and Refs. [38, 39] agree for equal fermion pairs in the final state.

[5]Although not stated in Ref. [37], mass-singular parts have been dropped there in the numerical evaluation [46] rendering a thorough comparison of the (mf′) and (ff′) parts impossible. Comparing the sum of all three contributions, i.e. the complete non-factorizable correction factor, our result differs from the sum read off from Ref. [37].

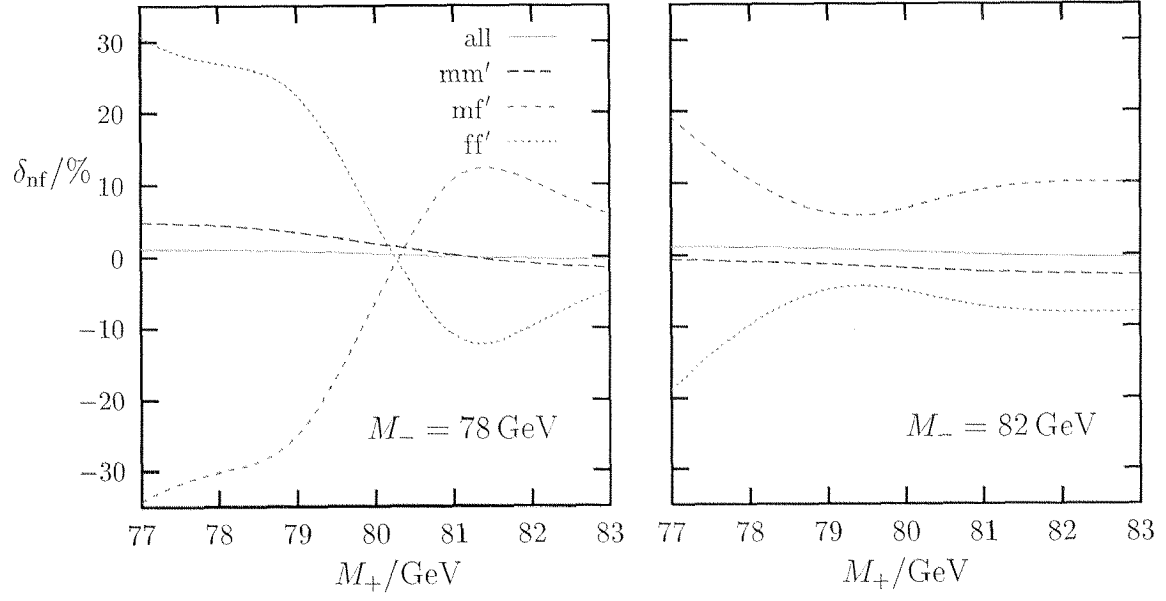Figure 3.6: Relative non-factorizable correction factor to the differential cross section for the phase-space configuration given in the text. The curves labelled mm', mf', and ff' correspond to the curves A, B, and C of Ref. [37], respectively.
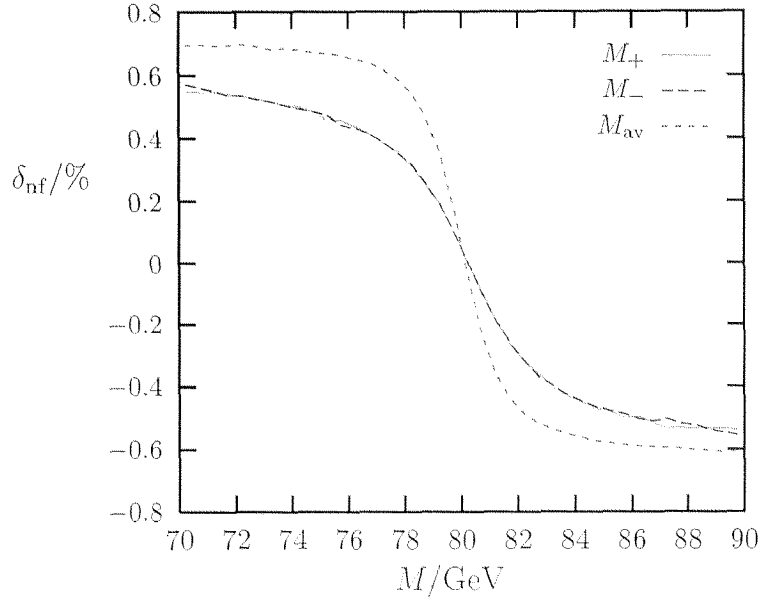

Figure 3.7: Relative non-factorizable corrections to the single invariant-mass distributions $d\sigma/dM_\pm$ and $d\sigma/dM_{av}$ for the CM energy $\sqrt{s} = 184\,\text{GeV}$.

Δ_+	Δ_-						
	-1	$-1/2$	$-1/4$	0	$1/4$	$1/2$	1
-1	0.81	0.64	0.52	0.38	0.22	0.07	-0.16
$-1/2$	0.64	0.52	0.40	0.24	0.08	-0.07	-0.25
$-1/4$	0.52	0.40	0.28	0.13	-0.02	-0.15	-0.31
0	0.38	0.24	0.13	0.00	-0.13	-0.24	-0.37
$1/2$	0.22	0.08	-0.02	-0.13	-0.24	-0.32	-0.43
$1/4$	0.07	-0.07	-0.15	-0.24	-0.32	-0.39	-0.48
1	-0.16	-0.25	-0.31	-0.37	-0.43	-0.48	-0.54

Table 3.1: Relative non-factorizable corrections in per cent to the double invariant-mass distribution $d\sigma/dM_+dM_-$ for the CM energy $\sqrt{s} = 184\,\text{GeV}$ and various values of $M_\pm$ specified in terms of their distance from M_W in units of Γ_W, i.e. $\Delta_\pm = (M_\pm - M_W)/\Gamma_W$.

the scalar integrals are parameterized by scalar invariants different from ours, leading to differences of the order of $|k_\pm^2 - M_W^2|/M_W^2$.

In Ref. [38], additionally, the decay-angular distribution $d\sigma/dM_-dM_+d\cos\theta_{W^+e^+}$ has been considered, where $\theta_{W^+e^+}$ is the decay angle between $\mathbf{k}_+$ and $\mathbf{k}_2$ in the laboratory system. Our results for this angular distribution are shown in Fig. 3.8. The cross section is small for $\cos\theta_{W^+e^+} \sim -1$, where the corrections are largest. Unfortunately the corresponding figure in Ref. [38] is not correct [47]. The authors of Ref. [38] have provided a corrected figure, which agrees reasonably well with Fig. 3.8, but does not show the kinks in the curve for $M_\pm = 78\,\text{GeV}$. The kinks are due to a logarithmic Landau singularity in the 4-point functions. If one employs the on-shell parameterization of phase space, as in Ref. [38], the Landau singularities appear at the boundary of phase space. Although no kinks appear in the physical phase space in this case, the Landau singularities still give rise to large corrections for $\cos\theta_{W^+e^+} \sim -1$. Since the kinks appear in a region where the cross section is small, they are not relevant for phenomenology. The issue of the kinks is further discussed in Section 3.4.3.

3.4.2 Numerical results for leptonic final state

In Fig. 3.9 we show the non-factorizable corrections to the single invariant-mass distribution $d\sigma/dM_+$ for various CM energies. While the corrections reach up to 1.3% for $\sqrt{s} = 172\,\text{GeV}$, they decrease with increasing energy and are less than 0.04% for $\sqrt{s} = 300\,\text{GeV}$. Note that the shape of the corrections is exactly what is naively expected. If a photon is emitted in the final state, the invariant mass of the fermion pair is smaller than the invariant mass of the resonant W boson, which is given by the invariant mass of the fermion pair plus photon. Since we calculate the corrections as a function of the

Figure 3.8: Relative non-factorizable corrections to the decay-angular distribution $\mathrm{d}\sigma/\mathrm{d}M_-\mathrm{d}M_+\mathrm{d}\cos\theta_{\mathrm{W}^+\mathrm{e}^+}$ for fixed values of the invariant masses $M_\pm$ and the CM energy $\sqrt{s} = 184\,\mathrm{GeV}$.
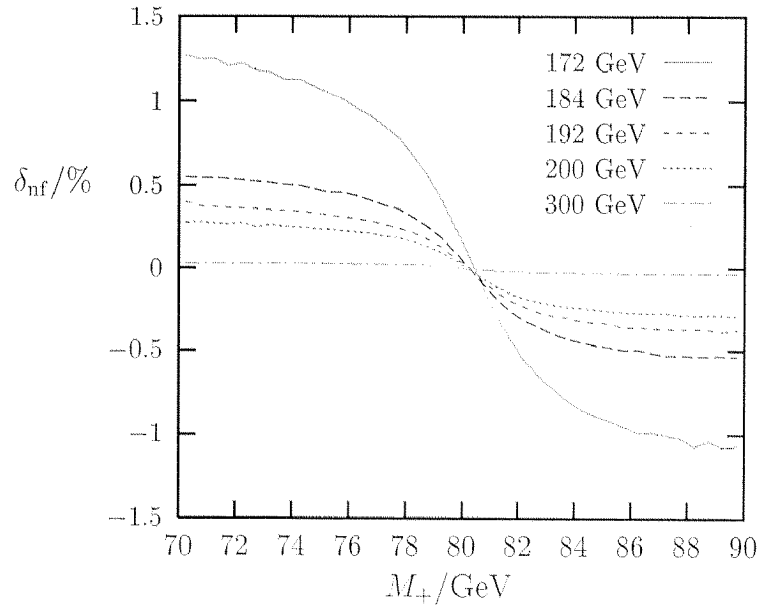
Figure 3.9: Relative non-factorizable corrections to the single invariant-mass distribution $\mathrm{d}\sigma/\mathrm{d}M_+$ for various CM energies.
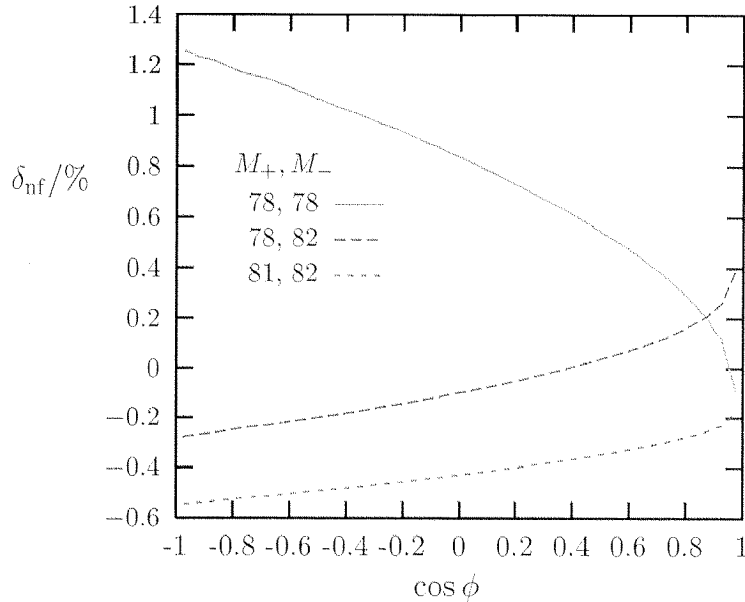
Figure 3.10: Relative non-factorizable corrections to the angular distribution $d\sigma/dM_- dM_+ d\cos\phi$ for fixed values of the invariant masses $M_\pm$ and the CM energy $\sqrt{s} = 184\,\mathrm{GeV}$.

$\sqrt{s}/\mathrm{GeV}$	172	184	192	200	300
$\Delta M_+/\mathrm{MeV}$	-2.0	-1.1	-0.8	-0.6	-0.09

Table 3.2: Shift of the maximum of the single invariant-mass distributions $d\sigma/dM_+$ induced by the non-factorizable corrections at various CM energies.

invariant masses of the fermion pairs, the cross section tends to increase for small invariant masses and decrease for large invariant masses.

The non-factorizable corrections distort the invariant-mass distribution and thus lead to a shift in the W-boson mass determined from the direct reconstruction of the decay products with respect to the actual W-boson mass. This shift can be estimated by the displacement of the maximum of the single-invariant-mass distribution caused by the corrections shown in Fig. 3.9. To this end, we determine the slope of the corrections for $M_+ = M_\mathrm{W}$, multiply this linearized correction to a simple Breit-Wigner factor, and determine the shift ΔM_+ of the maximum. The smallness of the correction allows us to evaluate ΔM_+ in linear approximation, leading to the simple formula

$$\Delta M_+ = \left(\frac{d\delta_{\mathrm{nf}}}{dM_+}\right)\Bigg|_{M_+=M_\mathrm{W}} \frac{\Gamma_\mathrm{W}^2}{8}. \qquad (3.4.2)$$

Extracting the slope from our numerical results we obtain the mass shifts shown in Table 3.2.

In Figs. 3.10 and 3.11 we show the effect of the non-factorizable corrections on various angular distributions. Since the non-factorizable corrections are independent of the production angle of the W bosons, it suffices to consider distributions involving the angles

65
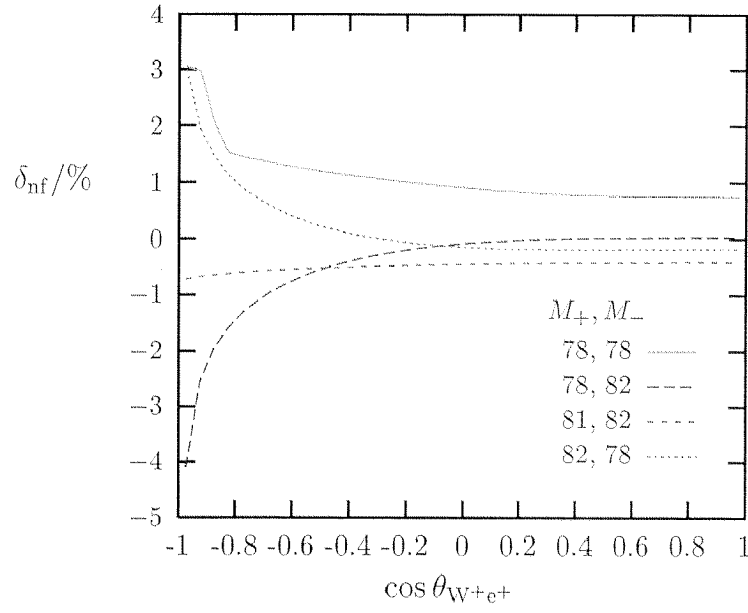
Figure 3.11: Relative non-factorizable corrections to the angular distribution $d\sigma/dM_-dM_+d\cos\theta_{e^+e^-}$ for fixed values of the invariant masses $M_\pm$ and a CM energy $\sqrt{s} = 184\,\text{GeV}$.
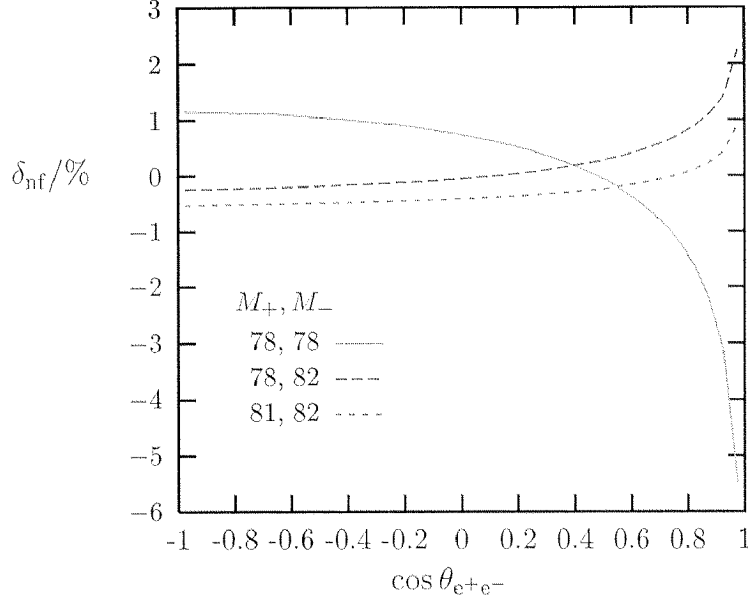
of the final-state fermions. We define all angles in the laboratory system, which is the CM system of the production process. The distribution over the angle ϕ between the two planes spanned by the momenta of the two fermion pairs in which the W bosons decay, i.e.

$$\cos\phi = \frac{(\mathbf{k}_1 \times \mathbf{k}_2)(\mathbf{k}_3 \times \mathbf{k}_4)}{|\mathbf{k}_1 \times \mathbf{k}_2||\mathbf{k}_3 \times \mathbf{k}_4|}, \tag{3.4.3}$$

is presented in Fig. 3.10. The corrections are of the order of 1% or less. Like the ϕ distribution, the distribution over the angle between positron and electron $\theta_{e^+e^-}$ (Fig. 3.11) is symmetric under the interchange of M_+ and M_-. As for the $\theta_{e^+W^+}$ distribution (Fig. 3.8), the corrections reach several per cent in the region where the cross section is small.

The distribution in the electron energy E_{e^-} is considered in Fig. 3.12. The corrections are typically of the order of 1%. Again the corrections become large where the cross section is small.

In Section 3.3.4 we have introduced a correction term that includes the full off-shell Coulomb singularity. The results for the non-factorizable corrections with this improvement are compared with those of the pure DPA in Fig. 3.13. For $\sqrt{s} = 184\,\text{GeV}$ the additional terms shift the non-factorizable corrections by up to 1.4% for $d\sigma/dM_{av}$ and by up to 0.8% for $d\sigma/dM_+$ for small invariant masses, whereas for large invariant masses there is practically no effect. The difference originates essentially from the differences between $1/\bar{\beta}$ and $1/\beta_W$ in (3.3.24). For large invariant masses, the explicit logarithms in (3.3.24) are small, i.e. the Coulomb singularity correction is minuscule, and this difference practically makes no effect. For small invariant masses, the logarithms are approximately $i\pi$ and the difference causes the effect seen in Fig. 3.13. In Table 3.3 we show the non-factorizable corrections to the double invariant-mass distribution, as in Table 3.1, but now with the

Figure 3.12: Relative non-factorizable corrections to the electron-energy distribution $d\sigma/dM_-dM_+dE_{e^-}$ for fixed values of the invariant masses $M_\pm$ and a CM energy $\sqrt{s} = 184\,\text{GeV}$.

Figure 3.13: Relative non-factorizable corrections to the single invariant-mass distributions $d\sigma/dM_+$ and $d\sigma/dM_{av}$ for a CM energy $\sqrt{s} = 184\,\text{GeV}$ with (lower curves) and without (upper curves) improved Coulomb-singularity treatment.

Δ_+	Δ_-						
	-1	$-1/2$	$-1/4$	0	$1/4$	$1/2$	1
-1	0.39	0.31	0.23	0.15	0.05	-0.04	-0.20
$-1/2$	0.31	0.28	0.20	0.10	-0.02	-0.13	-0.27
$-1/4$	0.23	0.20	0.13	0.03	-0.09	-0.19	-0.33
0	0.15	0.10	0.03	-0.08	-0.18	-0.27	-0.38
$1/2$	0.05	-0.02	-0.09	-0.18	-0.27	-0.35	-0.44
$1/4$	-0.04	-0.13	-0.19	-0.27	-0.35	-0.41	-0.49
1	-0.20	-0.27	-0.33	-0.38	-0.44	-0.49	-0.54

Table 3.3: Same as in Table 3.1 but with improved Coulomb-singularity treatment.

improved Coulomb-singularity treatment. We find a difference of up to half a per cent for small invariant masses but no effect for large ones. We mention that the difference between the entries in Tables 3.3 and 3.1 is directly given by the contribution (3.3.24) to $\Delta_{mm'}$, without any influence of the phase-space integration.

3.4.3 Discussion of intrinsic ambiguities

In the results presented so far, all scalar integrals were parameterized by s, s_{23}, s_{13}, s_{24}, and $k_\pm^2$ (parameterization 1). In DPA, however, the parameters of the scalar integrals are only fixed up to terms of order $k_\pm^2 - M_W^2$. We can for example parameterize the scalar integrals in terms of s, s_{23}, s_{123}, s_{234}, and $k_\pm^2$ (parameterization 2) instead. As a third parameterization, we fix all scalar invariants except for $k_\pm^2$ by their on-shell values, corresponding exactly to the approach of Ref. [38]. The results of these three parameterizations differ by non-doubly-resonant corrections.

The difference between parameterizations 1 and 2 is illustrated in Fig. 3.14 for the single invariant-mass distribution. The difference amounts to $\sim 0.1\%$. Note that for an invariant mass $M_+ = 70\,\text{GeV}$ we have $\alpha |M_W^2 - k_+^2|/M_W^2 \sim 0.002$ and would thus expect absolute changes in the non-factorizable corrections at this level.

For the non-factorizable corrections to the angular distributions, uncertainties of the same order are to be expected. The only exceptions are the distributions over the decay angles $\theta_{W^+e^+}$ and $\theta_{W^-e^-}$. Let us explain this for $\theta_{W^+e^+}$ in more detail: the non-factorizable correction contains the term $2\pi i \ln[1 + x_W M_W^2/(s_{13}+s_{23})]$, which can be evaluated by taking $(s_{13} + s_{23})$ directly or $(s_{123} - M_W^2)$ as input. This parameterization ambiguity can lead to larger uncertainties, because the above logarithm can become singular, and the location of this Landau singularity is shifted by the ambiguity. Since there is a one-to-one correspondence between s_{123} and $\theta_{W^+e^+}$ for fixed s and k_+^2, this logarithmic singularity is washed out if the angular integration over $\theta_{W^+e^+}$ is performed, but appears as a kink structure in
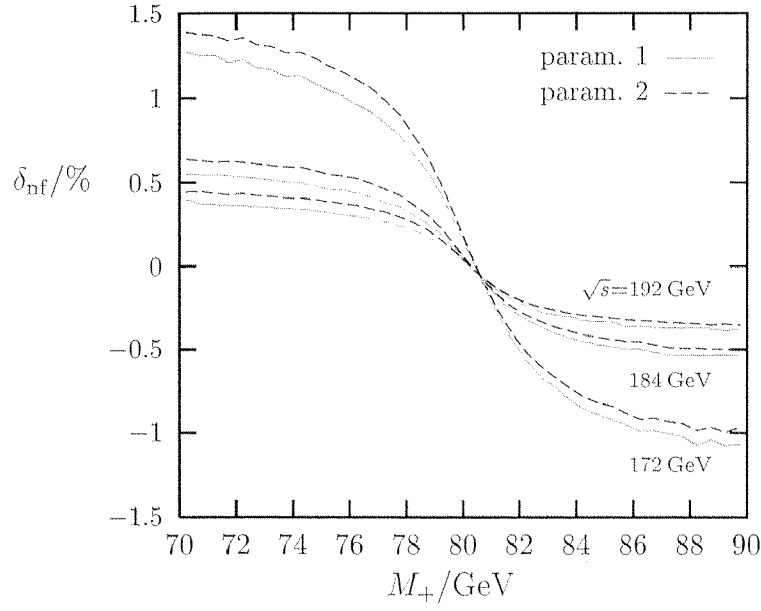
Figure 3.14: Relative non-factorizable corrections to the single invariant-mass distribution $d\sigma/dM_+$ for the CM energies 172, 184, and 192 GeV and two different parameterizations.
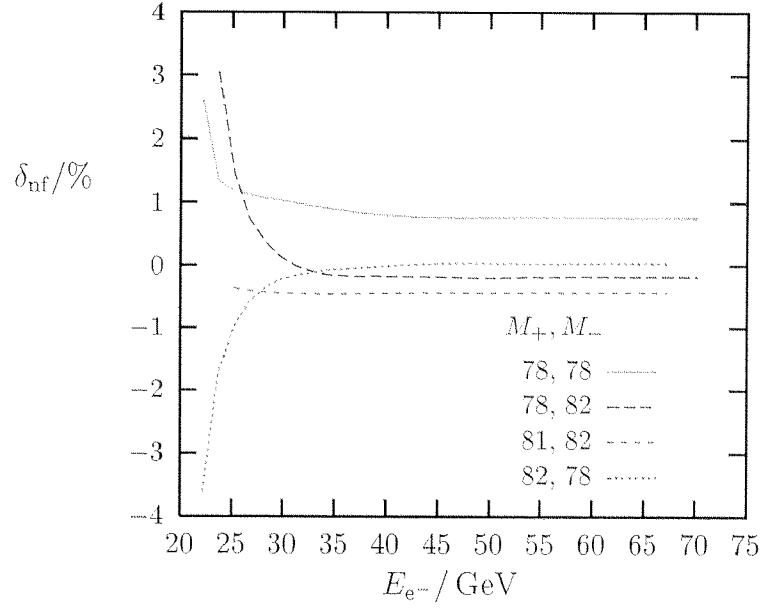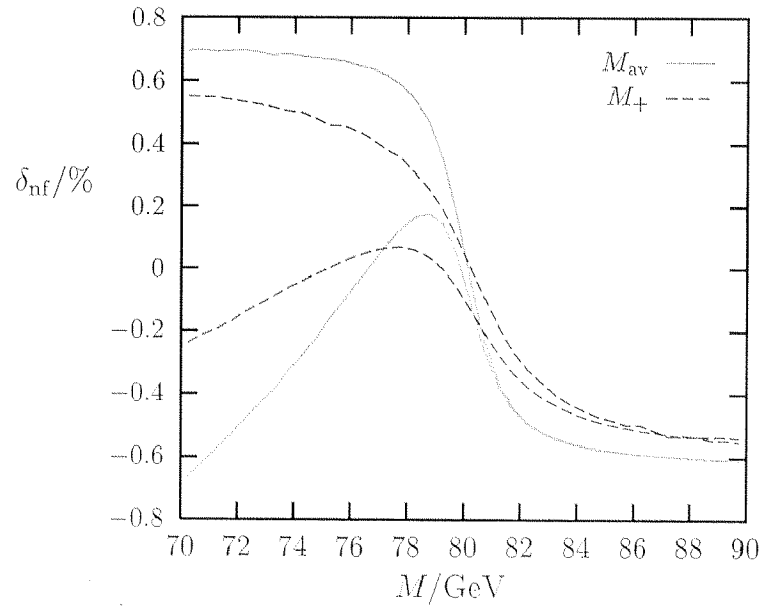

Figure 3.15: Relative non-factorizable corrections to the decay-angular distribution $d\sigma/dM_-dM_+d\cos\theta_{W^+e^+}$ for fixed values of the invariant masses $M_\pm$ and a CM energy $\sqrt{s} = 184\,\mathrm{GeV}$ using three different parameterizations, as specified in the text.

the angular distribution over this angle. Fig. 3.15 shows the non-factorizable corrections to this angular distribution for the three parameterizations. For $M_+ = 78\,\mathrm{GeV}$ we still have $\alpha|k_+^2 - M_\mathrm{W}^2|/M_\mathrm{W}^2 \sim 0.0004$. Apart from the regions where the Landau singularities appear, this is indeed of the order of the differences between the three parameterizations. When considering the Landau singularities, one should realize that the parameterization ambiguity of the locations of the singularities is not suppressed by a factor α, i.e. different parameterizations shift the locations at the level of $|k_+^2 - M_\mathrm{W}^2|/M_\mathrm{W}^2 \sim 0.05$. However, the impact of the corresponding kinks on observables is again suppressed with $\alpha|k_+^2 - M_\mathrm{W}^2|/M_\mathrm{W}^2$ if the angles are integrated over, since the singularities can only appear near the boundary of phase space and disappear from phase space exactly on resonance. Since the cross section is small where the Landau singularity appears, the effect is phenomenologically irrelevant.

3.4.4 Comparison between leptonic, semi-leptonic, and hadronic final state

The non-factorizable corrections to the invariant-mass distributions are different for different final states and in general also for the intermediate W^+ and W^- bosons.[6] The invariant-mass distributions to the intermediate $\mathrm{W}^\pm$ bosons coincide only if the complete process is CP-symmetric. In this context, CP symmetry does not distinguish between the different fermion generations, since we work in double-pole approximation and neglect fermion masses; in other words, the argument also applies to final states like $\nu_\mathrm{e} \mathrm{e}^+ \mu^- \bar{\nu}_\mu$ and $\mathrm{u}\bar{\mathrm{d}}\mathrm{s}\bar{\mathrm{c}}$, which are not CP-symmetric in the strict sense. Thus, we end up with equal distributions for the $\mathrm{W}^\pm$ bosons in the purely leptonic and purely hadronic channels, respectively, but not in the semi-leptonic case.

Fig. 3.16 shows the non-factorizable corrections to the single-invariant-mass distributions for leptonic, hadronic, and semi-leptonic final states at various centre-of-mass energies. We observe the same qualitative features for all final states; the corrections are positive below resonance and negative above. Quantitatively the differences between the corrections to the different final states are small; we note that the slopes of the corrections on resonance, which are responsible for the shift in the maximum of the distribution, are maximal for the leptonic final state. Therefore, we conclude that the W-boson mass determination by invariant-mass reconstruction at LEP2 is not significantly influenced by non-factorizable corrections.

The authors of Ref. [38, 39] have also calculated [47] the non-factorizable corrections to the single-invariant-mass distributions shown in Fig. 3.16 for $\sqrt{s} = 172\,\mathrm{GeV}$ and $184\,\mathrm{GeV}$. They find good agreement with our results for positive invariant masses. However, their corrections are antisymmetric and therefore differ from our results for negative invariant

---

[6]In Ref. [38, 39] and in the preprint version of Ref. [40] it has been argued that the relative non-factorizable corrections to pure invariant-mass distributions are identical for all final states in $\mathrm{e}^+\mathrm{e}^- \to$ WW $\to$ 4 fermions and vanish for Z-pair-mediated four-fermion production. This was deduced from the assumption that (up to charge factors) the non-factorizable corrections become symmetric under the separate interchanges $k_1 \leftrightarrow k_2$ and $k_3 \leftrightarrow k_4$ after integration over all decay angles. Although the function Δ for the relative correction has this property, this assumption is not correct, because the differential lowest-order cross section is not symmetric under these interchanges.
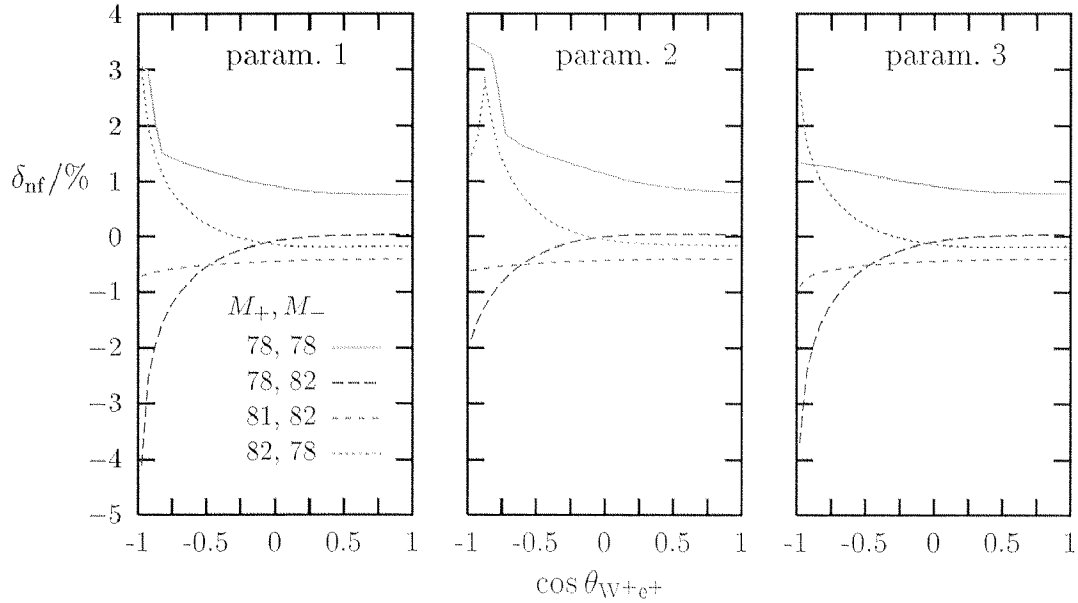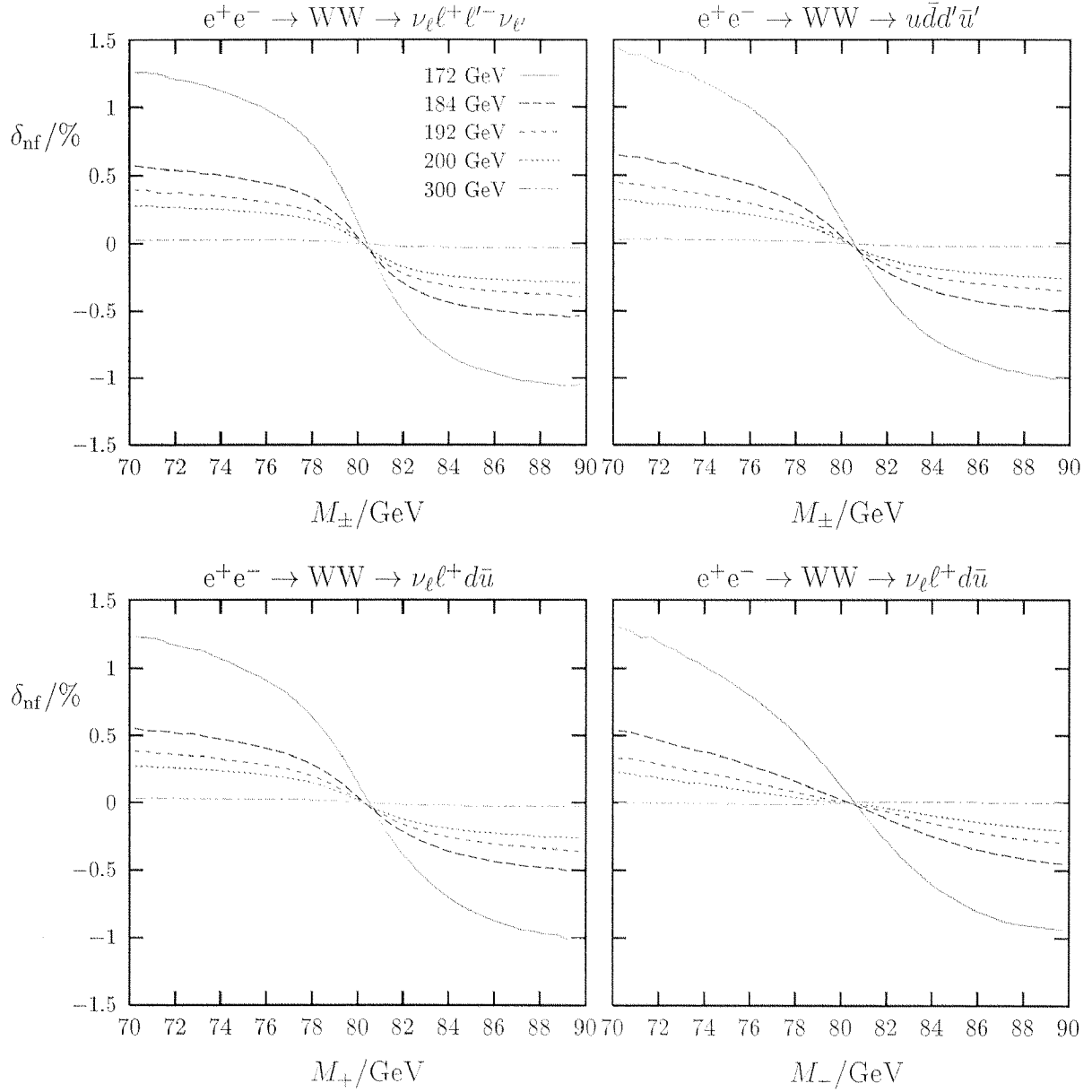
Figure 3.16: Relative non-factorizable corrections to the single-invariant-mass distributions $d\sigma/dM_{\pm}$ for $e^+e^- \to WW \to 4$ fermions with different final states for various centre-of-mass energies.

masses. The differences are of the order of non-doubly-resonant corrections and due to different parameterizations of the corrections.

In the previous sections, we investigated the influence of the non-factorizing corrections on various angular and energy distributions with fixed invariant masses for the final-state fermion pairs. We have repeated this analysis for hadronic and semi-leptonic final states and found corrections of the same order of magnitude, viz. of typically 1% at LEP2 energies.

3.4.5 Numerical results for Z-pair production

For the production channels via a resonant Z-boson pair, $e^+e^- \to ZZ \to 4$ fermions, we have $f_1 = f_2$ and $f_3 = f_4$. Owing to Bose symmetry the lowest-order cross section $d\sigma_{\mathrm{Born}}$ is invariant under the set of interchanges $(k_1, k_2) \leftrightarrow (k_3, k_4)$. This symmetry, which is respected by the non-factorizable corrections, implies that the single-invariant-mass distributions to each of the final-state fermion pairs of the two Z-boson decays are equal. CP invariance leads to the additional symmetry with respect to $(p_+, k_1, k_2) \leftrightarrow (p_-, k_4, k_3)$; after integration over the Z-pair production angle this substitution reduces to $(k_1, k_2) \leftrightarrow (k_4, k_3)$. In view of non-factorizable corrections it is also interesting to inspect the behaviour of $d\sigma_{\mathrm{Born}}$ under the replacements $k_1 \leftrightarrow k_2$ and $k_3 \leftrightarrow k_4$ separately, since terms in $d\sigma_{\mathrm{Born}}$ that are symmetric in at least one of these substitutions do not contribute to $d\sigma_{\mathrm{nf}}$ if all decay angles are integrated over. This is a direct consequence of the antisymmetry of δ_{nf} in each of the substitutions $k_1 \leftrightarrow k_2$ and $k_3 \leftrightarrow k_4$, which follows from (3.3.2) and $Q_1 = Q_2$, $Q_3 = Q_4$.

In order to study the behaviour of $d\sigma_{\mathrm{Born}}$ under the replacements $k_1 \leftrightarrow k_2$ and $k_3 \leftrightarrow k_4$, it is convenient to consider the helicity amplitudes for the two signal diagrams for $e^+e^- \to ZZ \to 4$ fermions, which contain two resonant Z-boson propagators. These amplitudes are proportional to the right- and left-handed couplings $g_i^\pm = v_i \mp a_i$ of each fermion $f_i = f_1, f_3$ to the Z boson. As can be seen from the explicit form of the amplitudes, the substitution $k_1 \leftrightarrow k_2$ transforms the helicity amplitudes to those with reversed helicities of the fermions f_1 and $\bar{f}_2 = \bar{f}_1$ apart from changing the couplings $g_1^\pm$ into $g_1^\mp$. Therefore, the differential lowest-order cross section, i.e. the squared helicity amplitudes summed over all final-state polarizations, can be split into two parts: one is symmetric in $k_1 \leftrightarrow k_2$ and proportional to $[(g_1^+)^2 + (g_1^-)^2]/2 = v_1^2 + a_1^2$, the other is anti-symmetric and proportional to $[(g_1^-)^2 - (g_1^+)^2]/2 = 2v_1 a_1$. The analogous reasoning applies to the substitution $k_3 \leftrightarrow k_4$. After performing the angular integrations, we finally find that the lowest-order cross section is proportional to $(v_1^2 + a_1^2)(v_3^2 + a_3^2)$, and the non-factorizable correction proportional to $4Q_1 v_1 a_1 Q_3 v_3 a_3$, where the charge factors Q_i stem from the correction factor δ_{nf}. Comparing pure invariant-mass distributions for different final states, the ratios of the non-factorizable corrections should be of the same order of magnitude as the ratios of the corresponding coupling factors,

$$F = \left| \frac{4Q_1 v_1 a_1 Q_3 v_3 a_3}{(v_1^2 + a_1^2)(v_3^2 + a_3^2)} \right|. \tag{3.4.4}$$
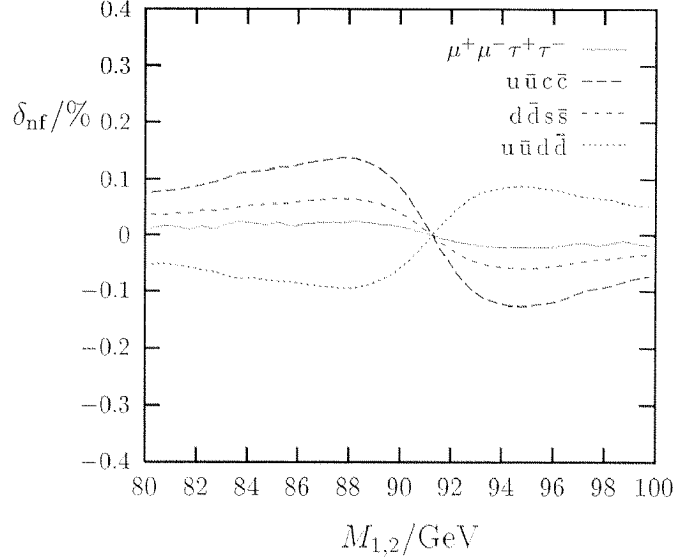
Figure 3.17: Relative non-factorizable corrections to the single-invariant-mass distributions $\mathrm{d}\sigma/\mathrm{d}M_{1,2}$ for $e^+e^- \to ZZ \to 4\,$fermions with different final states for $\sqrt{s} = 192\,\mathrm{GeV}$.

The factors F take the following values:

$f_1 f_3$	$\ell\ell$	ℓu	ℓd	uu	ud	dd
F	0.04	0.09	0.06	0.21	0.14	0.10

$$(3.4.5)$$

where ℓ, u, d generically refer to leptons, up-type quarks and down-type quarks, respectively. The reason for the smallness of the factors F is different for leptons and quarks: for leptons the suppression is due to the small coupling v_i to the vector current, for quarks the factor F is reduced by the relative charges Q_i.

Fig. 3.17 shows the non-factorizable corrections to the single-invariant-mass distributions $\mathrm{d}\sigma/\mathrm{d}M_{1,2}$, where $M_{1,2}$ denote the invariant masses of the first and second fermion–anti-fermion pairs, respectively. The ratios of the different curves are indeed of the order of magnitude of the ratios of the factors F given in (3.4.5). For equal signs of Q_1 and Q_3 the shape of the corrections is similar to the shape of the corrections to $e^+e^- \to WW \to 4\,$fermions, for opposite signs of Q_1 and Q_3 the shape is reversed. The corrections by themselves are very small and phenomenologically unimportant. The smallness of these corrections can be qualitatively understood by comparing the factors F of (3.4.4) for the ratios of the couplings with the corresponding one for the W-pair-mediated processes. For $e^+e^- \to WW \to 4\,$leptons we simply have $F = 1$, because in the LEP2 energy range the purely left-handed t-channel diagram dominates the cross section, and no systematic compensations are induced by symmetries. Therefore, the factors in (3.4.5) should directly give an estimate for the suppression of δ_{nf} for $e^+e^- \to ZZ \to 4\,$fermions with respect to four-lepton production via a W-boson pair. Comparing the corrections for energies with the same distance from the respective on-shell pair-production thresholds, i.e. the curve for $\sqrt{s} = 184\,\mathrm{GeV}$ in the W-boson case (Fig. 3.16) with the curves for $\sqrt{s} = 192\,\mathrm{GeV}$ in the Z-boson case (Fig. 3.17), we find reasonable agreement with
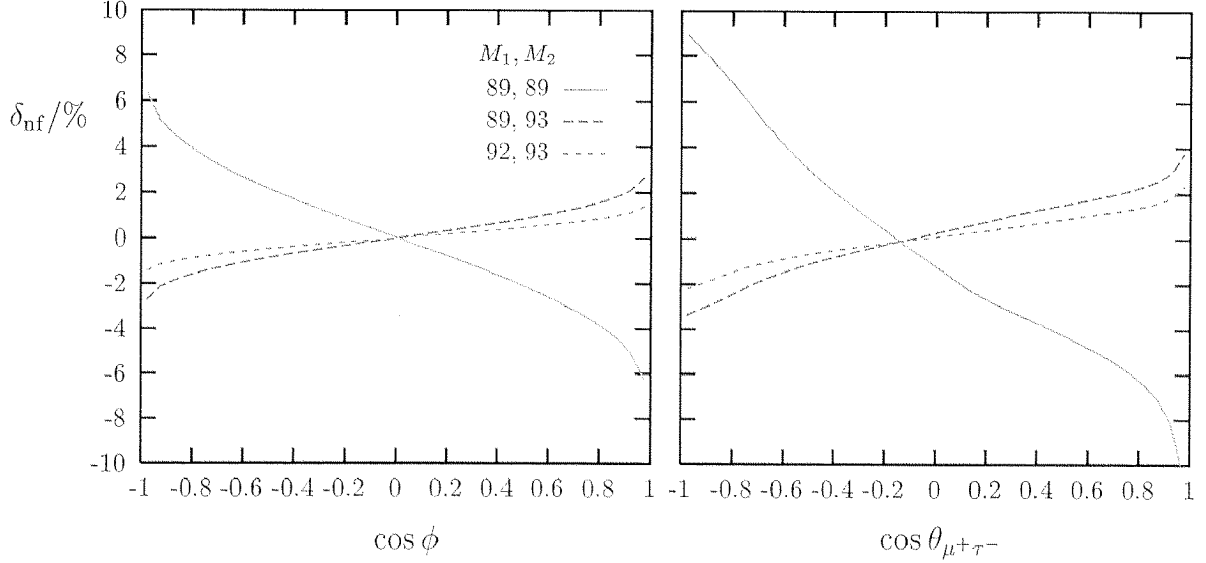
73

Figure 3.18: Relative non-factorizable corrections to the angular distributions $\mathrm{d}\sigma/\mathrm{d}M_1\mathrm{d}M_2\mathrm{d}\cos\phi$ and $\mathrm{d}\sigma/\mathrm{d}M_1\mathrm{d}M_2\mathrm{d}\cos\theta_{\mu^+\tau^-}$ in $e^+e^- \to ZZ \to \mu^-\mu^+\tau^-\tau^+$ for fixed values of the invariant masses $M_{1,2}$ and $\sqrt{s} = 192\,\mathrm{GeV}$.

our expectation. The authors of Ref. [38, 39] have reproduced the corrections shown in Fig. 3.17 with good agreement [47].

Finally, we inspect the impact of non-factorizable corrections to some angular distributions in Z-pair-mediated four-fermion production for fixed values of the invariant masses $M_{1,2}$. Since the presence of the suppression factor F relies on the assumption that the phase-space integration is symmetric under $k_1 \leftrightarrow k_2$ and $k_3 \leftrightarrow k_4$, this suppression in general does not apply to angular distributions. However, partial suppressions occur, e.g., if the integration is still symmetric under one of these substitutions and, in particular, for quarks in the final state because of their smaller charges. Two examples for angular distributions without any suppression are illustrated in Fig. 3.18 for the purely leptonic final state $\mu^-\mu^+\tau^-\tau^+$. The angle ϕ is defined by the two planes spanned by the momenta of the two fermion pairs in which the Z bosons decay,

$$\cos\phi = \frac{(\mathbf{k}_1 \times \mathbf{k}_2)(\mathbf{k}_3 \times \mathbf{k}_4)}{|\mathbf{k}_1 \times \mathbf{k}_2||\mathbf{k}_3 \times \mathbf{k}_4|}, \qquad (3.4.6)$$

and $\theta_{\mu^+\tau^-}$ denotes the angle between the momenta of the μ^+ and the τ^-, respectively. The shapes of the curves in Fig. 3.18, specifically the curves for the distribution in $\cos\phi$, nicely reflect the approximate anti-symmetric behaviour in the angular dependence, which leads to the suppression in the invariant-mass distributions. The size of the corrections turns out to be at the level of a few per cent, i.e. they are not necessarily negligible in precision predictions. Note, however, that the cross section for Z-pair production is only one tenth of the W-pair production cross section.

74

Chapter 4

Radiative corrections to $e^+e^- \rightarrow W^+W^- \rightarrow 4f$

As discussed in the introduction, the cross section for $e^+e^- \rightarrow W^+W^- \rightarrow 4f$ should be known with an accuracy of 1% or better in order to cope with the experimental precision at LEP2. This requires the calculation of the $\mathcal{O}(\alpha)$ corrections to the processes $e^+e^- \rightarrow W^+W^- \rightarrow 4f$.

The leading radiative corrections, like the running of the electromagnetic coupling constant, universal corrections associated with the ρ parameter, the Coulomb singularity, and the resummed leading-logarithmic corrections from initial-state radiation (ISR), are already implemented in several event generators (see Ref. [30] and references therein). The neglected non-leading corrections can be estimated from the on-shell W-pair production [5, 48], where the full one-loop calculation differs from the one including only these leading effects by about 1-2% at LEP2 energies and 10-20% in the TeV range. Hence, the leading radiative corrections are in general not sufficient to match the experimental accuracy of LEP2.

The calculation of the full $\mathcal{O}(\alpha)$ corrections is extremely complicated since the number of diagrams is of the order of 10^3-10^4 including one-loop integrals with up to six propagators [49]. The numerical computation of these corrections is highly non-trivial because the tensor reduction to scalar integrals and the calculation of the one-loop integrals with five and more propagators cause numerical instabilities. Furthermore, the numerical integration via Monte Carlo techniques is rather slow for such complex calculations.

Approximations for radiative corrections beyond the leading level have been calculated by two groups. A first calculation of the complete doubly-resonant $\mathcal{O}(\alpha)$ radiative corrections to the four-fermion processes $e^+e^- \rightarrow W^+W^- \rightarrow 4f$ has been discussed in Ref. [50]. There a semi-analytic approach has been used with different matrix elements for different phase-space regions and for different observables. Moreover, the four-fermion phase space has been factorized into the phase space of the on-shell W-pair production and of the on-shell W decays and the integrations of the two invariant masses of the intermediate W bosons. For the numerical discussion, only results for leptonic processes have been included. The authors of Ref. [50] have found a large shift of the Breit–Wigner line shape due to logarithms of the form $\ln(m_f^2/s)$ resulting from final-state radiation (FSR). These logarithms are due to the absence of collinear photons in the definition of the invariant

mass of the W boson. In realistic observables, collinear photons cannot be resolved from charged fermions, except for muons, and have to be included in the reconstructed invariant mass of the corresponding W boson.

In Ref. [51], a four-fermion event generator has been presented, including all $\mathcal{O}(\alpha)$ radiative corrections to the on-shell W-pair production, $e^+e^- \to W^+W^-$, with exponentiation of the universal corrections from photon radiation off initial-state $e^\pm$ and off the $W^\pm$ bosons. Leading-logarithmic corrections from FSR have been included in this Monte Carlo generator in Ref. [52]. However, non-leading $\mathcal{O}(\alpha)$ corrections to the W decays and the non-factorizable corrections are missing. The results of Ref. [50] have been qualitatively confirmed by the calculations of Ref. [52].

Hence, a Monte Carlo generator including the complete doubly-resonant $\mathcal{O}(\alpha)$ corrections is needed in order to match the accuracy of LEP2 and to take into account realistic experimental situations.

4.1 Strategy of the calculation

In this chapter, we consider the virtual corrections to the processes

$$e^+(p_+) + e^-(p_-) \;\to\; W^+(k_+) + W^-(k_-) \;\to\; f_1(k_1) + \bar{f}_2(k_2) + f_3(k_3) + \bar{f}_4(k_4) \quad (4.1.1)$$

and the complete bremsstrahlung processes

$$e^+(p_+) + e^-(p_-) \;\to\; f_1(k_1) + \bar{f}_2(k_2) + f_3(k_3) + \bar{f}_4(k_4) + \gamma(q), \qquad (4.1.2)$$

where the relative charges of the fermions f_i are represented by Q_i with $i = 1, \ldots, 4$. The masses of the external fermions are neglected, except where this would lead to mass singularities. For the virtual corrections, the momenta of the intermediate W bosons read

$$k_+ = k_1 + k_2, \qquad k_- = k_3 + k_4. \qquad (4.1.3)$$

Furthermore, the square of the complex W-boson mass is defined by $M^2 = M_W^2 - \mathrm{i}M_W\Gamma_W$, and the center-of-mass (CM) energy is $\sqrt{s}$.

4.1.1 Doubly-resonant virtual corrections

The diagrams of four-fermion production can be classified into the doubly-resonant, singly-resonant, and non-resonant diagrams according to the number of resonant W-boson propagators. Hence, the amplitude of the virtual corrections can be written in the following way after implementation of the finite W-boson width:

$$\mathcal{M}_{\mathrm{virt}} = \underbrace{\frac{R_{+-}(k_+^2, k_-^2, \theta)}{(k_+^2 - M^2)(k_-^2 - M^2)}}_{\text{doubly-resonant}} + \underbrace{\frac{R_+(k_+^2, k_-^2, \theta)}{k_+^2 - M^2} + \frac{R_-(k_+^2, k_-^2, \theta)}{k_-^2 - M^2}}_{\text{single-resonant}} + \underbrace{N(k_+^2, k_-^2, \theta)}_{\text{non-resonant}}, \quad (4.1.4)$$

where the variable θ symbolizes all phase-space variables, except for the invariant masses $k_\pm^2$ of the W bosons.

Since the matrix elements of non-doubly-resonant diagrams are suppressed by a factor $\alpha \Gamma_W \ln(\ldots)/(\pi M_W) \approx 0.1\%$, a reasonable approach is to include only the doubly-resonant diagrams into the calculation. However, the naive inclusion of the doubly-resonant diagrams yields gauge-dependent results and the reliability of this approximation is unclear.

In order to separate the doubly-resonant corrections in a gauge-invariant way, the pole scheme has been proposed in Ref. [11, 12], where the matrix element is expanded about the complex W-boson masses. Since the complete matrix element is gauge-invariant, the single terms of the pole expansion are also gauge-invariant. If only the leading term is kept, the expansion is known as the double-pole approximation (DPA):

$$\mathcal{M}_{\text{virt}}^{\text{DPA}} = \frac{R_{+-}(M^2, M^2, \theta)}{(k_+^2 - M^2)(k_-^2 - M^2)}. \tag{4.1.5}$$

Note that the residue is taken at the complex pole resulting in complex kinematical invariants. In order to avoid the calculation of one-loop integrals for complex invariants, the W width is neglected in the numerator of (4.1.5), where the neglected terms are suppressed by a factor Γ_W/M_W and thus negligible in DPA.

For the application of the DPA on the virtual corrections, a set of eight independent phase-space variables including $k_\pm^2$ has to be chosen, which determine the momenta of the final-state fermions uniquely. For several choices of the parameterization of the phase space, the DPA differs only in non-doubly-resonant contributions. Note that in general events can be outside of the physical phase-space boundaries for on-shell W bosons (see Section 3.4.3). A relatively simple choice that generates only events within the physical phase-space domain is given in Appendix B.

The DPA is not valid near threshold since the phase-space region where both W bosons are resonant is suppressed by the kinematical factor $\lambda^{\frac{1}{2}}(s, k_+^2, k_-^2)$ (see (C.8)). Therefore, the singly-resonant corrections are as important as the doubly-resonant corrections at threshold. On the other hand, for some processes the non-doubly-resonant contributions can be enhanced by nearly on-shell virtual photons. This enhancement can be avoided by introducing appropriate phase-space cuts in the calculation.

In DPA the virtual corrections can be classified into factorizable and non-factorizable ones [5, 12, 42]. The square of the matrix element of the virtual corrections reads in DPA

$$|\mathcal{M}_{\text{virt}}^{\text{DPA}}|^2 = |\mathcal{M}_f|^2 + |\mathcal{M}_{\text{Born}}|^2 \delta_{\text{nf}}^{\text{virt}}. \tag{4.1.6}$$

where $\mathcal{M}_f$, $\mathcal{M}_{\text{Born}}$, and $\delta_{\text{nf}}^{\text{virt}}$ are the matrix elements of the factorizable corrections, the Born matrix element defined in (3.1.8), and the non-factorizable correction factor, respectively.

Factorizable virtual corrections

The factorizable virtual corrections are defined by the product of the on-shell matrix elements of the W-pair production and the W decays and the (transverse parts of the) W propagators (see Fig. 4.1):

$$\mathcal{M}_f = \sum_{\lambda_+, \lambda_-} \frac{1}{(k_+^2 - M^2)(k_-^2 - M^2)} \Big(\delta \mathcal{M}^{e^+ e^- \to W^+ W^-} \mathcal{M}_{\text{Born}}^{W^+ \to f_1 \bar{f}_2} \mathcal{M}_{\text{Born}}^{W^- \to f_3 \bar{f}_4} \tag{4.1.7}$$

$$+ \mathcal{M}_{\text{Born}}^{e^+ e^- \to W^+ W^-} \delta \mathcal{M}^{W^+ \to f_1 \bar{f}_2} \mathcal{M}_{\text{Born}}^{W^- \to f_3 \bar{f}_4} + \mathcal{M}_{\text{Born}}^{e^+ e^- \to W^+ W^-} \mathcal{M}_{\text{Born}}^{W^+ \to f_1 \bar{f}_2} \delta \mathcal{M}^{W^- \to f_3 \bar{f}_4} \Big),$$
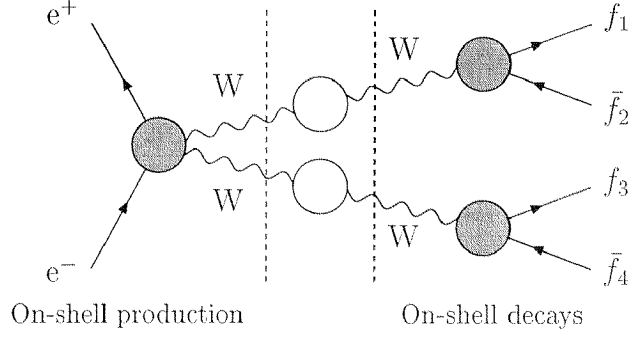
Figure 4.1: Factorizable corrections to $e^+e^- \to 4f$

where $\delta\mathcal{M}^{e^+e^-\to W^+W^-}$, $\delta\mathcal{M}^{W^+\to f_1\bar{f}_2}$, and $\delta\mathcal{M}^{W^-\to f_3\bar{f}_4}$ denote the one-loop amplitudes of the respective subprocesses. The sum runs over the physical polarizations $\lambda_\pm$ of the $W^\pm$ bosons.

Since the on-shell W-pair production and the on-shell W-decays are gauge-invariant processes, the factorizable corrections are also gauge-invariant. The results of the on-shell W-pair production and the on-shell W-boson decay are explicitly given in Ref. [53] and Ref. [54], respectively, and can be implemented in the Monte Carlo program, where we have to take care of the spin correlations of the W bosons in the production and decay subprocesses. The virtual corrections are build up by scalar form factors, which include all one-loop integrals, and standard matrix elements, which depend on the polarization vectors and spinors of the external particles. In DPA the form factors depend exclusively on the W-production angle and can be evaluated very fast by an expansion in Legendre polynomials [55].

Non-factorizable virtual corrections

The non-factorizable virtual corrections are defined as the difference between the virtual corrections to the complete four-fermion process in DPA and the factorizable virtual corrections. A representative set of diagrams contributing to the non-factorizable corrections are shown in Figs. 3.1 and 3.2. The matrix element of the non-factorizable virtual corrections $\mathcal{M}_{\mathrm{nf}}^{\mathrm{virt}}$ factorize to the Born matrix element in DPA (see Chapter 3 for more details):

$$\mathcal{M}_{\mathrm{nf}}^{\mathrm{virt}} = \mathcal{M}_{\mathrm{Born}}\delta_{\mathrm{nf}}^{\mathrm{virt}}, \tag{4.1.8}$$

where the correction factor $\delta_{\mathrm{nf}}^{\mathrm{virt}}$ is relatively simple and explicitly given in Section 3.3.3. Since the factorizable and the complete virtual corrections are gauge-invariant, the non-factorizable corrections are also gauge-invariant.

Note that the non-factorizable corrections involve logarithms of the form $\ln(k_\pm^2 - M^2)$, which become singular in the limit $k_\pm^2 \to M^2$. Therefore, these corrections are calculated for off-shell phase space, i.e. $k_\pm^2 \neq M^2$, while the off-shellness $(k_\pm^2 - M^2)$ is neglected whenever possible.

4.1.2 On the definition of the reconstructed W-boson mass

In Chapter 3, the non-factorizable virtual and real corrections have been calculated in DPA, where the integration over the photon momentum of the real corrections is performed analytically. As for the virtual corrections, the non-factorizable real corrections depend on the choice of the independent phase-space parameters in DPA. These parameters are fixed while the integration over the photon momentum is performed. To apply the DPA on the non-factorizing real corrections, two of these parameters are identified with the invariant masses of the W bosons. Owing to the presence of the bremsstrahlung photon the definition of these invariant masses is not unique. For different definitions the result for the real non-factorizable corrections differs by doubly-resonant contributions, as discussed in detail in Section 3.1.4. The reason is that the resonant W-boson propagator $1/[(k_+ + q)^2 - M^2]$ is constant, if the invariant mass is defined by $(k_+ + q)^2$, but depends on the photon momentum q for the invariant mass k_+^2. Therefore, the calculable observables are restricted to the actual parameterization of the phase space in a semi-analytic calculation. For instance, only invariant-mass distributions, where the W-boson masses are defined by $k_\pm^2$, can be calculated with the results of Chapter 3.

A DPA including all $\mathcal{O}(\alpha)$ corrections for four-fermion production has been worked out in Ref. [50]. As in Chapter 3, a semi-analytic approach has been used in Ref. [50], where, for the invariant mass distributions, the W-boson masses have been defined by invariant masses of the fermion–antifermion pairs, i.e. $M_\pm^2 = k_\pm^2$, resulting in large corrections from collinear radiation of bremsstrahlung photons off final-state fermions. These originate from logarithms of the form $\ln(m_f^2/s)$ and yielding large distortions of the peak position of the Breit–Wigner line shape at the CM energy 184 GeV of -77 MeV, -38 MeV, and -20 MeV for $e^+\nu_e$, $\mu^+\nu_\mu$, and $\tau^+\nu_\tau$, respectively. In practice, the invariant masses of W bosons have to be reconstructed in a more realistic way.

In realistic experimental situations, the final-state quarks are observed as jets. Photons radiated collinear to these jets cannot be resolved, and the photon momentum is included in the jet momentum. On the other hand, the momentum of the neutrino can only be calculated from the missing momentum of the final-state particles. In this way the neutrino momentum includes also the momenta due to emission of photons collinear to the beam [56]. Note that the reconstruction of the neutrino momentum is possible for semi-leptonic final states, but not for purely leptonic final states, where two neutrinos are involved. Furthermore, it is very difficult to separate collinear photons from electrons. However, photons can be resolved from muons even when they are collinear. Therefore, only a few observables, like the invariant-mass distribution $d\sigma/dM_-$ with $M_-^2 = k_-^2$ of the process $e^+e^- \rightarrow u\bar{d}\mu^-\bar{\nu}_\mu$, are directly sensitive to the distortion due to large corrections from FSR. In any case, a Monte Carlo generator is required in order to take into account realistic experimental situations.

4.1.3 Overlapping resonances in the bremsstrahlung process

The definition of a suitable approximation for the real corrections is made difficult by overlapping resonances of the W-bosons. In the bremsstrahlung process, the W-boson propagators differ depending on whether the bremsstrahlung photon is emitted from initial-state
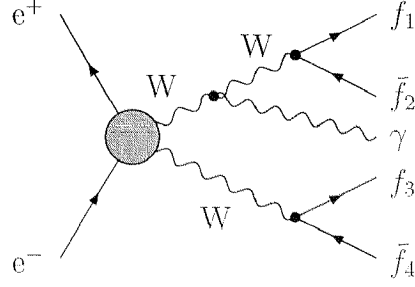
Figure 4.2: Diagram with overlapping resonances

particles or from the decay products of the W boson. Both types of propagators are present in Fig. 4.2 where the poles of the propagators are located at $k_-^2 = M^2$, $k_+^2 = M^2$, and $(k_+ + q)^2 = M^2$. Therefore, the expansion of the cross section about $k_+^2 = M^2$ and $k_-^2 = M^2$, like in the case of the virtual corrections, is not suitable.

The matrix element of the bremsstrahlung process can be written in the following way (see Section 3.1.5):

$$\mathcal{M}_{\text{real}} = \frac{\mathcal{R}(k_+, k_-, q)}{(k_+^2 - M^2)(k_-^2 - M^2)} + \frac{\mathcal{R}_+(k_+, k_-, q)}{[(k_+ + q)^2 - M^2](k_-^2 - M^2)}$$
$$+ \frac{\mathcal{R}_-(k_+, k_-, q)}{(k_+^2 - M^2)[(k_- + q)^2 - M^2]} + \mathcal{N}(k_+, k_-, q), \tag{4.1.9}$$

where $\mathcal{N}$ includes the matrix elements of all non-doubly-resonant diagrams. The factorizable corrections of the cross section are the squares of the single terms corresponding to $\mathcal{R}$, $\mathcal{R}_+$, and $\mathcal{R}_-$, while the non-factorizable corrections are the interferences between these terms.

In the hard photon region, $E_\gamma \gg \Gamma_W$, the two resonances of the W^+ bosons located at $k_+^2 = M^2$ and $(k_+ + q)^2 = M^2$ are well separated in phase space. Only the factorizable corrections contribute in this region in DPA, and the non-factorizable corrections vanish in DPA. For soft photons, $E_\gamma \ll \Gamma_W$, the resonances almost coincide, and the photon momentum can be neglected in the resonant propagators. However, for semi-soft photons with an energy $E_\gamma = \mathcal{O}(\Gamma_W)$, the resonances overlap. Thus the definition of an appropriate approximation is rather complicated and, hence, the reliability becomes unclear.

4.1.4 Inclusion of the real corrections

In order to avoid the problem of overlapping resonances, the bremsstrahlung process is taken into account exactly.

The bremsstrahlung processes are already studied in Chapter 2 including all diagrams. For the numerical discussion, the processes $e^+e^- \rightarrow \nu_\mu \mu^+ \tau^- \bar{\nu}_\tau$, $e^+e^- \rightarrow u \bar{d} \mu^- \bar{\nu}_\mu$, and $e^+e^- \rightarrow u\bar{d}s\bar{c}$ are considered. These are the processes with the smallest number of diagrams within the leptonic, semi-leptonic, and hadronic process classes. Note that the radiative corrections for any leptonic process are equivalent to the radiative corrections for $e^+e^- \rightarrow \nu_\mu \mu^+ \tau^- \bar{\nu}_\tau$ in DPA, in the absence of logarithms $\ln(m_f^2/s)$ from FSR. The same

80

is valid for $e^+e^- \rightarrow u\,\bar{d}\,\mu^-\bar{\nu}_\mu$ and $e^+e^- \rightarrow u\,\bar{d}\,s\,\bar{c}$ concerning semi-leptonic and hadronic processes, respectively.

4.2 Subtraction method

When calculating radiative corrections for four-fermion production, one has to take care of the singularities of the real and virtual radiative corrections. According to the Bloch–Nordsieck theorem [57] the infrared singularities cancel between the virtual and real part. Furthermore, collinear singularities, i.e. mass singularities, appear in the radiative corrections and are regularized by the fermion masses which are neglected otherwise. These singularities originate from collinear photon emission from light external fermions and show up as large logarithms $\ln(m_f^2/s)$. For inclusive enough observables, these collinear singularities cancel between the real and virtual radiative corrections owing to the Kinoshita–Lee–Nauenberg theorem [58], except for the mass singularities remaining from initial-state radiation (ISR) or resulting from renormalization. Two methods are exist for the treatment of the singularities in a Monte Carlo generator: *phase-space slicing* and the *subtraction method*.

Phase-space slicing splits the integration domain by a small separation cut into a part which includes all singularities and a finite part. For infrared singularities the splitting is usually done by a cut on the photon energy, for collinear singularities by a separation angle between the photon and the particle which emits the photon. The integral of the singular part over the photon momentum is analytically performed with an appropriate regularization, and terms of order of the cut parameter are neglected. In this way the singularities are extracted and can be added to the virtual part of the radiative corrections. Both the singular and the finite part of the radiative cross section depend logarithmically on the cut parameter. This dependence must cancel in the complete result. The logarithms of the separation cut are determined in the singular part by analytical integration. On the other hand, they must be compensated by numerical calculation of the corresponding logarithms included in the finite part of the cross section. Therefore, the cut has to be small enough that terms of order of the cut parameter can be neglected in the singular part, but large enough to obtain numerically stable results.

In contrast to phase-space slicing, the subtraction method requires no cut parameter. We use the subtraction method since we expect a better convergence behaviour. This method has been mostly applied for NLO predictions in massless QCD [59, 60][1] where the singularities are usually regularized dimensionally. In Electroweak Standard Model processes it is more convenient to introduce an infinitesimal photon mass as a regularization parameter for infrared singularities and to use small fermion masses for the regularization of the collinear singularities. In order to apply the subtraction method to four-fermion production, this method is formulated for mass regularization.

In the following, only singularities for photon emission off nearly massless external fermions are considered. Other singularities like collinear singularities of diagrams where a virtual photon decays into two external fermions have to be excluded by appropriate

---

[1]The subtraction method for massive particles can be found in Refs. [61, 62].

cuts. The subtraction method described in the following is based on the *dipole formalism* of S. Catani and M.H. Seymour [59]. The results of this section have been worked out independently by S. Dittmaier [61]. Comparing both results we find full consistence.

In the dipole formalism, various mappings are constructed from the five-particle phase space of the bremsstrahlung process $e^+e^- \rightarrow 4f\gamma$ into the four-particle phase space of the non-radiative process $e^+e^- \rightarrow 4f$. These mappings are required to obtain a process-independent formulation of the subtraction method. Each mapping corresponds to a certain singular behaviour of the differential cross section. According to these mappings, the five-particle phase space $\Phi^{(5)}$ splits into a four-particle phase space $\Phi^{(4)}$ and a remaining one-particle phase space, which contains the singularities:

$$\int \mathrm{d}\Phi^{(5)} = \int_0^1 \mathrm{d}x_1 \mathrm{d}x_2 \int \mathrm{d}\Phi^{(4)}(x_1 p_1, x_2 p_2) \int \mathrm{d}\Phi_{ik} \qquad (4.2.1)$$

with $i, k = 1, \ldots 6$. In the following, particles 1, 2 are initial-state fermions and $3, \ldots, 6$ final-state fermions. For the discussion of the subtraction method, all particle momenta are denoted by p_i and the photon momentum by q.

The arguments of $\mathrm{d}\Phi^{(4)}(x_1 p_1, x_2 p_2)$ indicate that the final-state momenta are calculated for incoming momenta $x_1 p_1$ and $x_2 p_2$. The one-particle phase space is decomposed into integrations over Φ_{ik} and over the momentum fractions of the incoming momenta x_1 and x_2. In this way, all different splittings of the five-particle phase space fit in this formula. The variables x_1 and x_2 are partly fixed by δ-distributions included in definition of Φ_{ik}.

For each mapping a subtraction term $\mathcal{V}_{ik}$ is constructed in such a way that it matches the singular behaviour of the cross section of the bremsstrahlung process in a certain phase-space region and that it can be analytically integrated over Φ_{ik}. The subtraction term is subtracted from the real corrections and added to the virtual corrections after analytic integration over Φ_{ik}:

$$\int \mathrm{d}\Phi^{(5)} \left| \mathcal{M}_{\mathrm{Born}}^{(5)} \right|^2 \mathcal{O}\left(\Phi^{(5)}\right) + \int \mathrm{d}\Phi^{(4)} 2\,\mathrm{Re}\left\{ \mathcal{M}_{\mathrm{virt}}^{(4)} \mathcal{M}_{\mathrm{Born}}^{(4)*} \right\} \mathcal{O}\left(\Phi^{(4)}\right)$$

$$= \int \mathrm{d}\Phi^{(5)} \left[\left| \mathcal{M}_{\mathrm{Born}}^{(5)} \right|^2 \mathcal{O}\left(\Phi^{(5)}\right) - \sum_{\substack{i,k=1 \\ i \neq k}}^{6} \mathcal{V}_{ik}\, \mathcal{O}\left(\Phi^{(4)}\left(\Phi^{(5)}\right)\right) \right]$$

$$+ \int_0^1 \mathrm{d}x_1 \mathrm{d}x_2 \int \mathrm{d}\Phi^{(4)}(x_1 p_1, x_2 p_2)\, \mathcal{O}\left(\Phi^{(4)}\right)$$

$$\times \left\{ 2\,\mathrm{Re}\left(\mathcal{M}_{\mathrm{virt}}^{(4)} \mathcal{M}_{\mathrm{Born}}^{(4)*} \right) \delta(1 - x_1)\delta(1 - x_2) + \sum_{\substack{i,k=1 \\ i \neq k}}^{6} \left[\int \mathrm{d}\Phi_{ik}\, \mathcal{V}_{ik} \right] \right\}, \quad (4.2.2)$$

where $\mathcal{M}_{\mathrm{Born}}^{(4)}$, $\mathcal{M}_{\mathrm{Born}}^{(5)}$, and $\mathcal{M}_{\mathrm{virt}}^{(4)}$ are the matrix elements of the tree-level process, the bremsstrahlung process, and the virtual corrections, respectively. The experimental situation, e.g. cuts, are included in the definition of the observable $\mathcal{O}$. Note that the observable $\mathcal{O}$ depends on the momenta of the four-particle or five-particle phase spaces. All integrations are performed numerically, except for the integration over Φ_{ik} which is performed analytically.

In this way, a part of the real corrections including the singularities is transferred to the virtual corrections. The difference between the cross section of the bremsstrahlung process

and the subtraction terms includes no singularities and hence can be integrated over the whole phase space. Note that it is not allowed to exclude the soft-photon region from the integration domain where the cross section of the bremsstrahlung process becomes infrared singular, since the infrared singularities have to cancel between the real and virtual corrections. This is in accordance with the fact, that it is not possible to separate experimentally photons with infinitesimal small energies from charged particles.

The situation for collinear singularities is different since collinear singularities show up as large logarithms of small but finite fermion masses. If fermion masses are used as regularization parameters, the phase-space region where the photon becomes collinear to an external fermion has to be included in the integration domain.

4.2.1 Behaviour of the cross section for collinear photons

As a first step, the collinear limit of the cross section for ISR is considered. It is convenient to calculate the collinear limit of the cross section in an axial gauge, where the photon polarization sum runs only over transverse polarizations and hence interference contributions do not involve collinear singularities. A photon with momentum q is emitted from an unpolarized initial-state fermion with momentum p_a, mass m_a, and relative charge Q_a. The relevant part of the cross section multiplied by the polarization sum of the photon reads

$$
\left[\frac{i}{\not{p}_a - \not{q} - m_a}(-ieQ_a)\gamma_\mu(\not{p}_a + m_a)ieQ_a\gamma_\nu \frac{-i}{\not{p}_a - \not{q} - m_a} \right] \left[-g^{\mu\nu} + \frac{q^\mu n^\nu + q^\nu n^\mu}{qn} \right]
$$

$$
= e^2 Q_a^2 \left[\frac{(1-x)\not{p}_a - \not{q}}{p_a q} \left(\frac{x}{1-x} - \frac{m_a^2}{p_a q} \right) + \frac{m_a}{p_a q} \left(\frac{2}{1-x} - \frac{m_a^2}{p_a q} \right) + \frac{\not{n}}{nq} \right]
$$

$$
+ \frac{e^2 Q_a^2}{p_a q} \left(\frac{1}{x} P(x) - \frac{m_a^2}{p_a q} \right) x \not{p}_a \tag{4.2.3}
$$

with $n^2 = 0$, $qn \neq 0$, $x = 1 - (nq)/(np_a)$, and the splitting function is given by

$$
P(x) = \frac{1+x^2}{1-x}. \tag{4.2.4}
$$

The arbitrary vector n is introduced to define the polarization of the photon.

The factor $(1-x)\not{p}_a - \not{q}$ vanishes in the collinear limit. Only the last term on the right-hand side proportional to $x\not{p}_a$ is singular in the collinear limit $q \to (1-x)p_a$. Hence, the collinear limit for photon radiation off unpolarized initial-state particles yields

$$
\left| \mathcal{M}^{(5)}_{\text{collinear}}(p_a, q) \right|^2 = \frac{e^2 Q_a^2}{p_a q} \left[\frac{1}{x} P(x) - \frac{m_a^2}{p_a q} \right] \left| \mathcal{M}^{(4)}_{\text{Born}}(xp_a) \right|^2. \tag{4.2.5}
$$

The behaviour of the cross section for polarized particles in the collinear limit can be found in Ref. [63]:

$$
\left| \mathcal{M}^{(5)}_{\text{collinear}}(p_a, \sigma_a, q) \right|^2 = \frac{e^2 Q_a^2}{p_a q} \left\{ \left[\frac{1}{x} P(x) - \frac{1+x^2}{x} \frac{m_a^2}{2p_a q} \right] \left| \mathcal{M}^{(4)}_{\text{Born}}(xp_a, \sigma_a) \right|^2 \right.
$$

$$
\left. + \frac{(1-x)^2}{x} \frac{m_a^2}{2p_a q} \left| \mathcal{M}^{(4)}_{\text{Born}}(xp_a, -\sigma_a) \right|^2 \right\} \tag{4.2.6}
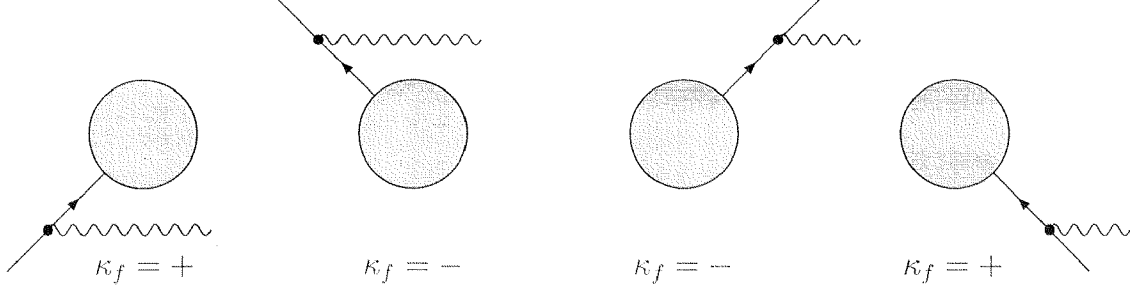$$

Figure 4.3: Value of κ_f for the different photon radiation off fermions

with the helicity σ_a of the initial-state fermion a. In the following all results are calculated for helicity eigenstates of the external fermions.

For massive fermions the collinear limit involves a helicity-flip term proportional to the square of the fermion mass, called finite-mass term. Note that if the cross section of the bremsstrahlung process is calculated for vanishing fermion masses the finite-mass terms are missing and have to be added to the cross section of the bremsstrahlung process or skipped in the corresponding subtraction terms in (4.2.2).

In order to be able to combine the collinear and soft limit in Section 4.2.3, we use charge conservation

$$\kappa_i Q_i = - \sum_{\substack{k \\ i \neq k}} \kappa_k Q_k \tag{4.2.7}$$

to obtain

$$\left| \mathcal{M}^{(5)}_{\text{collinear}}(p_a, \sigma_a, q) \right|^2 = - \sum_{\substack{k \\ k \neq a}} \frac{\kappa_a \kappa_k e^2 Q_a Q_k}{p_a q} \left\{ \left[\frac{1}{x} P(x) - \frac{1 + x^2}{x} \frac{m_a^2}{2 p_a q} \right] \left| \mathcal{M}^{(4)}_{\text{Born}}(x p_a, \sigma_a) \right|^2 \right.$$
$$\left. + \frac{(1 - x)^2}{x} \frac{m_a^2}{2 p_a q} \left| \mathcal{M}^{(4)}_{\text{Born}}(x p_a, -\sigma_a) \right|^2 \right\}. \tag{4.2.8}$$

The sign κ_i refers to charge flow of fermion i into or out of the diagram, respectively, which is illustrated in Fig. 4.3.

For FSR, q has to be replaced by $-q$:

$$\left| \mathcal{M}^{(5)}_{\text{collinear}}(p_i, \sigma_i, q) \right|^2 = - \sum_{\substack{k \\ k \neq i}} \frac{\kappa_i \kappa_k e^2 Q_i Q_k}{p_i q} \left\{ \left[P(z) - \frac{1 + z^2}{z} \frac{m_i^2}{2 p_i q} \right] \left| \mathcal{M}^{(4)}_{\text{Born}}\left(\frac{p_i}{z}, \sigma_i \right) \right|^2 \right.$$
$$\left. + \frac{(1 - z)^2}{z} \frac{m_i^2}{2 p_i q} \left| \mathcal{M}^{(4)}_{\text{Born}}\left(\frac{p_i}{z}, -\sigma_i \right) \right|^2 \right\} \tag{4.2.9}$$

with $z = (n p_i)/(n p_i + n q)$, where the particle i is a final-state particle.
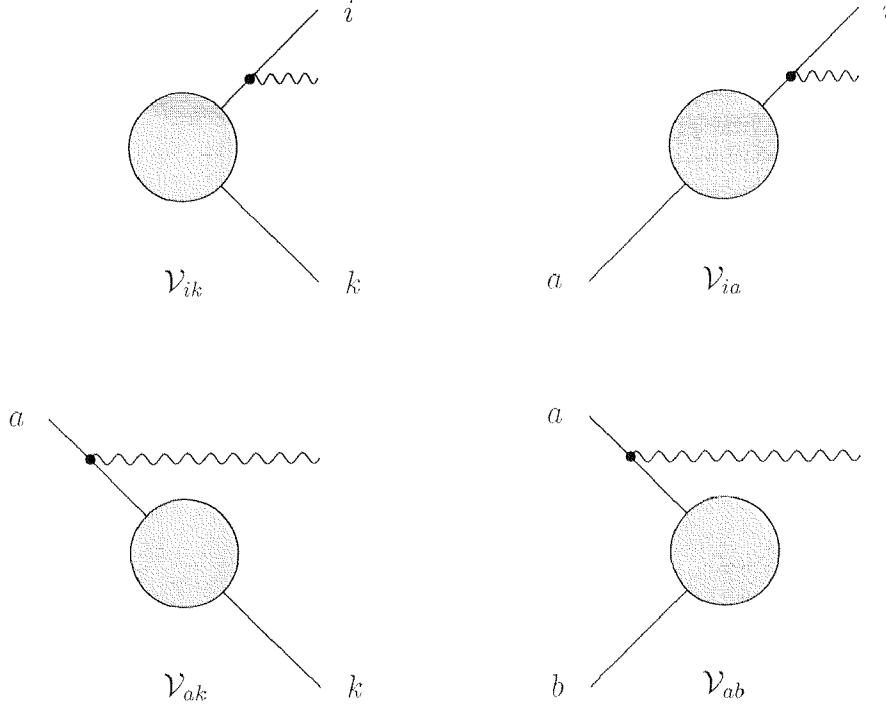
84

Figure 4.4: Diagrams for different combinations of initial-state or final-state emitter and spectator

4.2.2 Soft-photon approximation of the cross section

The infrared limit is given by the well known soft-photon approximation

$$\left|\mathcal{M}^{(5)}_{\text{soft}}\right|^2 = -\sum_{i,k} \frac{\kappa_i \kappa_k e^2 Q_i Q_k p_i p_k}{(p_i q)(p_k q)} \left|\mathcal{M}^{(4)}_{\text{Born}}\right|^2 . \tag{4.2.10}$$

After applying partial fractioning

$$\frac{p_i p_k}{(p_i q)(p_k q)} = \frac{p_i p_k}{[(p_i + p_k)q](p_k q)} + \frac{p_i p_k}{[(p_i + p_k)q](p_i q)} \tag{4.2.11}$$

and distributing the finite-mass term with $i = k$ with the help of charge conservation (4.2.7) to the terms with $i \neq k$, the soft limit reads

$$\left|\mathcal{M}^{(5)}_{\text{soft}}\right|^2 = -\sum_{\substack{i,k \\ i \neq k}} \frac{\kappa_i \kappa_k e^2 Q_i Q_k}{p_i q} \left[\frac{2 p_i p_k}{(p_i + p_k)q} - \frac{m_i^2}{p_i q} \right] \left|\mathcal{M}^{(4)}_{\text{Born}}\right|^2 . \tag{4.2.12}$$

In this way, the soft-photon approximation (4.2.12) is written in a similar way as the collinear limits (4.2.8) and (4.2.9).

4.2.3 Construction of the subtraction terms

The subtraction terms have to be constructed in such a way that they reproduce both the soft and collinear limit of the cross section. The soft-photon limit (4.2.12) depends

on two momenta p_i and p_k. Particle i is called emitter and k spectator, since the soft-photon approximation is singular if the photon becomes collinear to the emitter, but not if the photon is collinear to the spectator. Since the mass of the spectator regularizes no singularities, it is neglected in the following calculations. The diagrams corresponding to the four possible combinations of initial-state or final-state emitter and spectator are shown in Fig. 4.4.

Although the following results are formulated for four-fermion production, they can be applied to all processes where the external particles are light charged fermions and any other massless or massive neutral particles. Note that it is some freedom in the definition of the subtraction term and the separation of the one-particle phase space. In the following, all initial-state particles are denoted by the indices a or b with $a \neq b$ and $a, b = 1, 2$.

Final-state emitter with final-state spectator

Firstly, the case is considered where the emitter and spectator are final-state particles. A suitable subtraction term is defined by[2]

$$
\mathcal{V}_{ik} = -\frac{\kappa_i \kappa_k e^2 Q_i Q_k}{p_i q} \left\{ \left[\frac{2}{1 - z_{ik}(1 - y_{ik})} - (1 + z_{ik}) - \frac{1 + z_{ik}^2}{z_{ik}} \frac{m_i^2}{2 p_i q} \right] \left| \mathcal{M}_{\mathrm{Born}}^{(4)}(\tilde{p}_i, \sigma_i, \tilde{p}_k) \right|^2 \right.
$$
$$
\left. + \frac{(1 - z_{ik})^2}{z_{ik}} \frac{m_i^2}{2 p_i q} \left| \mathcal{M}_{\mathrm{Born}}^{(4)}(\tilde{p}_i, -\sigma_i, \tilde{p}_k) \right|^2 \right\} \tag{4.2.13}
$$

with the momenta of the four-particle phase space

$$
\tilde{p}_i = p_i + q - \frac{y_{ik}}{1 - y_{ik}} p_k, \qquad \tilde{p}_k = \frac{1}{1 - y_{ik}} p_k \tag{4.2.14}
$$

and the variables

$$
z_{ik} = \frac{p_i p_k}{p_i p_k + p_k q}, \qquad y_{ik} = \frac{p_i q}{p_i p_k + p_i q + p_k q}, \tag{4.2.15}
$$

where the indices i and k mark the emitter and the spectator, respectively.

The subtraction term obeys the soft limit (4.2.12) for $z_{ik} \to 1$ and $y_{ik} \to 0$, which can be verified with the help of

$$
\frac{1}{1 - z_{ik}(1 - y_{ik})} = \frac{p_i q + p_k q + p_i p_k}{(p_i + p_k) q}. \tag{4.2.16}
$$

Furthermore, if the momentum n after (4.2.9) is identified with the momentum of the spectator p_k, the subtraction term reproduces the cross section in the collinear limit, i.e. $y_{ik} \to 0$, $z_{ik} \to z$, and $\tilde{p}_i \to p_i/z$, (4.2.9).

The subtraction term is proportional to the Born matrix element $\mathcal{M}_{\mathrm{Born}}^{(4)}$ which depends on the momenta $\tilde{p}_i$ and $\tilde{p}_k$ of the four-particle phase space. These momenta are fixed for the analytical integration over Φ_{ik}. The momenta $\tilde{p}_i$ and $\tilde{p}_k$ are chosen in such a way that they fulfil momentum conservation

$$
0 = K + p_i + p_k + q = K + \tilde{p}_i + \tilde{p}_k \tag{4.2.17}
$$

---

[2]Note that the actual definition of the subtraction term of Ref. [61] differs by a factor $1 - y_{ik}$.

and the on-shell conditions of the four-particle phase space

$$\tilde{m}_i^2 = m_i^2 + \lambda^2 \to 0, \qquad \tilde{m}_k^2 = 0. \tag{4.2.18}$$

The momentum K is the sum of the momenta of the external particles, except for the emitter, the spectator, and the photon. The infinitesimal photon mass is denoted by λ.

The next step is to relate the momenta of the five-particle phase space to the momenta of the four-particle phase space and the variables z_{ik} and y_{ik} of the one-particle phase space. Therefore, we apply the mappings

$$p_i \mapsto y_{ik}, z_{ik}, k_\perp : p_i = \left(\frac{y_{ik}}{1 - y_{ik}} \frac{1}{1 - z_{ik}} - \frac{z_{ik}}{1 - z_{ik}} \frac{\lambda^2}{p_k q} \right) p_k + \frac{z_{ik}}{1 - z_{ik}} q + k_\perp, \tag{4.2.19}$$

$$p_k \mapsto \tilde{p}_k \qquad : p_k = (1 - y_{ik})\tilde{p}_k, \tag{4.2.20}$$

$$q \mapsto \tilde{p}_i \qquad : q = (1 - z_{ik})\tilde{p}_i - y_{ik} z_{ik} \tilde{p}_k + \frac{z_{ik}}{1 - z_{ik}} \frac{\lambda^2}{\tilde{p}_i \tilde{p}_k} \tilde{p}_k - (1 - z_{ik})k_\perp \tag{4.2.21}$$

with $k_\perp p_k = k_\perp q = 0$ and find the splitting of the five-particle phase space into the four-particle phase space determined by the momenta $\tilde{p}_i$ and $\tilde{p}_k$ and the remaining one-particle phase space:

$$\int \frac{d^4 p_i}{(2\pi)^3} \frac{d^4 p_k}{(2\pi)^3} \frac{d^4 q}{(2\pi)^3} \delta(p_i^2 - m_i^2)\theta(p_{i,0})\delta(p_k^2)\theta(p_{k,0})\delta(q^2 - \lambda^2)\theta(q_0)\delta^{(4)}(K - p_i - p_k - q)$$

$$= \int_0^1 dx_1 dx_2 \int \frac{d^4 \tilde{p}_i}{(2\pi)^3} \frac{d^4 \tilde{p}_k}{(2\pi)^3} \delta(\tilde{p}_i^2 - m_i^2 - \lambda^2)\theta(\tilde{p}_{i,0})\delta(\tilde{p}_k^2)\theta(\tilde{p}_{k,0})\delta^{(4)}(K - \tilde{p}_i - \tilde{p}_k) \int d\Phi_{ik}$$
$$\tag{4.2.22}$$

with the integral over the separated one-particle phase space

$$\int d\Phi_{ik} = \frac{\tilde{p}_i \tilde{p}_k}{8\pi^2} \delta(1 - x_1)\delta(1 - x_2) \int_0^{2\pi} \frac{d\phi_{k_\perp}}{2\pi} \int_0^1 dz_{ik} \int_0^1 dy_{ik}(1 - y_{ik})$$

$$\times \theta \left(y_{ik} - \frac{\lambda^2 z_{ik}^2 + m_i^2(1 - z_{ik})^2}{z_{ik}(1 - z_{ik})2\tilde{p}_i \tilde{p}_k} \right). \tag{4.2.23}$$

The additional integrations over x_1 and x_2 are introduced in order to match the definitions of (4.2.1). The masses λ and m_i in the δ-distribution of (4.2.22) can be neglected since they do not regularize singularities. The step function θ in (4.2.23) results from the requirement $k_\perp^2 < 0$ of (4.2.21) and regularizes all singularities. It can be verified in the rest frame of $p_i + p_k$ that $k_\perp$ is a space-like vector. The variable $\phi_{k_\perp}$ is the solid angle of $k_\perp$ with respect to p_k in the rest frame of $p_i + p_k$. Since the subtraction term does not depend on $\phi_{k_\perp}$ the integration over $\phi_{k_\perp}$ yields 2π. Note that the Born cross section included in the subtraction term $\mathcal{V}_{ik}$ depends exclusively on the momenta of the four-particle phase space, which are fixed for the integration over z_{ik} and y_{ik}.

Finally, the subtraction term is integrated over the one-particle phase space yielding

$$\int d\Phi_{ik}\mathcal{V}_{ik} = -\frac{\kappa_i \kappa_k e^2 Q_i Q_k}{8\pi^2} \delta(1 - x_1)\delta(1 - x_2)$$

$$\times \left\{ \left[\mathcal{L}(\lambda^2, m_i^2, 2\tilde{p}_i \tilde{p}_k) + \frac{5}{2} - \frac{2}{3}\pi^2 \right] \left| \mathcal{M}_{\text{Born}}^{(4)}(\tilde{p}_i, \sigma_i, \tilde{p}_k) \right|^2 + \frac{1}{2} \left| \mathcal{M}_{\text{Born}}^{(4)}(\tilde{p}_i, -\sigma_i, \tilde{p}_k) \right|^2 \right\}$$

$$+ \mathcal{O}(\lambda) + \mathcal{O}(m_i) \tag{4.2.24}$$

with

$$\mathcal{L}(\lambda^2, m_i^2, 2\tilde{p}_i\tilde{p}_k) = \frac{1}{2}\ln^2\left(\frac{\lambda^2}{2\tilde{p}_i\tilde{p}_k}\right) - \frac{1}{2}\ln^2\left(\frac{\lambda^2}{m_i^2}\right) + \frac{3}{2}\ln\left(\frac{m_i^2}{2\tilde{p}_i\tilde{p}_k}\right) + \ln\left(\frac{\lambda^2}{m_i^2}\right), \quad (4.2.25)$$

where the photon mass is neglected with respect to the fermion masses, i.e. $\lambda \ll m_i$.

Final-state emitter with initial-state spectator

Next, the subtraction term for final-state emitter and initial-state spectator is considered. The subtraction term with the correct collinear and soft limit is defined by

$$\mathcal{V}_{ia} = -\frac{\kappa_i \kappa_a e^2 Q_i Q_a}{p_i q}\left\{\left[\frac{2}{2 - z_{ia} - x_{ia}} - 1 - z_{ia} - \frac{1 + z_{ia}^2}{z_{ia}}\frac{m_i^2}{2p_i q}\right]\frac{1}{x_{ia}}\left|\mathcal{M}_{\text{Born}}^{(4)}(\tilde{p}_i, \sigma_i, \tilde{p}_a)\right|^2\right.$$
$$\left. + \frac{(1 - z_{ia})^2}{z_{ia}}\frac{m_i^2}{2p_i q}\frac{1}{x_{ia}}\left|\mathcal{M}_{\text{Born}}^{(4)}(\tilde{p}_i, -\sigma_i, \tilde{p}_a)\right|^2\right\} \quad (4.2.26)$$

with the momenta of the four-particle phase space

$$\tilde{p}_i = p_i + q - (1 - x_{ia})p_a, \qquad \tilde{p}_a = x_{ia}p_a, \quad (4.2.27)$$

and the variables

$$z_{ia} = \frac{p_i p_a}{p_i p_a + p_a q}, \qquad x_{ia} = \frac{p_i p_a + p_a q - p_i q}{p_i p_a + p_a q}. \quad (4.2.28)$$

Similarly to the previous section, the momenta $\tilde{p}_i$ and $\tilde{p}_a$ fulfil momentum conservation and the on-shell requirement for the external particles of the four-particle phase space.

In order to separate the integral over the one-particle phase space from the integral over the five-particle phase space, the following mappings are used:

$$p_i \mapsto x_{ia}, z_{ia}, k_\perp : p_i = \left(\frac{1 - x_{ia}}{1 - z_{ia}} - \frac{z_{ia}}{1 - z_{ia}}\frac{\lambda^2}{p_a q}\right)p_a + \frac{z_{ia}}{1 - z_{ia}}q + k_\perp, \quad (4.2.29)$$

$$q \mapsto \tilde{p}_i \qquad : q = (1 - z_{ia})\tilde{p}_i - (1 - x_{ia})z_{ia}p_a + \frac{z_{ia}}{1 - z_{ia}}\frac{\lambda^2}{\tilde{p}_i p_a}p_a - (1 - z_{ia})k_\perp \quad (4.2.30)$$

with $k_\perp p_a = k_\perp q = 0$. They result in the splitting of the phase space

$$\int \frac{\mathrm{d}^4 p_i}{(2\pi)^3}\frac{\mathrm{d}^4 q}{(2\pi)^3}\delta(p_i^2 - m_i^2)\theta(p_{i,0})\delta(q^2 - \lambda^2)\theta(q_0)\delta^{(4)}(K + p_a - p_i - q)$$

$$= \int_0^1 \mathrm{d}x_a \mathrm{d}x_b \int \frac{\mathrm{d}^4\tilde{p}_i}{(2\pi)^3}\delta(\tilde{p}_i^2 - m_i^2 - \lambda^2)\theta(\tilde{p}_{i,0})\delta^{(4)}(K + \tilde{p}_a - \tilde{p}_i)\int \mathrm{d}\Phi_{ia} \quad (4.2.31)$$

with

$$\int \mathrm{d}\Phi_{ia} = \frac{\tilde{p}_i p_a}{8\pi^2}\delta(x_{ia} - x_a)\delta(1 - x_b)\int_0^{2\pi}\frac{\mathrm{d}\phi_{k_\perp}}{2\pi}\int_0^1 \mathrm{d}z_{ia}$$

$$\times \theta\left((1 - x_{ia}) - \frac{\lambda^2 z_{ia}^2 + m_i^2(1 - z_{ia})^2}{z_{ia}(1 - z_{ia})2\tilde{p}_i p_a}\right), \quad (4.2.32)$$

where $\phi_{k_\perp}$ is the solid angle with respect to p_a in the rest frame of $p_a + p_i$. Since the spectator is an initial-state particle, the four-particle phase space becomes x_a-dependent and the one-particle phase space is included in the x_a-integration. As in the previous case the θ-function originates from $k_\perp^2 < 0$ of the mapping (4.2.30) and regularizes all singularities. Furthermore, the masses m_i and λ can be omitted in the δ-distribution of (4.2.31).

Since the subtraction term does not depend of $\phi_{k_\perp}$, the integration over $\phi_{k_\perp}$ yields 2π. Moreover, the Born cross section included in the subtraction term does not depend on z_{ia}, but is a function of x_{ia}. In order to avoid the analytic integration over the Born cross section, the subtraction term is integrated for fixed Born cross section at $x_{ia} = 1$. The x_{ia}-dependence of the Born cross section is taken into account with the help of the $+$-distribution, which is defined as usual by

$$\int_0^1 \mathrm{d}x\, g(x)[f(x)]_+ = \int_0^1 \mathrm{d}x[g(x) - g(1)]f(x), \qquad (4.2.33)$$

where $g(x)$ is an arbitrary test function.

The integration of subtraction term yields

$$\int \mathrm{d}\Phi_{ia} \mathcal{V}_{ia} = -\frac{\kappa_i \kappa_a e^2 Q_i Q_a}{8\pi^2} \delta(1 - x_b)$$
$$\times \left\{ \left\{ \left[\mathcal{L}(\lambda^2, m_i^2, 2\tilde{p}_i \tilde{p}_a) + 1 - \frac{\pi^2}{2} \right] \delta(1 - x_a) + \left[\frac{2}{1 - x_a} \ln\left(\frac{2 - x_a}{1 - x_a}\right) - \frac{3}{2}\frac{1}{1 - x_a} \right]_+ \right\} \right.$$
$$\left. \times \frac{1}{x_a} \left| \mathcal{M}_{\text{Born}}^{(4)}(\tilde{p}_i, \sigma_i, \tilde{p}_a) \right|^2 + \frac{1}{2}\delta(1 - x_a) \left| \mathcal{M}_{\text{Born}}^{(4)}(\tilde{p}_i, -\sigma_i, \tilde{p}_a) \right|^2 \right\}$$
$$+ \mathcal{O}(\lambda) + \mathcal{O}(m_i) \qquad (4.2.34)$$

with $\lambda \ll m_i$ and the function $\mathcal{L}$ defined in (4.2.25). The mass and infrared singularities of (4.2.34) have a similar form as in (4.2.24). Note that the $+$-distribution acts on the matrix element, the observable $\mathcal{O}$ (see (4.2.2)), and the momenta $\tilde{p}_i$ and $\tilde{p}_a$. Here and in the following case, the momenta of the four-particle phase-space are implicitly understood to be functions of x_a with $x_a = x_{ia}$.

Initial-state emitter with final-state spectator

Borrowing the previous definitions of the momenta of the four-particle phase space (4.2.27) and of the variables x_{ia} and z_{ia} (4.2.28), an appropriate subtraction term is defined by

$$\mathcal{V}_{ai} = -\frac{\kappa_a \kappa_i e^2 Q_a Q_i}{p_a q} \left\{ \left[\frac{2}{2 - x_{ia} - z_{ia}} - 1 - x_{ia} - (1 + x_{ia}^2)\frac{m_a^2}{2p_a q} \right] \frac{1}{x_{ia}} \left| \mathcal{M}_{\text{Born}}^{(4)}(\tilde{p}_a, \sigma_a, \tilde{p}_i) \right|^2 \right.$$
$$\left. + (1 - x_{ia})^2 \frac{m_a^2}{2p_a q}\frac{1}{x_{ia}} \left| \mathcal{M}_{\text{Born}}^{(4)}(\tilde{p}_a, -\sigma_a, \tilde{p}_i) \right|^2 \right\}. \qquad (4.2.35)$$

As in the previous case, the mappings

$$q \mapsto x_{ia}, z_{ia}, k_\perp : q = \frac{1 - x_{ia}}{z_{ia}} p_a + \left(\frac{1 - z_{ia}}{z_{ia}} - \frac{1 - x_{ia}}{z_{ia}}\frac{m_a^2}{p_a p_i} \right) p_i + k_\perp, \qquad (4.2.36)$$

$$p_i \mapsto \tilde{p}_i \qquad : p_i = \{z_{ia}\tilde{p}_i - (1 - x_{ia})(1 - z_{ia})p_a - z_{ia}k_\perp\}$$
$$\times \left\{ \frac{z_{ia}[\tilde{p}_i p_a + (1 - x_{ia})m_a^2]}{z_{ia}\tilde{p}_i p_a - (1 - z_{ia})(1 - x_{ia})m_a^2} \right\} \tag{4.2.37}$$

with $k_\perp p_a = k_\perp p_i = 0$ result in the splitting of the phase-space integral

$$\int \frac{\mathrm{d}^4 p_i}{(2\pi)^3} \frac{\mathrm{d}^4 q}{(2\pi)^3} \delta(p_i^2)\theta(p_{i,0})\delta(q^2 - \lambda^2)\theta(q_0)\delta^{(4)}(K + p_a - p_i - q)$$
$$= \int_0^1 \mathrm{d}x_a \mathrm{d}x_b \int \frac{\mathrm{d}^4 \tilde{p}_i}{(2\pi)^3}\delta(\tilde{p}_i^2 - \lambda^2 + (1 - x_a)^2 m_a^2)\theta(\tilde{p}_{i,0})\delta^{(4)}(K + \tilde{p}_a - \tilde{p}_i) \int \mathrm{d}\Phi_{ai} \tag{4.2.38}$$

with

$$\int \mathrm{d}\Phi_{ai} = \int_0^{2\pi} \frac{\mathrm{d}\phi_{k_\perp}}{2\pi} \int_0^1 \mathrm{d}x_{ia} \int_0^1 \mathrm{d}z_{ia} \delta(x_a - x_{ia})\delta(1 - x_b)$$
$$\times \frac{\tilde{p}_i p_a + (1 - x_{ia})m_a^2}{8\pi^2} \left\{ \frac{z_{ia}[\tilde{p}_i p_a + (1 - x_{ia})m_a^2]}{z_{ia}\tilde{p}_i p_a - (1 - z_{ia})(1 - x_{ia})m_a^2]} \right\}$$
$$\times \theta\left(1 - \frac{m_i^2 z_{ia}^2 + m_a^2(1 - x_{ia})^2[(1 - z_{ia})^2 + z_{ia}^2]}{(1 - z_{ia})z_{ia}(1 - x_{ia})2\tilde{p}_i p_a}\right). \tag{4.2.39}$$

The variable $\phi_{k_\perp}$ is the solid angle between p_a and $k_\perp$ in the rest frame of $p_a + p_i$ and the masses λ and m_a can be omitted in (4.2.38). The θ-function results from $k_\perp^2 < 0$.

The integration of the subtraction term over z_{ia} and x_{ia} for fixed p_a and $\tilde{p}_i$ provides

$$\int \mathrm{d}\Phi_{ai}\mathcal{V}_{ai} = -\frac{\kappa_a \kappa_i e^2 Q_a Q_i}{8\pi^2}\delta(1 - x_b)$$
$$\times \left\{ \left\{ \left[\mathcal{L}(\lambda^2, m_a^2, 2\tilde{p}_a\tilde{p}_i) - \frac{1}{4} - \frac{\pi^2}{6}\right]\delta(1 - x_a) + \left[\frac{2}{1 - x_a}\ln\left(\frac{1 - x_a}{2 - x_a}\right)\right]_+ \right. \right.$$
$$\left. - [P(x_a)(\ln(1 - x_a) + 1)]_+ - [P(x_a)]_+ \ln\left(\frac{m_a^2}{2p_a\tilde{p}_i}\right) \right\}\frac{1}{x_a}\left|\mathcal{M}_{\text{Born}}^{(4)}(\tilde{p}_a, \sigma_i, \tilde{p}_i)\right|^2$$
$$\left. + \left\{\frac{1}{2}\delta(1 - x_a) + [1 - x_a]_+\right\}\frac{1}{x_a}\left|\mathcal{M}_{\text{Born}}^{(4)}(\tilde{p}_a, -\sigma_a, \tilde{p}_i)\right|^2 \right\}$$
$$+ \mathcal{O}(\lambda) + \mathcal{O}(m_a) \tag{4.2.40}$$

with $\lambda \ll m_a$ and the function $\mathcal{L}$ defined in (4.2.25). The x_a-independent singularities are similar to the previous integrated subtraction term. Extra x_a-dependent mass singularities appear in (4.2.40) and are proportional to the splitting function $P(x_a)$.

While in Ref. [61] the momentum $\tilde{p}_a$ has been fixed for the x_{ia}-integration, here we fix the momentum p_a. Although the actual form of the subtraction terms are different, the results for integrated observables are the same. One can reproduce the result of Ref. [61] with

$$\int_0^1 \mathrm{d}x_a [P(x_a)]_+ \ln\left(\frac{m_a^2}{2p_a\tilde{p}_i}\right)g(x_a)$$
$$= \int_0^1 \mathrm{d}x_a \left\{ [P(x_a)]_+ \ln\left(\frac{m_a^2}{2\tilde{p}_a\tilde{p}_i}\right) + \left(\frac{5}{4} - \frac{\pi^2}{3}\right)\delta(1 - x_a)\right\}g(x_a). \tag{4.2.41}$$

Initial-state emitter with initial-state spectator

Finally, the subtraction terms for initial-state emitter and spectator are considered. The subtraction term reads

$$
\mathcal{V}_{ab} = -\frac{\kappa_a \kappa_b e^2 Q_a Q_b}{p_a q} \left\{ \left[\frac{2}{1 - x_{ab}} - 1 - x_{ab} - (1 + x_{ab}^2)\frac{m_a^2}{2 p_a q} \right] \frac{1}{x_{ab}} \left| \mathcal{M}_{\text{Born}}^{(4)}(\tilde{p}_a, \sigma_a, \tilde{p}_b) \right|^2 \right.
$$
$$
\left. + (1 - x_{ab})^2 \frac{m_a^2}{2 p_a q} \frac{1}{x_{ab}} \left| \mathcal{M}_{\text{Born}}^{(4)}(\tilde{p}_a, -\sigma_a, \tilde{p}_b) \right|^2 \right\} \tag{4.2.42}
$$

with the momenta of the four-particle phase space

$$
\tilde{p}_a = x_{ab} p_a, \qquad \tilde{p}_b = p_b \tag{4.2.43}
$$

and the variables

$$
v_{ab} = \frac{p_a q}{p_a p_b}, \qquad x_{ab} = \frac{p_a p_b - p_a q - p_b q}{p_a p_b}. \tag{4.2.44}
$$

Since the momenta of the four-particle phase space have to fulfil momentum conservation, the momenta p_i of the final-state particles are also modified:

$$
\tilde{p}_i^\mu = p_i^\mu - \frac{(K + \tilde{K}) p_i}{(K + \tilde{K}) K} (K + \tilde{K})^\mu + \frac{2 K p_i}{K^2} \tilde{K}^\mu \tag{4.2.45}
$$

with following auxiliary momenta

$$
K = p_a + p_b - q = \sum_{i=3}^{6} p_i, \qquad \tilde{K} = \tilde{p}_a + \tilde{p}_b = \sum_{i=3}^{6} \tilde{p}_i. \tag{4.2.46}
$$

Equation (4.2.45) is a proper Lorentz transformation of the momenta p_i into $\tilde{p}_i$ in the massless limit.[3]

The mapping from the five-particle phase space into the four-particle phase space reads

$$
q \mapsto x_{ab}, v_{ab}, k_\perp : q = \left[v_{ab} - (1 - x_{ab} - v_{ab})\frac{m_a^2}{p_a p_b} \right] p_b + (1 - x_{ab} - v_{ab}) p_a + k_\perp \tag{4.2.47}
$$

with $k_\perp p_a = k_\perp p_b = 0$.

Hence, the splitting of the phase-space integral takes the form

$$
\prod_i \int \frac{\mathrm{d}^4 p_i}{(2\pi)^3} \frac{\mathrm{d}^4 q}{(2\pi)^3} \delta(p_i^2 - m_i^2)\theta(p_{i,0})\delta(q^2 - \lambda^2)\theta(q_0)\delta^{(4)}(p_a + p_b - \textstyle\sum_i p_i - q)
$$
$$
= \int_0^1 \mathrm{d}x_a \mathrm{d}x_b \prod_i \int \frac{\mathrm{d}^4 \tilde{p}_i}{(2\pi)^3}\delta(\tilde{p}_i^2 - \tilde{m}_i^2)\theta(\tilde{p}_{i,0})\delta^{(4)}(\tilde{p}_a + \tilde{p}_b - \textstyle\sum_i \tilde{p}_i) \int \mathrm{d}\Phi_{ab} \tag{4.2.48}
$$

---

[3]The mapping of the final-state particles coincides with Ref. [59] for vanishing fermion masses.

with

$$\int \mathrm{d}\Phi_{ab} = \frac{p_a p_b}{8\pi^2} \int_0^{2\pi} \frac{\mathrm{d}\phi_{k_\perp}}{2\pi} \int_{-\frac{m_a^2+\lambda^2}{2p_a p_b}}^{1} \mathrm{d}x_{ab} \int_0^{1-x_{ab}} \mathrm{d}v_{ab}\delta(x_a - x_{ab})\delta(1 - x_b)$$

$$\times\, \theta\left(v_{ab} - \frac{(1 - x_{ab} - v_{ab})^2 m_a^2 + \lambda^2}{(1 - x_{ab} - v_{ab})2p_a p_b}\right). \tag{4.2.49}$$

The variable $\phi_{k_\perp}$ is the solid angle between p_a and $k_\perp$ in the rest frame of $p_a + p_b$. The masses $\tilde{m}_i$ of the final-state particles of the four-particle phase space,

$$\tilde{m}_i^2 = m_i^2 - [(1 - x_{ab}^2)m_a^2 + \lambda^2]$$
$$\times\left[\left(\frac{Kp_i + \tilde{K}p_i}{K^2 + K\tilde{K}}\right)^2 + 4\left(\frac{Kp_i}{K^2}\right)^2 - 4\frac{(Kp_i + \tilde{K}p_i)Kp_i}{(K^2 + K\tilde{K})K^2}\right], \tag{4.2.50}$$

can be replaced in (4.2.48) by the masses m_i of the final-state particles of the five-particle phase space after neglecting m_a and λ. The θ-function is due to the requirement $k_\perp^2 < 0$.

Finally, the integrated subtraction term is given:

$$\int \mathrm{d}\Phi_{ab}\mathcal{V}_{ab} = -\frac{\kappa_a \kappa_b e^2 Q_a Q_b}{8\pi^2}\delta(1 - x_b)$$

$$\times \left\{\left\{\left[\mathcal{L}(\lambda^2, m_a^2, 2\tilde{p}_a\tilde{p}_b) + \frac{3}{2} - \frac{\pi^2}{3}\right]\delta(1 - x_a) + [P(x_a)]_+\left[\ln\left(\frac{2p_a p_b}{m_a^2}\right) - 1\right]\right\}\right.$$

$$\times \frac{1}{x_a}\left|\mathcal{M}_{\mathrm{Born}}^{(4)}(\tilde{p}_a, \sigma_a, \tilde{p}_b)\right|^2 + \left\{\frac{1}{2}\delta(1 - x_a) + [1 - x_a]_+\right\}\frac{1}{x_a}\left|\mathcal{M}_{\mathrm{Born}}^{(4)}(\tilde{p}_a, -\sigma_a, \tilde{p}_b)\right|^2\right\}$$

$$+\, \mathcal{O}(\lambda) + \mathcal{O}(m_a) \tag{4.2.51}$$

with $\lambda \ll m_a$ and the function $\mathcal{L}$ defined in (4.2.25). The momentum $\tilde{p}_a$ is implicitly understood to be a function of x_a with $x_a = x_{ab}$.

4.2.4 Remarks to four-fermion production

Since the virtual corrections are calculated in DPA, the integrated subtraction terms that are added to the virtual radiative corrections have to be treated in the right way to achieve the correct cancellations of the singularities. However, it is not possible to apply the DPA to the whole integrated subtraction terms because the x_a-dependent parts are evaluated for reduced CM energies $\sqrt{x_a s}$, which are below the W-pair production threshold for small x_a, where the DPA is not possible. Therefore, the integrated subtraction terms have to be divided into two parts, one including all x_a-dependent terms and a second which is evaluated in DPA including all infrared and mass singularities, except for the x_a-dependent mass singularities resulting from ISR. Here, the following decomposition is used:

$$\int \Phi_{ik}\mathcal{V}_{ik} \sim V_{ik}^{\mathrm{DPA}} + V_{ik}^{\mathrm{off\text{-}shell}}, \tag{4.2.52}$$

$$V_{ik}^{\mathrm{DPA}} = -\frac{\kappa_i \kappa_k e^2 Q_i Q_k}{8\pi^2}\delta(1 - x_1)\delta(1 - x_2)\mathcal{L}(\lambda^2, m_i^2, 2\tilde{p}_i^{\mathrm{on}}\tilde{p}_k^{\mathrm{on}})$$

$$\times \left|\mathcal{M}_{\mathrm{Born}}^{(4)}(\tilde{p}_i^{\mathrm{on}}, \sigma_i, \tilde{p}_k^{\mathrm{on}})\right|^2 \tag{4.2.53}$$

with $i, k = 1, \ldots, 6$, and the on-shell momenta defined in (B.1). The function $\mathcal{L}$ is defined in (4.2.25). Different choices of the decomposition (4.2.52) of the subtraction terms differ only in non-doubly-resonant contributions.

The singularities of (4.2.53) cancel with the singularities of the virtual corrections, while x_a-dependent mass singularities remain in $V_{ik}^{\text{off-shell}}$ from ISR. Moreover, in the integral over the five-particle phase space of (4.2.2), the cuts applied to the bremsstrahlung process and to the individual subtraction terms are different, because the observable $\mathcal{O}$ depends on the five-particle phase space for the bremsstrahlung process, but on the four-particle phase space in the case of the subtraction terms. Hence, one should take care of the correct implementation of cuts in the phase-space generators, if the subtraction terms are involved in the calculation.

4.3 Numerical results

For the numerical discussion, the radiative corrections are evaluated as described in the previous sections, i.e. the virtual corrections are calculated in DPA, and the complete bremsstrahlung process $e^+e^- \to 4f\gamma$ is included for the real corrections. Although polarized cross sections can be calculated in our approach, only unpolarized cross sections are considered in this thesis.

The fixed-width scheme and following input parameters are used for the numerical discussion:

$$\alpha = 1/137.0359895, \qquad G_\mu = 1.16639 \times 10^{-5}\,\text{GeV}^{-2}, \qquad M_\text{H} = 300\,\text{GeV},$$

$$M_\text{W} = 80.26\,\text{GeV}, \qquad \Gamma_\text{W} = 2.08174\,\text{GeV}, \qquad M_\text{Z} = 91.1884\,\text{GeV},$$

$$\Gamma_\text{Z} = 2.4971\,\text{GeV},$$

$$(4.3.1)$$

except for Section 4.3.3 where the input is given explicitly. If not stated otherwise, the weak mixing angle is defined by $c_\text{W} = M_\text{W}/M_\text{Z}$, $s_\text{W}^2 = 1 - c_\text{W}^2$, and the following fermion masses are used:

$$m_\text{e} = 0.51099906\,\text{MeV}, \qquad m_\mu = 105.658389\,\text{MeV}, \qquad m_\tau = 1.7771\,\text{GeV},$$

$$m_\text{u} = 47\,\text{MeV}, \qquad m_\text{c} = 1.55\,\text{GeV}, \qquad m_\text{t} = 165.26\,\text{GeV},$$

$$m_\text{d} = 47\,\text{MeV}, \qquad m_\text{s} = 150\,\text{MeV}, \qquad m_\text{b} = 4.7\,\text{GeV}, \qquad (4.3.2)$$

where the light quark masses are adjusted in such a way that the experimentally measured hadronic vacuum polarization is reproduced.

The input parameters coincide with those of Ref. [50], except for the additional Z-boson width. The finite Z width is required, since the momenta of the bremsstrahlung process are generated for off-shell W bosons. For vanishing Z-boson width, the matrix element of the bremsstrahlung process becomes singular if the real photon has the energy $E_\gamma = \sqrt{s} - M_\text{Z}$. This singularity is due to diagrams where the incoming electron and positron annihilate into a virtual Z boson after radiation of a bremsstrahlung photon. The virtual corrections are evaluated for vanishing Z-boson width.

If not stated otherwise, we use the G_μ parameterization, where the Fermi constant G_μ and the fine structure constant α are related by

$$G_\mu = \frac{\alpha\pi}{\sqrt{2}M_W^2 s_w^2}\frac{1}{1 - \Delta r}. \qquad (4.3.3)$$

The symbol Δr denotes the radiative corrections to the muon decay. The cross section in G_μ parameterization can be obtained from the results in the on-shell renormalization scheme in the following way:

$$d\sigma^{G_\mu} = d\sigma_{\text{Born}}^{G_\mu}(1 + \delta^{G_\mu})$$

with

$$d\sigma_{\text{Born}}^{G_\mu} = \frac{d\sigma_{\text{Born}}^\alpha}{(1 - \Delta r)^4}, \qquad \delta^{G_\mu} = \frac{d\sigma_{\text{virt}}^\alpha + d\sigma_{\text{real}}^\alpha}{d\sigma_{\text{Born}}^\alpha} - 4\Delta r^{\text{1-loop}}. \qquad (4.3.4)$$

The quantities $\sigma_{\text{Born}}^\alpha$, $\sigma_{\text{virt}}^\alpha$, and $\sigma_{\text{real}}^\alpha$ denote the tree-level cross section, the virtual, and the real corrections, respectively, calculated in the one-shell renormalization scheme with the free parameters $\alpha(0)$, M_W, M_Z, M_H, and m_f. The value of Δr can be calculated from (4.3.3) and the one-loop corrections to the muon decay yield $\Delta r^{\text{1-loop}} = 0.0373994$ for the set of input parameters (4.3.1) and (4.3.2).

4.3.1 Total cross section and angular distributions

In order to compare our results with the results of Ref. [50], the doubly-resonant electroweak $\mathcal{O}(\alpha)$ radiative corrections are calculated for the leptonic process $e^+e^- \to \nu_\mu\mu^+\tau^-\bar{\nu}_\tau$ and the LEP2 energy $184\,\text{GeV}$. In Ref. [50], the DPA is applied to both the matrix element and the four-fermion phase space, except for the Breit–Wigner propagators. The integrations of the Breit–Wigner propagators over the invariant masses $k_\pm^2$ are extended to the full range $(-\infty, +\infty)$, resulting in

$$\int_{-\infty}^\infty dk_\pm^2 \frac{1}{k_\pm^2 - M_W^2 + iM_W\Gamma_W} = \frac{\pi}{M_W\Gamma_W}. \qquad (4.3.5)$$

In contrast to Ref. [50], the radiative corrections in our approach are evaluated as described in the previous sections with the exact bremsstrahlung process, and the virtual corrections are taken in DPA. Whereas in Ref. [50], the momenta are generated for on-shell W bosons, we use the exact off-shell phase space for the calculation of the radiative corrections. The DPA-Born cross section is evaluated in the same way as done in Ref. [50], in particular with on-shell phase space, in order to have a common normalization of the relative corrections. Moreover, the real photon is recombined with a charged final-state fermion if their invariant mass is smaller than all other invariant masses $m(\gamma, f)$, where γ denotes the photon and f an initial- or final-state charged fermion.

CM-energy dependence of the total cross section

In Fig. 4.5 the total cross section and the corresponding relative correction factor δ are given as a function of the CM energy. The radiative corrections are large and negative,

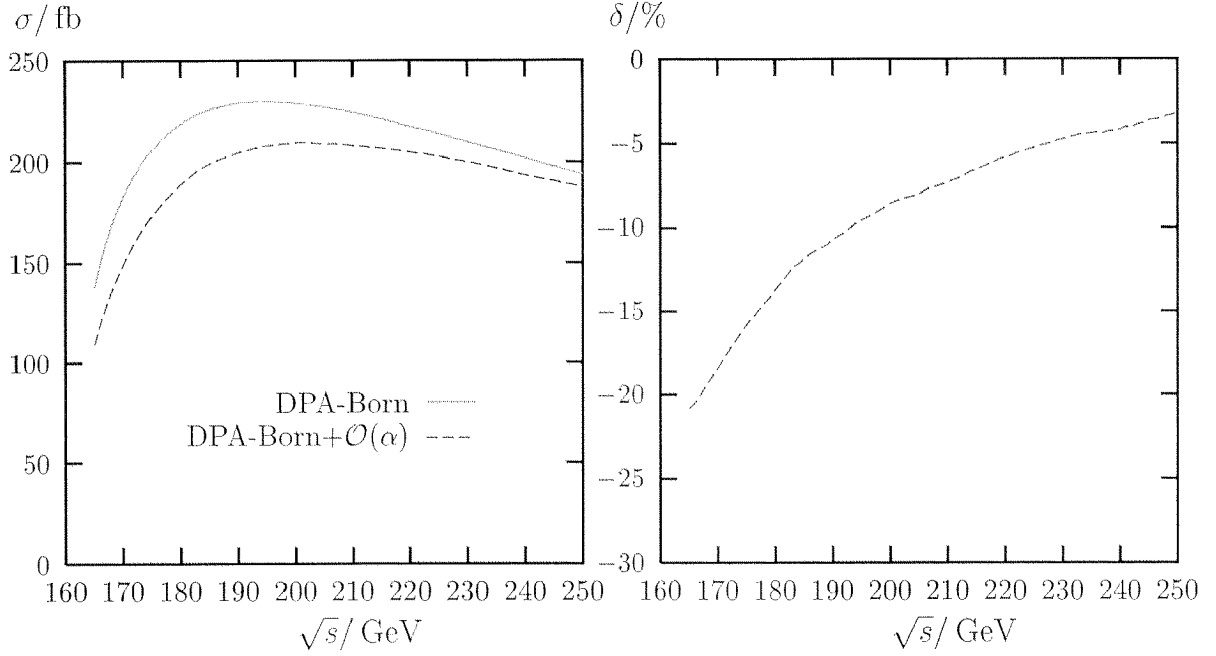Figure 4.5: CM-energy dependence of the total cross section and the relative corrections for the process $e^+e^- \to \nu_\mu \mu^+ \tau^- \bar{\nu}_\tau$

especially close to the W-pair threshold. This effect is due to real-photon ISR, which effectively reduces the available energy of the W-pair production subprocess, combined with the fact, that near the W-pair threshold the cross section is rapidly decreasing with decreasing energy. The large corrections result from diagrams of the bremsstrahlung process where the real photon is emitted from an initial-state electron or positron.

The DPA-Born cross section agrees very well with Fig. 8 of Ref. [50]. The curve for the cross section including $\mathcal{O}(\alpha)$ corrections agrees for high energies, but differs for low energies. For instance, the cross section at 165 GeV is about 7% larger than the cross section taken from Fig. 8 of Ref. [50]. Above 190 GeV the relative corrections agree very well with the results of Fig. 9 in Ref. [50]. Note that the dominating corrections resulting from ISR are evaluated in Ref. [50] in DPA with on-shell phase space, i.e. $k_\pm^2 = M_W^2$, but calculated in our approach with the full off-shell kinematics. This could account for the deviation to Ref. [50].

Production-angle distribution

The production-angle distribution is shown in Fig. 4.6. This distribution is, in particular, important in order to get more strict bound on the non-standard triple-gauge-boson couplings. The radiative corrections are negative, and increase in size with decreasing production angles. The origin of the distortion of the distribution can be traced back to hard initial-state photonic corrections. Hard-photon emission boosts the CM system of the W bosons, causing a migration of events from regions with large cross section in the CM system (e.g. forward direction) to regions with small cross section in the laboratory system (e.g. backward direction).
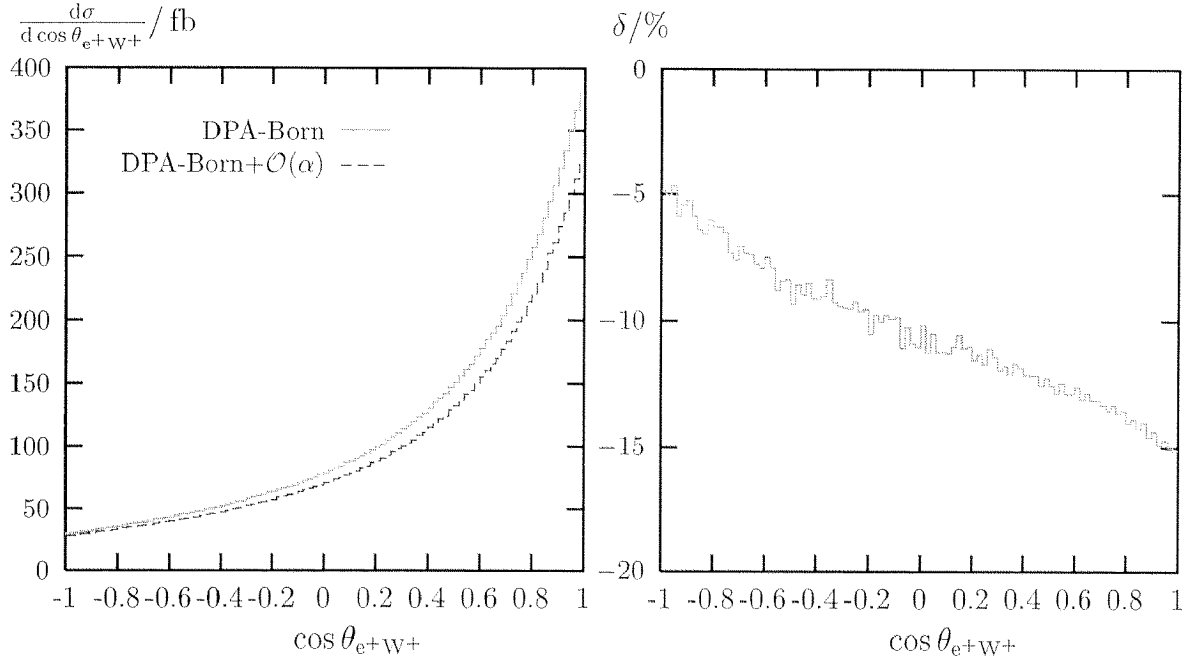
Figure 4.6: Production-angle distribution for the CM energy $\sqrt{s} = 184\,\text{GeV}$ and the process $e^+e^- \to \nu_\mu \mu^+ \tau^- \bar{\nu}_\tau$

Our result based on the DPA-Born cross section agrees very well with Fig. 10 of Ref. [50]. The relative corrections are about one per cent larger than the results of Ref. [50] for small scattering angles and agree for large scattering angles . Note that the total cross section of Ref. [50] is about one per cent smaller than our result at $\sqrt{s} = 184\,\text{GeV}$.

Decay-angle distribution

The decay-angle distribution of the final-state μ^+ with respect to the W^+ boson in the laboratory frame can be found in Fig. 4.7. As in the case of the production-angle distribution, the large corrections are mainly due to hard-photon boost effects. The radiative corrections are negative and large for small decay angles.

The differential cross sections of Fig. 4.7 agree very well with Fig. 16 of Ref. [50]. Deviations of about one per cent are visible from the relative radiative corrections shown in Fig. 17 of Ref. [50].

4.3.2   Invariant-mass distribution

For the definition of realistic observables the momentum of collinear photons have to be recombined with the momentum of the nearest fermion, except for a muon in the final state, as discussed in Section 4.1.2. Otherwise logarithms of the form $\ln(m_f^2/s)$ remain from FSR in the invariant-mass distributions. These logarithms are not calculable in our approach, which is explained in the following: we use the subtraction method, where all mass singularities, which appear for inclusive observables, are transferred from the real part to the virtual part of the radiative corrections with the help of subtraction terms
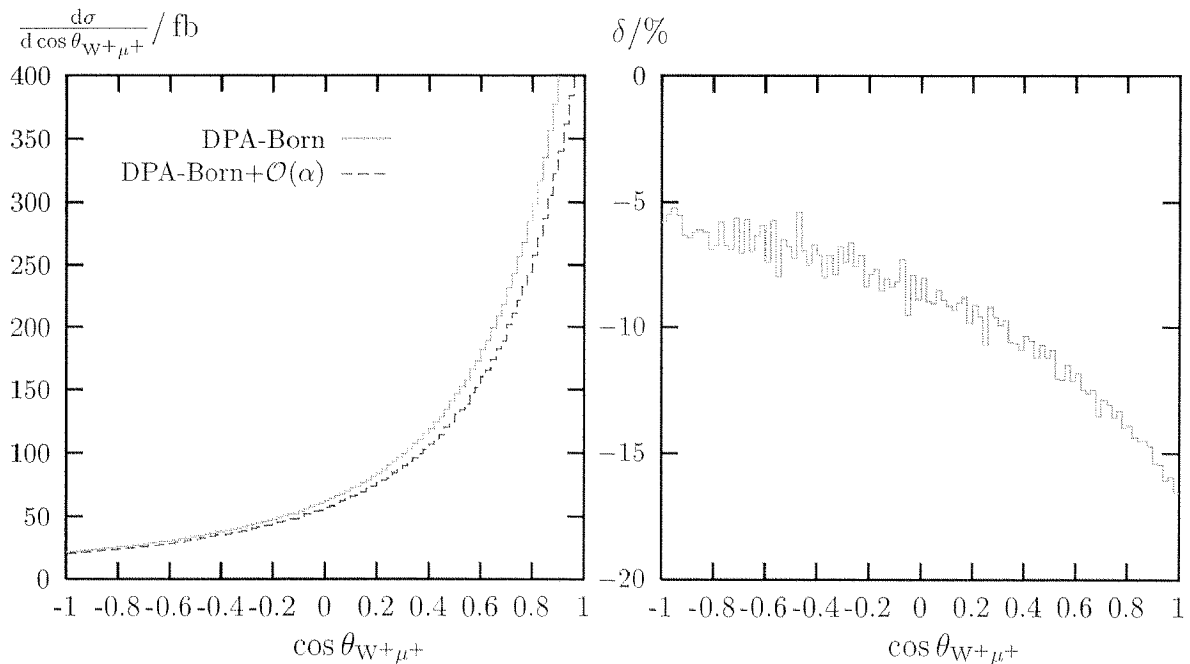
Figure 4.7: Decay-angle distribution of the μ^+ with respect to the W^+ in the laboratory frame for the CM energy $\sqrt{s} = 184\,\text{GeV}$ and the process $e^+e^- \to \nu_\mu \mu^+ \tau^- \bar{\nu}_\tau$

and the fermion masses are neglected everywhere, except for the mass singularities. For observables, which are not inclusive in the collinear region, like invariant-mass distributions without recombination cuts, the phase-space integration over the difference of the bremsstrahlung cross section and the corresponding subtraction terms in (4.2.2) becomes divergent for vanishing fermion masses. Therefore, a comparison with the invariant-mass distribution of Ref. [50] is not possible, since the calculation is performed without recombination cuts.

The following photon recombination procedure is used. All photons within a cone of $5°$ around the beams are discarded. Next, the photon is recombined with the nearest final-state charged fermion, more precisely, with the fermion that has the smallest invariant mass with the photon. Finally, all events are discarded if a charged final-state fermion is within a cone of $10°$ around the beams. The recombination cuts read:

recomb a: $m(f, \gamma) < 5\,\text{GeV}$,

recomb b: $m(f, \gamma) < 25\,\text{GeV}$,

where $m(f, \gamma)$ denotes the invariant mass of a final-state charged fermion and the photon.

For the invariant-mass distributions, the Born cross section is calculated with the complete matrix element and off-shell kinematics. The radiative corrections are evaluated as in the previous section.

The invariant-mass distributions are shown in Figs. 4.8, 4.9, 4.10, and 4.11 for two recombination cuts and two CM energies: the LEP2 energy $184\,\text{GeV}$ and a possible linear collider energy $500\,\text{GeV}$. The results include the leptonic process $e^+e^- \to \nu_\mu \mu^+ \tau^- \bar{\nu}_\tau$, the semi-leptonic process $e^+e^- \to u\bar{d}\,\mu^- \bar{\nu}_\mu$, and the hadronic process $e^+e^- \to u\bar{d}s\bar{c}$. Note
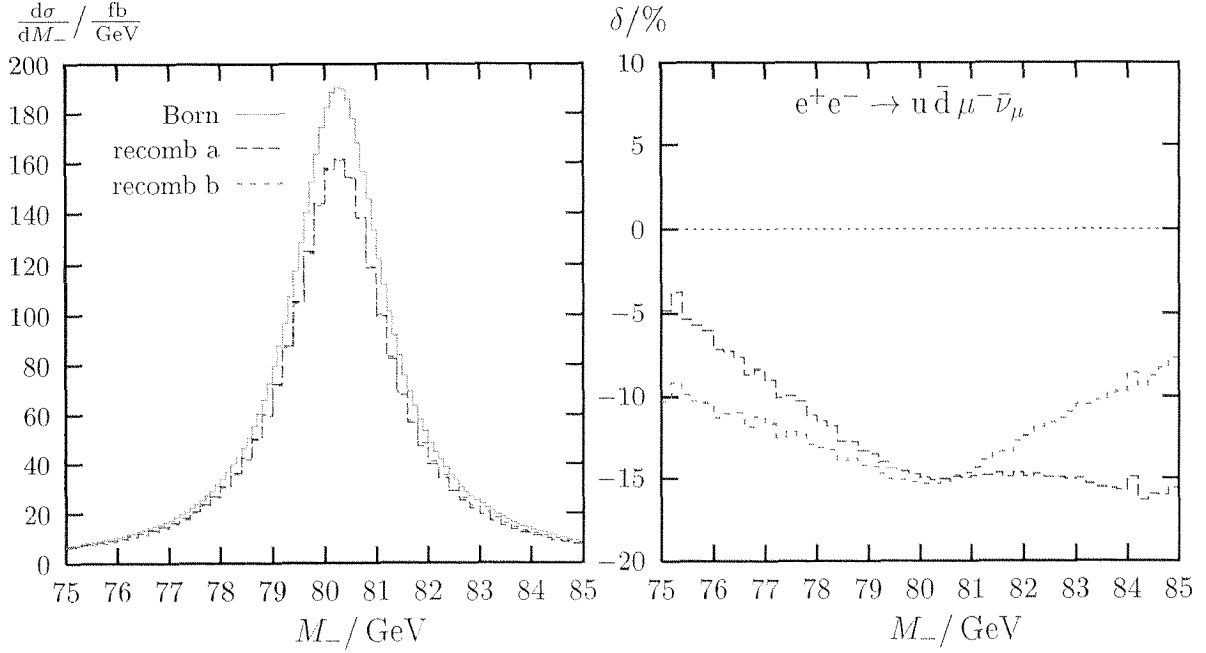
Figure 4.8: Invariant-mass distributions for different photon-recombination cuts and energy $\sqrt{s} = 184\,\text{GeV}$

that the radiative corrections of all leptonic processes are equivalent in DPA if no mass singularities remain from FSR. The same is true for the semi-leptonic and hadronic process classes.

As discussed in Section 4.3.1, the large negative radiative corrections for 184 GeV originate from hard-photon ISR, which reduces the available CM energy for the W-pair production subprocess, combined with the fact that the total cross section of the W-pair production subprocess is steeply decreasing for decreasing CM energy near threshold. Since the linear-collider energy 500 GeV is far away from threshold and the cross section of the W-pair production is slowly decreasing for increasing energies for $\sqrt{s} \lesssim 500\,\text{GeV}$, the relative corrections are small and positive.

Apart from the large reduction of the cross section for 184 GeV due to ISR, a distortion of the Breit–Wigner line shape is caused by FSR, which can be explained as follows: if the event is outside the recombination cuts, the invariant W-boson masses are defined by the momenta of the corresponding fermion–antifermion pairs:

$$M_+^2 = k_+^2 = (k_1 + k_2)^2, \qquad M_-^2 = k_-^2 = (k_3 + k_4)^2, \tag{4.3.6}$$

where $k_1, \ldots, k_4$ are the momenta of the final-state fermions. For FSR, one of the two resonant W bosons decays not only into a fermion–antifermion pair, but also in a bremsstrahlung photon. Thus, the corresponding W-boson propagator,

$$P\left((k_\pm + q)^2\right) = \frac{1}{\left[(k_\pm + q)^2 - M^2\right]}, \tag{4.3.7}$$

depends in addition on the photon momentum q and leads to a shift of the Breit–Wigner line shape to smaller invariant masses. These effects are especially large without recombination cuts since mass singularities remain from FSR [50]. With recombination cuts, the
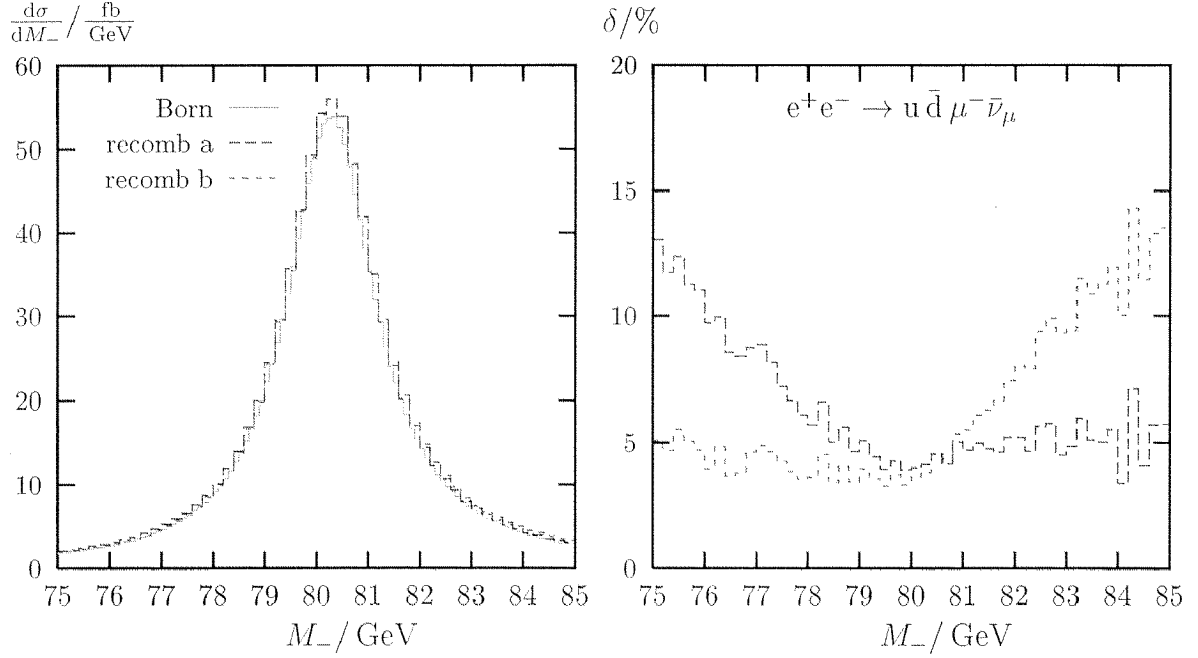
Figure 4.9: Invariant-mass distributions for different photon-recombination cuts and energy $\sqrt{s} = 500\,\text{GeV}$

mass singularities disappear and are effectively replaced by logarithms depending on these cuts. A small recombination cut leads to large distortions of the Breit–Wigner resonance shape, while large recombination cuts yield relatively small effects.

If the photon is inside the recombination cuts, it is combined with the nearest charged fermion and hence is included in the invariant mass of the corresponding resonant W boson:

$$M_+^2 = (k_+ + q)^2 \quad \text{or} \quad M_-^2 = (k_- + q)^2. \tag{4.3.8}$$

The resonance of the W-boson propagator,

$$P(k_\pm^2) = \frac{1}{[k_\pm^2 - M^2]}, \tag{4.3.9}$$

which do not depend on the photon momentum, is located at larger invariant masses, i.e. $M_\pm > M_W$, where $M_\pm$ is defined in (4.3.8). This leads to a shift of the Breit–Wigner line shape to larger invariant masses.

These effects all visible in Figs. 4.8, 4.9, 4.10, and 4.11. For $M_\pm \lesssim M_W$, the relative corrections increase for decreasing invariant masses due to propagators defined in (4.3.7) and events, which are outside the recombination cuts. This effect is large for small recombination cuts, as expected from the previous discussion. On the other hand, for $M_\pm \gtrsim M_W$ the relative corrections increase for increasing invariant mass owing to the propagators defined in (4.3.9) and events, where the photon is recombined with the nearest fermion. This effect is visible for the large recombination cut b. Both effects result in a shift and a broadening of the Breit–Wigner line shape.

$\sqrt{s}$/ GeV	189	500	2000	10000
σ/ fb	1284.9(5)	570.4(3)	83.4(6)	6.52(1)

Table 4.1: Comparison with Table 3 of Ref. [22]: Total cross section of the process $e^+e^- \to$ u $\bar{d}\,\mu^-\bar{\nu}_\mu\gamma$ with the photon mass $m_\gamma = 10^{-6}\,\mathrm{GeV}$

Note that the radiative corrections from FSR include the squares of the charges of the final-state fermions, which emit the bremsstrahlung photons. Thus, the FSR corrections are proportional to $Q_{l^\pm}^2 = 1$ for invariant-mass distributions of W-bosons, which decay into leptons, and proportional to $Q_q^2 + Q_{\bar{q}}^2 = 5/9$, if the W-boson decays into a quark–antiquark pair.

4.3.3 Test of the subtraction method

In Table 3 of Ref. [22], the sum of the soft-photon cross section with $E_\gamma < \omega$ and the hard-photon cross section with photon energy $E_\gamma > \omega$ of the process $e^+e^- \to$ u $\bar{d}\mu^-\bar{\nu}_\mu\gamma$ is given for several values of the separation cut ω, in order to show the independence on the parameter ω. Since the soft-photon cross section depends on the photon mass $m_\gamma = 10^{-6}\,\mathrm{GeV}$, it is not a physical observable. However, it is a good test for the implementation of the subtraction method.

In Ref. [22], the fixed-width scheme and the following input parameters have been used: $M_W = 80.23\,\mathrm{GeV}$, $\Gamma_W = 2.085\,\mathrm{GeV}$, $M_Z = 91.1888\,\mathrm{GeV}$, $\Gamma_Z = 2.4974\,\mathrm{GeV}$, $m_e = 0.51099906\,\mathrm{MeV}$, $m_u = 5\,\mathrm{MeV}$, $m_d = 10\,\mathrm{MeV}$, and $s_W^2 = 0.22591$. All couplings have been parameterized by $\alpha(M_W) = 1/128.07$, except for the couplings of the bremsstrahlung photon which have been parameterized by $\alpha = 1/137.0359895$.

Our results for these input parameters are shown in Table 4.1 and agree well within the statistical error, apart from the CM energy 10 TeV, where the numerical integration is most complicated.
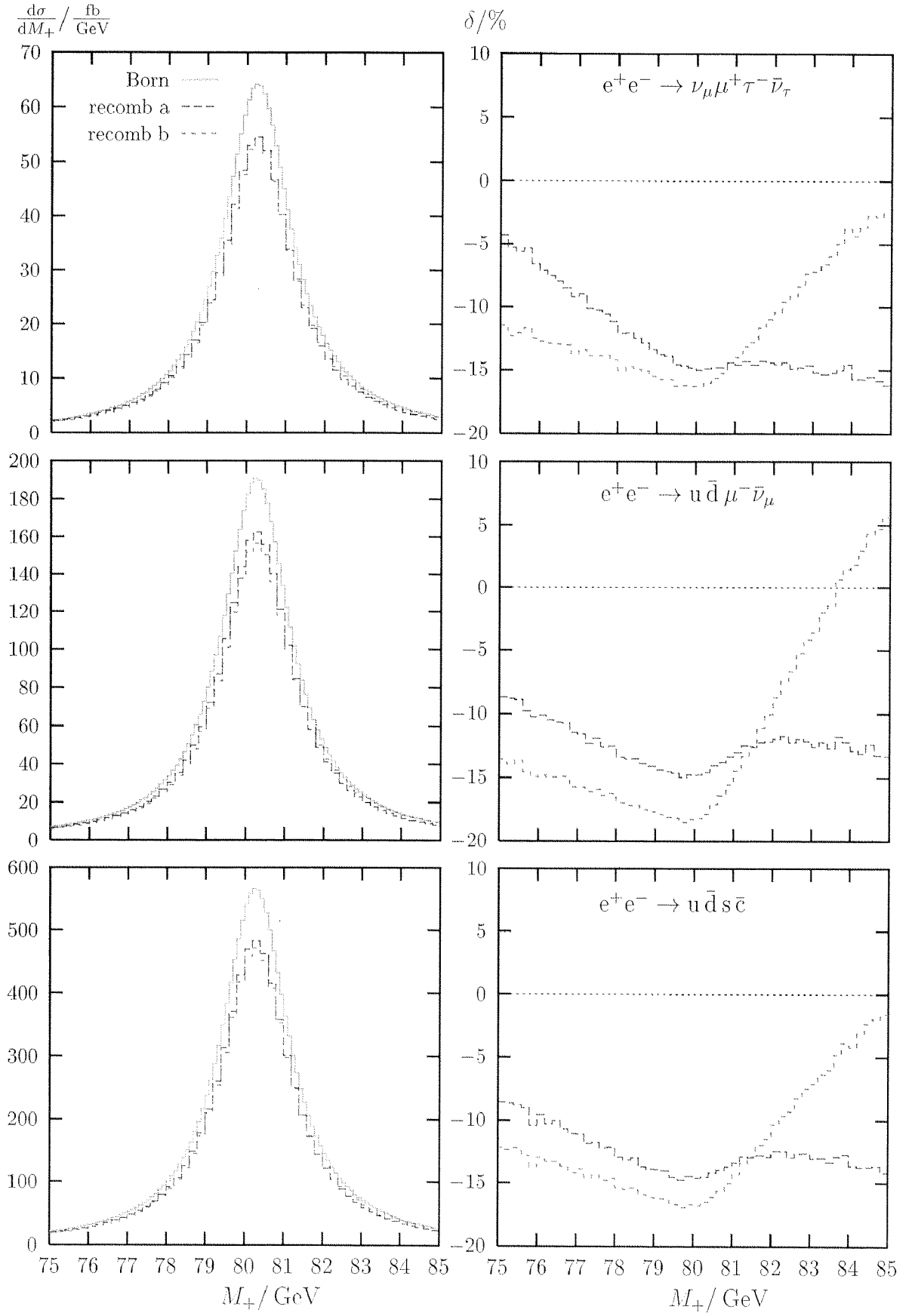
Figure 4.10: Invariant-mass distributions for different photon-recombination cuts, different processes, and energy $\sqrt{s} = 184\,\text{GeV}$
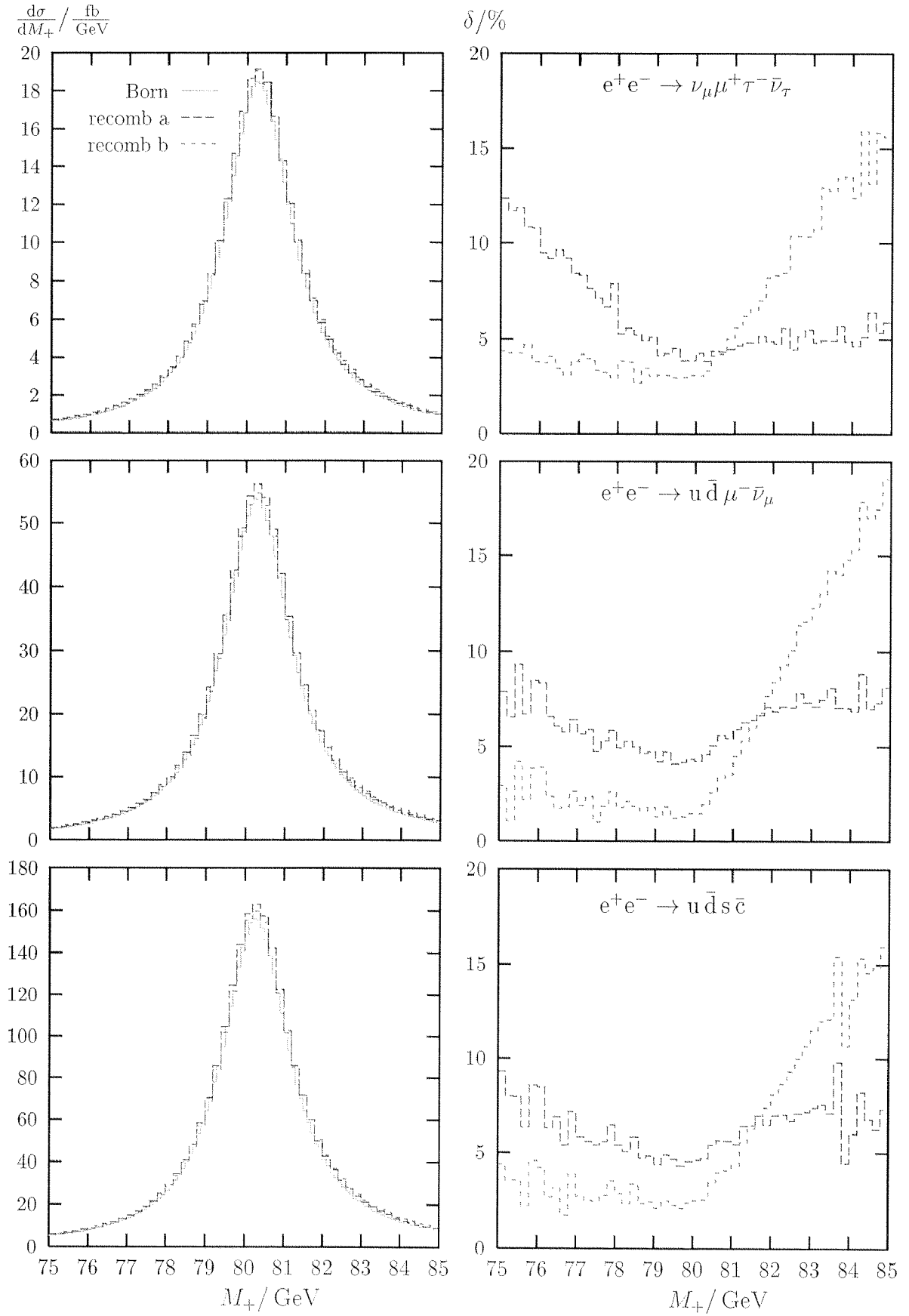
$\frac{\mathrm{d}\sigma}{\mathrm{d}M_+} / \frac{\mathrm{fb}}{\mathrm{GeV}}$

$\delta/\%$

Born
recomb a
recomb b

$e^+e^- \to \nu_\mu \mu^+ \tau^- \bar{\nu}_\tau$

$e^+e^- \to u\bar{d}\,\mu^- \bar{\nu}_\mu$

$e^+e^- \to u\bar{d}\,s\bar{c}$

$M_+/$ GeV

$M_+/$ GeV

Figure 4.11: Invariant-mass distributions for different photon-recombination cuts, different processes, and energy $\sqrt{s} = 500\,\mathrm{GeV}$

Appendix

A Calculation of real and virtual corrections

A.1 Useful definitions

In the main text, we have already used the following short-hand expressions,

$$\beta_{\mathrm{W}} = \sqrt{1 - \frac{4M_{\mathrm{W}}^2}{s} + i\epsilon},$$

$$x_{\mathrm{W}} = \frac{\beta_{\mathrm{W}} - 1}{\beta_{\mathrm{W}} + 1},$$

$$\beta = \sqrt{1 - \frac{4M^2}{s}},$$

$$\bar{\beta} = \frac{\sqrt{\lambda(s, k_+^2, k_-^2)}}{s},$$

$$\kappa_{\mathrm{W}} = \sqrt{\lambda(M_{\mathrm{W}}^4, s_{13}s_{24}, s_{14}s_{23}) - i\epsilon},$$

$$\Delta_M = \frac{|k_+^2 - k_-^2|}{s}, \tag{A.1}$$

where

$$\lambda(x, y, z) = x^2 + y^2 + z^2 - 2xy - 2xz - 2yz. \tag{A.2}$$

The evaluation of one-loop n-point functions naturally leads to the usual dilogarithm,

$$\mathrm{Li}_2(z) = -\int_0^z \frac{\mathrm{d}t}{t} \ln(1 - t), \qquad |\arc(1 - z)| < \pi, \tag{A.3}$$

and its analytically continued form

$$\mathcal{L}i_2(x, y) = \mathrm{Li}_2(1 - xy) + [\ln(xy) - \ln(x) - \ln(y)]\ln(1 - xy),$$
$$|\arc(x)|, |\arc(y)| < \pi. \tag{A.4}$$

A.2 Calculation of the real bremsstrahlung integrals

In this appendix we describe a general method for evaluating the bremsstrahlung 3- and 4-point integrals defined in (3.2.15). We make use of the generalized Feynman-parameter representation [64]

$$\frac{1}{\prod_{i=1}^n N_i'} = \Gamma(n) \int_0^\infty \mathrm{d}x_1 \cdots \mathrm{d}x_n \frac{\delta(1 - \sum_{i=1}^n \alpha_i x_i)}{(\sum_{i=1}^n N_i' x_i)^n}, \tag{A.5}$$

where the real variables $\alpha_i \geq 0$ are arbitrary, but not all equal to zero simultaneously. The sum $\sum_{i=1}^{n} N_i' x_i$ must be non-zero over the entire integration domain.

We first consider the 3-point integral $\mathcal{C}_0$. We only need the difference between the general IR-finite integral and the corresponding IR-divergent on-shell integral,

$$
\mathcal{C}_0(p_1, p_2, 0, m_1, m_2) - \mathcal{C}_0\left(p_1, p_2, \lambda, \sqrt{p_1^2}, \sqrt{p_2^2}\right)
$$

$$
= \int \frac{\mathrm{d}^3 \mathbf{q}}{\pi q_0} \left\{ \frac{1}{(2p_1 q + p_1^2 - m_1^2)(2p_2 q + p_2^2 - m_2^2)} - \frac{1}{(2p_1 q)(2p_2 q)} \right\}\bigg|_{q_0 = \sqrt{\mathbf{q}^2 + \lambda^2}}, \quad (A.6)
$$

which is UV-finite and Lorentz-invariant. Extracting the signs σ_i of p_{i0} via definition (3.2.29), and assuming for the moment $\sigma_i \operatorname{Re}(p_i^2 - m_i^2) > 0$, the Feynman-parameter representation (A.5) can be applied to each term in the integrand of (A.6). The integration over $\mathrm{d}^3 \mathbf{q}$ can be carried out and yields

$$
\mathcal{C}_0(p_1, p_2, 0, m_1, m_2) - \mathcal{C}_0\left(p_1, p_2, \lambda, \sqrt{p_1^2}, \sqrt{p_2^2}\right) \qquad (A.7)
$$

$$
= \sigma_1 \sigma_2 \int_0^\infty \mathrm{d}x_1 \mathrm{d}x_2 \, \delta\left(1 - \sum_{i=1}^2 \alpha_i x_i\right) \frac{\ln(\lambda^2) + \ln\left[\left(\sum_{i=1}^2 \tilde{p}_i x_i\right)^2\right] - 2\ln\left[\sum_{i=1}^2 \sigma_i (p_i^2 - m_i^2) x_i\right]}{2\left(\sum_{i=1}^2 \tilde{p}_i x_i\right)^2}.
$$

Putting for instance $\alpha_1 = 0$ and $\alpha_2 = 1$, and using

$$
\int_0^\infty \mathrm{d}x \left(\frac{1}{x + z_1} - \frac{1}{x + z_2}\right) \ln(1 + zx) = \mathcal{L}i_2(z_1, z) - \mathcal{L}i_2(z_2, z), \qquad (A.8)
$$

where $|\operatorname{arc}(z_{1,2}, z, z\,z_{1,2})| < \pi$, the remaining one-dimensional integration and the analytical continuations to arbitrary complex $(p_i^2 - m_i^2)$ are straightforward.

Next we consider the IR-finite 4-point function

$$
\mathcal{D}_0(p_1, p_2, p_3, 0, m_1, m_2, m_3)
$$

$$
= \int \frac{\mathrm{d}^3 \mathbf{q}}{\pi q_0} \frac{1}{(2p_1 q + p_1^2 - m_1^2)(2p_2 q + p_2^2 - m_2^2)(2p_3 q + p_3^2 - m_3^2)}\bigg|_{q_0 = |\mathbf{q}|}. \qquad (A.9)
$$

For $\sigma_i \operatorname{Re}(p_i^2 - m_i^2) > 0$ we can proceed as above and find

$$
\mathcal{D}_0(p_1, p_2, p_3, 0, m_1, m_2, m_3) = \sigma_1 \sigma_2 \sigma_3 \int_0^\infty \mathrm{d}x_1 \mathrm{d}x_2 \mathrm{d}x_3 \frac{\delta\left(1 - \sum_{i=1}^3 \alpha_i x_i\right)}{\left[\sum_{i=1}^3 \sigma_i (p_i^2 - m_i^2) x_i\right]\left(\sum_{i=1}^3 \tilde{p}_i x_i\right)^2}.
$$
$$
(A.10)
$$

Again, the two-dimensional integration over the Feynman parameters and the analytical continuations in $(p_i^2 - m_i^2)$ are straightforward.

Finally, we inspect the IR-divergent 4-point function

$$
\mathcal{D}_0\left(p_1, p_2, p_3, \lambda, \sqrt{p_1^2}, m_2, \sqrt{p_3^2}\right) = \int \frac{\mathrm{d}^3 \mathbf{q}}{\pi q_0} \frac{1}{(2p_1 q)(2p_2 q + p_2^2 - m_2^2)(2p_3 q)}\bigg|_{q_0 = \sqrt{\mathbf{q}^2 + \lambda^2}}. \qquad (A.11)
$$

Instead of applying the Feynman-parameter representation directly, it is more convenient to extract the infrared singularity by subtracting and adding an IR-divergent 3-point function containing the same IR structure. Since the difference between the 4- and 3-point functions is IR-finite, we can regularize the IR divergence in these two integrals in a more convenient way. Therefore, we write

$$\mathcal{D}_0\left(p_1, p_2, p_3, \lambda, \sqrt{p_1^2}, m_2, \sqrt{p_3^2}\right) = \lim_{m^2 \to p_1^2} \left[\mathcal{D}_0\left(p_1, p_2, p_3, 0, m, m_2, \sqrt{p_3^2}\right) \right.$$

$$\left. - \frac{1}{p_2^2 - m_2^2} \mathcal{C}_0\left(p_1, p_3, 0, m, \sqrt{p_3^2}\right) + \frac{1}{p_2^2 - m_2^2} \mathcal{C}_0\left(p_1, p_3, \lambda, \sqrt{p_1^2}, \sqrt{p_3^2}\right) \right], \qquad \text{(A.12)}$$

i.e. we regularize the IR divergence in the 4-point function by the off-shellness $p_1^2 - m^2 \neq 0$. Both the 4-point function as well as the difference of 3-point functions can be treated as above, yielding straightforward Feynman-parameter integrals according to (A.7) and (A.10), respectively. The limit $m^2 \to p_1^2$ can easily be taken after the integrations have been performed.

A.3 Explicit results for scalar integrals

Loop integrals in double-pole approximation

The following one-loop integrals are required for the calculation of the non-factorizable corrections in Sections 3.3.2 and 3.3.3. The 2-point and 3-point functions of the (mm), (mf), and (im) corrections read in DPA:

$$\frac{1}{k_+^2 - M^2} \left\{ B_0(k_+, 0, M) - \left[B_0\left(k_+, 0, M\right) \right]_{k_+^2 = M^2} \right\} - \left[B_0'\left(k_+, \lambda, M_{\mathrm{W}}\right) \right]_{k_+^2 = M_{\mathrm{W}}^2}$$

$$\sim \frac{1}{M_{\mathrm{W}}^2} \left\{ \ln\left(\frac{\lambda M_{\mathrm{W}}}{-K_+} \right) + 1 \right\}, \qquad \text{(A.13)}$$

$$C_0(k_2, k_+, 0, m_2, M) - \left[C_0(k_2, k_+, \lambda, m_2, M_{\mathrm{W}}) \right]_{k_+^2 = M_{\mathrm{W}}^2}$$

$$\sim -\frac{1}{M_{\mathrm{W}}^2} \left\{ \ln\left(\frac{m_2^2}{M_{\mathrm{W}}^2} \right) \ln\left(\frac{-K_+}{\lambda M_{\mathrm{W}}} \right) + \ln^2\left(\frac{m_2}{M_{\mathrm{W}}} \right) + \frac{\pi^2}{6} \right\}, \qquad \text{(A.14)}$$

$$C_0(p_+, k_+, 0, m_{\mathrm{e}}, M) - \left[C_0(p_+, k_+, \lambda, m_{\mathrm{e}}, M_{\mathrm{W}}) \right]_{k_+^2 = M_{\mathrm{W}}^2}$$

$$\sim \frac{1}{t - M_{\mathrm{W}}^2} \left\{ \ln\left(\frac{m_{\mathrm{e}} M_{\mathrm{W}}}{M_{\mathrm{W}}^2 - t} \right) \left[\ln\left(\frac{-K_+}{M_{\mathrm{W}}^2 - t} \right) + \ln\left(\frac{-K_+}{\lambda^2} \right) + \ln\left(\frac{m_{\mathrm{e}}}{M_{\mathrm{W}}} \right) \right] + \frac{\pi^2}{6} \right\}. \quad \text{(A.15)}$$

In the (mm') correction the following combination of 3-point functions appears in the strict DPA:

$$C_0(k_+, -k_-, 0, M, M) - \left[C_0(k_+, -k_-, \lambda, M_{\mathrm{W}}, M_{\mathrm{W}}) \right]_{k_\pm^2 = M_{\mathrm{W}}^2}$$

$$\sim \frac{1}{s\beta_{\mathrm{W}}} \left\{ -\mathcal{L}i_2\left(\frac{K_-}{K_+}, x_{\mathrm{W}} \right) + \mathcal{L}i_2\left(\frac{K_-}{K_+}, x_{\mathrm{W}}^{-1} \right) + \mathrm{Li}_2(1 - x_{\mathrm{W}}^2) + \pi^2 + \ln^2(-x_{\mathrm{W}}) \right.$$

$$\left. + 2\ln\left(\frac{K_+}{\lambda M_{\mathrm{W}}} \right) \ln(x_{\mathrm{W}}) - 2\pi i \ln(1 - x_{\mathrm{W}}^2) \right\}. \qquad \text{(A.16)}$$

In order to include the full off-shell Coulomb singularity, one has to add

$$\frac{2\pi\mathrm{i}}{s\bar{\beta}}\ln\left(\frac{\beta+\Delta_M-\bar{\beta}}{\beta+\Delta_M+\bar{\beta}}\right)-\frac{2\pi\mathrm{i}}{s\beta_{\mathrm{W}}}\ln\left(\frac{K_++K_-+s\beta_{\mathrm{W}}\Delta_M}{2\beta_{\mathrm{W}}^2 s}\right) \tag{A.17}$$

to the r.h.s. of (A.16).

For the (if), (mf'), and (ff') corrections we need the following 4-point functions:

$$D_0(p_+,k_+,k_2,\lambda,m_{\mathrm{e}},M,m_2)\sim\frac{1}{t_{+2}K_+}\left\{2\ln\left(\frac{m_{\mathrm{e}}m_2}{-t_{+2}}\right)\ln\left(\frac{\lambda M_{\mathrm{W}}}{-K_+}\right)-\ln^2\left(\frac{m_2}{M_{\mathrm{W}}}\right)-\frac{\pi^2}{3}\right.$$
$$\left.-\ln^2\left(\frac{m_{\mathrm{e}}M_{\mathrm{W}}}{M_{\mathrm{W}}^2-t}\right)-\mathrm{Li}_2\left(1-\frac{t-M_{\mathrm{W}}^2}{t_{\pm i}}\right)\right\}, \tag{A.18}$$

$$D_0(0)=D_0(-k_4,k_++k_3,k_2+k_3,0,M,M,0)$$
$$\sim\frac{1}{\kappa_{\mathrm{W}}}\sum_{\sigma=1,2}(-1)^\sigma\left\{\mathcal{L}i_2\left(-\frac{s_{13}+s_{23}}{M_{\mathrm{W}}^2}-\mathrm{i}\epsilon,-x_\sigma\right)+\mathcal{L}i_2\left(-\frac{M_{\mathrm{W}}^2}{s_{23}+s_{24}}+\mathrm{i}\epsilon,-x_\sigma\right)\right.$$
$$\left.-\mathcal{L}i_2\left(x_{\mathrm{W}},-x_\sigma\right)-\mathcal{L}i_2\left(x_{\mathrm{W}}^{-1},-x_\sigma\right)-\ln\left(1+\frac{s_{24}}{s_{23}}\right)\ln(-x_\sigma)\right\}, \tag{A.19}$$

$$\text{with}\qquad x_1=\frac{s_{24}z}{M_{\mathrm{W}}^2},\qquad x_2=\frac{M_{\mathrm{W}}^2}{s_{13}z},\qquad z=\frac{M_{\mathrm{W}}^4+s_{13}s_{24}-s_{14}s_{23}+\kappa_{\mathrm{W}}}{2s_{13}s_{24}}, \tag{A.20}$$

$$D_0(1)=D_0(-k_-,k_+,k_2,0,M,M,m_2)$$
$$\sim\frac{1}{K_+(s_{23}+s_{24})+K_-M_{\mathrm{W}}^2}\left\{\sum_{\tau=\pm1}\left[\mathcal{L}i_2\left(\frac{K_+}{K_-},x_{\mathrm{W}}^\tau\right)-\mathcal{L}i_2\left(-\frac{M_{\mathrm{W}}^2}{s_{23}+s_{24}}+\mathrm{i}\epsilon,x_{\mathrm{W}}^\tau\right)\right]\right. \tag{A.21}$$
$$\left.-2\,\mathcal{L}i_2\left(\frac{K_+}{K_-},-\frac{s_{23}+s_{24}}{M_{\mathrm{W}}^2}-\mathrm{i}\epsilon\right)-\ln\left(\frac{m_2^2}{M_{\mathrm{W}}^2}\right)\left[\ln\left(\frac{K_+}{K_-}\right)+\ln\left(-\frac{s_{23}+s_{24}}{M_{\mathrm{W}}^2}-\mathrm{i}\epsilon\right)\right]\right\},$$

$$D_0(2)=D_0(-k_3,k_+,k_2,\lambda,m_3,M,m_2)$$
$$\sim\frac{1}{K_+s_{23}}\left\{-\mathrm{Li}_2\left(-\frac{s_{13}}{s_{23}}\right)-\frac{\pi^2}{3}+2\ln\left(-\frac{s_{23}}{m_2m_3}-\mathrm{i}\epsilon\right)\ln\left(\frac{-K_+}{\lambda M_{\mathrm{W}}}\right)-\ln^2\left(\frac{m_2}{M_{\mathrm{W}}}\right)\right.$$
$$\left.-\ln^2\left(-\frac{s_{13}+s_{23}}{m_3 M_{\mathrm{W}}}-\mathrm{i}\epsilon\right)\right\}, \tag{A.22}$$

$$D_0(3)=D_0(-k_3,-k_-,k_2,\lambda,m_3,M,m_2)=D_0(2)\big|_{K_+\leftrightarrow K_-,m_2\leftrightarrow m_3,s_{13}\leftrightarrow s_{24}}, \tag{A.23}$$

$$D_0(4)=D_0(-k_3,-k_-,k_+,0,m_3,M,M)=D_0(1)\big|_{K_+\leftrightarrow K_-,m_2\leftrightarrow m_3,s_{13}\leftrightarrow s_{24}}. \tag{A.24}$$

Bremsstrahlung integrals in double-pole approximation

In the (mm') interference corrections the following combination of 3-point functions appears:

$$\mathcal{C}_0(k_+,k_-,0,M,M^*)-\left[\mathcal{C}_0(k_+,k_-,\lambda,M_{\mathrm{W}},M_{\mathrm{W}})\right]_{k_\pm^2=M_{\mathrm{W}}^2}$$
$$\sim\left\{C_0(k_+,-k_-,0,M,M)-\left[C_0(k_+,-k_-,\lambda,M_{\mathrm{W}},M_{\mathrm{W}})\right]_{k_\pm^2=M_{\mathrm{W}}^2}\right\}\Big|_{K_-\to-K_-^*}$$

106

$$- \frac{2\pi\mathrm{i}}{s\beta_{\mathrm{W}}} \ln\left[\frac{K_+ + K_-^* x_{\mathrm{W}}}{\mathrm{i}\lambda M_{\mathrm{W}}(1 - x_{\mathrm{W}}^2)} \right]. \tag{A.25}$$

For the (mf′) and (ff′) interference corrections the following 4-point functions are required:

$$\widetilde{\mathcal{D}}_0(0) = -D_0(k_4, k_+ - k_3, k_2 - k_3, 0, M_-, M_+, 0)$$
$$\sim -D_0(0) + \frac{2\pi\mathrm{i}}{\kappa_{\mathrm{W}}}\left\{ \ln\left(-x_{\mathrm{W}}\frac{s_{23}}{M_{\mathrm{W}}^2} \right) + \ln\left[1 + \frac{s_{13}}{s_{23}}(1 - z) \right] + \ln\left[1 + \frac{s_{24}}{s_{23}}(1 - z) \right] \right.$$
$$\left. - \ln\left(1 + \frac{s_{13}}{M_{\mathrm{W}}^2} z x_{\mathrm{W}} \right) - \ln\left(1 + \frac{s_{24}}{M_{\mathrm{W}}^2} z x_{\mathrm{W}} \right) \right\}, \tag{A.26}$$

with z from (A.20),

$$\mathcal{D}_0(1) = \mathcal{D}_0(k_-, k_+, k_2, 0, M^*, M, m_2)$$
$$\sim D_0(1)\Big|_{K_- \to -K_-^*} + \frac{2\pi\mathrm{i}}{K_+(s_{23} + s_{24}) - K_-^* M_{\mathrm{W}}^2}\left[2\ln\left(1 - \frac{K_+}{K_-^*}\frac{s_{23} + s_{24}}{M_{\mathrm{W}}^2} \right) \right.$$
$$\left. - \ln\left(1 + \frac{K_+}{K_-^* x_{\mathrm{W}}} \right) - \ln\left(1 + \frac{x_{\mathrm{W}} M_{\mathrm{W}}^2}{s_{23} + s_{24}} \right) - \ln\left(\frac{m_2^2}{M_{\mathrm{W}}^2} \right) \right], \tag{A.27}$$

$$\mathcal{D}_0(2) = \mathcal{D}_0(k_3, k_+, k_2, \lambda, m_3, M, m_2)$$
$$\sim D_0(2) + \frac{2\pi\mathrm{i}}{K_+ s_{23}} \ln\left[\frac{K_+ s_{23}}{\mathrm{i}\lambda m_2(s_{13} + s_{23})} \right], \tag{A.28}$$

$$\mathcal{D}_0(3) = \mathcal{D}_0(k_3, k_-, k_2, \lambda, m_3, M^*, m_2)$$
$$\sim -D_0(3)\Big|_{K_- \to -K_-^*} + \frac{2\pi\mathrm{i}}{K_-^* s_{23}} \ln\left[\frac{\mathrm{i}K_-^* m_2}{\lambda(s_{23} + s_{24})} \right], \tag{A.29}$$

$$\mathcal{D}_0(4) = \mathcal{D}_0(k_3, k_-, k_+, 0, m_3, M^*, M)$$
$$\sim -D_0(4)\Big|_{K_- \to -K_-^*} + \frac{2\pi\mathrm{i}}{K_-^*(s_{13} + s_{23}) - K_+ M_{\mathrm{W}}^2}\left[\ln\left(1 + \frac{K_-^* x_{\mathrm{W}}}{K_+} \right) - \ln\left(1 + \frac{x_{\mathrm{W}} M_{\mathrm{W}}^2}{s_{13} + s_{23}} \right) \right]. \tag{A.30}$$

We note that the logarithmic terms on the r.h.s. of (A.26) yield purely imaginary contributions if $(s_{13} + s_{23}) > -M_{\mathrm{W}}^2 x_{\mathrm{W}}$, $(s_{23} + s_{24}) > -M_{\mathrm{W}}^2 x_{\mathrm{W}}$, and κ_{W} is imaginary. These conditions are fulfilled on resonance. Off resonance, this is no longer true near the boundary of phase space. But since these conditions are only violated in a fraction of phase space of order $|k_\pm^2 - M_{\mathrm{W}}^2|/M_{\mathrm{W}}^2$, which is irrelevant in DPA (compare the discussion of the relevance of the Landau singularities in Section 3.4.3), it would even be allowed to replace $\widetilde{\mathcal{D}}_0(0)$, which is real, by $-\operatorname{Re}\{D_0(0)\}$, as it was done in Refs. [38, 39].

B Four-fermion momenta for on-shell W bosons

In order to define a DPA for the virtual corrections of four-fermion production, one has to project the four-fermion momenta for off-shell intermediate W bosons to the ones, where

the W bosons are on shell. Therefore, eight independent parameters have to be chosen, which determine the four-fermion phase space uniquely and include the invariant masses of the resonant W bosons $k_\pm^2$. One possible choice is to fix the directions of the particles W^+, f_1, and f_3 in the CM frame of the initial-state e^+e^- pair while taking the limit $k_\pm^2 \to M_W^2$. This results in the on-shell projection:

$$k_{+0}^{\mathrm{on}} = \frac{\sqrt{s}}{2}, \quad \mathbf{k}_+^{\mathrm{on}} = \frac{\mathbf{k}_+}{|\mathbf{k}_+|}\frac{\sqrt{s}}{2}\beta_W, \quad k_-^{\mathrm{on}} = p_+ + p_- - k_+^{\mathrm{on}},$$

$$k_1^{\mathrm{on}} = k_1\frac{M_W^2}{2k_1 k_+^{\mathrm{on}}}, \quad k_2^{\mathrm{on}} = k_+^{\mathrm{on}} - k_1^{\mathrm{on}}, \quad k_3^{\mathrm{on}} = k_3\frac{M_W^2}{2k_3 k_-^{\mathrm{on}}}, \quad k_4^{\mathrm{on}} = k_-^{\mathrm{on}} - k_3^{\mathrm{on}} \qquad \text{(B.1)}$$

with $k_+ = k_1 + k_2$ and $k_- = k_3 + k_4$. The momenta of the initial-state $e^\pm$ are denoted by $p_\pm$ and the momenta of the final-state fermions by $k_i, i = 1, \ldots, 4$. The on-shell momenta are marked by the superscript 'on'.

C   Construction of phase-space generators

The scattering amplitude of a given process includes usually a lot of different propagators corresponding to the different diagrams. The different propagators peak in different phase-space regions and, therefore, slow down the convergence of the numerical integration or cause numerical instabilities. If the differential cross section varies too much, the result and, in particular, the statistical error of the Monte Carlo integration can not be trusted.

As described in Section 2.2, the multichannel approach is applied to obtain accurate predictions for the processes $e^+e^- \to 4f(+\gamma)$, where each channel is responsible for a diagram or a class of diagrams with the same propagators. A channel is defined by the mappings from random numbers to the momenta of the event. For each diagram, a phase-space generator is constructed in such a way that the corresponding propagators are smoothed by the Jacobian of the specific mapping. To do so, the inverse of the Jacobian of the channel has to simulate the cross section in those regions of phase space where the cross section becomes large. The construction of the phase-space generators is explained in the following (see in addition Refs. [26, 65, 66]).

C.1   Smoothing propagators depending on time-like momenta

Diagrams usually involve several propagators depending on time-like or space-like momenta. In this section, diagrams which depend only on propagators with time-like momenta are considered. It is appropriate to decompose the integral over the phase space into several integrals over the invariants of the propagators and the remaining integrals over the angles in appropriate rest frames. Each invariant is mapped to a random number r such that the integral takes the following form:

$$\int_{s_{\min}}^{s_{\max}} \mathrm{d}s = \int_0^1 \frac{\mathrm{d}r}{g_s(s(r), m^2, \nu, s_{\min}, s_{\max})} \qquad \text{(C.1)}$$

with $0 \le r \le 1$ and the density g_s defined by

$$\frac{1}{g_s(s(r), m^2, \nu, s_{\min}, s_{\max})} = \frac{\mathrm{d}h(r, m^2, \nu, s_{\min}, s_{\max})}{\mathrm{d}r}. \qquad \text{(C.2)}$$

The mapping of the random number r into the invariant s

$$s(r) = h(r, m^2, \nu, s_{\min}, s_{\max}) \tag{C.3}$$

has to be chosen such that the density g_s simulates the behaviour of the integrand in the region where the integrand is large. This is called *importance sampling*, because more events are sampled in the important integration region of s in which the integrand becomes large. Thus, it is a reasonable approach to require that the density has to include the inverse of the propagator.

The mappings belonging to the different propagator types read:

- **Propagator with vanishing width** [26] : $\quad \sigma \propto 1/|s - m^2|^2$

$$h(r, m^2, \nu, s_{\min}, s_{\max}) = \left[r(s_{\max} - m^2)^{1-\nu} + (1-r)(s_{\min} - m^2)^{1-\nu} \right]^{\frac{1}{1-\nu}} + m^2,$$

$$g_s(s, m^2, \nu, s_{\min}, s_{\max}) = \frac{1 - \nu}{\left[(s_{\max} - m^2)^{1-\nu} - (s_{\min} - m^2)^{1-\nu} \right](s - m^2)^{\nu}} \tag{C.4}$$

for $\nu \neq 1$ and

$$h(r, m^2, 1, s_{\min}, s_{\max}) = \exp\left[r\ln(s_{\max} - m^2) - (1-r)\ln(s_{\min} - m^2) \right] + m^2,$$

$$g_s(s, m^2, 1, s_{\min}, s_{\max}) = \frac{1}{\left[\ln(s_{\max} - m^2) - \ln(s_{\min} - m^2) \right](s - m^2)} \tag{C.5}$$

for $\nu = 1$.

- **Breit–Wigner propagator:** $\quad \sigma \propto 1/[(s - M_V^2)^2 + M_V^2 \Gamma_V^2]$

$$h(r, M_V^2 - iM_V\Gamma_V, 2, s_{\min}, s_{\max}) = M_V\Gamma \tan\left[y_1 + (y_2 - y_1)r \right] + M_V^2,$$

$$g_s(s, M_V^2 - iM_V\Gamma, 2, s_{\min}, s_{\max}) = \frac{M_V\Gamma_V}{(y_2 - y_1)[(s - M_V^2)^2 + M_V^2\Gamma_V^2]} \tag{C.6}$$

with

$$y_{1/2} = \arctan\left(\frac{s_{\min/\max} - M_V^2}{M_V\Gamma_V} \right). \tag{C.7}$$

These mappings are applicable not only for the Mandelstam variable s, but also for the absolute value of the Mandelstam variables $|t|$ and $|u|$.

The parameter ν can be tuned to optimise the Monte Carlo integration and should be chosen $\gtrsim 1$. The naive expectation $\nu = 2$ is not necessarily the best choice, because the propagator poles of the differential cross section are partly cancelled in the collinear limit. Note that the mappings (C.4) and (C.5) are undefined for $\nu \geq 1$ and $s_{\min} \leq m^2$.

Since all fermion masses are neglected in our calculations for four-fermion production, m can be omitted in (C.4) and (C.5). However, I found it convenient to use a small negative mass parameter $m^2 = -a$ to avoid numerical problems for $s_{\min} = 0$.

Isotropic decay into two particles

Phase-space generators of diagrams, which include only propagators depending on time-like momenta, can be composed by isotopic particle decays. Therefore, the isotopic decay is described in the following.

A particle with momentum p decays into two particles with momenta k_1 and k_2. The momenta of the initial-state particle and the masses of the final-state particles are fixed. The polar angle ϕ^* and azimuthal angle θ^* in the rest frame of the decaying particle are suitable integration variables:

$$\int d\Phi_d(p, m_1^2, m_2^2) = \int d^4k_1 d^4k_2 \delta(k_1^2 - m_1^2)\theta(k_{10})\delta(k_2^2 - m_2^2)\theta(k_{20})\delta^{(4)}(p - k_1 - k_2)$$

$$= \frac{\lambda^{\frac{1}{2}}(p^2, m_1^2, m_2^2)}{8p^2} \int_0^{2\pi} d\phi^* \int_{-1}^1 d\cos\theta^* \tag{C.8}$$

with the function λ defined in (A.2). For the numerical integration using the Monte Carlo technique, the angles have to be expressed by random numbers r_1 and r_2 with $0 \le r_1, r_2 \le 1$:

$$\int d\Phi_d(p, m_1^2, m_2^2) = \frac{1}{g_d(p^2, m_1^2, m_2^2)} \int_0^1 dr_1 dr_2 \tag{C.9}$$

with $\phi = 2\pi r_1$, $\cos\theta^* = 2r_2 - 1$, and the density

$$g_d(p^2, m_1^2, m_2^2) = \frac{2p^2}{\lambda^{\frac{1}{2}}(p^2, m_1^2, m_2^2)\pi}. \tag{C.10}$$

Since the laboratory frame usually does not coincide with the rest frame of the decaying particle, the proper Lorentz transformation is introduced. The Lorentz transformation of momentum k into the rest frame of the particle with momentum p is defined by

$$k' = \mathcal{B}(p_0, \mathbf{p})k \tag{C.11}$$

with the explicit form (see e.g. Ref. [65])

$$k_0' = \gamma k_0 + \mathbf{b}\mathbf{k}, \qquad \mathbf{k}' = \mathbf{k} + \mathbf{b}\frac{\mathbf{b}\mathbf{k}}{1 - \gamma} + \mathbf{b}k_0, \tag{C.12}$$

where $\mathbf{b} = -\mathbf{p}/m$, $\gamma = p_0/m$ and $m = \sqrt{p^2}$. The inverse Lorentz transform is obtained by substituting $\mathbf{p}$ into $-\mathbf{p}$. For instance, if the momentum k is identical to p, the particle is transformed into its rest frame and vice versa:

$$p^* = \mathcal{B}(p_0, \mathbf{p})p, \qquad p = \mathcal{B}(p_0, -\mathbf{p})p^* \tag{C.13}$$

with $p^* = (m, 0, 0, 0)^{\mathrm{T}}$.

Since the decay is isotropic, the orientation of the coordinate system can be arbitrarily chosen and the momenta of the outgoing particles read

$$k_1 = \mathcal{B}(p_0, -\mathbf{p})\mathcal{R}(\phi^*, \cos\theta^*)\begin{pmatrix} \frac{p^2 + k_1^2 - k_2^2}{2\sqrt{p^2}} \\ 0 \\ 0 \\ \frac{\lambda^{\frac{1}{2}}(p^2, k_1^2, k_2^2)}{2\sqrt{p^2}} \end{pmatrix}, \qquad k_2 = p - k_1 \tag{C.14}$$
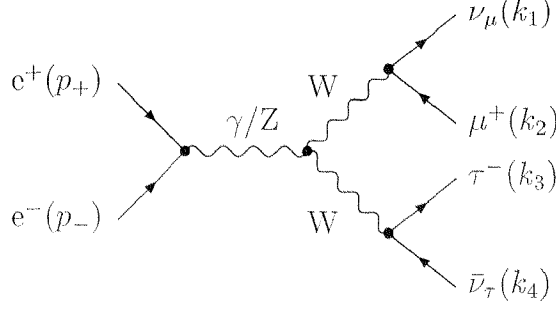
Figure 4.12: Diagram with two resonant W bosons of the process $e^+e^- \to \nu_\mu \mu^+ \tau^- \bar{\nu}_\tau$

with the explicit rotation

$$\mathcal{R}(\phi^*, \cos\theta^*) = \begin{pmatrix} 1 & 0 & 0 & 0 \\ 0 & \cos\phi^* & \sin\phi^* & 0 \\ 0 & -\sin\phi^* & \cos\phi^* & 0 \\ 0 & 0 & 0 & 1 \end{pmatrix} \begin{pmatrix} 1 & 0 & 0 & 0 \\ 0 & \cos\theta^* & 0 & \sin\theta^* \\ 0 & 0 & 1 & 0 \\ 0 & -\sin\theta^* & 0 & \cos\theta^* \end{pmatrix}. \tag{C.15}$$

Example

As an example, a phase-space generator for the diagram of Fig. 4.12 is constructed. For both intermediate particles, photon or Z boson, only one generator is required, since the corresponding propagator is fixed by the momenta of the initial-state particles and, hence, no mapping is needed. The phase-space integral can be decomposed of the integrals over the invariants of the intermediate W bosons, the W-pair production, and the two W decays:

$$\int d\Phi = \int_0^{p^2} dk_+^2 \int_0^{\left(\sqrt{p^2} - \sqrt{k_+^2}\right)^2} dk_-^2 \int d\Phi_d(p, k_+^2, k_-^2)$$
$$\times \int d\Phi_d(k_+, k_1^2, k_2^2) \int d\Phi_d(k_-, k_3^2, k_4^2) \tag{C.16}$$

with $p = p_+ + p_-$, $k_+ = k_1 + k_2$, and $k_- = k_3 + k_4$. The invariant masses of the W-boson propagators are determined by

$$k_+^2 = h(r_1, M_W^2 - iM_W\Gamma_W, 2, 0, p^2), \tag{C.17}$$

$$k_-^2 = h\left(r_2, M_W^2 - iM_W\Gamma_W, 2, 0, \left(\sqrt{p^2} - \sqrt{k_+^2}\right)^2\right) \tag{C.18}$$

with the function h defined in (C.6). The total density reads

$$g_{\text{tot}} = g_s(k_+^2, M_W^2 - iM_W\Gamma_W, 2, 0, p^2) g_s\left(k_-^2, M_W^2 - iM_W\Gamma_W, 2, 0, \left(\sqrt{p^2} - \sqrt{k_+^2}\right)^2\right)$$
$$\times g_d(p^2, k_+^2, k_-^2) g_d(k_+^2, k_1^2, k_2^2) g_d(k_-^2, k_3^2, k_4^2). \tag{C.19}$$

including the two W-boson propagators.

111

C.2 The *t*-channel diagram of a 2 → 2 particle process

So far, only phase-space generators for diagrams with propagators depending on time-like momenta are considered. The simplest diagram including virtual particles with space-like momenta is the *t*-channel diagram of a 2 → 2 particle scattering process which is outlined in the following.

Two particles with momenta p_+ and p_- transform into two particles with momenta k_1 and k_2, where the momenta of the initial-state particles and the masses of the final-state particles are fixed. Furthermore, the diagram includes a propagator depending on the Mandelstam variable $t = (p_+ - k_1)^2$ which has to be smoothed.

The calculation is performed in the rest frame of $p = p_+ + p_-$ with the 3-axis in $\mathbf{p}_+$ direction. The momenta of the external particles take the form

$$
p_\pm^* = \begin{pmatrix} \frac{p^2 + p_\pm^2 - p_\mp^2}{2\sqrt{p^2}} \\ 0 \\ 0 \\ \pm \frac{\lambda^{\frac{1}{2}}(p^2, p_+^2, p_-^2)}{2\sqrt{p^2}} \end{pmatrix}, \qquad k_1^* = \mathcal{R}(\phi^*, \cos\theta^*) \begin{pmatrix} \frac{p^2 + k_1^2 - k_2^2}{2\sqrt{p^2}} \\ 0 \\ 0 \\ \frac{\lambda^{\frac{1}{2}}(p^2, k_1^2, k_2^2)}{2\sqrt{p^2}} \end{pmatrix}, \qquad \text{(C.20)}
$$

and $k_2^* = p_+^* + p_-^* - k_1^*$. Since the invariant mass of the propagator t depends exclusively on the azimuthal angle $\cos\theta^*$,

$$
t = k_1^2 + p_+^2 - \frac{(p^2 + k_1^2 - k_2^2)(p^2 + p_+^2 - p_-^2) - \lambda^{\frac{1}{2}}(p^2, k_1^2, k_2^2)\lambda^{\frac{1}{2}}(p^2, p_+^2, p_-^2)\cos\theta^*}{2p^2}, \quad \text{(C.21)}
$$

the phase-space integral can be converted into an integral over the polar angle ϕ^* and over the absolute value of the Mandelstam variable t:

$$
\int \mathrm{d}\Phi_p(p_+, p_-, m_1^2, m_2^2)
$$

$$
= \int \mathrm{d}^4 k_1 \mathrm{d}^4 k_2 \delta^{(4)}(p - p_1 - p_2)\delta\left(k_1^2 - m_1^2\right)\theta(k_{10})\delta\left(k_2^2 - m_2^2\right)\theta(k_{20})
$$

$$
= \frac{1}{4\lambda^{\frac{1}{2}}(p^2, p_+^2, p_-^2)} \int_0^{2\pi} \mathrm{d}\phi^* \int_{-t_{\max}}^{-t_{\min}} \mathrm{d}|t|, \qquad \text{(C.22)}
$$

where the integration boundaries can be calculated from (C.21) with $-1 \leq \cos\theta^* \leq 1$. Like in the previous section, the polar angle ϕ^* and the invariant t of the propagator are determined by

$$
\phi^* = 2\pi r_1, \qquad |t| = h(r_2, m^2, \nu, -t_{\max}, -t_{\min}) \qquad \text{(C.23)}
$$

resulting in

$$
\int \mathrm{d}\Phi_p(p_+, p_-, k_1^2, k_2^2) = \int_0^1 \mathrm{d}r_1 \int_0^1 \mathrm{d}r_2 \frac{1}{g_p(p^2, p_+^2, p_-^2, t, m^2, \nu, t_{\min}, t_{\max})} \qquad \text{(C.24)}
$$

with the density

$$
g_p(p^2, p_+^2, p_-^2, t, m^2, \nu, t_{\min}, t_{\max}) = \frac{2}{\pi}\lambda^{\frac{1}{2}}(p^2, p_+^2, p_-^2)g_s(-t, m^2, \nu, -t_{\max}, -t_{\min}). \quad \text{(C.25)}
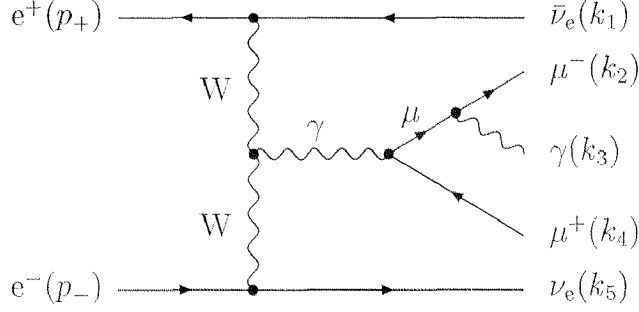$$

Figure 4.13: An example for a multi-peripheral diagram contributing to the process $e^+e^- \to \nu_e\bar{\nu}_e\mu^-\mu^+\gamma$

To obtain the momenta of the final-state particles in the laboratory frame, a rotation and a proper Lorentz transformation are performed:

$$k_i = \mathcal{B}(p_0, -\mathbf{p})\mathcal{R}(-\hat{\phi}, \cos\hat{\theta})k_i^* \tag{C.26}$$

with $i = 1, 2$ and the angles

$$\hat{\phi} = \begin{cases} \arctan\left(\frac{\hat{p}_{+2}}{\hat{p}_{+1}}\right) & , \quad \hat{p}_{+1} > 0 \\ \arctan\left(\frac{\hat{p}_{+2}}{\hat{p}_{+1}}\right) + \pi & , \quad \hat{p}_{+1} < 0 \end{cases}, \qquad \cos\hat{\theta} = \frac{\hat{p}_{+3}}{|\hat{\mathbf{p}}_+|} \tag{C.27}$$

with $\hat{p}_+ = \mathcal{B}(p_0, \mathbf{p})p_+$.

In order to make the numerical integration more efficient, cuts can already be introduced in the generation of the event, i.e. an upper limit on t or on $\cos\theta^*$. Since the Mandelstam variable t is Lorentz invariant the cut on t is valid in arbitrary frames. Angular cuts have to be transformed into the rest frame of the incoming particles.

C.3   Phase-space generator for a multi-peripheral diagram

The multi-peripheral diagram of Fig. 4.13 is investigated as an example, because it involves all types of propagators. In the following, all fermion masses are neglected and the following definitions are used:

$$k_{23} = k_2 + k_3, \qquad k_{234} = k_2 + k_3 + k_4, \qquad k_{1234} = k_1 + k_2 + k_3 + k_4,$$
$$q_+ = p_+ - k_1, \qquad q_- = p_- - k_5, \qquad p = p_+ + p_-. \tag{C.28}$$

The infrared and collinear singularities are excluded by a lower limit on $k_{23}^2 > k_{23,\text{min}}^2$.

The phase-space integral

$$\int d\Phi = \int_{k_{23,\text{min}}^2}^{p^2} dk_{23}^2 \int_{k_{23}^2}^{p^2} dk_{234}^2 \int_{k_{234}^2}^{p^2} dk_{1234}^2 \int d\Phi_p(p_+, p_-, k_{1234}^2, k_5^2)$$
$$\times \int d\Phi_p(p_+, q_-, k_1^2, k_{234}^2) \int d\Phi_d(k_{234}, k_{23}^2, k_4^2) \int d\Phi_d(k_{23}, k_2^2, k_3^2) \tag{C.29}$$

113

is decomposed of two scattering processes and two particle decays. The intermediate particles of this decomposition are the virtual particles and an additional fictitious particle with momentum k_{1234}. The invariant masses of the external particles of the scattering processes and particle decays have to be determined first:

$$k_{23}^2 = h(r_1, 0, \nu_1, k_{23,\text{min}}^2, p^2), \tag{C.30}$$

$$k_{234}^2 = h(r_2, 0, \nu_2, k_{23}^2, p^2), \tag{C.31}$$

$$k_{1234}^2 = h(r_3, 0, 0, k_{234}^2, p^2). \tag{C.32}$$

As a second step, the momenta of the final-state particles are calculated:

$$\boxed{p_+ + p_- \to k_{1234} + k_5}$$

The initial-state electron and positron transforms into the final-state ν_e and a fictitious particle with momentum k_{1234}. The invariant mass of the W-boson propagator is determined by

$$|q_-^2| = h(r_4, M_W^2 - iM_W\Gamma_W, 2, 0, p^2 - k_{1234}^2), \tag{C.33}$$

where the boundaries are taken from (C.21). The momenta can be calculated according to Section C.2.

$$\boxed{p_+ + q_- \to k_1 + k_{234}}$$

The incoming particles are the initial-state positron and the incoming virtual W boson which couples to the initial-state electron. Note, that the momentum of the incoming W boson is fixed by the momentum of the initial-state electron and the already calculated momentum of the final-state ν_e. The invariant mass of the W-boson propagator reads

$$|q_+^2| = h(r_5, M_W^2 - iM_W\Gamma_W, 2, 0, (k_{1234}^2 - k_{234}^2)(k_{1234}^2 - q_-^2)/k_{1234}^2) \tag{C.34}$$

with the boundaries calculated from (C.21). In this way, the momenta of the final-state $\bar{\nu}_e$ and the virtual photon are determined.

$$\boxed{k_{234} \to k_{23} + k_4}$$

The virtual photon decays isotropically into the final-state μ^+ and the virtual μ according to Section C.1.

$$\boxed{k_{23} \to k_2 + k_3}$$

Finally, the virtual μ decays isotropically into the final-state μ^- and the final-state γ.

The total density reads

$$
\begin{aligned}
g_{\text{tot}} = {} & g_s(k_{23}^2, 0, \nu_1, k_{23,\text{min}}^2, p^2)g_s(k_{234}^2, 0, \nu_2, k_{23}^2, p^2)g_s(k_{1234}^2, 0, 0, k_{234}^2, p^2) \\
& \times g_p(p^2, 0, 0, q_-^2, M_W^2 - iM_W\Gamma_W, 2, 0, p^2 - k_{1234}^2) \\
& \times g_p(k_{1234}^2, 0, q_-^2, q_+^2, M_W^2 - iM_W\Gamma_W, 2, 0, (k_{1234}^2 - k_{234}^2)(k_{1234}^2 - q_-^2)/k_{1234}^2) \\
& \times g_d(k_{234}^2, k_{23}^2, 0)g_d(k_{23}^2, 0, 0)
\end{aligned}
\tag{C.35}
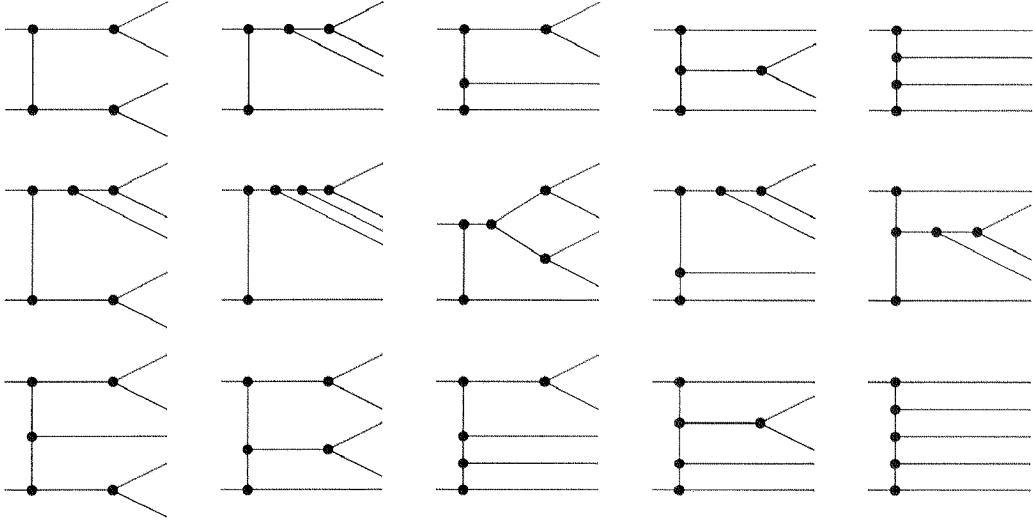$$

and includes all propagators of this diagram.

114

Figure 4.14: The generic phase-space generators symbolized by the topologies of the corresponding diagrams

C.4 Remarks on four-fermion production

In this way, five generic phase-space generators for $e^+e^- \rightarrow 4f$ and ten for $e^+e^- \rightarrow 4f\gamma$ are constructed. The topologies corresponding to the phase-space generators for the processes $e^+e^- \rightarrow 4f$ are shown in the first row of Fig. 4.14 and the topologies corresponding to $e^+e^- \rightarrow 4f\gamma$ can be found in the second and third row of Fig. 4.14. For each generic generator the order of the external particles and the mappings for each propagator can be chosen. In particular, flat mappings of a subset of propagators correspond to topologies where these propagators are contracted. With the help of these generators all propagators of the cross section are smoothed. Special phase-space generators for interference contributions to the cross section are not constructed.

For the process $e^+e^- \rightarrow e^+e^-e^+e^-\gamma$ with 1008 diagrams 928 different channels are included in the calculation. The difference is due to diagrams where the initial-state e^+e^- pair couples to a virtual photon or Z boson. Since the invariant masses of the virtual photon and Z-boson are fixed by the CM energy, only one phase-space generator is required for both diagrams. For instance, the diagram of Fig. 4.12 corresponds to the first topology of Fig. 4.14, where the mapping of the propagator which couples to both incoming particles is flat, i.e. $\nu_i = 0$.

Phase-space generators for diagrams with a quartic-gauge-boson vertex are also included. This diagrams have one propagator less than the other diagrams. Therefore, one propagator in Fig. 4.14 is omitted and the mapping of the invariant of this propagator is flat.

The order of the particle decays, the $2 \rightarrow 2$ particle processes, and the determination of the invariants influence the convergence behaviour of the numerical integration, since the integration domains of the single mappings depend on the already fixed invariants and momenta. In particular, the invariant masses of decaying particles in a decay chain are not independent of each other. To improve the numerical stability, the invariants of the virtual massless particles that couple to external particles should be calculated first, applying already the cuts in the generation of the momenta. In the here discussed Monte Carlo program, invariant-mass cuts are used for the propagators of the virtual

particles with time-like momenta. For the virtual particles with space-like momenta only one angular cut is applied to the first $2 \to 2$ particle process. Note, that the angular cut does not influence the boundaries of the integrations over the invariants of the virtual or fictitious particles with time-like momenta, which are calculated at the beginning.

For the numerical integration of the subtraction terms, additional phase-space generators are constructed, which take into account the propagators of the Born-cross section included in the subtraction terms. Since the Born cross section depends on the four-particle phase space, the four-particle momenta have to be generated first with the phase-space generators for the processes $e^+e^- \to 4f$. These momenta are then mapped into the five-particle phase space according to the different mappings defined Section 4.2.3.

Besides momentum conservation and the requirements on the momenta of external particles, i.e. $k_i^2 = m_i^2$ and $k_{i0} \geq 0$, the phase-space volume is a very helpful variable to test the phase-space generators. For massless external particles, the phase-space volume can be calculated analytically as follows

$$\int \prod_{i=1,n} \mathrm{d}^4 k_i \delta(k_i^2) \theta(k_{i0}) \delta^{(4)}(p - \sum_{i=1}^n k_i) = \left(\frac{\pi}{2}\right)^{n-1} \frac{p^{2n-4}}{\Gamma(n)\Gamma(n-1)}, \tag{C.36}$$

where n is the number of final-state particles (see e.g. Ref. [67]).

Bibliography

[1] S.L. Glashow, *Nucl. Phys.* **22** (1961) 579;
S. Weinberg, *Phys. Rev. Lett.* **19** (1967) 1264;
A. Salam, in Elementary Particle Theory, ed. H. Svartholm (Almqvist and Wiksell, Stockholm, 11968),p. 367;
S.L. Glashow, J. Illiopoulos and L. Maiani, *Phys. Rev.* **D2** (1970) 1285.

[2] G. 't Hooft, *Nucl. Phys.* **B33** (1971) 173; *Nucl. Phys.* **B35** (1971) 167;
E. Kraus, *Ann. Phys.* **262** (1998) 155.

[3] G. Gounaris et al., in *Physics at LEP2*, eds. G. Altarelli, T. Sjöstrand and F. Zwirner (CERN 96-01, Geneva, 1996), Vol. 1, p. 525, hep-ph/9602352.

[4] Z. Kunszt et al., in *Physics at LEP2*, eds. G. Altarelli, T. Sjöstrand and F. Zwirner (CERN 96-01, Geneva, 1996), Vol. 1, p. 141, hep-ph/9602352.

[5] W. Beenakker et al., in *Physics at LEP2*, eds. G. Altarelli, T. Sjöstrand and F. Zwirner (CERN 96-01, Geneva, 1996), Vol. 1, p. 79, hep-ph/9602351.

[6] J.-F. Grivaz et al., in *Conceptual Design of a 500 GeV* e^+e^- *Linear Collider with Integrated X-ray Laser Facility*, eds. R. Brinkmann, G. Materlik, J. Rossbach and A. Wagner (DESY 97-048, Hamburg, 1997), Vol. 1, p. 1.

[7] U. Baur and D. Zeppenfeld, *Phys. Rev. Lett.* **75** (1995) 1002.

[8] Y. Kurihara, D. Perret-Gallix and Y. Shimizu, *Phys. Lett.* **B349** (1995) 367.

[9] E.N. Argyres et al., *Phys. Lett.* **B358** (1995) 339.

[10] W. Beenakker et al., *Nucl. Phys.* **B500** (1997) 255.

[11] R.G. Stuart, *Phys. Lett.* **B262** (1991) 113;
H. Veltman, *Z. Phys.* **C62** (1994) 35;
A. Aeppli, F. Cuypers and G.J. van Oldenborgh, *Phys. Lett.* **B314** (1993) 413.

[12] A. Aeppli, G.J. van Oldenborgh and D. Wyler, *Nucl. Phys.* **B428** (1994) 126.

[13] A. Denner, *Fortschr. Phys.* **41** (1993) 307.

[14] G. Bélanger and F. Boudjema, *Phys. Lett.* **B288** (1992) 201;
G. Abu Leil and W.J. Stirling, *J. Phys.* **G21** (1995) 517;
W.J. Stirling and A. Werthenbach, DTP-99-30, hep-ph/9903315 and *Eur. Phys. J.* **C12** (2000) 441;
G. Bélanger el al., *Eur. Phys. J.* **C13** (2000) 283.

[15] A. Aeppli and D. Wyler, *Phys. Lett.* **B262** (1991) 125.

[16] A. Aeppli, doctoral thesis, Universität Zürich (1992).

[17] G.J. van Oldenborgh, P.J. Franzini and A. Borrelli, *Comput. Phys. Commun.* **83** (1994) 14.

[18] G.J. van Oldenborgh, *Nucl. Phys.* **B470** (1996) 71.

[19] J. Fujimoto et al., *Nucl. Phys. (Proc. Suppl.)* **37B** (1994) 169.

[20] F. Caravaglios and M. Moretti, *Z. Phys.* **C74** (1997) 291.

[21] A. Denner, S. Dittmaier, M. Roth and D. Wackeroth, *Nucl. Phys.* **B560** (1999) 33.

[22] F. Jegerlehner and K. Kolodziej, *Eur. Phys. J.* **C12** (2000) 77.

[23] F.A. Berends, R. Kleiss and R. Pittau, *Nucl. Phys.* **B424** (1994) 308 and *Comput. Phys. Commun.* **85** (1995) 437.

[24] K. Fujikawa, *Phys. Rev.* **D7** (1973) 393;
M. Bacé and N.D. Hari Dass, *Ann. Phys.* **94** (1975) 349;
B.W. Lee and R.E. Shrock, *Phys. Rev.* **D16** (1977) 1444;
M.B. Gavela, G. Girardi, C. Malleville and P. Sorba, *Nucl. Phys.* **B193** (1981) 257;
N.G. Deshpande and M. Nazerimonfared, *Nucl. Phys.* **B213** (1983) 390;
F. Boudjema, *Phys. Lett.* **B187** (1987) 362;
A. Denner, S. Dittmaier and R. Schuster, *Nucl. Phys.* **B452** (1995) 80.

[25] S. Dittmaier, *Phys. Rev.* **D59** (1999) 016007.

[26] F.A. Berends, P.H. Daverveldt and R. Kleiss, *Nucl. Phys.* **B253** (1985) 441 and *Comput. Phys. Commun.* **40** (1986) 285;
J. Hilgart, R. Kleiss and F. Le Diberder, *Comput. Phys. Commun.* **75** (1993) 191.

[27] R. Kleiss and R. Pittau, *Comput. Phys. Commun.* **83** (1994) 141.

[28] M. Böhm, W. Hollik and H. Spiesberger, *Fortschr. Phys.* **34** (1986) 687;
A. Denner, S. Dittmaier and G. Weiglein, *Nucl. Phys.* **B440** (1995) 95.

[29] D. Bardin et al., *Nucl. Phys. (Proc. Suppl.)* **37B** (1994) 148.

[30] D. Bardin et al, in *Physics at LEP2*, eds. G. Altarelli, T. Sjöstrand, F. Zwirner, CERN 96-01, Vol. 2, p. 3, hep-ph/9709270.

[31] E. Boos and Th. Ohl, *Phys. Rev. Lett.* **83** (1999) 480.

[32] T. Stelzer and W.F. Long, *Comput. Phys. Commun.* **81** (1994) 357;
E. Murayama, I. Watanabe and K. Hagiwara, KEK report 91-11, 1992.

[33] R.G. Stuart, in Z^0 *Physics*, ed. J. Tran Thanh Van (Editions Frontieres, Gif-sur-Yvette, 1990) p. 41.

[34] C.G. Papadopoulos, *Phys. Lett.* **B352** (1995) 144.

[35] F. Boudjema et al, in *Physics at LEP2*, eds. G. Altarelli, T. Sjöstrand, F. Zwirner, CERN 96-01, Vol. 1, p. 207, hep-ph/9601224.

[36] V.S. Fadin, V.A. Khoze and A.D. Martin, *Phys. Rev.* **D49** (1994) 2247 and *Phys. Lett.* **B320** (1994) 141;
K. Melnikov and O. Yakovlev, *Phys. Lett.* **B324** (1994) 217.

[37] K. Melnikov and O.I. Yakovlev, *Nucl. Phys.* **B471** (1996) 90.

[38] W. Beenakker, F.A. Berends and A.P. Chapovsky, *Phys. Lett.* **B411** (1997) 203.

[39] W. Beenakker, F.A. Berends and A.P. Chapovsky, *Nucl. Phys.* **B508** (1997) 17.

[40] A. Denner, S. Dittmaier and M. Roth, *Nucl. Phys.* **B519** (1998) 39.

[41] A. Denner, S. Dittmaier and M. Roth, *Phys. Lett.* **B429** (1998) 145.

[42] W. Beenakker and A. Denner, *Int. J. Mod. Phys.* **A9** (1994) 4837;
G. Montagna, O. Nicrosini and F. Piccinini, *Riv. Nuovo Cim.* **21** (1998) 1.

[43] G. 't Hooft and M. Veltman, *Nucl. Phys.* **B153** (1979) 365;
W. Beenakker and A. Denner, *Nucl. Phys.* **B338** (1990) 349;
A. Denner, U. Nierste and R. Scharf, *Nucl. Phys.* **B367** (1991) 637.

[44] D.B. Melrose, *Nuovo Cimento* **XLA** (1965) 181;
W.L. van Neerven and J.A.M. Vermaseren, *Phys. Lett.* **B137** (1984) 241.

[45] V.S. Fadin, V.A. Khoze and A.D. Martin, *Phys. Lett.* **B311** (1993) 311;
D. Bardin, W. Beenakker and A. Denner, *Phys. Lett.* **B317** (1993) 213;
V.S. Fadin et al., *Phys. Rev.* **D52** (1995) 1377.

[46] K. Melnikov and O.I. Yakovlev, private communication.

[47] W. Beenakker, F.A. Berends and A.P. Chapovsky, private communication.

[48] M. Böhm, A. Denner and S. Dittmaier, *Nucl. Phys.* **B376** (1992) 29 and *Nucl. Phys.* **B391** (1993) 483;
S. Dittmaier, *Acta Phys. Pol.* **B28** (1997) 619.

[49] A. Vicini, *Acta Phys. Pol.* **B29** (1998) 2847.

[50] W. Beenakker, A.P. Chapovsky and F.A. Berends, *Phys. Lett.* **B435** (1998) 233;
W. Beenakker, A.P. Chapovsky and F.A. Berends, *Nucl. Phys.* **B548** (1999) 3.

[51] S. Jadach et al., *Phys. Lett.* **B417** (1998) 326.

[52] S. Jadach et al., UTHEP-98-0502, hep-ph/9907436.

[53] M. Böhm et al., *Nucl. Phys.* **B304** (1988) 463;
J. Fleischer, F. Jegerlehner and M. Zrałek, *Z. Phys.* **C42** (1989) 409;
W. Beenakker, K. Kołodziej and T. Sack, *Phys. Lett.* **B258** (1991) 469;
W. Beenakker, F.A. Berends and T. Sack, *Nucl. Phys.* **B367** (1991) 287;
K. Kołodziej and M. Zrałek, *Phys. Rev.* **D43** (1991) 3619;
J. Fleischer, F. Jegerlehner and K. Kołodziej, *Phys. Rev.* **D47** (1993) 830.

[54] D.Yu. Bardin, S. Riemann and T. Riemann, *Z. Phys.* **C32** (1986) 121;
F. Jegerlehner, *Z. Phys.* **C32** (1986) 425;
A. Denner and T. Sack, *Z. Phys.* **C46** (1990) 653.

[55] A. Denner, S. Dittmaier, M. Roth and D. Wackeroth, $\mathcal{O}(\alpha)$ *corrections to* $e^+e^- \rightarrow$ WW $\rightarrow$ 4 fermions$(+\gamma)$ *in double-pole approximation,* in preparation.

[56] A. Ballestrero and R. Chierici, *Phys. Lett.* **B422** (1998) 305.

[57] F. Bloch and A. Nordsieck, *Phys. Rev.* **52** (1937) 54.

[58] T. Kinoshita, *J. Mod. Phys.* **3** (1962) 650;
T.D. Lee and M. Nauenberg, *Phys. Rev.* **133** (1964) 1549.

[59] S. Catani and M.H. Seymour, *Phys. Lett.* **B378** (1996) 287, *Nucl. Phys.* **B485** (1997) 291 and *Nucl. Phys.* **B510** (1998) 503.

[60] R.K. Ellis, D.A. Ross and A.E. Tarrano, *Nucl. Phys.* **B178** (1981) 421;
S.D. Ellis, Z. Kunszt and D.E. Soper, *Phys. Rev.* **D40** (1989) 2188;
Z. Kunszt and D.E. Soper, *Phys. Rev.* **D46** (1992) 192;
S. Frixione, Z. Kunszt and A. Signer, *Nucl. Phys.* **B467** (1996) 399;
Z. Nagy and Z. Trócsányi, *Nucl. Phys.* **B486** (1997) 189.

[61] S. Dittmaier, *Nucl. Phys.* **B565** (2000) 69.

[62] M.L. Mangano, P. Nason and G. Ridolfi, *Nucl. Phys.* **B373** (1992) 295.

[63] V.N. Beier, V.S. Fadin and V.A. Khoze, *Nucl. Phys.* **B65** (1973) 381;
F.A. Berends et al., *Nucl. Phys.* **B206** (1982) 61;
R. Kleiss, *Z. Phys.* **C33** (1987) 433.

[64] I.T. Todorov, *Analytic properties of Feynman diagrams in quantum field theory* (Pergamon Press, Oxford, 1971);
R. Scharf and J.B. Tausk, *Nucl. Phys.* **B412** (1994) 523.

[65] E. Byckling and K. Kajantie, *Particle Kinematics* (John Wiley & Sons, London, 1973), p. 158ff.

[66] V. Barger and R. Phillips, *Collider Physics* (Addison-Wesley, Redwood City, 1987), p. 397ff.

[67] R. Kleiss, W.J. Stirling and S.D. Ellis, *Comput. Phys. Commun.* **40** (1986) 359;

Curriculum Vitae

Personal data

Name: Roth, Markus
Date of birth: March 8, 1969
Place of birth: Werneck, Germany
Nationality: German

Education

Since 1996: Ph. D. student under the supervision of Dr. Ansgar Denner and Prof. Zoltan Kunszt at the ETH Zürich and the Paul Scherrer Institute, Switzerland.

1996: Ph. D. student under the supervision of Dr. Ansgar Denner at the University of Würzburg.

1995 – 1996: Compulsory military service

1989 – 1995: Diploma student in physics at the University of Würzburg, Germany. Thesis title: *"High-energy approximation of massive Feynman-integrals"*

1988: Abitur at the Alexander–von–Humboldt-Gymnasium, Schweinfurt, Germany.

Publications

- **Predictions for all processes $e^+e^- \to 4\,$fermions $+\,\gamma$,**
  A. Denner, S. Dittmaier, M. Roth and D. Wackeroth, *Nucl. Phys.* **B560** (1999) 33.

- **Further numerical results on non-factorizable corrections to $e^+e^- \to 4\,$fermions,**
  A. Denner, S. Dittmaier and M. Roth, *Phys. Lett.* **B429** (1998) 145.

- **Non-factorizable photonic corrections to $e^+e^- \to WW \to 4\,$fermions,**
  A. Denner, S. Dittmaier and M. Roth, *Nucl. Phys.* **B519** (1998) 39.

- **High-energy approximation of one-loop Feynman integrals,**
  M. Roth and A. Denner, *Nucl. Phys.* **B479** (1996) 495.

Acknowledgements